



POLITECNICO DI MILANO  
DEPARTMENT OF MECHANICAL ENGINEERING  
DOCTORAL PROGRAMME IN MECHANICAL ENGINEERING

---

DESIGN, DEVELOPMENT AND ENGINEERING OF A  
BENCH FOR TESTING LOWER LIMB PROSTHESIS, WITH  
FOCUS ON HIGH-TECHNOLOGICAL SOLUTIONS

Doctoral Dissertation of:  
**Cristiano Marinelli**

Supervisor:  
**Prof. Ferruccio Resta**

Tutor:  
**Prof. Maurizio Vedani**

The Chair of the Doctoral Program:  
**Prof. Bianca Maria Colosimo**



---

## Acknowledgments

---

This work was performed at the Department of Mechanical Engineering of Politecnico di Milano under the supervision of Prof. Ferruccio Resta and Prof. Hermes Giberti. First and foremost, I would like to thank them for giving me the extraordinary opportunity to work in such an inspiring environment. The knowledge and experience gained during these years are the most precious things I have ever got. Moreover, their contribution and support was essential for the successful completion of the research project. In this regard, special thanks also go to Prof. Manuela Galli and Eng. Chiara Rigoldi for giving me access to the gait analysis laboratory (Lab. L. Divieti, Department of Biomedical Engineering, Politecnico di Milano, via Golgi 39, 20133 Milan, Italy) and for the many fruitful discussions. I am also sincerely indebted to Eng. Giacomo Lenzoni for his technical contribution and interest in the topic.

Thanks a lot to the colleagues and friends at our Department for their help, support and all the fun we had together. It has been a rewarding experience to spend time especially with my office mates (Andrea, Davide, Rajesh, Leonardo, Pawel, Navid, Binbin, Alireza, Arash, Simone and Gianluca). You are among the most brilliant guys I have ever met and I wish you the best. The same applies to Damiano, Andrea and Filippo.

I am also extremely grateful to my family, especially to my mother for her unceasing support, unconditional love and extraordinary fortitude. The achievement of this result is especially one merit of yours. Last, but not least, thanks to my girlfriend Costanza for her compelling optimism and infinite generosity demonstrated during this period. Your personality is the best I have ever seen, that's why I love you.

Cristiano  
Milano, May 2016



---

## Abstract

---

In the recent past, lower-limb prostheses technological advancement mostly concerned the possibility of integrating ever smaller and more powerful electronic components instead of new materials and topologies. For instance, the electronic knee prostheses currently on the market guarantee maximum yield through sensors and actuators that allow to adjust in real time the characteristics and thus the response of the device itself. Although sophisticated, products currently on the market are far from able to guarantee the same opportunities of their biological counterpart. On the one hand, developing a commercially viable prosthesis that is humanlike as well as economical is a challenging design problem. On the other hand, suitable development and verification methods are missing. Indeed, the legislation in force merely identifies structural tests to verify that the prostheses ensure adequate strength properties during their use. Test methods for the assessment of the functional performances of the whole prostheses are missing. Hardware-In-the-Loop simulation concept represents a useful approach from this point of view. Indeed, it allows to integrate the user behavior into the prosthetic development process removing the limitations related to in-vivo tests. However, the realization of a reliably operating physical solution requires the development of complex mechanical design and sophisticated control strategies. The considerations and the steps performed by the author to achieve these goals are reported in this document. In particular, the bench definition process is performed in order to overcome the most significant challenges of gait simulators, i.e. operating at physiologically correct velocities, applying full scale ground reaction forces and simulating motion in all three planes (sagittal, coronal and transverse).

*Keywords:* *prostheses, test bench, gait simulator, hardware-in-the-loop.*



---

## Summary

---

**T**HIS research topic deals with the development of a bench for testing above knee lower limb prostheses. The idea of developing such a bench is established after a careful evaluation of the requirements and test methods defined by the International Standards Organization (ISO) to assess the conformity of the mentioned devices. These standards merely identify structural tests whose purpose is just to verify that the prostheses, and their individual components, are able to ensure adequate strength properties during their use. Proofs are therefore generally performed using simple servo-hydraulic testing systems. Clearly, they are not suitable for assessing the functional performances of the prosthetic devices, i.e. the ability to assist the amputee while walking or performing other locomotor functions.

These limitations have prompted the manufacturers and the research centers to take advantage of in-vivo test methods, that is, relying on the contribution and the opinion of amputees. However, this solution entails a series of problems that severely slow down the development of new prosthetic devices. On the other hand, robotic testing implies a lot of advantages over human gait trials. This approach allows indeed to integrate the user behavior in an automatic testing procedure while removing all the limitations associated with the employment of a real person.

Despite the need to perform such type of test is not recent, the development of solutions that share the same purpose has been very slow in recent years. Among these there is no system able to completely achieve the aforementioned purpose, to the best of the author's knowledge. From this the need to study new test machines that allow to:

- assess the functional performances of different lower-limb prostheses (especially modern ones);
- make comparison between them;
- support industries in the design and development of more powerful prosthetic devices;
- satisfy the demand of more functional lower limb prostheses by amputees and restore their full rehabilitation.

---

The bench has therefore to guarantee the sequential replication of movements and loads that distinguish a normal leg during the execution of the stride. Humanoid robots such as mechatronic systems that require the development of complex kinematic and mechanical design and the definition of stable and adaptable control strategies. Many considerations must then be done upon the advantages of using different solutions in terms of mechanism architecture and control algorithms before developing a reliably operating physical solution. This document reports the steps and considerations made by the author to achieve these goals. Here is a brief overview of the main contents of the Chapters.

In Chapter 1 the technological advancement of prosthetic knee joints is analyzed in order to emphasize the limits of the test methods currently defined by the legislation in force, i.e. the ISO 10328:2006. Thereafter, the advantages of in-vitro testing procedures over in-vivo gait trials are enunciated so as to legitimize the relevance of this study.

Since the intention is to integrate the user behavior into an automatized testing procedure, the main features of the gait are successively analyzed in Chapter 2. In particular, both the kinematic and dynamic information necessary are extracted starting from the rough data acquired during a gait analysis session.

In Chapter 3 the general layout of the system is defined according to the kinematic and dynamic requirements of gait and the considerations already made by other authors involved in the realization of gait simulators. In particular, at the end of this process the resulting machine is divided into three major subsystems:

- one for reproducing the longitudinal loads;
- one for reproducing the vertical loads;
- one for reproducing the motion of the hip.

These are analyzed and developed separately in the next three Chapters (4,5,6). Experimental tests are also performed in order to extract useful design information.

In Chapter 7, the models developed so far are finally integrated within a single simulation environment in order to verify the merits of the proposed solutions and check the ability of the system to reproduce the phenomenon in-vitro as a whole.

The achieved results demonstrate the validity of the choices undertaken and encourage the development of more refined real solutions.

---

# Contents

---

<b>1 State-of-the-art</b>	<b>1</b>
1.1 Introduction . . . . .	1
1.2 The problem: amputation and rehabilitation . . . . .	1
1.3 Knee prosthetic joint . . . . .	4
1.3.1 Passive joints . . . . .	4
1.3.2 Semi-active joints . . . . .	5
1.3.3 Active joints . . . . .	7
1.4 Legislation in force . . . . .	10
1.5 In-vitro testing . . . . .	15
1.6 Hardware-In-the-Loop . . . . .	16
1.7 Lower-limb prostheses test bench . . . . .	17
1.8 State-of-the-art concluding remarks . . . . .	21
<b>2 Gait analysis</b>	<b>23</b>
2.1 Introduction . . . . .	23
2.2 Basic features of the walk . . . . .	23
2.3 Gait analysis methods . . . . .	26
2.4 Requirements . . . . .	30
2.4.1 Kinematic requirements . . . . .	30
2.4.2 Dynamic requirements . . . . .	37
2.5 Gait analysis concluding remarks . . . . .	40
<b>3 System synthesis</b>	<b>41</b>
3.1 Introduction . . . . .	41
3.2 General layout . . . . .	41
3.3 Residual limb subsystem . . . . .	43
3.4 Ground subsystem . . . . .	45
3.5 System synthesis concluding remarks . . . . .	46

## Contents

---

<b>4 Longitudinal loading subsystem</b>	<b>49</b>
4.1 Introduction . . . . .	49
4.2 Longitudinal axis design . . . . .	49
4.2.1 Mechanism identification . . . . .	49
4.2.2 Motor-reducer unit selection . . . . .	50
4.3 Operation procedure . . . . .	56
4.4 Control architecture . . . . .	56
4.5 Position control . . . . .	58
4.5.1 Mathematical model . . . . .	58
4.5.2 Control synthesis . . . . .	59
4.5.3 Law of motion profile . . . . .	62
4.6 Force control . . . . .	63
4.6.1 Friction model . . . . .	63
4.6.2 Control synthesis . . . . .	65
4.6.3 Force profile . . . . .	66
4.7 Numerical simulation . . . . .	67
4.7.1 Nonlinear numerical model . . . . .	68
4.7.2 Preliminary results . . . . .	68
4.7.3 Position/force control with self-adjusting matrix . . . . .	70
4.7.4 Final results . . . . .	73
4.8 Experimental testing . . . . .	73
4.8.1 Experimental setup . . . . .	74
4.8.2 LabView control program . . . . .	75
4.8.3 Experimental trial . . . . .	75
4.9 Longitudinal loading subsystem concluding remarks . . . . .	76
<b>5 Vertical loading subsystem</b>	<b>79</b>
5.1 Introduction . . . . .	79
5.2 Mechanical architecture . . . . .	79
5.2.1 Actuator . . . . .	80
5.2.2 Mechanism architecture . . . . .	81
5.2.3 Measurement set-up . . . . .	82
5.3 Structural design . . . . .	86
5.3.1 Vertical guide system . . . . .	86
5.3.2 Lower plate . . . . .	87
5.3.3 Intermediate plate connected to the air spring . . . . .	88
5.3.4 Intermediate plate connected to the flexible foils . . . . .	89
5.3.5 Upper plate . . . . .	90
5.4 Operation procedure . . . . .	92
5.5 Mathematical model . . . . .	93
5.5.1 Air spring model . . . . .	94
5.5.2 Servo-valve model . . . . .	95
5.5.3 Mechanical load model . . . . .	97
5.6 Numerical simulation . . . . .	98
5.6.1 Linear analysis . . . . .	98
5.6.2 Nonlinear analysis . . . . .	107
5.7 Realization and characterization . . . . .	110

5.7.1	Realization and assembly . . . . .	111
5.7.2	Control system . . . . .	112
5.7.3	Calibration . . . . .	114
5.8	Vertical loading subsystem concluding remarks . . . . .	121
<b>6</b>	<b>Residual limb subsystem</b>	<b>123</b>
6.1	Introduction . . . . .	123
6.2	ABB IRB 6620 . . . . .	123
6.3	Kinematic and dynamic analysis . . . . .	125
6.4	ABB IRB 6620 optimization analysis . . . . .	129
6.5	Prosthesis grasping solution . . . . .	132
6.6	Residual limb subsystem concluding remarks . . . . .	134
<b>7</b>	<b>Numerical model of the entire system</b>	<b>135</b>
7.1	Introduction . . . . .	135
7.2	ADAMS-MATLAB/Simulink co-simulation . . . . .	135
7.3	Numerical model of the mechanical system . . . . .	136
7.4	Numerical model of the control system . . . . .	138
7.5	Operation and results . . . . .	139
7.6	Numerical model of the entire system concluding remarks . . . . .	143
<b>8</b>	<b>Conclusions</b>	<b>145</b>
<b>A</b>	<b>Anatomical frames</b>	<b>149</b>
A.1	Thigh coordinate system . . . . .	149
A.2	Shank coordinate system . . . . .	150
A.3	Foot coordinate system . . . . .	150
A.4	Global coordinate system . . . . .	151
<b>B</b>	<b>Angular convention</b>	<b>153</b>
B.1	Cardan and Eulerian angles . . . . .	153
B.2	Cardan convention: position . . . . .	153
B.3	Cardan convention: velocity and acceleration . . . . .	154
B.3.1	Angular velocity . . . . .	154
B.3.2	Angular acceleration . . . . .	154
<b>Bibliography</b>		<b>157</b>



---

## List of Figures

---

1.1 Amputations levels and reasons . . . . .	2
1.2 Transfemoral prosthesis main components . . . . .	3
1.3 Mono- and poly-centric knee prosthetic joint . . . . .	4
1.4 Passive knee joint currently on the market . . . . .	5
1.5 Semi-active knee joint currently on the market . . . . .	6
1.6 Active prosthesis having motors directly coupled at the joints . . . . .	8
1.7 Active prosthesis driven by pneumatic actuators . . . . .	8
1.8 Active prosthesis exploiting the concept of Series Elastic Actuators . . . . .	9
1.9 Active prosthesis exploiting a non linear passive transmission . . . . .	9
1.10 Kind of prostheses considered in the standard 10328:2006 . . . . .	10
1.11 Main loading configurations according to the standard 10328:2006 . . . . .	11
1.12 Schematic representation of the test configurations A (1.12a) and B (1.12b)	12
1.13 Real representation of the test configurations A (1.13a) and B (1.13b) . .	12
1.14 Examples of experimental setup compliant with the requirements in force	13
1.15 In-vivo test performed by a disabled volunteer . . . . .	14
1.16 In-vivo test performed by an able-bodied volunteer . . . . .	14
1.17 Bench for testing car engines . . . . .	16
1.18 Bench for testing pantographs . . . . .	16
1.19 Bench for testing satellite rendezvous and docking . . . . .	16
1.20 Bench for testing ventricular and aortic prosthetic valves . . . . .	16
1.21 Anatomical planes . . . . .	18
1.22 Test bench developed by Natsakis et al. . . . .	19
1.23 Test bench developed by Giberti et al. . . . .	19
1.24 Test bench developed by Zhang et al. . . . .	20
1.25 Test bench developed by Richter et al. . . . .	20
1.26 Test bench developed by Kim and Oh . . . . .	20
1.27 Test bench developed by Thiele et al. . . . .	21
1.28 Test bench developed by Aubin et al. . . . .	21
2.1 Controlateral rotation of the upper and lower part of the body during normal walking . . . . .	24

## List of Figures

---

2.2 Main phases of the gait cycle . . . . .	25
2.3 Example of EMG sensor . . . . .	26
2.4 Example of magnetic sensor . . . . .	26
2.5 Example of force plate . . . . .	27
2.6 Example of insole sensor . . . . .	27
2.7 Examples of electro-goniometer and relative application . . . . .	27
2.8 Example of accelerometer and relative application . . . . .	28
2.9 Example of optical motion capture system and relative application . . . . .	28
2.10 Panoramic view of the gait analysis laboratory . . . . .	29
2.11 Laboratory measurement equipment . . . . .	29
2.12 Pose of the femur embedded reference system over time . . . . .	30
2.13 Davis markers scheme . . . . .	31
2.14 Orientation of a body in three dimensions . . . . .	32
2.15 Initial and final hip orientation . . . . .	33
2.16 Sequence of intrinsic rotations according to the ( $ZXY$ ) Cardan convention	33
2.17 Axes convention adopted at the hip . . . . .	34
2.18 Hip linear displacement components of subject 1, 2, 3 and 4 . . . . .	34
2.19 Hip angular displacement components of subject 1, 2, 3 and 4 . . . . .	35
2.20 Reference hip linear displacement components . . . . .	35
2.21 Reference hip angular displacement components . . . . .	35
2.22 Motion simplification . . . . .	36
2.23 Reference hip velocity components . . . . .	37
2.24 Reference hip acceleration components . . . . .	37
2.25 Trajectories of some anatomical points within the sagittal plane . . . . .	37
2.26 Axes convention adopted at the foot . . . . .	38
2.27 Force components acting on the right foot of the subjects 1, 2, 3 and 4 . . . . .	38
2.28 Reference force components . . . . .	38
2.29 Loads acting on the hip . . . . .	39
2.30 Power to be delivered at the hip joint . . . . .	39
2.31 Hip and foot diagrams . . . . .	40
3.1 Initial (3.1a) and final (3.1b) topology of the system . . . . .	42
3.2 Overview of the system architecture . . . . .	43
3.3 Manipulators with serial (3.3a) and parallel (3.3b) kinematic architecture	44
3.4 Overview of the system architecture . . . . .	47
4.1 Linear guide kinematic data . . . . .	50
4.2 Linear guide dynamic data . . . . .	50
4.3 Representative picture of the linear guide . . . . .	50
4.4 Schematic representation of a mechanical system made up of motor, transmission, and load . . . . .	51
4.5 Schematic representation of mechanical load driven by the motor-reducer unit . . . . .	53
4.6 Law of motion of the foot in longitudinal direction . . . . .	54
4.7 External load applied to the carriage . . . . .	54
4.8 Reference hip linear displacement components . . . . .	54
4.9 Reference hip angular displacement components . . . . .	54

---

**List of Figures**

4.10 Useful reduction ratio range associated to each motor . . . . .	55
4.11 Brushless motor kinematic and dynamic data . . . . .	55
4.12 Planetary gearbox kinematic data . . . . .	55
4.13 Representative picture of the motor-reducer unit . . . . .	55
4.14 Schematic representation of the hybrid control architecture . . . . .	57
4.15 Block diagram of the mechanical system during position control . . . . .	59
4.16 Block diagram of the P/PI position controlled system . . . . .	60
4.17 Block diagram of the resulting PID position controlled system . . . . .	60
4.18 Frequency response function of the closed loop system . . . . .	61
4.19 Step response function of the closed loop system . . . . .	61
4.20 Position, velocity and acceleration profiles considered during this study	62
4.21 Possible velocity profiles . . . . .	63
4.22 Coulomb friction model . . . . .	64
4.23 Karnopp friction model . . . . .	64
4.24 SimMechanics friction block . . . . .	65
4.25 Block diagram of the PID force controlled system . . . . .	66
4.26 Actual and approximated longitudinal force reference . . . . .	67
4.27 Block diagram of the horizontal actuating system numerical model . . . . .	68
4.28 Force reference and actual trend . . . . .	69
4.29 Position reference and actual trend . . . . .	69
4.30 Switch signal . . . . .	69
4.31 Actual position of both the carriage and the foot . . . . .	70
4.32 Torque supplied by the motor to drive the carriage according to the hybrid control strategy . . . . .	70
4.33 Schematic representation of the mixed control architecture . . . . .	71
4.34 Trend of the selection matrix as a function of the vertical reaction force considering different values in terms of $\alpha$ . . . . .	72
4.35 Block diagram of the strategy for modulating the reference force signal through the Z-shaped function . . . . .	72
4.36 Torque supplied by the motor to drive the carriage according to the mixed control strategy . . . . .	73
4.37 Connection diagram of the longitudinal actuating subsystem experimental setup . . . . .	74
4.38 NI-SCB 68 screw terminal connector block . . . . .	75
4.39 PCI NI-6229 DAQ board . . . . .	75
4.40 LabVIEW programming environment . . . . .	76
4.41 Experimental result in terms of torque supplied by the motor and velocity of the carriage . . . . .	77
4.42 Experimental trend of the friction coefficient as a function of the carriage velocity . . . . .	77
4.43 Numerical trend of the friction coefficient as a function of the carriage velocity . . . . .	77
5.1 Examples of air spring available on the market . . . . .	81
5.2 Out of alignment working conditions allowed by the air spring considered during this study . . . . .	81
5.3 Basic configuration of the vertical actuating mechanism . . . . .	82

## List of Figures

---

5.4 Solution developed by Tarabini et al. for identifying the mass matrix of people . . . . .	83
5.5 Load cell implemented . . . . .	84
5.6 Solution for measuring the load in longitudinal direction . . . . .	85
5.7 Solution for measuring the load in vertical direction . . . . .	85
5.8 Spherical joints implemented . . . . .	86
5.9 Linear potentiometer implemented . . . . .	86
5.10 Schematic representation of the final solution . . . . .	86
5.11 Mechanism sections . . . . .	86
5.12 Commercial components constituting the vertical guide system . . . . .	87
5.13 Final design of the lower plate . . . . .	88
5.14 Final design of the intermediate plate connected to the air spring . . . . .	89
5.15 Final design of the intermediate plate connected to the flexible foils . . . . .	89
5.16 FE analysis of the intermediate plate connected to the flexible foils . . . . .	90
5.17 Final design of the upper plate . . . . .	90
5.18 First FE analysis of the upper plate . . . . .	91
5.19 Second FE analysis of the upper plate . . . . .	91
5.20 Final rendering of the vertical loading subsystem . . . . .	91
5.21 Working phases of the vertical loading subsystem . . . . .	93
5.22 Schematic representation of the air spring . . . . .	94
5.23 Foot ground penetration contact model . . . . .	98
5.24 Block diagram of the air spring open loop control system . . . . .	99
5.25 Block diagram of the air spring closed loop control system . . . . .	99
5.26 Schematic representation of the vertical loading subsystem during the stable contact phase . . . . .	99
5.27 Model considered during the application of the Euler method . . . . .	99
5.28 Datasheet diagram of the thrust force supplied by the spring as a function of the inner pressure and the elongation . . . . .	101
5.29 Stiffness of the air spring as a function of the inner pressure . . . . .	101
5.30 Root locus of the system about each equilibrium point . . . . .	103
5.31 Bode frequency response of the dynamic system about each equilibrium point . . . . .	103
5.32 Bode frequency response of the dynamic system and its reduced version . . . . .	105
5.33 Gain and phase margins representation of the open loop controlled system . . . . .	106
5.34 Step response of the closed-loop system about each equilibrium point . . . . .	106
5.35 Bode frequency response of the closed-loop system about each equilibrium point . . . . .	107
5.36 Block diagram of the vertical loading subsystem developed using Simulink and SimMechanics . . . . .	107
5.37 Block diagram of the pneumatic actuator developed using Simulink . . . . .	108
5.38 Approximated force reference and actual load applied to the foot . . . . .	108
5.39 Elastic force due to the inner stiffness of the bellows . . . . .	108
5.40 Approximated force reference and actual load applied to the foot with the new set of gains . . . . .	109
5.41 Switch signal . . . . .	109

5.42 Vertical real force reference and actual load applied to the foot with the new set of gains . . . . .	110
5.43 Vertical position of both the foot and the support surface . . . . .	110
5.44 Absolute pressure within the air spring . . . . .	110
5.45 Commercial and custom made pieces . . . . .	111
5.46 Upper an lower part constituting the vertical loading subsystem . . . . .	111
5.47 Representative picture of the vertical loading subsystem accommodated on the linear guide . . . . .	111
5.48 Connection diagram of the vertical loading subsystem . . . . .	112
5.49 LabVIEW programming environment . . . . .	112
5.50 Load cells calibration experimental setup . . . . .	113
5.51 Servo-valve and elbow gasket implemented . . . . .	114
5.52 Vertical loading subsystem accommodated on the universal testing machine . . . . .	115
5.53 Block diagram of the overall experimental setup . . . . .	116
5.54 Thrust force supplied by the vertical loading subsystem as a function of the relative pressure and the elongation of the spring . . . . .	116
5.55 Stiffness of the vertical loading subsystem in vertical direction as a function of the absolute pressure . . . . .	117
5.56 Comparison of the force through the custom measurement setup and the universal testing machine load cell . . . . .	117
5.57 Average error committed through the custom measurement setup as a function of the relative pressure . . . . .	118
5.58 Bode diagram of the servo-valve transfer function . . . . .	119
5.59 Force read through the custom measurement setup and the universal testing machine during the first dynamic test . . . . .	120
5.60 Trend of the friction force of the vertical loading subsystem . . . . .	120
5.61 Ability of the system to track a constant force reference despite the disturbance imposed in terms of motion . . . . .	121
6.1 ABB IRB 6620 industrial 6-axis robot . . . . .	124
6.2 ABB IRB 6620 available workspace . . . . .	124
6.3 Reference hip linear displacement components . . . . .	125
6.4 Reference hip angular displacement components . . . . .	125
6.5 Reference hip linear displacement components . . . . .	125
6.6 Reference hip angular displacement components . . . . .	125
6.7 Representation of the robot model built in MSC Adams . . . . .	126
6.8 Main robot reference frames . . . . .	126
6.9 Joints angular position computed in MSC Adams before optimization .	127
6.10 Joints angular velocity computed in MSC Adams before optimization .	127
6.11 Joints torques computed in MSC Adams considering no loads at the hip	127
6.12 Joints torques computed in MSC Adams considering the loads at the hip	127
6.13 Joints powers computed in MSC Adams considering the loads at the hip	128
6.14 ABB RobotStudio simulation environment . . . . .	128
6.15 Orientation of the TF with respect to the end-effector . . . . .	130
6.16 Trend of the objective function during the optimization procedure . . .	130
6.17 Joints angular position computed in MSC Adams after optimization . .	131

## List of Figures

---

6.18 Joints angular velocity computed in MSC Adams after optimization . . . . .	131
6.19 Joints torques computed in MSC Adams after optimization . . . . .	131
6.20 Joints powers computed in MSC Adams after optimization . . . . .	131
6.21 Prosthetic tubular adapter . . . . .	132
6.22 SolidWorks representation of the grasping solution . . . . .	133
6.23 SolidWorks representation of the grasping solution mounted on the robot	133
7.1 Schematic representation of the co-simulation model . . . . .	136
7.2 Representation of the mechanical model of the overall system built in ADAMS . . . . .	137
7.3 Representation of the control system built in MATLAB/Simulink . . . . .	139
7.4 Comparison of the main co-simulation results with the corresponding gait instants . . . . .	139
7.5 Trajectory followed by the foot in the sagittal plane . . . . .	140
7.6 Vertical reaction force achieved by means of the model and corresponding gait trend . . . . .	140
7.7 Horizontal reaction force achieved by means of the model and corresponding gait trend . . . . .	141
7.8 Vertical displacement of both the force plate and the foot . . . . .	141
7.9 Horizontal displacement of both the force plate and the foot . . . . .	141
7.10 Absolute pressure within the air spring . . . . .	142
7.11 Torque applied by the brushless motor connected to the linear guide . .	142
7.12 Torques at the joints of the robot . . . . .	142
A.1 Anatomical landmarks . . . . .	149

---

## List of Tables

---

2.1 Primary kinematic and dynamic requirements . . . . .	40
4.1 Main characteristics of the Lenze motors considered during the selection procedure . . . . .	53
4.2 Parameters for the selection of the motor-reducer unit . . . . .	55
4.3 Position control PID gains . . . . .	61
4.4 Friction model parameters . . . . .	65
4.5 Analysis of the force components correlation . . . . .	66
5.1 Parameters of the foot-ground contact model . . . . .	98
5.2 Initial conditions of the dynamic system about each equilibrium position . . . . .	102
5.3 Bellows stiffness as a function of the inner pressure . . . . .	102
5.4 Steady-state gain corresponding to each equilibrium point . . . . .	104
5.5 Load cells sensitivity . . . . .	113
5.6 Parameters obtained by applying the Ziegler-Nichols method about each equilibrium point . . . . .	119
5.7 Relations for computing the PID according to the Ziegler-Nichols . . . . .	119
6.1 Primary kinematic information of the ABB IRB 6620 robot . . . . .	124
B.1 Cardan convention for computing the orientation matrix . . . . .	154



---

# CHAPTER **1**

---

## **State-of-the-art**

---

### **1.1 Introduction**

---

Nowadays, the application of advanced technology solutions allows humans to delegate most of their tasks to machines. Due to traumas, diseases or birth defects, these technologies are frequently exploited to restore the full reintegration of a patient who suffered the amputation of a limb. From this point of view, prostheses aim to replicate the shape and functionality of the corresponding missing anatomical structures. However, products currently on the market are far from able to guarantee the same opportunities of their biological counterparts. This deficiency is principally due to the lack of suitable development and verification procedures. As a consequence, the aim of the present work is to define new methods for testing and developing more properly a particular category of prosthesis, the transfemoral one.

### **1.2 The problem: amputation and rehabilitation**

---

In Italy every year about 5000 amputation surgery are performed [52]. In particular, the lower limbs are the most affected, with 91.7% of the total amount of interventions (Fig. 1.1). The main causes leading doctors to perform this kind of operation are:

- peripheral vascular diseases and cancers;
- traumas and accidents;
- congenital disorders or birth defects.

Regardless of the reason, the amputation of a limb is a traumatic event both in physical and psychological terms. The possibility of having a substitute of the limb is therefore necessary to restore the full recovery of a patient. From this point of view, pros-

## Chapter 1. State-of-the-art

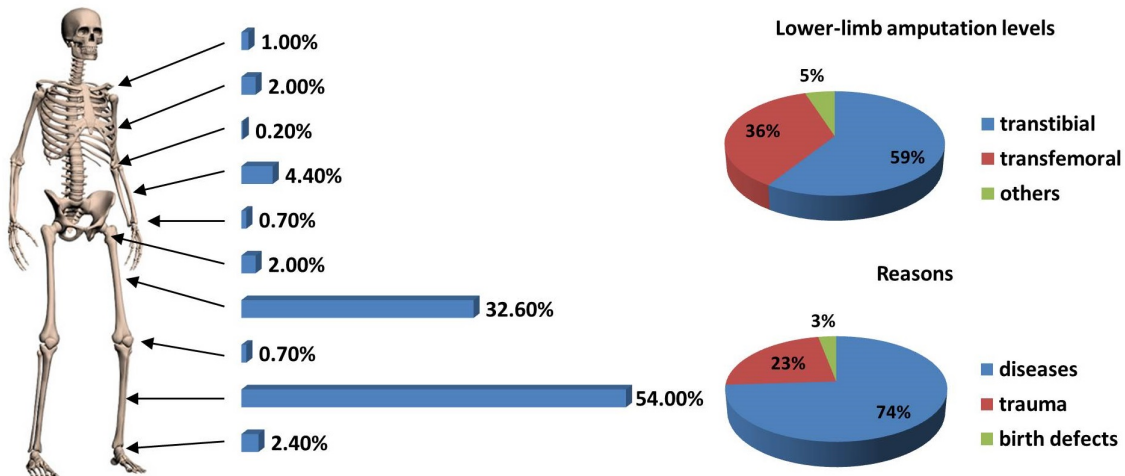


**Figure 1.1: Amputations levels and reasons**

thetic devices aim to replicate the shape and functionality of the corresponding missing anatomical structure.

There are basically two types of prosthesis for replacing the lower limb depending on whether the amputation is performed above or below the knee (Fig. 1.1). These are respectively called transfemoral and transtibial. The former is more complex because it reproduces the foot and the ankle as well as the knee, probably the most problematic prosthetic component of this category.

Regardless of the kind considered, there are two approaches to build a prosthesis: exoskeletal or endoskeletal. The second type has completely replaced the first one. Its modular structure allows indeed to achieve a higher level of versatility in the realization of the prosthesis. As a consequence, the device can be adapted and adjusted to suit the patient and his level of activity. Focusing on endoskeletal devices, the four major components of the above-knee prosthesis are represented and described below (Fig. 1.2):

- **Socket**

It's the rigid element in contact with the stump of the amputee. Its function is therefore to create a point for connecting and aligning the rest of the prosthesis. It is custom-made for each patient.

- **Knee joint**

It is the element linking the rest of the prosthesis to the socket. Thus, it strongly influences the overall performance of the device. In particular, it should ensure stability in orthostatic (i.e. quiet standing) position and a correct dynamic response during walking. The component is chosen based on the activity level and the particular needs of each amputee.

- **Pylon**

It corresponds to the tibia in a healthy subject, and it consists in a variable-length tube which links the knee to the prosthetic foot. The diameter is standard, i.e. 30mm.

## **1.2. The problem: amputation and rehabilitation**

- Foot-ankle system

This component allows the subject to interact with the ground such as the corresponding biological counterpart. There are many varieties on the market. The final choice is carried out according to the use foreseen for the entire prosthesis.



**Figure 1.2:** Transfemoral prosthesis main components

A broad variety of sockets, knees, pylons, feet, and ankles are available and can be combined to produce the prosthesis that best meets the needs of each individual amputee. The final choice depends on the following factors:

- the physical and mental conditions of the user;
- the status and the length of the stump;
- the disability level of the user;
- the presence of associated disabling diseases;
- the age;
- the activity level of the user;
- the environmental conditions in which the prosthesis is used;
- the technology advancement in the field.

In terms of prosthetic knees, the technological level reached by modern devices allows amputees to recover an adequate lifestyle, but still different from the normal one. An overview of the prosthetic knees currently on the market is briefly given below.

### **1.3 Knee prosthetic joint**

---

The prosthetic industry has developed many devices to face the need to replace the knee joint. These may be divided in three main categories:

- passive;
- semi-active;
- active.

A review of their main features is given below.

#### **1.3.1 Passive joints**

Passive joints consist in simple kinematic chains (either crank, glyph, 4- or 6-bar mechanisms) integrating mechanical elements (springs and dampers) whose physical characteristics are modifiable only off-line. The kinematics chains establish the position of the center of rotation of the shank with respect to the thigh. Single-axis and multi-axis schemes are possible (Fig. 1.3).

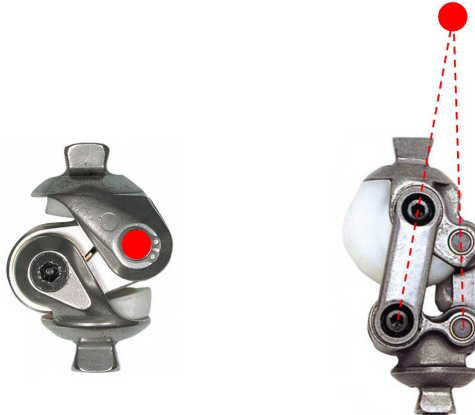


**Figure 1.3: Mono- and poly-centric knee prosthetic joint**

The mechanical elements determine instead the motion possibilities of the mechanism. The combination of these elements determines the resistance of the joint to rotate during both the stance and the swing phase, that are respectively the phases during which the foot is in contact with and off the ground. In particular, the resistance must prevent the knee to buckle during the stance phase of walking and the shank from moving forward too fast during the swing phase. For example, here is the description of some passive devices.

- The Total Knee (Össur, Iceland, Fig. 1.4a) is a multi-axis device integrating a hydraulic circuit for controlling the amount of resistance during swing phase. Stance stability is mechanically ensured by means of a 4-bar mechanism.

### 1.3. Knee prosthetic joint

- The Mercury (Blatchford Endolite, USA, Fig. 1.4b) is a single-axis prosthetic knee whose stance and swing phase control is accomplished through a hydraulic cylinder.
- The NK-1 (Nabtesco, Japan, Fig. 1.4c) is a single axis device integrating a pneumatic circuit and an advanced weight-activated brake system for controlling respectively the swing and stance phase of walking.
- The NK-6 (Nabtesco, Japan, Fig. 1.4d) provides a great stability in the stance phase by means of a 6-bar mechanism. Swing smoothness is guaranteed by a hydraulic cylinder.



**Figure 1.4:** Passive knee joint currently on the market

The behavior of these devices, in terms of flexion-extension angle, completely rely on the dynamic characteristics of the gait. As a result, they do not provide the maximum support and the maximum yield in every situation. These aids are therefore generally recommended for patients who do not have a very active life.

#### 1.3.2 Semi-active joints

Semi-active prostheses offer some improvements over mechanically passive devices. The introduction of active components (sensors, processing units, actuators) and devoted control strategies allow to tune the damping level, and then the resistance of the prostheses in real-time as a function of some gait parameters. Thus, they are frequently referred to as variable-damping knee prostheses. Within the group of microprocessor controlled knee joints, there are differences referring to units generating internal resistance, sensor technology and control strategy [13]. Here is a brief description of the most successful products currently on the market.

- The SmartIP (Blatchford Endolite, USA, Fig. 1.5a) employs a pneumatic circuit and motorized valves for modulating the damping of the artificial joint during the swing phase.
- The C-Leg (Otto Bock, Germany, Fig. 1.5b) utilizes a hydraulic circuit instead of a pneumatic one and a dedicated control system for dissipating mechanical energy during both the stance and swing phase according to actual dynamics.

## Chapter 1. State-of-the-art

- The Orion2 (Batchford Endolite, USA, Fig. 1.5c) and the Hybrid Knee (Nabtesco, Japan) are single-axis devices integrating both a hydraulic and a pneumatic unit. Stance and swing controls are ensured by regulating in real-time the flow through the corresponding valves.
  - In the RheoKnee (Össur, Iceland, Fig. 1.5d) the resistance during the whole stride is continuously adjusted by changing the magnetic field and therefore the viscosity of the magnetorheological fluid in the embedded hydraulic circuit.



**Figure 1.5:** Semi-active knee joint currently on the market

Despite the differences referring to sensor technology, the generation of the control signal is generally performed according to position and force sources of information coming from strain gauges and either linear or angular potentiometers. Such information allow to detect the walking phase and therefore to choose the control strategy to be applied, providing greater comfort to the user. Often the ‘finite-state’ approach is employed to adjust the control parameters and obtain the desired resistance profile during the stride [15]. From this point of view, the simplest, and therefore most widespread solution is splitting the gait cycle in two states: the stance and the swing. The knee joint is locked throughout the entire phase of stance. On the other hand, damping is appropriately adjusted over the swing phase. Researchers have even attempted to use electromyographic (EMG) signals measured from the residual limb and sophisticated control algorithms, such as fuzzy logic and neural network, to adapt the behavior of the prosthesis. However, classification of the information coming from sensors and therefore estimation/recognition of the user intent is still an open issue [2, 39, 63].

Several scientific studies have been conducted to quantitatively compare mechanically passive knees with variable-damping devices in terms of gait metabolism, kinetics, and kinematics [42, 45]. The results of these studies indicate that microprocessor controlled prosthetic knee joints offer significant advantages over the mechanically passive counterpart in terms of stability, energy consumption, comfort, and versatility. Nevertheless, much work remains to be done for restoring the pre-morbid activity level of amputees. Although sophisticated, the current solutions are indeed not yet able to completely reestablish the original joint function, which is the result of a complex evolution process. In particular, the reproduction of the following physiological aspects is still an open issue [75, 83]:

- the intrinsic impedance of the corresponding biological structure;
- the energy storage and return of a real knee;
- the ability of muscles to perform active work.

The latter is in particular the main aspect commonly associated to prosthetic deficiencies. Indeed, the inability to deliver joint power significantly impairs the ability of these prostheses to completely restore many locomotive functions, such as sit-to-stand maneuvers, stair/slope ascent ambulation, as well as level walking; despite energy requirements of the knee during the latter task are largely dissipative. From this point of view, the efforts made by some researchers gave birth to a new device category, the active prostheses; where ‘active’ refers to the ability of generating a positive work at the knee by gaining energy from a supply source. Different solution have been proposed in the literature but none is currently available on the market. Here is a review of the main advances introduced over the last ten years to fulfill the above mentioned requirements.

### 1.3.3 Active joints

First approaches to the design of powered prostheses mainly focused on the use of single-motor transmission systems directly coupled to the knee joint to generate the desired torque at the joint itself. The torque necessary to adjust the angular position of the prosthetic device was in particular computed based on the angular state of the sound limb [15, 44]. Such approach, known as echo control [35], eliminates the need for the mathematical model of the gait cycle during implementation of the control process. However, it introduces major drawbacks. Firstly, the desired position trajectories are typically computed based on the measurement of the sound side leg trajectory, which restricts the approach to only unilateral amputees, and also presents the problem of instrumenting the sound side leg. Secondly, suitable motion tracking requires an output stiffness too high to replicate the characteristic impedance of the biological structure. As a consequence, this approach forces the amputee to react to the artificial limb rather than interact with it and therefore returns a behavior far from the corresponding physiological one [30]. For this reason, the echo control was soon abandoned in favor of the impedance-based approach. According to this method, torque at the joint is generated by approximating the behavior of the knee as the combination of finite states consisting of passive spring and damper. For example, the behavior of the knee within a given state can be represented using a linear spring and a linear damper as follows [49]:

$$\tau = -k(\theta - \theta_{eq}) - b\dot{\theta},$$

where  $\tau$  is the command torque,  $\theta$  denotes the joint angle, and  $\dot{\theta}$  represents the joint angular velocity. The three remaining parameters,  $\theta_{eq}$ ,  $k$  and  $b$ , are respectively the set point of the spring, the stiffness and the damping coefficient. By varying these parameters it is possible both to perform active work and to adjust the apparent impedance of the device. Power can be generated by switching between appropriate equilibrium positions (of the spring) in each finite state. Impedance can be adjusted by tuning the physical parameters. In addition, the joint behavior results locally passive, that is, at any given state the prosthesis comes to rest at a local equilibrium point. From the user

## Chapter 1. State-of-the-art

point of view, the impedance control enhances therefore both the reliability and predictability of the device. However, two problems are associated with this solution. On the one hand, the impedance profile to be reproduced is not exactly known since quantitative data on physiological knee joint impedance during gait are still missing [66]. Indeed, assessment of this information is almost impossible because the inherent non-linear behavior of the anatomical joint. Nevertheless, following the assumption that knowledge of physiological impedance could facilitate control design, several research groups are currently working on quantifying physiological joint impedance during gait. On the other hand, existing hardware components are inherently too stiff to allow the replication of the estimated physiological stiffness templates, whatever they are. For instance, both in [15] and [30] the active torque about the knee is produced by means of a DC brushed motor actuating a ball-screw mechanism directly coupled to the joint. Harmonic drive gears are used by other authors [93] (Fig. 1.6).

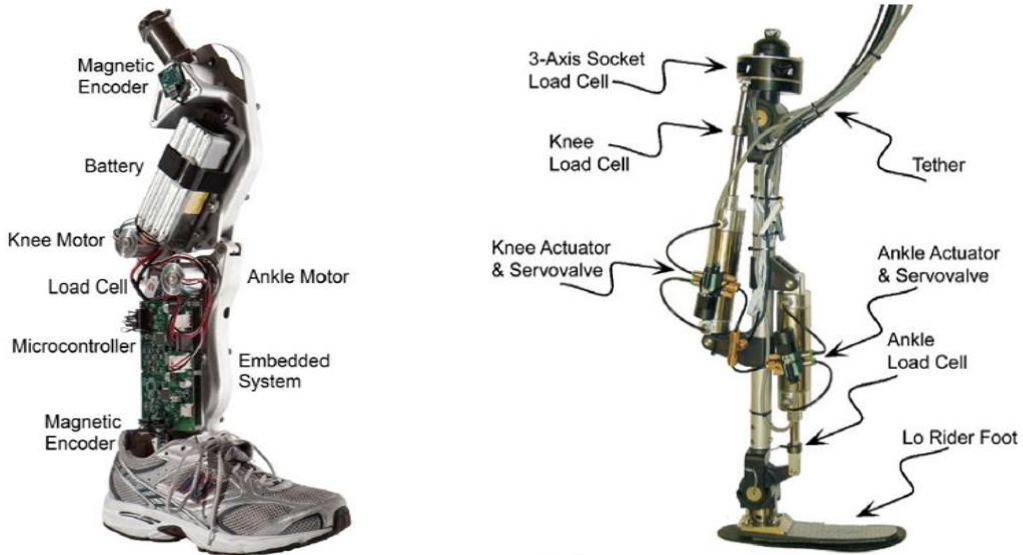


**Figure 1.6:** Active prosthesis having motors directly coupled at the joints

**Figure 1.7:** Active prosthesis driven by pneumatic actuators

While these components are ideal for high-stiffness applications, because of their high bandwidth and high positioning precision, they fail to reproduce the impedance profile of a biological joint [66]. Attempts have been made to solve this problem. A pneumatically powered device is for example proposed in [77] (Fig. 1.7). However, no quantitative information about the resulting intrinsic stiffness is reported in the paper. On the other hand, promising results are obtained based on the idea of Series Elastic Actuator (SEA), i.e. the introduction of compliant elements in series with the motors. Besides guaranteeing a correct reproduction of the impedance, this solution entails indeed also other advantages from the prosthetic application point of view:

- improves force control performance;
- protects the transmission mechanically from impacts;
- makes devices safer to interact with humans;

### 1.3. Knee prosthetic joint

- has the potential for energy storage.

For instance, a powered knee prosthesis with two series-elastic actuators positioned in parallel in an agonist-antagonist arrangement is proposed in [56] (Fig. 1.8). Motors can be independently used to control the knee angle at which each spring is engaged and therefore to establish different stiffness levels. Despite the possibility of arbitrarily vary the physical stiffness, the employment of two actuators entails higher weight and complexity, which are undesired characteristics in prosthetic applications. In this regard, a nonlinear transmission able to change the actuator stiffness as a function of joint angle is proposed in [66] (Fig. 1.9). Compared to the previous approach this solution does not need a second actuator, but the awareness of joint stiffness-angle relationship before designing. Unfortunately, this information is not yet accessible. Then, a totally active prosthesis for lower limb amputees is far from realizable in short time.

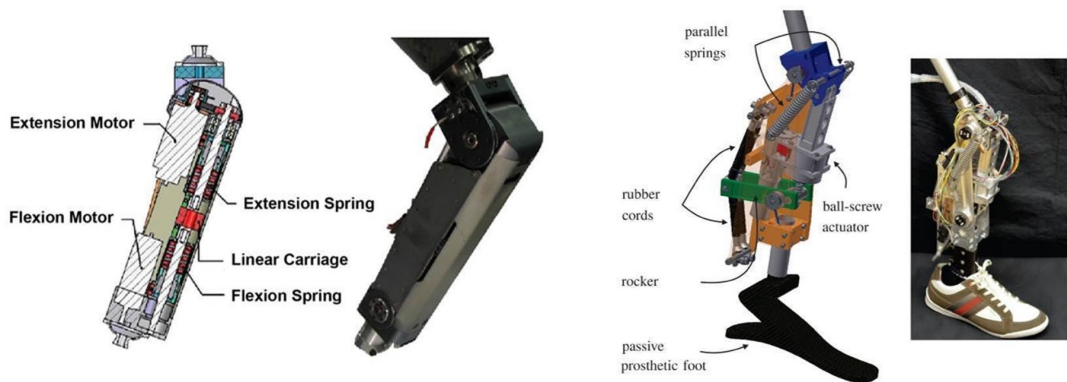


**Figure 1.8:** Active prosthesis exploiting the concept of Series Elastic Actuators    **Figure 1.9:** Active prosthesis exploiting a non linear passive transmission

Nevertheless, motivated by the potential of modern technologies, nowadays researchers are trying to develop devices to help impaired individuals to walk in a more natural way. However, there are several factors limiting the general use and commercialization of these devices. On the one hand, developing a commercially viable powered prosthesis that is humanlike in its weight, size, strength, and impedance, while still being energetically economical and noise free, is a challenging design problem. On the other hand, suitable verification methods to verify and increase both the strength and the functional properties of the prostheses are missing. The standard currently in force has indeed some gaps from this point of view. As a consequence, commercial transfemoral prostheses remain limited to energetically passive devices, that is, the joints of the prostheses can either store or dissipate energy, but cannot provide net power over a gait cycle. These devices cannot accurately replicate the exactness of human locomotion. As a result, the gait of transfemoral amputees is asymmetric, and tasks where able-bodied subjects heavily rely on positive knee joint power require considerable adaptation of the motor pattern [66]. Not surprisingly, transfemoral amputees experience clinical problems, such as back pain, as well as higher metabolic energy requirements when using variable-damping knee technology [56].

## **1.4 Legislation in force**

---

The experimental tests on prosthetic elements are designed so as to ensure that the devices or their individual components have adequate safety properties during their use. Requirements and test methods relative to lower-limb prostheses are collected by the International Organization for Standardization (ISO) in the standard 10328:2006, ‘Prosthetics - Structural testing of lower-limb prostheses - Requirements and test methods’ [1]. Such document covers the following aspects:

1. definition, identification, selection and preparation of test samples;
2. designation of the test categories;
3. configuration of the experimental setup;
4. description of the test loading conditions and test loading levels;
5. specification of the test equipment compliance;
6. execution of the experimental procedure;
7. verification of the performance requirements fulfillment.

Despite these instructions apply to several types of prostheses (Fig. 1.10), the aforementioned items are analyzed below by referring just to transfemoral complete structures.

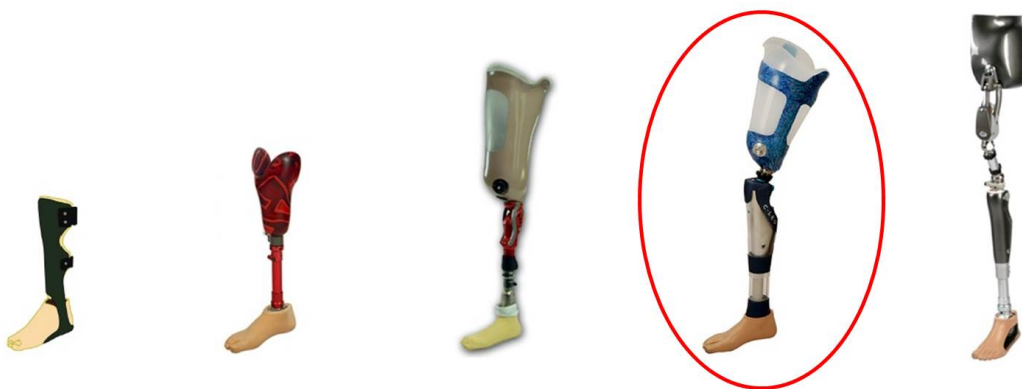


**Figure 1.10: Kind of prostheses considered in the standard 10328:2006**

For a transfemoral prosthesis, a complete structure consists of a knee unit and ankle unit or ankle attachment with all parts between. It may also contain parts above the knee unit, including the socket, and below the ankle unit or ankle attachment, including the foot unit (Sec. 1.2). Regardless of the prosthetic portion considered, aim of the standard is to assess that the sample ensures suitable strength properties during practice. However, the complexity of the load actions to which a lower-limb prosthesis is subjected during use by the amputee cannot be simulated through a single test procedure. The standard identifies therefore two critical situations during which most likely the stresses are greater and consequently prescribes two principal tests. These critical situations are referred to as condition A and B:

#### 1.4. Legislation in force

- condition A: maximum loading occurring early in the stance phase of walking.;
- condition B: maximum loading occurring late in the stance phase of walking.

The corresponding walking stages are shown in the following figure (Fig. 1.11).

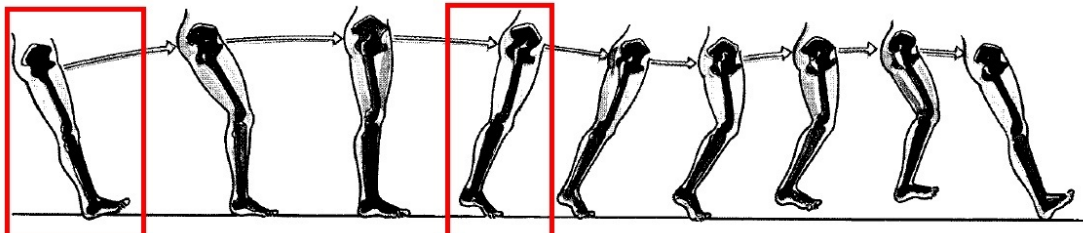


**Figure 1.11:** Main loading configurations according to the standard 10328:2006

Each test is characterized by own configuration and loading conditions. These features are analyzed below.

Once established a reference system, the instructions provided in the standard contribute to place both the test sample and the load so as to reproduce the above two most critical load situations as realistically as possible. In particular, the test sample and the load are not aligned in order to produce compound loadings by the application of a single test force. The schematic illustrations of both the test configurations are shown (Fig. 1.12). For the sake of clarity, also the pictures of a transfemoral prosthesis under test at the laboratories of Politecnico di Milano are reported (Fig. 1.13).

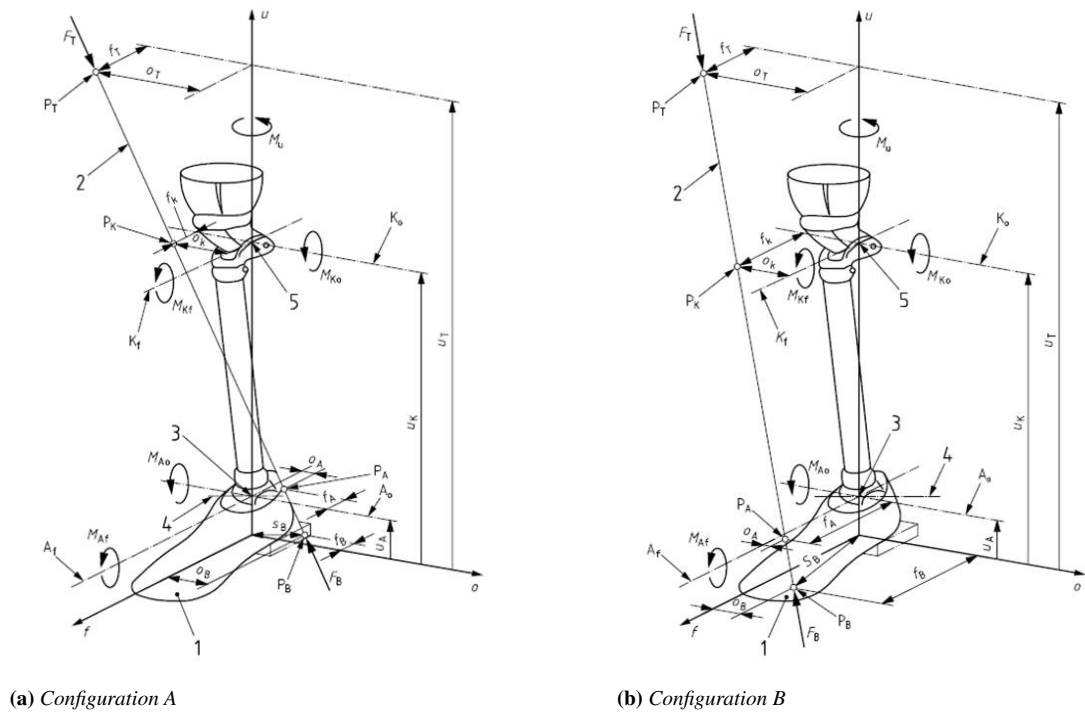
Given a configuration, the specimen undergoes three different loading conditions in order to evaluate its strength considering different working situations:

- proof strength (PS):  
static load representing an occasional severe event, which can be sustained by the prosthetic device/structure and still allow it to function as intended;
- ultimate strength (US):  
static load representing a gross single event, which can be sustained by the prosthetic device/structure but which could render it thereafter unusable;
- fatigue strength (FS):  
cyclic load which can be sustained by the prosthetic device/structure for a given number of cycles.

The entity of the loads to be applied to the prosthesis is reported in the document as a function of the loading condition (PS, US, FS) as well as of a severity factor which depends on the patient's weight category. The approval requires the specimen to support the loads associated to each test in the way intended by the standard. As a consequence, the tests are monitored both in terms of load and displacement to assess any structural failure. The standard finally defines accuracy requirements both in terms of preparation and execution of the tests so that evaluations can be properly carried out. For more information refer to the standard itself.

Clearly, the current international standard merely identifies static and cyclic structural tests just to verify that the prostheses, or their individual components, are able to

## Chapter 1. State-of-the-art



(a) Configuration A

(b) Configuration B

**Figure 1.12:** Schematic representation of the test configurations A (1.12a) and B (1.12b)



(a) Configuration A

(b) Configuration B

**Figure 1.13:** Real representation of the test configurations A (1.13a) and B (1.13b)

#### 1.4. Legislation in force

ensure adequate strength properties during their use. Accordingly, strength tests have been performed so far using simple servo-hydraulic testing systems [55] (Fig. 1.14).

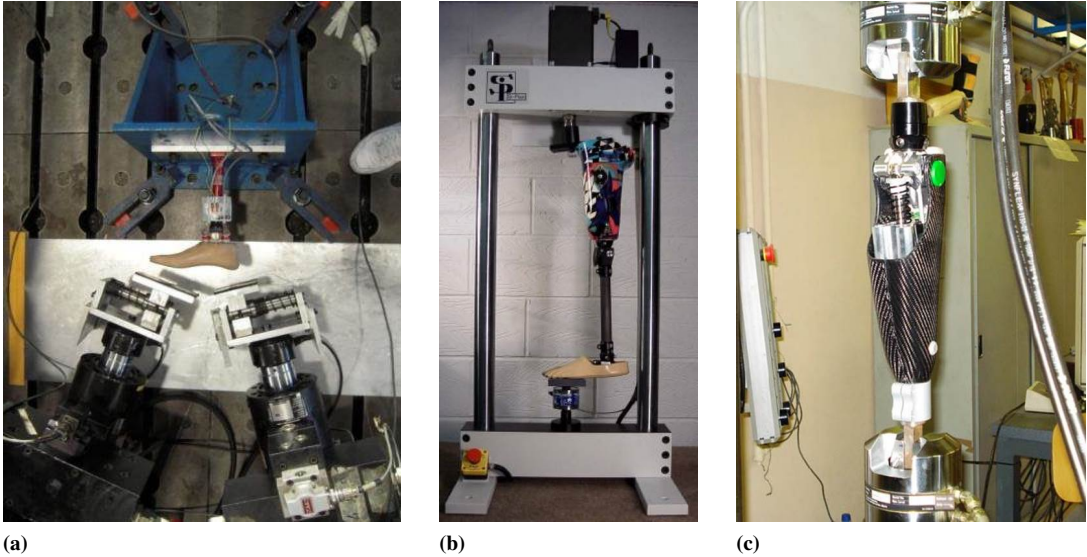


**Figure 1.14:** Examples of experimental setup compliant with the requirements in force

Obviously, these methods are not suitable for assessing the functional performances of the prosthetic devices, that is, the ability to assist the amputee while walking. However, this was not the primary requirement of the period because the available devices were just passive. In fact, although the standard is in force since 2006, the test methods and the performance requirements are the outcome of a series of meetings held under the aegis of the International Society for Prosthetics and Orthotics (ISPO) around the middle of the twentieth century. The final one was held in Philadelphia, USA, in 1977. The test procedures may therefore not be applicable to prostheses different from those used in the consensus, such as modern electronic prosthetic devices. Indeed, in the recent past, the prosthetic technological advancement mostly concerned the possibility of integrating ever smaller and more powerful electronic components instead of new materials and topologies. For instance, the modern semi-active knee prostheses (Sec. 1.3) guarantee maximum yield by means of sensors and actuators that allow to adjust in real time the damping and thus the response of the device itself. The evaluation of these solutions requires controlled field trials in addition to the laboratory tests specified in this International Standard. The ISO itself acknowledges the limits of the standard stating:

*“Ideally, additional laboratory tests should be carried out to deal with function, wear and tear, new material developments, environmental influences and user activities as part of the evaluation procedure. There are no standards for such tests, so appropriate procedures will need to be determined.”.*

These limitations have prompted the manufacturers and research centers to take advantage of in-vivo test methods (Fig. 1.15). This technique implies the possibility to find amputees ready to provide their contribution and opinion. Obviously, this solution

## Chapter 1. State-of-the-art

---

entails a series of problems, including:

- mean controllability and repeatability of the test procedure;
- inadequate reliability of the results;
- poor safety level;
- lack of volunteers with a technical background.

The development of new prosthetic devices is severely slowed down by these aspects, especially the last one. Indeed, the field trials should be repeated whenever significant design changes are made to the prosthesis. Not surprisingly, some research centers have developed specific supports for fitting the prosthesis under study on able-bodied subjects (Fig. 1.16). For instance, an able-bodied testing adaptor is used in [77] and [30] to assess the performances of a transfemoral prosthesis without the participation of an amputee.

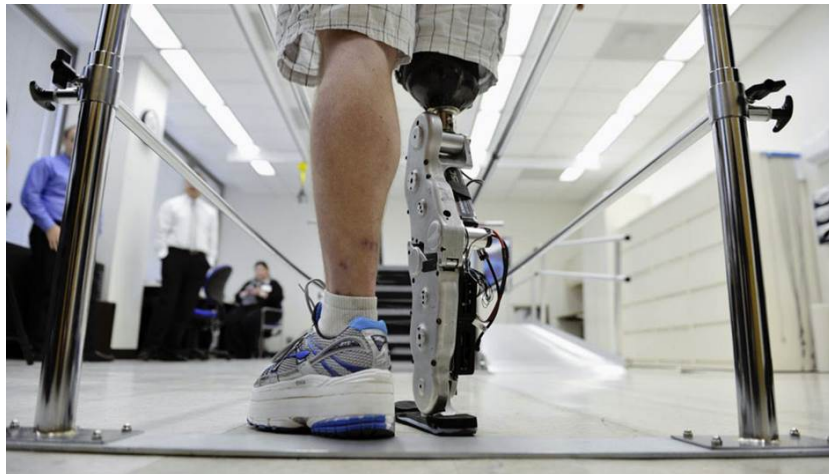


**Figure 1.15:** *In-vivo test performed by a disabled volunteer*

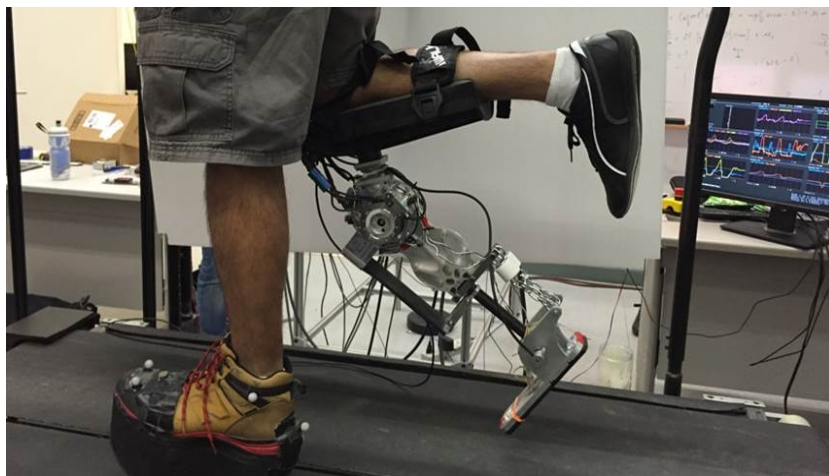


**Figure 1.16:** *In-vivo test performed by an able-bodied volunteer*

## **1.5. In-vitro testing**

---

Obviously both these approaches are inappropriate. From this the need to study new test methods that allow to:

- assess the functional performances of different lower-limb prostheses (especially modern ones);
- make comparison between them;
- support industries in the design and development of more powerful prosthetic devices;
- satisfy the demand of more functional lower limb prostheses by amputees and restore their full rehabilitation.

According to this, the purpose of the present work is to suggest a solution and assess its possibility of reproducing working conditions more realistic than the methodologies provided by the International Standard in force.

### **1.5 In-vitro testing**

---

The analysis performed in the previous sections revealed the need to take advantage of new test methods in order to develop ever more powerful lower-limb prosthetic devices. Indeed, the ability to run functional tests exclusively in-vivo (human gait trials) severely limits their progress both in terms of time and results. This need is quite common in the engineering field. Indeed, the same problems arise whenever addressing the design of a new system. Although in some cases the best way to develop a product is to test its properties under real operating conditions, frequently laboratory tests are a more efficient way. This strategy is superior due to four main factors:

- cost;
- duration;
- safety;
- feasibility.

For instance, the high design costs of a car do not allow to wait for the completion of the entire system before testing the performance of the engine [86], the suspension [60] or any other component. Thus, devoted test rigs are developed in parallel to the system in order to test the performance of the individual parts ahead (Fig. 1.17).

The same applies in the railway sector (Fig. 1.18). The possibility of simulating the mechanical interaction between the pantograph and the overhead equipment before operation is for example an important issue in the design of high-speed railways [28].

In other cases, the need to perform laboratory tests is primarily determined by the impossibility to perform field trials. For instance, spacecraft operations, such as satellite rendezvous and docking, must be carefully designed and thoroughly verified before a real space mission can be launched [53] (Fig. 1.19). Prosthetics implanted within the human body suffer from the same problem (Fig. 1.20). Ethical and technical reasons discourage indeed in-vivo measurements [37, 59].



**Figure 1.17:** Bench for testing car engines

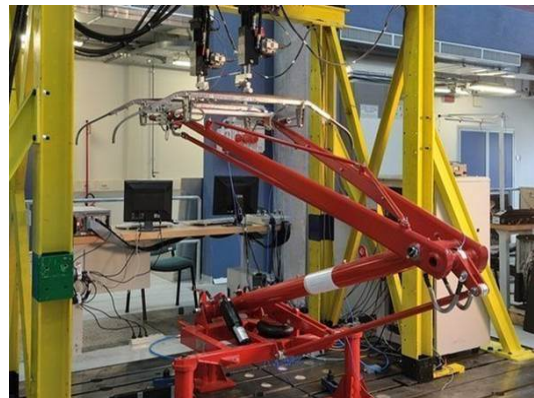


**Figure 1.18:** Bench for testing pantographs

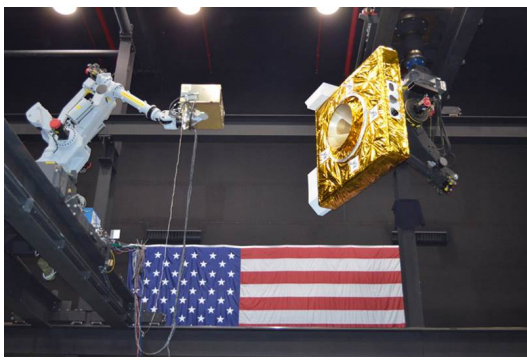


**Figure 1.19:** Bench for testing satellite rendezvous and docking



**Figure 1.20:** Bench for testing ventricular and aortic prosthetic valves

Other simulations are mainly performed in the fields of power engineering and robotics. Regardless of the application, a test designed according to this logic is referred to as Hardware-In-the-Loop (HIL) simulation.

## 1.6 Hardware-In-the-Loop

---

Simulations performed according to the HIL techniques allow to verify the performance of the units under study by reproducing in-vitro the working conditions under which they must operate [9]. The components making this task possible are:

- sensors: collect data about quantities of interest during the test;
- actuators: allow to reproduce the desired operating conditions by performing the commands delivered by the controller;
- wirings: connect sensors and actuators to the controller;
- mathematical models: emulate what not physically reproduced through the actuators.

This approach is particularly useful when the need is to anticipate the verification on components or subsystems already in the designing stage. The response of the prototype allows indeed to evaluate in advance and safely how the final product behaves

## **1.7. Lower-limb prostheses test bench**

---

during operation. Furthermore, this technique allows to simulate the most different operating conditions and to facilitate the execution of long test procedures. In conclusion, the development of semi-active and active prostheses would benefit more from the execution of in-vitro than in-vivo tests. Specific conditions that warrant the use of HIL simulation during prosthetic development include:

- Enhancing the quality of testing

The reproducibility, the controllability, and the possibility to arbitrarily instrument the prosthesis provide access to more reliable and detailed information about the system behavior.

- Reducing the development schedules

The physiological needs of an amputee introduce unavoidable dead times. On the other hand, a test rig may be operated continuously for a long period of time.

- Versatility

A robotic simulator allows to quickly change the prosthesis under test, the scenario and the working conditions. In addition, it enables to simulate irregular situations that volunteers for ethical and safety reasons cannot perform, such as stumble.

It is therefore foreseen that robotic testing of prostheses will play a greater role than human gait trials in the development process of the dynamic characteristics of prosthetic devices. The need to perform such type of test is not recent [36]. Nevertheless, the development of solutions that share the same purpose has been very slow in recent years. Here is a review of the most interesting solutions reported in the literature.

## **1.7 Lower-limb prostheses test bench**

---

Different mechanical solutions for testing the functional properties of lower-limb prostheses according the HIL technique are available in the literature. There are systems for assessing the performances of either transfemoral or transtibial prostheses. These solutions exhibit common characteristics:

- the partition of the machine in two subsystems interacting with the prosthesis, i.e. the ground and the limb;
- the reproduction of a more or less extended part of the limb depending on the type of prosthesis under study;

but also differences:

- the sort of movements and loads to be simulated;
- the technologies adopted;
- the control strategies implemented.

The design differences are principally influenced by the number of degrees of freedom taken into account. There are indeed gait simulators developed either in 2 or 3 dimensions. The former exclusively reproduce the aspects of the phenomenon occurring in the sagittal plane (Fig. 1.21). The other, instead, even those occurring in the transverse and frontal planes (Fig. 1.21).

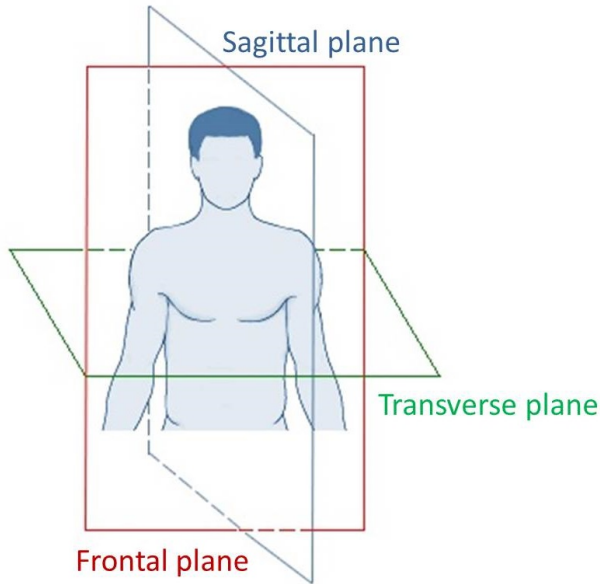


**Figure 1.21:** Anatomical planes

These approaches comply with different needs. Those in two dimensions endorse the simplification of the system. On the other hand, the three-dimensional ones give priority to the complete reproduction of the phenomenon. This aspect looks essential if the intention is to evaluate the ability of the prosthesis to completely replace the function of the healthy limb. Nevertheless, most of the authors restrict the functionality of their test systems so as to reproduce only the sagittal characteristics of the phenomenon pretending that out of plane deviations are reasonably lower and therefore negligible. In fact, it is just a way to reduce the number of degrees of freedom considered, and then the complexity of the issue.

Different in-plane solutions, in terms of mechanical architecture, have been proposed for the sake of simplicity. Two representative as well different examples of setup suitable for assessing the functional performances of transtibial prostheses are given in [61] and [31]. The former, that is the gait simulator developed by Natsakis et al., is actually designed to study the foot-ground contact force using cadaveric specimens. However, it may be useful to investigate the dynamics of transtibial prostheses. The bench consists of a metallic frame bearing a linear guide and a force platform. The specimen is attached to the carriage of the linear guide via a hinge joint representing the knee. Both the carriage and the hinge are actuated by servo-electric motors to simulate respectively the horizontal progression and the rotation of the knee joint within the sagittal plane. Meanwhile, a pneumatic actuator below the platform controls its vertical motion to achieve the correct reproduction of the vertical ground reaction force. A representation of the bench is shown below (Fig. 1.22).

Also the solution proposed by Giberti et al. is mainly designed for testing transtibial prostheses in the sagittal plane (Fig. 1.23). However, the degrees of freedom are reproduced and actuated in a totally different way. Movements and loads in vertical direction are played by means of a hydraulic actuator at the hinge representing the hip joint. Conversely, the horizontal motion component is introduced at the ground by

## 1.7. Lower-limb prostheses test bench

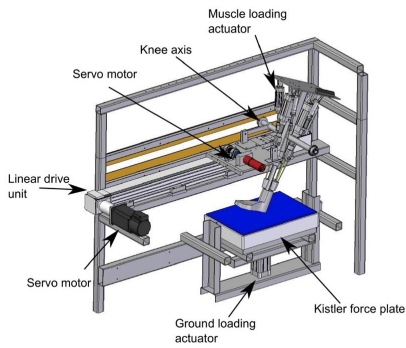


**Figure 1.22:** Test bench developed by Natsakis et al.

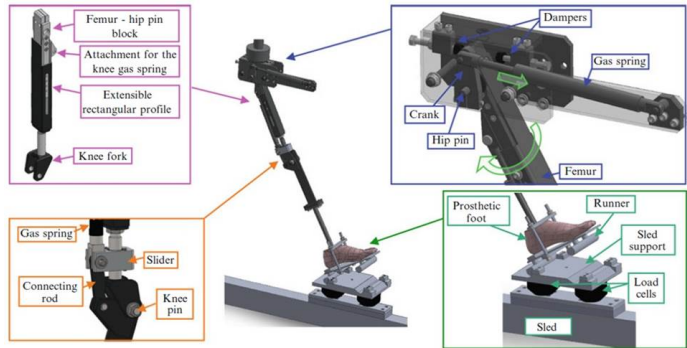


**Figure 1.23:** Test bench developed by Giberti et al.

moving the surface supporting the foot via a linear guide actuated by an electric servomotor. Finally, lockable gas springs allow selective rotation of the hip and knee joints during stance phase as well as a smooth position recovery during the swing phase. Such design differences entail opposite advantages and disadvantages. The decision, performed by Natsakis et al., to actively control all the available degrees of freedom allows for a more accurate reproduction of the kinematic and dynamic aspects of the phenomenon. On the other hand, the behavior of the system proposed by Giberti et al. depends passively on the dynamic characteristics of the gesture, especially in terms of rotations at the joints. As a result, the corresponding solution is not completely able to reproduce the sought characteristics of walking. However, the additional reproduction of the hip rotation provides two significant benefits over the solution proposed by Natsakis et al., it allows to:

- perform, with a limited number of changes, also tests on transfemoral prostheses;
- delegate the horizontal motion component to the ground.

The latter aspect is especially relevant. The reproduction of the horizontal motion at the ground introduces indeed the possibility to perform several cycles of the phenomenon *in loco*, that is, limiting the size of the machine. Apparently, the same considerations have been performed by Zhang et al. in [92] (Fig. 1.24). The architecture of their bench is indeed similar to that of Giberti et al.. However, the authors introduce servo-motors at the hip and knee joints to actively drive the angular position of the segments of the limb, overcoming the main problems observed in [31].

Although the authors of the last two solutions claim the possibility to test transfemoral prostheses, there are no evidences supporting this opportunity. However, their architecture does not differ much from that designed to test above knee prostheses. Here are some of the examples reported in the literature.

The machine design proposed by Richter et al. [69] is limited to three degrees of freedom, namely hip horizontal, vertical and angular displacements, which are the minimum required to reproduce two-dimensional gait patterns. The vertical motion stage is performed by means of a brushless DC motor directly coupled to a ballscrew-driven vertical slide. The rotary motion stage is accomplished via a motor carried by the vertical slide itself. Finally, since the machine has a fixed vertical axis, a treadmill is used as

a walking surface to reproduce the horizontal motion. Both the hip and the ground actuating subsystems are attached to the green rigid frame shown in the figure (Fig. 1.25). This setup guarantees the possibility to perform the gait cycle over and over again as well as the opportunity to assess the prosthesis performance under different working conditions and irrespective of prosthetic device considered. The robot has indeed full authority over hip vertical and angular displacement. As a consequence the actuation, sensing and control hardware allows other tasks than trajectory control, such as force control, hybrid force/trajectory control and impedance control.



**Figure 1.24:** Test bench developed by Zhang et al.



**Figure 1.25:** Test bench developed by Richter et al.

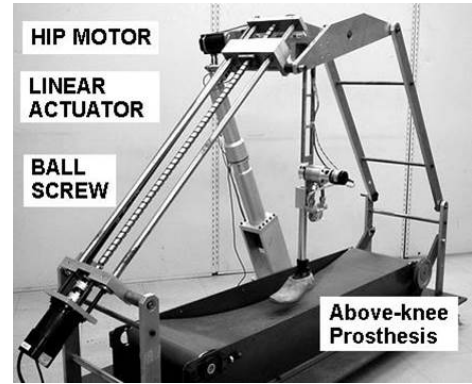


**Figure 1.26:** Test bench developed by Kim and Oh

Higher level of realism may be achieved by adding other linear and rotational degrees of freedom to the machine. For instance in [46], Kim and Oh introduce an additional degree of freedom which allows the hip to perform the horizontal movements besides the already mentioned vertical and angular displacements (Fig. 1.26). Such joint is indeed characterized by the superposition of two speed terms in forward direction: one is constant and the other is variable with zero mean. The first has no effect on the dynamics of the system. The second one determines a distribution of inertial loads that can play a fundamental role in terms of the response of the knee, especially during the swing phase. Although this aspect is not considered in [81], the simulator developed by Thiele et al. is designed to reproduce the phenomenon in three dimensions using five servo-hydraulic actuators. In particular, the hip module consists of three serially coupled actuators for the movement of flexion/extension, of adduction/abduction and of inversion/eversion. On the other hand, the foot module consists of two serially coupled actuators for vertical and horizontal movements of the instrumented foot plate which record ground reaction forces. This simulator is shown in figure (Fig. 1.27). Results obtained by means of it are good especially during the stance phase. However, major deviations from gait analysis data occur during swing phase both in terms of movements and loads at the hip and knee joints. This is probably due to the erroneous inertial load distribution achievable by constraining the linear displacements of the hip. As a consequence also the thigh and the shank movements differ significantly from the target values during the swing phase.

Finally, for the sake of completeness, a simulator useful for testing transtibial prostheses in three dimensions is reported (Fig. 1.28). The system developed in [7] exploits a 6-DOFs parallel kinematic manipulator (PKM) to drive the motion of a force plate so

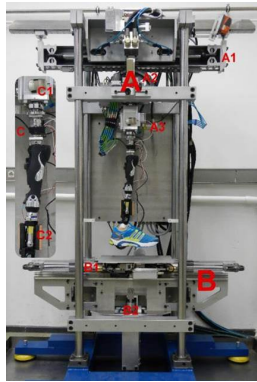


**Figure 1.27:** Test bench developed by Thiele et al.

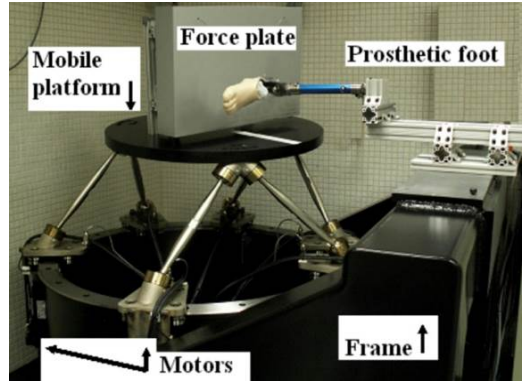


**Figure 1.28:** Test bench developed by Aubin et al.

as to load the prosthesis fixed in the space according to sought gait standards. In particular, the trajectory to be followed is computed through an iterative learning algorithm removing the problems related to changing control strategy (from position to force and vice versa). Beyond the logic implemented, the intrinsic characteristics of the PKM allow to:

- simulate the phenomenon in three dimensions;
- apply forces similar to the real ones.

However, the benefits are effective just at frequencies much lower than the real ones. Indeed, the higher the gait rate considered, the larger the error in reproducing the contact force in terms of magnitude. Moreover, such a design choice significantly increases the complexity of the system.

## 1.8 State-of-the-art concluding remarks

Different options are available to investigate the biomechanics of transfemoral amputee locomotion for design optimization of intelligent knee prostheses. Among these in-vitro gait simulations demonstrate several advantages over in-vivo experimentation. In-vivo experiments are indeed limited due to many reasons, such as subject dependence/reliance and poor controllability/repeatability of the process. Conversely, the possibility to design studies ad hoc and run them continuously is a major advantage of in-vitro simulations. Furthermore, since the test condition is highly controllable, the effect of specific parameters can be studied in isolation and safely when performing such kind of simulations.

Although the need to perform this type of test is not recent, solutions able to faithfully reproduce both the kinematic and dynamic aspects of walking do not yet exist. The systems analyzed in this chapter achieve acceptable results only in one domain. Moreover, not during both the stance and the swing phase. In-vivo testing is therefore still widespread. Anyway, the few works reported in the literature have proven that robot-based testing is a useful approach for investigating human locomotion. According to the above mentioned considerations, the aim of this research activity is to develop an in-vitro gait simulator for testing trans-femoral prostheses, especially modern ones,

## **Chapter 1. State-of-the-art**

---

and assess their functional properties. In particular, the definition process is performed in order to overcome the three significant challenges of gait simulators highlighted in this chapter, i.e.:

- operating at physiologically correct velocities;
- applying full scale ground reaction forces;
- simulating motion in all three planes (sagittal, coronal and transverse).

Humanoid robots such as these are mechatronic systems that require the development of complex kinematic and mechanical design and the definition of stable and adaptable control strategies. Many considerations must then be done upon the advantages of using different solutions in terms of mechanism architecture and control algorithms before developing a reliably operating physical solution. This document reports the steps and considerations made by the author to achieve these goals. In this regard, the kinematic and dynamic aspects of walking to be simulated are first analyzed in the next chapter.

---

# CHAPTER 2

---

## Gait analysis

---

### 2.1 Introduction

---

This research topic deals with the development of a bench for testing lower limb prostheses. In particular, the purpose of the bench is to assess the functional performances of the device under test by reproducing working conditions more realistic than those suggested by the International Organization for Standardization (ISO). Indeed, as extensively explained in the literature review chapter, the requirements and test methods currently in force are suitable just to assess the capacity of the prosthesis to withstand, one by one, the restricted set of worst loads occurring at different foot-ground contact instants. Since the bench must guarantee the sequential replication of movements and loads that distinguish the execution of the whole stride, the features of human locomotion to be reproduced have been initially analyzed. In particular, the basic notions about walking, and the tools for quantifying it, are first introduced in this chapter. Afterwards, the kinematic and dynamic data useful in the development process of the bench are extracted and analyzed.

### 2.2 Basic features of the walk

---

Upright bipedal walking, intended as cyclical repetition of the stride, is the result of a complex evolutionary adaptation process as well as the fundamental hallmark that distinguishes humans from other primates. In order to fully investigate the complex set of resulting movements, the analysis should start from the biochemical signals generated by the central nervous system. However, from the mechanical point of view, this phenomenon can be simply interpreted as the result of a complex interaction between internal, external and inertial forces, performed in order to propel the body forward and simultaneously maintain its standing stability, i.e. the posture. The external forces

## Chapter 2. Gait analysis

---

are the actions exerted by the environment on the biological system, such as the force beneath each foot in contact with the ground and the gravity. The internal forces are generated instead by an admirable regulatory system, made up of muscles and neurons, whose aim, under physiological conditions, is to selectively activate the body segments both in timing and intensity so as to ensure the achievement of the sought dynamic equilibrium. Finally, the inertial loads must obviously be considered for the second law of Newton.

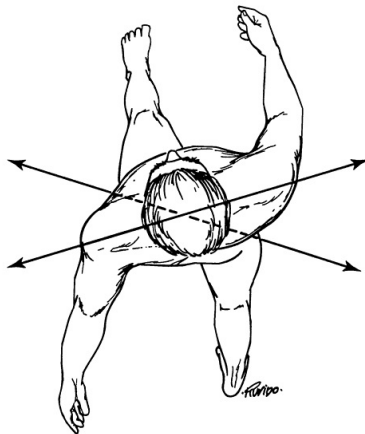


**Figure 2.1:** Controlateral rotation of the upper and lower part of the body during normal walking

It is worth to emphasize that the contribution of each body segment is important for achieving the final result. This means that pelvis, spine, arms and head must move in synchrony with the legs to ensure the correct execution of the gesture while minimizing the energy expenditure [65]. This aspect can be simply understood considering that arm swinging during normal bipedal walking helps to neutralize the angular momentum produced by the contralateral rotation of the lower part of the body and to reduce therefore energy expenditure [58] (Fig. 2.1).

Walking is therefore an extraordinarily complex phenomenon to be examined in its entirety for proper interpretation. This aspect is essential whenever the research is conducted for clinical purposes. Indeed, a disorder in any segment of the body can have consequences on the overall individual's gait pattern. However, during walking the body may be divided into two functional units: the passenger and the locomotor [16, 65]. Head, arms, and trunk are the passenger unit because they are carried rather than directly contributing to the act of walking. The small amount of active control performed by these segments in normal conditions has not proved to be essential, especially in terms of progression and stability rather than energy conservation. The possibility to carry packages is an evidence from this point of view. Thus, the mechanics of the locomotor, constituted by the lower limbs and the pelvis body segments, may be analyzed separately if there is no need to identify the correlation between the units.

This habit is quite common in the literature [25, 41, 47, 65]. As a consequence, the behavior of the locomotor, or a portion thereof, can be artificially replicated as a single entity, that is, without simulating the entire body system. Only the behavior of the anatomical portions extending from the hips to the feet, i.e. the lower limbs, are therefore considered from now on.

## 2.2. Basic features of the walk

According to the mechanical analogy, each limb can be reduced for simplicity into an open kinematic chain composed of six passive elements (hip, thigh, knee, leg, ankle, foot), three of which are joints, and a high number of active components, the muscles. During the walk, the sequence of movements executed by these elements is called ‘gait cycle’ and can be divided into two well distinct periods: the ‘stance’ and the ‘swing phase’, namely the phases during which the same foot is respectively in contact with the ground and moving in the air (Fig. 2.2). Intuitively, each phase is characterized by different working conditions and therefore different behaviors:

- during stance the limb is in contact with the ground and supports the rest of the system;
- during swing the limb moves towards a new contact point before the beginning of a new cycle.

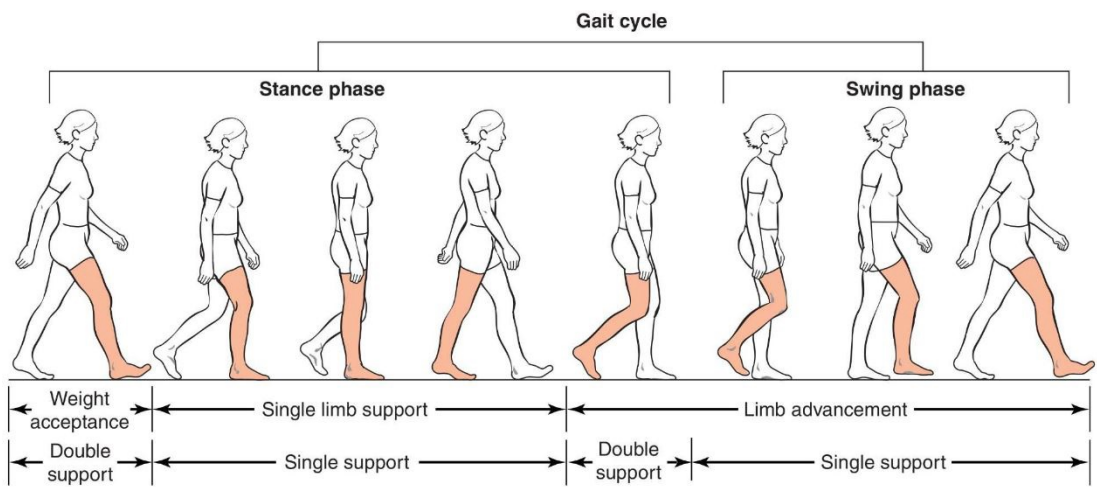


**Figure 2.2: Main phases of the gait cycle**

Clearly, both the phases are equally important for the correct reproduction of the gesture. None of them can therefore be ignored during simulation if the intention is to assess the ability of the prosthetic device to fully assist the amputee while walking. Moreover, their mutual energetic influence induces the need to reproduce the phenomenon by means of a single test procedure. Indeed, according to the conservation law, the phenomenon is characterized by a continuous energy transfer between the phases by opposite changes of the potential and the kinetic energy components [87]. As extensively pointed out in the literature review chapter (Sec. 1.3), energy storage is one of the most important aspects of the modern prosthetics design as well as the reproduction of the impedance profile of the biological counterpart and the ability to perform active work. Thus, it cannot be absolutely neglected during the testing phase.

As a result, the aim is therefore to replicate, by means of a single test procedure, the complex set of movements and loads characterizing the lower limb during both the stance and the swing phases of walking. In particular, since the intention is to develop a gait simulator for testing transfemoral prostheses, the machine must be able to replicate the series of motion patterns performed at the hip by the stump and the trend of forces acting on the prosthetic foot due to reaction with the ground.

## Chapter 2. Gait analysis

---

Once identified the phenomenon to be reproduced, walking is analyzed quantitatively to outline the kinematic and kinetic requirements of the test bench. The techniques adopted to perform this type of study are grouped under the name of ‘gait analysis’.

### 2.3 Gait analysis methods

---

Gait analysis consists in the calculation, quantification and interpretation of the quantities characterizing normal and pathological human locomotion. Even if some aspects of the gait can be evaluated by direct observation, the detailed assessment of the phenomenon requires laboratory measurements, i.e. the need for appropriate instruments and measurement protocols. Indeed, these add greater precision, provide information that cannot be obtained by eye and facilitate correlation of multiple factors [85]. In particular, an analysis requires the acquisition over time of three kinds of data to be complete:

- kinematic;
- kinetic;
- electromyographic (EMG).

Kinematic measurements, intended as positions and orientations of the body segments under study, allow to trace the movements of the joints. The main kinetic measurement is instead the foot-floor reaction force. By combining kinematic and kinetic data, it is possible to calculate the joints momentum and power. The joints angle, momentum and power, and the EMG from specific muscles, provide a detailed description of the mechanics of gait. Several techniques have been developed to access these data. Some of them are investigated below.

The acquisition of the electrical signal associated to muscle contraction is measured by means of surface electrodes. Modern EMG acquisition systems are wireless based in order to prevent wirings to obstruct the movement and therefore to jeopardize the test 2.3.



**Figure 2.3:** Example of EMG sensor



**Figure 2.4:** Example of magnetic sensor

Force plates are regularly used to collect data about the interaction of the feet with the ground (Fig. 2.5). There are different kind of force plates. Differences mainly rely on size, amount and nature of the loads to be measured. There exist in particular two different kind of technology to be used depending on whether the distribution of forces is either static or dynamic. In some cases it is better to take advantage of technologies based on strain gauges. In others, it is better to resort to piezoelectric sensors. The force

### 2.3. Gait analysis methods

measurement can alternatively be performed by inserting in the shoes insoles equipped with either piezoelectric, strain-gauged or capacitive sensors [10, 11, 29, 40] (Fig. 2.6). However, they are mostly prototypes not suitable to perform accurate acquisition of the loads at present.



**Figure 2.5:** Example of force plate



**Figure 2.6:** Example of insole sensor

The assortment is bigger from the kinematics point of view [48]. In particular, among all the available solutions, gait analysis using wearable sensors shows great prospects [79]. For instance, electro-goniometers have been used to record instantaneously the three-dimensional joint rotation of the lower extremities (Fig. 2.7).



(a)



(b)

**Figure 2.7:** Examples of electro-goniometer and relative application

Accelerometers and gyro-sensors have also been used for indirect measurement of angular displacements of limbs segments (Fig. 2.8). Other motion capture systems are built using magnetic sensors for quantifying some basic spatio-temporal information about gait (Fig. 2.4).

Despite gait analysis using wearable sensors is an inexpensive, convenient, and efficient manner of providing useful information, it is not the best. Modern motion capture systems provide more accurate three-dimensional representation of bones and joints action through optical instruments (Fig. 2.9). For instance, the spatial positions of either bright or reflective markers placed on key anatomical sites are determined over time via sophisticated computer-aided camera systems and their locations translated into body motion data through dedicated algorithms.

The selection of a particular technique depends on several aspects: cost, purpose of the data, size, transportability and many others. It is therefore not easy to understand which is the best without taking into account its application. Aim of this work is to replicate, as realistically as possible, the set of movements performed by the limb and

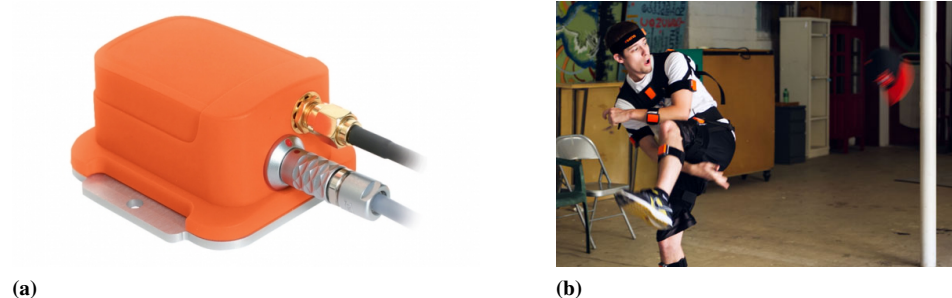


**Figure 2.8:** Example of accelerometer and relative application

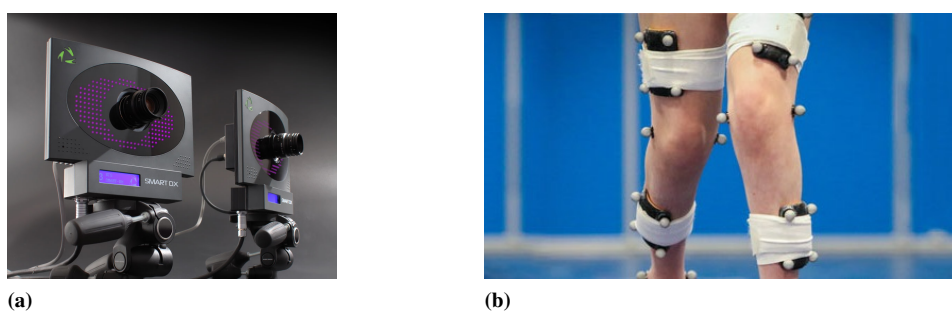


**Figure 2.9:** Example of optical motion capture system and relative application

the loads acting on its foot due to reaction with the ground. Hence, it is useless to access the electromyographic information. Conversely, the accuracy demand is high in terms of kinematic and dynamic data. However, their procurement is not easy. There are neither reference databases nor standard patterns accepted by the community. Moreover, the lack of uniformity in outcome presentation determined a large dispersion of the data in the recent past [88–90] and therefore great difficulties in terms of comparison of the results published by different laboratories in the literature. Not being able to take advantage of already available data, we relied on a devoted gait analysis laboratory for acquiring them; Laboratorio Luigi Divieti, Dip. Ing. Biomedica, Politecnico di Milano. On the one hand this approach provided significant advantages:

- the availability of data obtained through a solid and reliable measurement setup;
- the opportunity to arbitrarily define the trial protocols;
- the possibility to be supported by some of the foremost experts in the field of gait analysis.

On the other hand it resulted in a considerable drawback:

- the amount of acquired data required a careful and long phase of post-processing to achieve the desired results.

The main features of the measurement setup employed by the laboratory are listed below (Fig. 2.10).

### 2.3. Gait analysis methods

An optoelectronic system composed by 8 cameras (ELITE 2002, BTS spa, Italy (Fig. 2.11a)) is used to measure the three-dimensional coordinates of the reflective markers placed on the body of the voluntary subjects under study. The sampling rate of the camera system is  $100\text{Hz}$ .

The foot-ground contact reaction load components are measured by means of two staggered strain-gauge based 6 axis force platforms (AMTI Inc., USA (Fig. 2.11b 2.11c)) build in the floor, that is, embedded in the walkway. The sampling rate of the platform is  $500\text{Hz}$ .



**Figure 2.10:** Panoramic view of the gait analysis laboratory

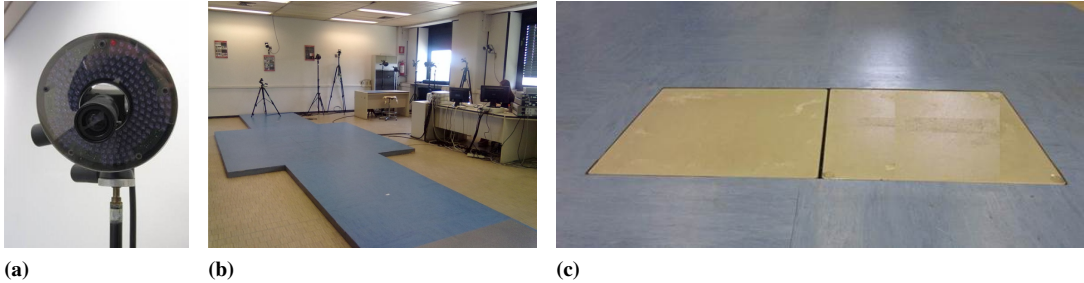


**Figure 2.11:** Laboratory measurement equipment

In terms of protocol, trials are performed by asking the volunteers to walk along a predetermined path assuming a natural cadence, i.e. a natural number of steps per minute and therefore a comfortable walking speed, after an acclimatization stage. It is worth to point out that, for simplicity as well as technical and safety reasons, trials are executed involving 4 healthy subjects. Although differences between healthy and disabled subjects exist in terms of strategy, this aspect should not undermine the validity of the study. Deviations of transfemoral amputees from normal walking are indeed very small and therefore not relevant in context different from the clinical one. In addition, such deviations may vary depending on the confidence of the amputee and the characteristics of the prosthesis in use, making it difficult to standardize the test. Finally, the intention of this study is to evaluate the ability of the prosthesis to restore the pre-morbid mobility level. According to author's opinion, reproducing movements and loads other than the physiological ones to assess the performance of the prosthesis is therefore illogical.

Data obtained during the laboratory sessions are processed and analyzed in the next section in order to identify the requirements of the set-up.

## 2.4 Requirements

---

Apart from being crucial for the detection and treatment of gait disorders, ‘gait analysis’, that is, the quantification of the factors governing the functionality of the lower extremities, has contributed significantly to the design of prostheses [64], orthoses [26], artificial limbs, exoskeletons [94] and other orthopedic robots [3,82]. Similarly, the data recorded during the aforementioned gait analysis session are used, in this context, to outline the requirements necessary for defining the set-up of the rig. Both kinematic and dynamic data are necessary to undertake the definition process of the machine. These quantities are extracted and analyzed below.

### 2.4.1 Kinematic requirements

The three-dimensional description of the lower-limb kinematics entails the need to describe, in each instant of time, the pose of the corresponding bony segments involved in the analysis. Being known the morphology of each hypothetically rigid segment, this is equivalent to define the pose of the triad embedded in each bone ( $X_iY_iZ_i$ ) with respect to the global reference system ( $X_gY_gZ_g$ ) (Fig. 2.12).

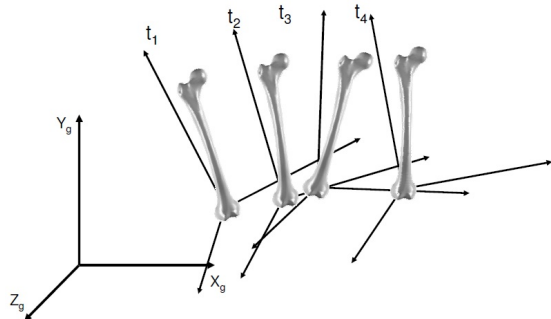


**Figure 2.12:** Pose of the femur embedded reference system over time

Six independent parameters are necessary to completely define the pose of each triad, i.e. as many as the degrees of freedom of a rigid body in space. These parameters state the location ( $x, y, z$ ) and the orientation ( $\alpha, \beta, \gamma$ ) of the orthogonal system embedded in the bony segment of interest with respect to the global reference frame. The identification of these parameters then implies the definition of a global reference system, and as many local reference frames as the number of body segments involved in the analysis. The definition of a global coordinate system is not a big deal. Its characteristics are reported in Appendix A. On the other hand, the reference frames associated to the bony segments of interest are built according to the position of some anatomical landmarks, which in turn are identified starting from the position components of the reflective body surface markers acquired during the gait analysis session. Body surface markers placement and acquisition are therefore crucial tasks. Indeed, results obtained by non-invasive measuring methods like this can be severely corrupted by the inaccuracies committed in the construction of the embedded coordinate systems. As a consequence, markers placement must fulfill some experimental requirements [20]:

1. sufficient measurements (three-image coordinates) should be available on the markers from the available cameras at any given time;

## 2.4. Requirements

2. for a given experiment, the light reflected from markers should be oriented within the field of view of a sufficient number of cameras;
3. the distance between three markers associated with each body segment and the offset of any marker from the line joining the other two should be sufficiently large so that error propagation from reconstructed marker coordinates to the bone orientation in space will be minimal;
4. the relative movement between markers and underlying bone should be minimal;
5. mounting the markers on the experimental subject should be a fast and easy operation;
6. it should be possible to place markers despite the presence of appliances such as orthoses, prostheses, or external fracture fixator.

Different positioning schemes have been developed by gait laboratories to comply with these requests. During this work, the markers are placed on the body of 4 healthy subjects according to the Davis protocol (Fig. 2.13). Such a protocol allows indeed to satisfy two important requirements: the external marker system is simple and yet rigorous enough to define the motion of the rigid body segments as fast and easily as possible [43].



**Figure 2.13:** Davis markers scheme

Regardless of the markers scheme adopted, the final embedded orthogonal coordinate systems must be defined so as to ensure repeatability in terms of results and consistency with the standard recommended by the ISB. Otherwise, it would be not

## Chapter 2. Gait analysis

---

possible to compare data between gait laboratories [20, 43]. For such reason the concept of anatomical triads has been introduced in the last decade [89, 90]. These triads own the property of repeatability because they are built using anatomical landmarks (identified by palpation) and points lying on anatomical planes (not directly accessible), including the hypothesis of rigidity of the bones [20]. The points and the rules useful for defining the embedded reference frames of the thigh, the shank and the foot are reported in Appendix A [89].

Once uniquely defined the anatomical triads embedded in each bony segments of the lower limbs, there remains the problem to switch from the position and orientation of the bony segments to the position and orientation of the anatomical joints. These data are easily computable once the coordinates of the bony embedded reference frame are known. The 3 position components of each joint center ( $x, y, z$ ) are indirectly computed by means of geometrical relations between the anatomical reference frames and some anatomical features of the subject under study [50]. On the other hand, the 3 orientation parameters ( $\alpha, \beta, \gamma$ ) are indirectly computed starting from the orientation matrix, which is obtained by projecting the unit vectors defining the orthogonal axes of the anatomical frames on the directions defined by the axes of the global reference one (direction cosines) (Fig. 2.14).

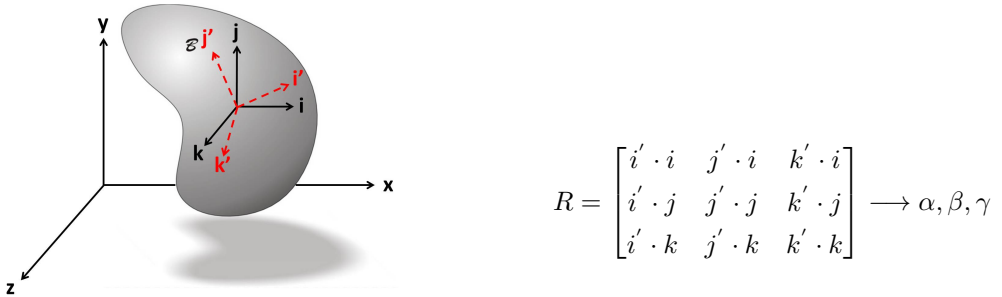


**Figure 2.14:** Orientation of a body in three dimensions

These 3 quantities may be defined as a set of finite rotations assumed to take place in sequence, either about the axes of the local coordinate system (intrinsic rotations) or about the axes of the global coordinate system (extrinsic rotations), to achieve the final orientation starting from an alignment situation [51]. However, the value assumed by these three parameters changes according to the convention adopted. In particular, according to either Euler [22, 43] or Cardan [19, 76] convention, there exist twelve possible sequences of rotation,  $\alpha, \beta$  and  $\gamma$ , giving the same result:

- Euler angles:  $(ZXZ), (XYX), (YZY), (ZYZ), (XZX), (YXY)$ ;
- Cardan angles:  $(XYZ), (YZX), (ZXY), (XZY), (ZYX), (YXZ)$ ;

For the sake of clarity, in the following example the  $(ZXY)$  Cardan sequence of intrinsic rotations is used for describing the final orientation of the hip starting from an initial alignment situation with the global reference frame (Fig. 2.15). The origins are assumed coincident for simplicity.

## 2.4. Requirements

The  $(ZXY)$  Cardan sequence is the convention generally adopted by the gait analysis laboratories for expressing the rotations according to the relevant clinical terminology: the  $Z$ -axis corresponds to the flexion-extension axis of the joint (Fig. 2.16a), the  $X$ -axis to the abduction-adduction axis (Fig. 2.16b), and the  $Y$ -axis to the internal-external rotation axis (Fig. 2.16c). On the other hand, the  $(XYZ)$  Cardan sequence of intrinsic rotations, that is, the Tait-Bryan convention generally used in robotics, is implemented during this work. Data are therefore reported according to this convention during the following analysis. Further information about the Cardan convention are given in Appendix B.

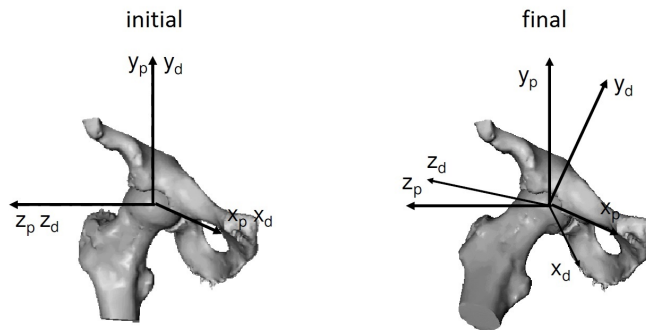


**Figure 2.15:** Initial and final hip orientation

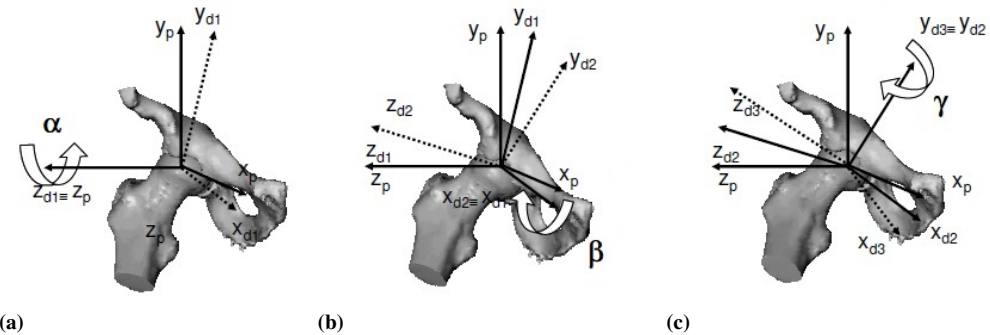


**Figure 2.16:** Sequence of intrinsic rotations according to the  $(ZXY)$  Cardan convention

The trends of the six variables ( $x, y, z, \alpha, \beta, \gamma$ ) describing the kinematics of the right hip of every volunteer are computed according to the considerations given above. Ankle and knee joint motion patterns are not considered since the bench is primarily intended for testing transfemoral prostheses. Each subject underwent several acquisitions. Thus, all the available trends are reported within the corresponding graphic (Fig. 2.18, 2.19) with reference to the coordinate system convention shown on the hip diagram (Fig. 2.17). In particular, the trends are represented in terms of percentage, rather than time, thus allowing normalization and therefore an easier comparison of the data. The exact duration of the cycle varies indeed as a function of the walking speed. Within each chart, initial foot strike occurs at 0%, and the second foot strike at 100%. In addition, since these data are contaminated with noise and have to be used for dynamic purposes, a low-pass filter is also applied. Despite studies have been performed to assess the fre-

## Chapter 2. Gait analysis

quency content of gait [6], the exact cutoff frequency is decided after harmonic content analysis. In particular, the final decision is to consider only contributions up to  $10\text{Hz}$  when dealing with kinematics.

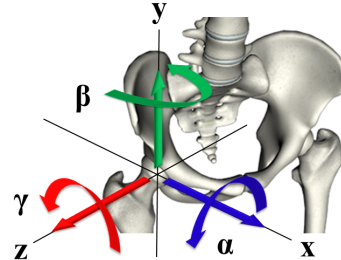


**Figure 2.17:** Axes convention adopted at the hip

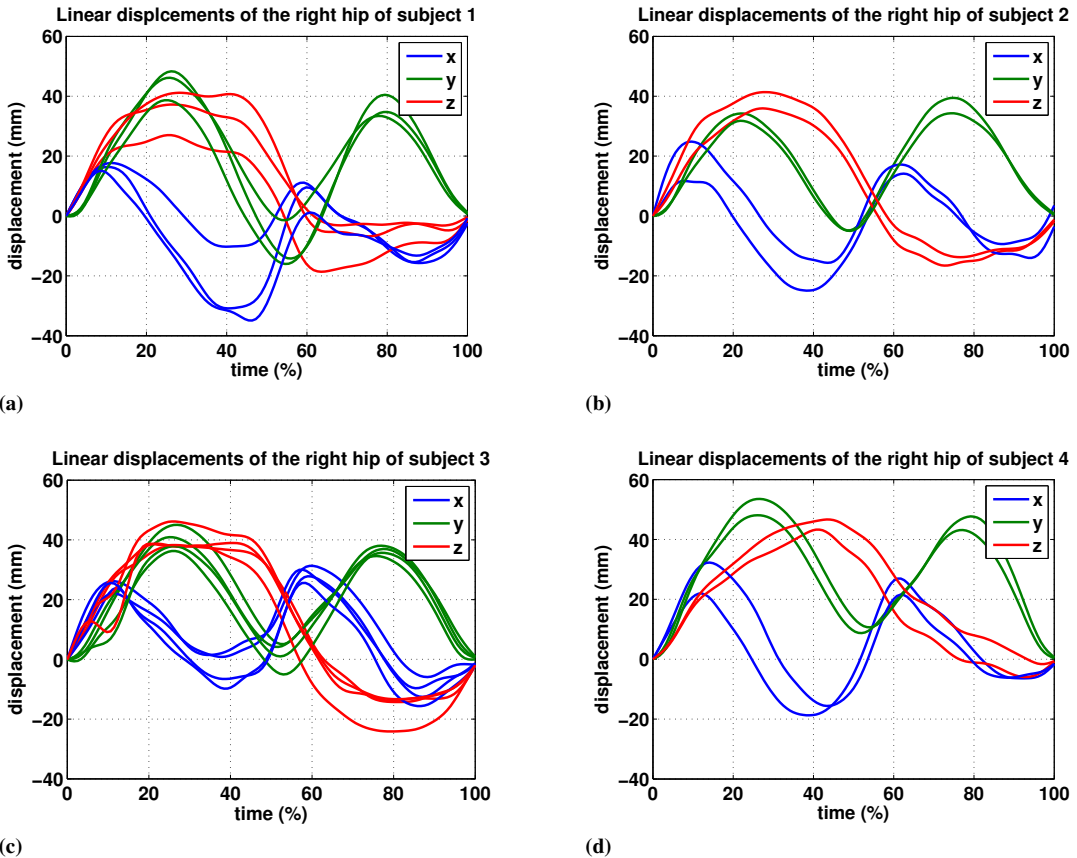


**Figure 2.18:** Hip linear displacement components of subject 1, 2, 3 and 4

The motion patterns are repeatable within each subject. On the other hand, they are slightly different among distinct persons. Nevertheless, movements performed during walking follow precise templates even if varying from a subject to another one. Thus, none of the available trends can be considered better or worse than the others. For this reason, the system requirements are extracted by considering only one acquisition. For the sake of clarity, the corresponding graphs are shown again. These trends are

## 2.4. Requirements

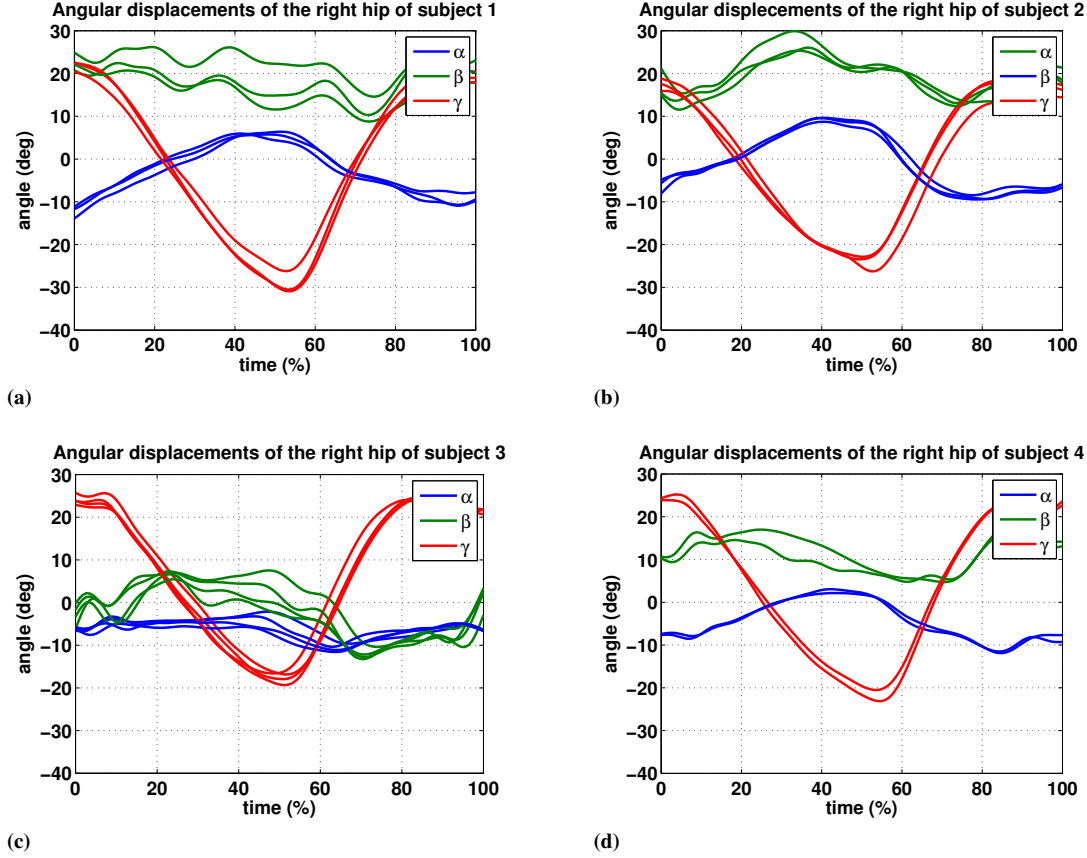


**Figure 2.19:** Hip angular displacement components of subject 1, 2, 3 and 4

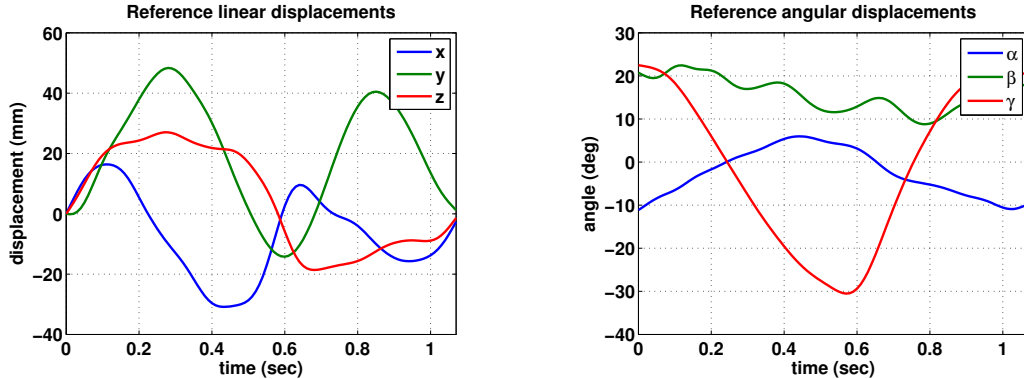


**Figure 2.20:** Reference hip linear displacement components **Figure 2.21:** Reference hip angular displacement components

represented in terms of time, rather than percentage. In particular, the cycle under study lasts 1.07 seconds.

These values match very closely the measurements published in the literature [19, 22, 76]. Starting from them, some important considerations are performed in order to define the requirements of the bench.

- Although the major arc of joint motion occurs in the sagittal plane, there also are

subtle actions occurring in the frontal and transverse planes. According to the literature, the application of these movements, albeit small, allows to enhance the stability as well as to minimize the energy expenditure [41]. As a consequence, they are not negligible if the intention is to evaluate the ability of the prosthesis under test to assist the amputee while walking. Three-dimensional motion reproduction is then required for completeness.

- The hip velocity along the  $x$  direction is given by the superposition of two contributions. Albeit variable, one has zero mean. Instead, the other is constant and determines the net progression of the whole body. Because only accelerations terms affect the dynamics of the prosthesis, there is no need to consider constant longitudinal speed. From a practical point of view, it is like considering a subject walking on a treadmill instead of forward with respect to the ground [46] (Fig. 2.22).

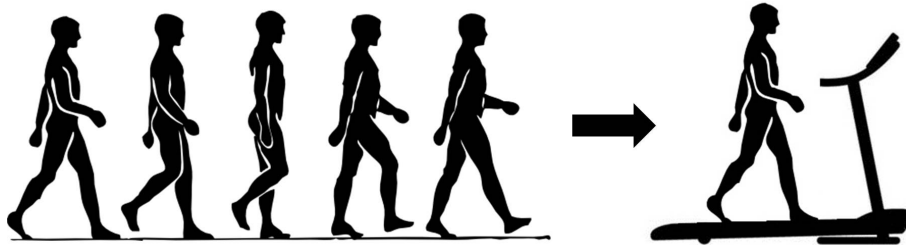


**Figure 2.22:** Motion simplification

The data are then processed in order to neglect the average velocity along the direction of progression, i.e. the  $x$ -axis. Ideally this is not necessary in the other two directions. However small deviations may occur even along these two. Thus, the average velocity along the  $y$ -axis and  $z$ -axis is subtracted from the corresponding values. From this point of view, it is worth noting that in the graphs shown above the trends are already processed so as to neglect the velocity constant terms. In particular, the linear displacements are represented in terms of deviation from the point  $[0, 0, 0]$ . As a consequence, the simulator has no reason to go on forward and test can take place in loco [46, 73]. Such a characteristic is very important because allows both to reduce the size of the machine and take advantage of the support provided by a frame fixed to the ground. The latter requirement is necessary especially to reduce the inertia of the system. According to the charts of the linear and angular components of both velocity and acceleration (Fig. 2.23, 2.24), the dynamics involved in the phenomenon is indeed very high (angular quantities are computed according rules reported in Appendix B). On the other hand, the local reproduction of the phenomenon induces the need to introduce horizontal motion of the ground along  $x$ , just as in a treadmill. To estimate the required stroke, the available kinematic data are finally processed so as to extract the trajectory followed by the main anatomical points under physiological conditions. This task is obviously performed taking into consideration only the plane of walking, i.e. the sagittal plane. The trend of the trajectory is reported in the following figure (Fig. 2.25).

## 2.4. Requirements

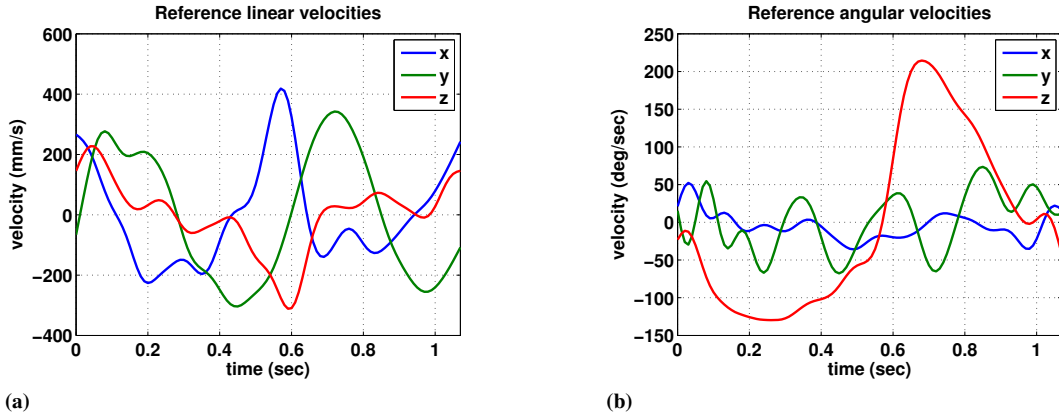


**Figure 2.23:** Reference hip velocity components

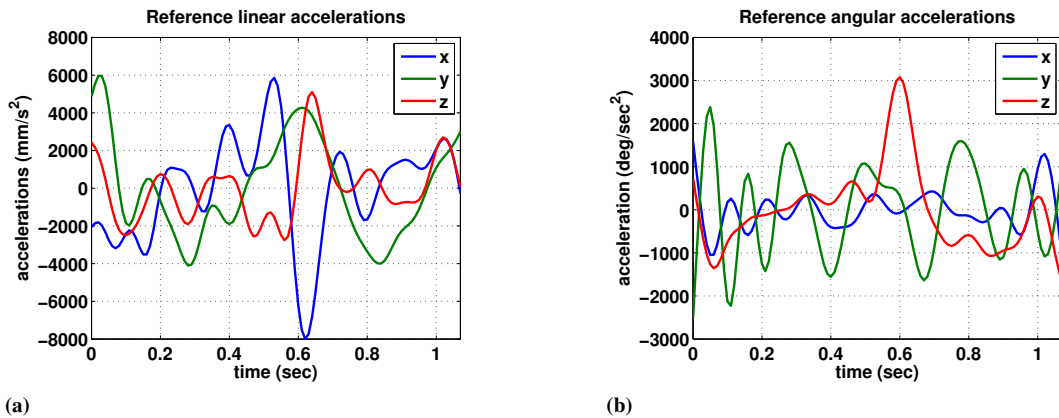


**Figure 2.24:** Reference hip acceleration components

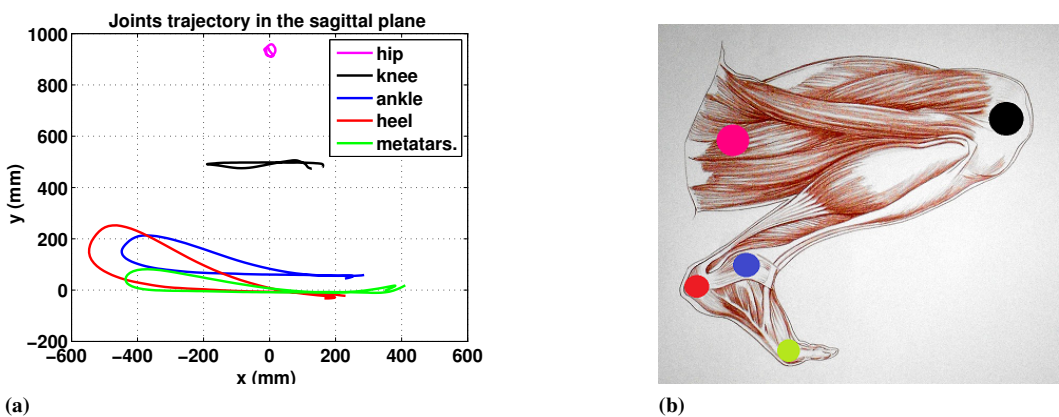


**Figure 2.25:** Trajectories of some anatomical points within the sagittal plane

### 2.4.2 Dynamic requirements

The ground reaction forces acting on the right foot are directly measured by means of a force platform. Each single component is the algebraic summation of the mass-

## Chapter 2. Gait analysis

acceleration product of all the body segments while the foot is in contact with the platform. In particular, each component reflects the acceleration due to gravity as well as the acceleration due to motion. Since the subjects involved have different body mass, as expected, the corresponding force components assume different value at a given instant. However, the trends are very similar to each other (Fig. 2.27) because the kinematic trends follow very specific templates. Anyway, this is not a problem. Once chosen the kinematic trends of a subject, it is appropriate to consider the corresponding force components. These are shown in the following charts (Fig. 2.28) with reference to the coordinate system convention shown on the foot diagram (Fig. 2.26). A low pass filter with 25Hz cutoff frequency is applied to reject the noise.

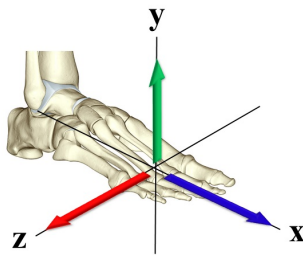


**Figure 2.26:** Axes convention adopted at the foot

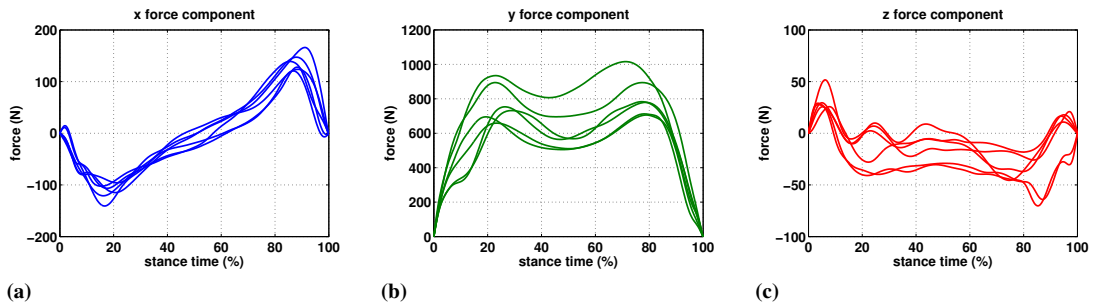


**Figure 2.27:** Force components acting on the right foot of the subjects 1, 2, 3 and 4

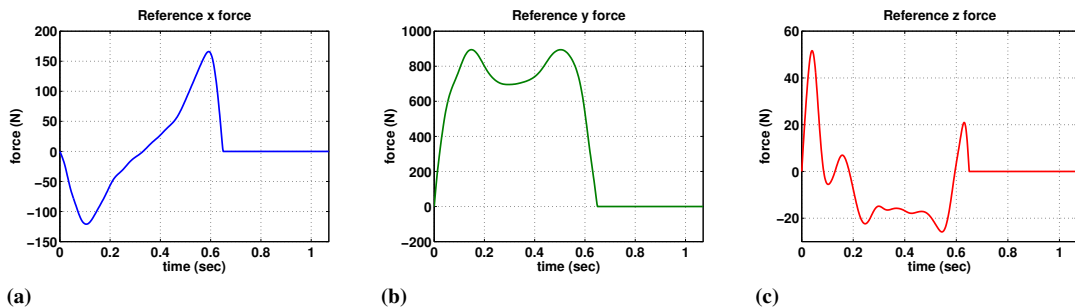


**Figure 2.28:** Reference force components

Also the kinetic data match very closely the measurements published in the literature [19, 22, 76].

## 2.4. Requirements

Once evaluated the reliability of the information, the dynamic and kinematic data available are processed in order to estimate the loads acting on the hip joint during the test procedure [84]. This evaluation is carried out by applying at the joints masses comparable to those of the prosthetic devices on the market rather than considering the mass distribution of a healthy limb, that is,  $5\text{kg}$  at the knee and  $2.5\text{kg}$  at the ankle. The results are reported in the following figures (Fig. 2.29).

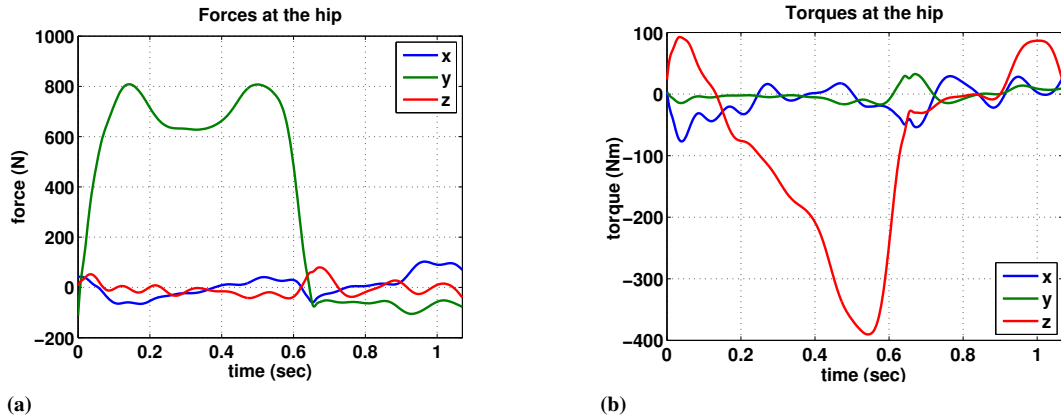


**Figure 2.29:** Loads acting on the hip

The trend of the linear forces are consistent with the results reported in the literature [27]. On the other hand, the torques are decisively bigger in terms of  $z$  component. Under physiological conditions, its maximum absolute value should be about twice the weight of the subject (around  $150\text{Nm}$  in this case) [27]. The difference is probably determined by the simplifications introduced both in terms of geometry and mass properties. Anyway, it is worth noting that the hip center undergoes a high kinematics as well as a high dynamics, especially during the stance phase, that is, during the initial 60% of the cycle. This aspect will probably induce some complications during the synthesis of the system. Indeed, most of the available technological solutions achieve high performance only in one domain at a time. The construction aspects of the bench are analyzed in the next chapter (Chap. 3). The loads and velocities of the hip center are finally used to calculate the power to be delivered by the system at the hip joint. Here are the graphs (Fig. 2.30).

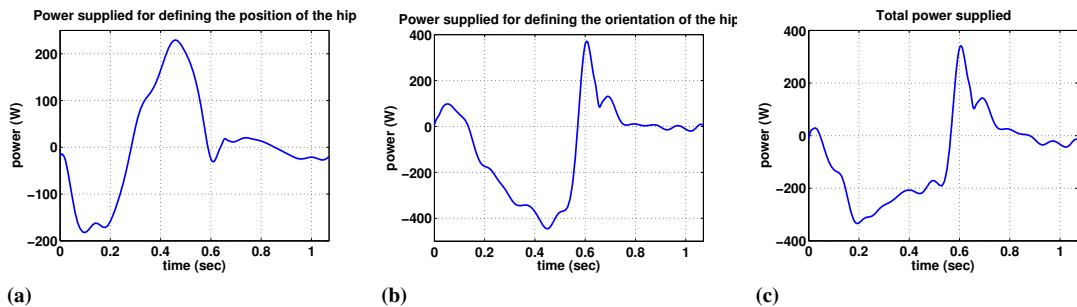


**Figure 2.30:** Power to be delivered at the hip joint

## 2.5 Gait analysis concluding remarks

The gait analysis performed in this chapter has allowed to extract useful information about the kinematic and dynamic characteristics of the phenomenon to be reproduced and consequently to estimate both the motion and payload capability of the simulator. In particular, during the data processing some important constructional aspects have come to light. Among these are: the possibility to replicate only the prosthetic limb rather than the entire body system and the possibility to simulate the stride in loco by neglecting the constant velocity terms of the hip in space. In addition, the three-dimensional reproduction of the gesture is required for completeness.

The fundamental quantities obtained considering the aforementioned observations are summarized in the following table according to the axes conventions reported on the hip and foot diagrams. (Tab. 2.1):

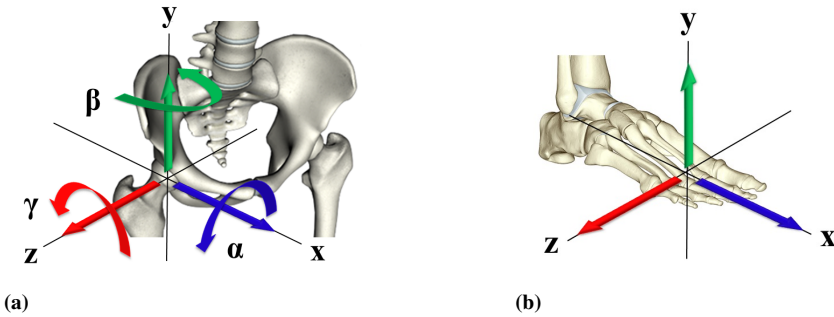


**Figure 2.31:** Hip and foot diagrams

**Table 2.1:** Primary kinematic and dynamic requirements

$\Delta x_{hip} = 47mm$	$\Delta y_{hip} = 63mm$	$\Delta z_{hip} = 46mm$
$\Delta \alpha_{hip} = 17deg$	$\Delta \beta_{hip} = 14deg$	$\Delta \gamma_{hip} = 53deg$
	$\Delta x_{foot} = 873mm$	
$max( \dot{x}_{hip} ) = 0.4 \cdot 10^3 mm/s$	$max( \dot{y}_{hip} ) = 0.3 \cdot 10^3 mm/s$	$max( \dot{z}_{hip} ) = 0.3 \cdot 10^3 mm/s$
$rms(\dot{x}_{hip}) = 0.2 \cdot 10^3 mm/s$	$rms(\dot{y}_{hip}) = 0.2 \cdot 10^3 mm/s$	$rms(\dot{z}_{hip}) = 0.1 \cdot 10^3 mm/s$
$max( \ddot{x}_{hip} ) = 8 \cdot 10^3 mm/s^2$	$max( \ddot{y}_{hip} ) = 6 \cdot 10^3 mm/s^2$	$max( \ddot{z}_{hip} ) = 5.1 \cdot 10^3 mm/s^2$
$rms(\ddot{x}_{hip}) = 2.7 \cdot 10^3 mm/s^2$	$rms(\ddot{y}_{hip}) = 2.6 \cdot 10^3 mm/s^2$	$rms(\ddot{z}_{hip}) = 1.7 \cdot 10^3 mm/s^2$
$max( \omega_{x,hip} ) = 52.3 deg/s$	$max( \omega_{y,hip} ) = 73.6 deg/s$	$max( \omega_{z,hip} ) = 214.5 deg/s$
$rms(\omega_{x,hip}) = 18.9 deg/s$	$rms(\omega_{y,hip}) = 38.5 deg/s$	$rms(\omega_{z,hip}) = 110.6 deg/s$
$max( \dot{\omega}_{x,hip} ) = 1.6 \cdot 10^3 deg/s^2$	$max( \dot{\omega}_{y,hip} ) = 2.5 \cdot 10^3 deg/s^2$	$max( \dot{\omega}_{z,hip} ) = 3.1 \cdot 10^3 deg/s^2$
$rms(\dot{\omega}_{x,hip}) = 445 deg/s^2$	$rms(\dot{\omega}_{y,hip}) = 1.1 \cdot 10^3 deg/s^2$	$rms(\dot{\omega}_{z,hip}) = 957.9 deg/s^2$
$max( F_{x,foot} ) = 166N$	$max( F_{y,foot} ) = 894N$	$max( F_{z,foot} ) = 52N$
$max( F_{x,hip} ) = 103N$	$max( F_{y,hip} ) = 808N$	$max( F_{z,hip} ) = 80N$
$max( M_{x,hip} ) = 77N/m$	$max( M_{y,hip} ) = 33N/m$	$max( M_{z,hip} ) = 390N$
$rms( W_{lin} ) = 109W$	$rms( W_{ang} ) = 213W$	$rms( W_{tot} ) = 176W$

These are used in the next chapter in order to perform the synthesis of the system.

---

# CHAPTER 3

---

## System synthesis

---

### 3.1 Introduction

---

In this chapter, the mechanical architecture of the system under study is defined according to the kinematic and dynamic requirements of gait (Sec. 2.4) and the considerations already made by other authors involved in the realization of gait simulators (Sec. 1.7). In particular, the factors leading to the division of the bench in two subsystems are analyzed before developing the corresponding physical solutions. In addition, some preliminary considerations about the operation procedure of the system are performed.

### 3.2 General layout

---

The definition of the mechanical architecture of the bench cannot overlook the amount of degrees of freedom (DOFs) to be reproduced. From this point of view, the literature (Chap. 1) states that the greater the number of DOFs considered, the more realistic the reproduction of the phenomenon is. Thus, according to the three-dimensional nature of the movements and loads analyzed in the previous chapter (Chap. 2), 9 DOFs are required to completely reproduce the gait cycle: the 6 (3 translations + 3 rotations) motion components of the hip in space and the 3 load components acting on the prosthetic foot due to reaction with the ground. Knee and ankle DOFs are neglected since the bench is principally intended to test transfemoral prosthetic devices (Fig. 3.1a).

Although the willingness to completely reproduce the phenomenon in three dimensions, possible simplifications are evaluated in order to reduce the complexity of the system architecture. The contribution of each independent DOF is therefore analyzed in terms of utility. This procedure is obviously undertaken starting from the considerations performed in the literature review chapter about gait simulator.

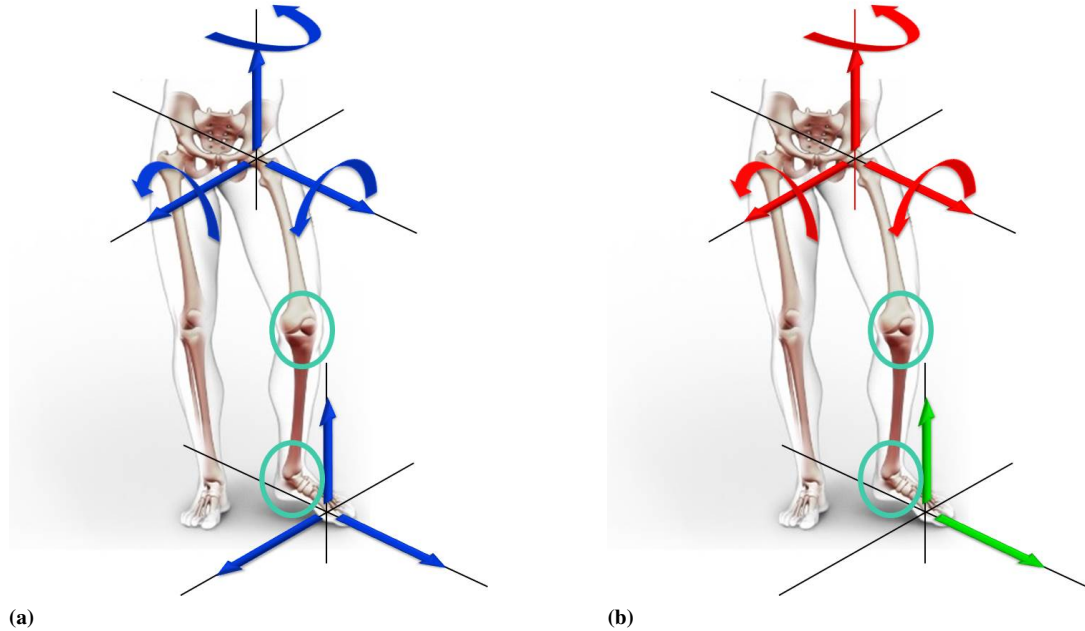


**Figure 3.1:** Initial (3.1a) and final (3.1b) topology of the system

For instance, the results reported in [81] show that the minimum number of DOFs necessary to properly reproduce the loading conditions during the stance phase equals 5. Three of them are used to set the orientation of the prosthesis in space. The others to load the foot in both the longitudinal and vertical direction. However, the suppression of the linear hip movements prevents the correct replication of the inertial loads acting on the prosthesis and consequently the possibility to test the device under realistic swing phase operating conditions [46, 81]. According to the analysis performed in Chapter 2, the task performed by the prosthesis during this period is essential from a functional point of view (Sec. 2.2). Moreover, all linear contributions are equally important since there are not significant differences between the linear components of acceleration (Sec. 2.4). Thus, it is strictly necessary to reproduce all the 6 movements of the hip in space.

Apparently, these 6 DOFs are sufficient to properly reproduce also the working conditions of the stance phase. The 3 linear DOFs can indeed be controlled alternately in terms of position and force to reproduce respectively both the movements and the loads acting at the hip. However, the limits of this solution have already been probed by other authors [7]. Systems in compliance with the kinematic and dynamic requirements of the phenomenon have an inertia so high to prevent the correct reproduction of the force reference, especially when operating at physiologically correct velocities. Moreover, the force control would result in deviation of the hip center from the desired trajectory preventing the possibility to correctly reproduce the kinematics characteristics of the phenomenon. As a consequence, the habit to split the machine in two subsystems interacting with the prosthesis [7, 31, 36, 46, 61, 69, 81, 92], i.e. the limb and the ground, is adopted during this work.

The distribution of the total amount of DOFs among subsystems is constrained instead by the following operation requirements:

### 3.3. Residual limb subsystem

- decouple the kinematic degrees of freedom from the dynamic ones;
- drive all the motion components of the fake leg during the swing phase.

The limb should therefore be able to perform all 6 possible movements. On the other hand, the application of loads to the foot is performed by means of the ground subsystem.

From this point of view, the force orthogonal to the sagittal plane is generally neglected by the majority of the authors [31, 36, 46, 61, 69, 81, 92]. Its magnitude is indeed much lower than those of the other two components (Sec. 2.4) and its reproduction may presumably be obtained as the result of the interaction of the foot with the ground. Same simplification is therefore adopted during this work. As a consequence, the system is defined in order to have 6 DOFs at the residual fake leg and 2 DOFs at the support surface representing the ground. A schematic representation of the system is given in figure (Fig. 3.1b).

The resultant number of DOFs considered is therefore 8. The use or development of a machine aimed at reproducing prosthetic gait considering 8 DOFs has not been reported, to the best of the author's knowledge. Thus, it consists in an innovative feature with respect to the state-of-the-art as well as a challenging design problem.

Once defined the topology, each subsystem is defined in order to meet both:

- the performance requirements (correctly reproducing the kinematics and dynamics of the phenomenon);
- the construction requirements (reducing the size as well as the time and cost of realization of the rig).

## 3.3 Residual limb subsystem

The definition of the residual limb subsystem consists in reproducing the sound joint closest to the prosthesis, i.e. the hip. The portion of the residual femur can indeed be replicated by designing a suitable rigid link (Fig. 3.2).



**Figure 3.2:** Overview of the system architecture

The complete mobility of the aforementioned articulation can be easily reproduced if the anatomical characteristics of the biological counterpart are excluded. For instance, this purpose can be achieved by using as many actuators as DOFs and a mechanism

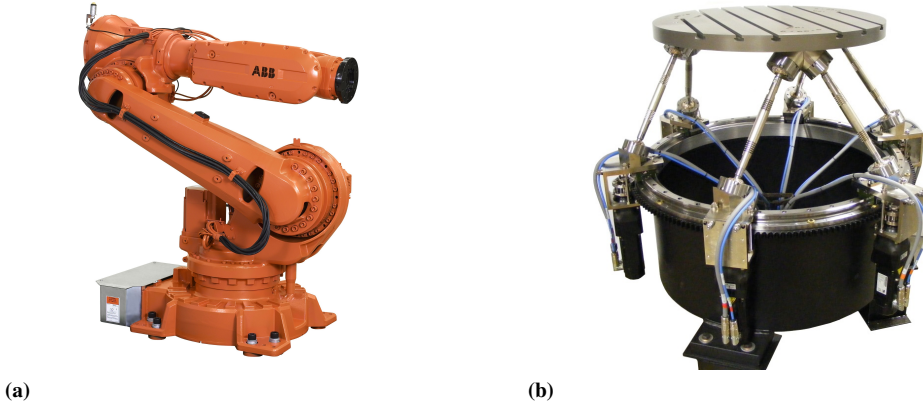


**Figure 3.3:** Manipulators with serial (3.3a) and parallel (3.3b) kinematic architecture

allowing their combination. Various solutions are possible to reproduce the 6 motion components of the hip in space (Sec. 2.4) but not all of them satisfy both the performance and the construction requirements. Among these are the need to accurately reproduce in loco phenomena characterized by a high dynamics, reducing as much as possible the time and cost of realization of the system. Commercial robots are relatively less expensive and more accessible than custom made ones. Despite the latter solution is more reliable, only commercial products are therefore considered for reproducing the kinematics of the hip during this preliminary study. Two options are basically available on the market:

- serial kinematic mechanisms (SKMs)(Fig. 3.3a);
- parallel kinematic mechanisms (PKMs) (Fig. 3.3b).

PKMs exhibit several advantages in terms of performance with respect to mechanisms having serial architecture. Namely, they can provide higher payload to weight ratio, higher stiffness, higher dynamic response. Therefore, PKMs can be seen as excellent candidates for designing powerful humanoid robots [21]. On the other hand, the typical higher workspace to size ratio of SKMs introduces major advantages in terms of versatility. In particular, it allows the simulation of other gait situations in addition to level walking, such as sitting, stumbling or near fall situations, extending the scope of the machine while limiting its overall size. Finally, although both the solutions are commercially available, the procurement of a SKM compliant with the kinematic and dynamic requirements of the application is easier. As a consequence, the intention is to use a commercial six-axes industrial robot with serial architecture for actuating the prosthetic specimen [37]. In summary, the characteristics that determined this choice are:

- broad workspace;
- compact size;
- high payload capability;
- easy procurement.

However, this kind of system introduces a major problem: it doesn't have very fast responding speed since it is designed for common industrial applications like working in an automobile assembly line. Hence, the need to introduce a compliant behavior in the main load direction, i.e. the vertical one, to address the sudden stress changes and the large disturbance forces arises despite of the high load capability. This is especially true in the initial stage of contact between the prosthetic foot and the force platform representing the ground [37]. However, many advanced robotic control techniques cannot be implemented because the low-level control plant is not accessible and the dynamic model of the manipulator (including the key model parameters) is not available from the manufacturer. As a consequence, the need to implement a suitable solution at the support surface representing the ground to prevent potentially dangerous situations arises. This is investigated below.

### **3.4 Ground subsystem**

---

The subsystem representing the ground must be able to periodically replicate the trend of the sagittal forces acting on the foot due to reaction with the ground. It is therefore essential to build a solution that can accurately measure and produce the aforementioned load components.

Different methods are available, but not all of them are suitable for the application. The solution is indeed inevitably influenced by the design choices of the residual limb subsystem. In particular, it is worth to consider the following two main aspects:

1. the decision to neglect the constant velocity terms of the hip so as to perform the phenomenon *in loco* induces the need to introduce a wide stroke in longitudinal direction (Sec. 2.4);
2. regardless of the payload capability, the 6-axis industrial robot entails the need to introduce a compliant behavior in the vertical direction (Sec. 3.3).

The ground subsystem is therefore the most critical component to be developed. Indeed, it introduces the need to define specific as well as different solutions in the aforementioned load directions. Nevertheless, a mechanism obtained as the series of two stand-alone tools provides 3 major advantages:

- decouples the individual movements;
- simplifies the mathematical model;
- allows to define two separate control strategies.

The solutions for driving the platform both in longitudinal and vertical direction can therefore be developed separately. Here is a brief overview of the considerations discussed in the following chapters.

Different solutions have been successfully implemented by other authors for reproducing the longitudinal motion of the surface representing the ground. For instance a treadmill and linear guide are exploited respectively in [69] and [31]. The endless belt of the former solution introduces major advantages. However, there is no evidence in the literature about its capability to reproduce the longitudinal load. The linear guide is therefore implemented during this work.

In vertical direction, electric actuators are excluded to avoid the risk of compromising the functionality of the robot rigidly connected to the prosthetic specimen. On the other hand, the idea is to drive the corresponding custom mechanism using a pneumatic actuator in order to take advantage of the compressibility of the gas to increase the compliance of the system and consequently its stability. Despite the dynamic characteristics of these devices are lower than those of the electromechanical counterpart, this kind of solution has already been used in other studies showing great reliability [61]. Thus, good results could presumably be obtained also in this context. Furthermore, the low mass of the pneumatic actuator contributes to reduce the inertia and therefore the stress at the motor driving the carriage of the linear guide.

Finally, from a functional point of view, the need is to control the ground subsystem alternatively in force or position depending on whether it is respectively in contact or not with the foot. The first strategy is active during the stance phase so as to reproduce the loads acting on the foot. On the other hand, the second one contributes to take the subsystem back in the initial position during the swing phase, that is, before the beginning of the next cycle. This occurs both in the longitudinal and vertical direction.

### **3.5 System synthesis concluding remarks**

---

The analysis undertaken in this chapter has allowed to identify the minimum number of DOFs necessary to completely reproduce the characteristics of the gait in-vitro. This information has been successively used to defined the mechanical architecture of the system. At the end of this procedure, the gait simulator exhibits 8 DOFs and is made of two main subsystems with 6 and 2 DOFs. These aim respectively to simulate the kinematics of the residual limb rigidly connected to prosthetic specimen and the loads acting on the prosthetic foot due to reaction with the ground. The first task is accomplished by a commercial 6-axis industrial robot which is controlled in terms of position during the entire gait cycle. On the other hand, the second subsystem is designed as the series of two standalone units in order to decouple the longitudinal and vertical force components. Regardless of the physical solution adopted, the intention is to control both the axes alternately in terms of force and position. The former strategy is active as long as the foot is in contact with the ground so as to reproduce the load acting on it, that is, during the stance phase. The other one contributes instead to take the subsystem back in the initial position before the beginning of the next cycle, that is, during the swing phase. A schematic illustration of the system is shown (Fig. 3.4).

Once the general layout of the set-up is defined, the need is to select the commercial components based on their capability of generating both the range of motion and the loads outlined in the gait analysis chapter. Then, custom pieces are designed to accommodate them. Finally, their mathematical models are developed for addressing the synthesis of suitable control strategies. These tasks are performed separately in the next chapters.

### **3.5. System synthesis concluding remarks**

---

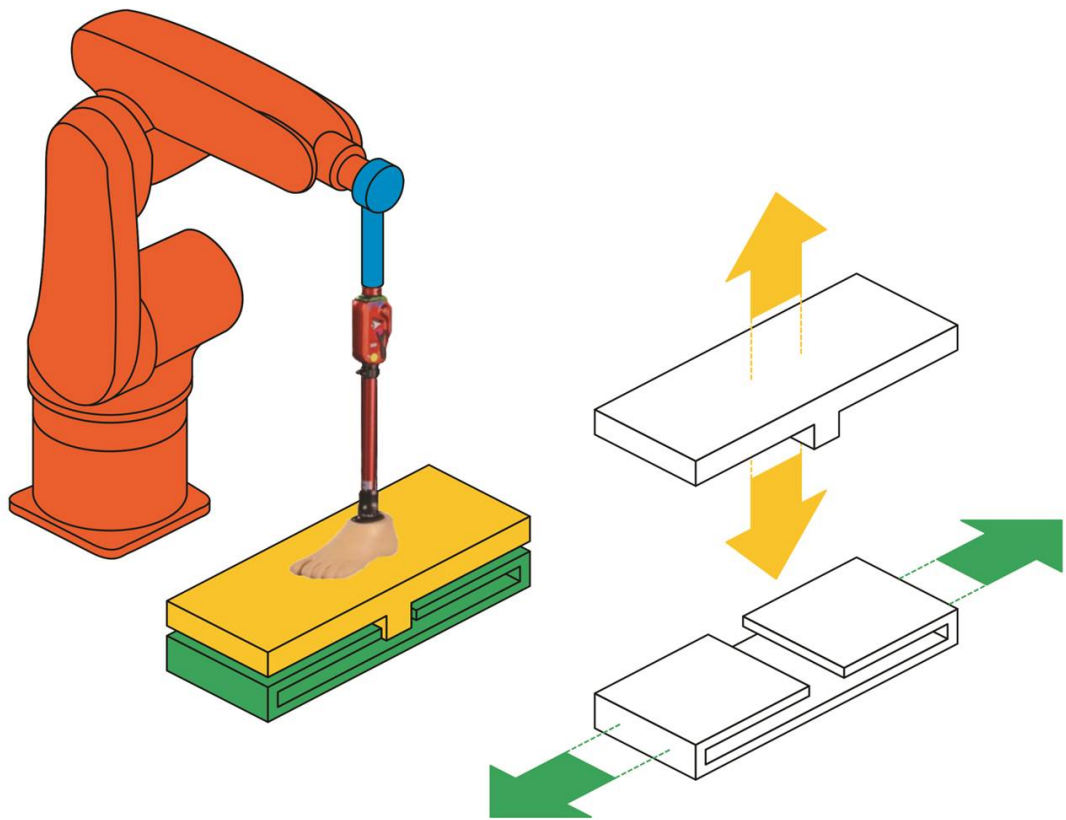


**Figure 3.4:** Overview of the system architecture



---

# CHAPTER 4

---

## Longitudinal loading subsystem

---

### 4.1 Introduction

---

This chapter deals with the development of the solution necessary for reproducing the longitudinal load acting on the prosthetic foot due to reaction with the ground. First of all the design choices are analyzed and the commercial components are selected based on both their compatibility and availability. Thereafter the operation procedure is reviewed and the mathematical model is set up in order to accomplish the synthesis of a suitable control strategy. The merits of the proposed solution are then tested and improved numerically. Finally, a series of experimental tests is performed in order to get familiar with the programming software, LabVIEW, and estimate the values assumed by certain parameters, which are useful for modeling purposes.

### 4.2 Longitudinal axis design

---

The development of the longitudinal loading subsystem involves two issues:

- the identification of a mechanism having a stroke suitable for the application;
- the selection of a motor-reducer unit having kinematic and dynamic characteristics suitable for the application.

These tasks are performed separately in the next two sections.

#### 4.2.1 Mechanism identification

Different solutions have been successfully implemented by other authors for reproducing the longitudinal motion of the platform representing the ground (Sec. 1.7). For

## Chapter 4. Longitudinal loading subsystem

instance, a treadmill and a linear guide are exploited respectively in [69] and [31]. Albeit the endless belt of the former solution facilitates the execution of several cycles, there is no evidence in the literature about its capability to reproduce the force rather than the displacement in the aforementioned horizontal direction. On the other hand, the linear guide has already been successfully used for loading purposes [12]. In addition, the threaded holes of the carriage facilitate the accommodation of the mechanism reproducing the vertical forces (Chap. 5). Although the need to take the carriage back in the initial position before the beginning of the next cycle, the linear guide is therefore employed during this work.

The model selected - NC Componenti LPA RH80-15 (Fig. 4.3) - is able to withstand the expected loads acting on the carriage within the sagittal plane and to supply the required stroke. Its main kinematic and dynamic characteristics are listed in the following tables (Tab. 4.1, 4.2).

**Figure 4.1:** Linear guide kinematic data

Maximal stroke	1.2m
Stroke per rotation	0.1/ $\pi$ m/rad
Maximal velocity	1.4m/s

**Figure 4.2:** Linear guide dynamic data

$F_x$	2200N
$F_y$	3900N
$F_z$	3900N
$M_x$	152Nm
$M_y$	740Nm
$M_z$	740Nm

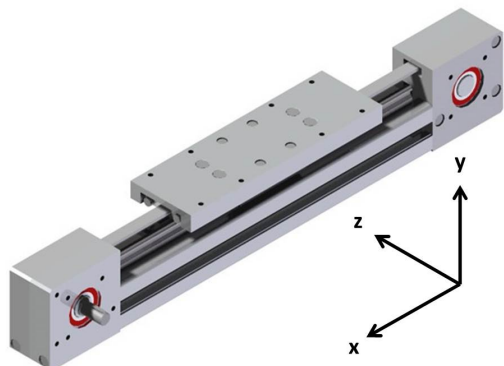


**Figure 4.3:** Representative picture of the linear guide

Once the linear guide has been selected, it is necessary to identify an electric motor and a transmission suitable for the application. The steps performed in order to achieve this goal are reported below.

### 4.2.2 Motor-reducer unit selection

Several aspects must be considered in order to properly select the motor-reducer unit, but from a practical point of view it is sufficient to verify the following ones [24]:

- the maximum torque and the maximum speed required by the application must not exceed those admitted by the motors,

$$\omega_m \leq \omega_{m,max},$$

$$T_m(\omega_m) \leq T_{m,max}(\omega_m);$$

- the root mean square value (RMS<sup>1</sup>) of the torque required by the application must

<sup>1</sup>The root mean square for a function over the time period  $T$  is:

$$x_{rms} = \sqrt{\frac{1}{T} \int_0^T x^2 dt}$$

## 4.2. Longitudinal axis design

be lower than the rated one,

$$T_{m,rms} \leq T_{m,N}.$$

Otherwise, the final performance and the service life of the electric motor would be inevitably compromised.

There are many straightforward procedures in the literature which are useful to select these components while respecting the conditions given above. The practical approach proposed by Giberti et al. [32] is implemented during this study. Firstly, the method is described referring to a general system made of motor, transmission and load. Then, it is applied considering the problem under study.

### Description of the selection method

A simple but general model of a servo-system is characterized by three key elements (Fig. 4.4): motor, transmission, and load.

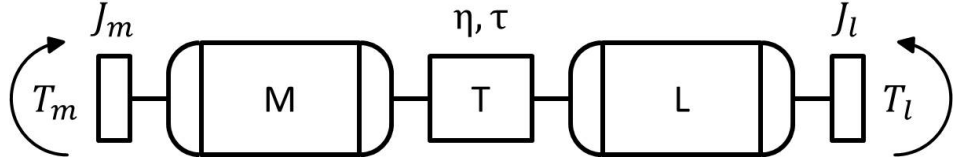


**Figure 4.4:** Schematic representation of a mechanical system made up of motor, transmission, and load

The equation describing its dynamics is achieved by using an energy approach [8]:

$$\eta [T_m \omega_m - J_m \dot{\omega}_m \omega_m] = T_l \omega_l + J_l \dot{\omega}_l \omega_l$$

where subscripts  $m$  and  $l$  stand respectively for the motor and the load.  $T$  indicates the torque,  $J$  the inertia,  $\eta$  the mechanical efficiency of the transmission,  $\tau$  the kinematic ratio, and  $\omega$  the angular velocity. By neglecting the loss in the transmission,  $\eta = 1$ , and introducing the relation between the upstream and downstream kinematic quantities,  $\tau = \omega_l / \omega_m$ , it is finally possible to obtain the expression of the motor torque,

$$T_m = \frac{J_m \dot{\omega}_l}{\tau} + \tau (T_l + J_l \dot{\omega}_l) = \frac{J_m \dot{\omega}_l}{\tau} + \tau T_l^*,$$

and its RMS value,

$$T_{m,rms}^2 = \frac{J_m^2}{\tau^2} \dot{\omega}_{l,rms}^2 + \tau^2 T_{l,rms}^{*2} + 2 J_m (\dot{\omega}_l T_l^*)_{mean},$$

Given this relation, the third inequality given above is rewritten so as to explicit two parameters, i.e.  $\alpha$  and  $\beta$ :

$$\begin{aligned} T_{m,N} &\geq T_{m,rms}, \\ \frac{T_{m,N}^2}{J_m} &\geq \tau^2 \frac{T_{l,rms}^{*2}}{J_m} + J_m \frac{\dot{\omega}_{l,rms}^2}{\tau^2} + 2 (T_l^* + \dot{\omega}_l)_{mean}, \\ \alpha &\geq \beta + \left[ T_{l,rms}^* \left( \frac{\tau}{\sqrt{J_m}} \right) - \dot{\omega}_{l,rms} \left( \frac{\sqrt{J_m}}{\tau} \right) \right]^2. \end{aligned}$$

## Chapter 4. Longitudinal loading subsystem

---

The *accelerating factor*,  $\alpha$ , is exclusively related to motor features reported in the manufacturer catalog,

$$\alpha = \frac{T_{m,N}^2}{J_m}.$$

On the other hand, the *load factor*,  $\beta$ , depends only on information related to the load and the working condition (applied load and law of motion),

$$\beta = 2 [\dot{\omega}_{l,rms} T_{l,rms}^* + (\dot{\omega}_l T_l^*)_{mean}] .$$

Since the residual squared term is always positive, or null, the inequality is verified whenever the factor  $\alpha$  is sufficiently greater than the factor  $\beta$ . If this is the case, the engine can be considered suitable for the application and the range of useful reduction ratios can be finally determined according to the following relations so as to respect the limitations imposed by the motor working range:

$$\alpha \geq \gamma + \beta \rightarrow 0 \leq \gamma \leq (\alpha - \beta)$$

$$\gamma = \left[ T_{l,rms}^* \left( \frac{\tau}{\sqrt{J_m}} \right) - \dot{\omega}_{l,rms} \left( \frac{\sqrt{J_m}}{\tau} \right) \right]^2 \rightarrow \tau_{min} \leq \tau \leq \tau_{max}$$

$$\sqrt{J_m} \frac{\sqrt{\alpha - \beta + 4\dot{\omega}_{l,rms} T_{l,rms}^*} - \sqrt{\alpha - \beta}}{2T_{l,rms}^*} \leq \tau \leq \sqrt{J_m} \frac{\sqrt{\alpha - \beta + 4\dot{\omega}_{l,rms} T_{l,rms}^*} + \sqrt{\alpha - \beta}}{2T_{l,rms}^*}.$$

In order to ensure the possibility to reach the maximum speed required by the load, a further parameter has to be considered,

$$\tau \geq \tau_{lim} = \frac{\omega_{l,max}}{\omega_{m,max}} \rightarrow \max(\tau_{min}, \tau_{lim}) \leq \tau \leq \tau_{max}.$$

These relations are used in the next section in order to select a motor-reducer unit suitable for the application.

### Application of the selection method

According to the considerations performed in the previous section the method proposed by Giberti et al. is applicable as long as the characteristics of the motor and load are known. These are investigated below.

From the engine point of view, it is claimed that synchronous servo-motors have preferable characteristics in automation application:

- low inertia;
- high power to weight ratio;
- broad working range, both in terms of torque and speed;
- high bandwidth;
- restrained dimensions.

## 4.2. Longitudinal axis design

On the other hand, the main drawback associated with the use of this kind of solution is the cost rise. Unlike other electric motors, the excitation of the stator circuit determining the rotation of the rotor is electronically controlled by means of an inverter. The cost of this device must therefore be considered. Nevertheless, this solution is implemented. The list of the engines considered during the application of the selection procedure described above are given in the following table along with their main characteristics (Tab. 4.1).

**Table 4.1:** Main characteristics of the Lenz motors considered during the selection procedure

	$\omega_{m,max}(rpm)$	$T_{m,max}(Nm)$	$T_{m,N}(Nm)$	$J_m(kgcm^2)$
MCS06C41	4050	2.4	0.6	0.16
MCS06I41	4050	6.2	1.5	0.3
MCS09L41	4050	32	4.5	2.8
MCS09D41	4050	9.5	2.3	1.1
MCS12L41	4050	56	11	10.6
MCS14P32	3225	105	21	34.7
MCS19F30	3000	86	21	65
MCS19P30	3000	190	64	160

The value assumed by  $\alpha$  can be uniquely computed using this information (Tab. 4.2).

On the other hand, the  $\beta$  parameter is computed through some known quantities related to the load. These are analyzed below referring to the schematic diagram of the system under study (Fig. 4.5).

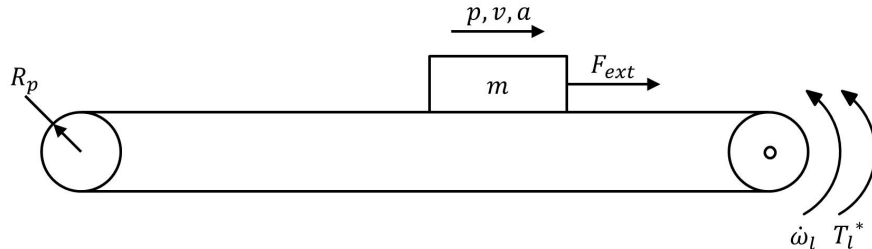


**Figure 4.5:** Schematic representation of mechanical load driven by the motor-reducer unit

The available kinematic data of the foot in longitudinal direction are used to estimate the law of motion of the carriage ( $p, v, a$ ). The position (Fig. 4.6a), the velocity (Fig. 4.6b), and the acceleration (Fig. 4.6c) trends are shown.

The external load ( $F_{ext}$ ) is none other than the force applied by the foot to the carriage during the stance phase. Its trend is shown (Fig. 4.7).

Finally, the mass of the system ( $m$ ) can be calculated by considering the contributions of both the carriage and the vertical actuation mechanism accommodated on it,

$$m = m_c + m_{vls} \approx 15kg.$$

Once obtained the angular acceleration,  $\dot{\omega}_l$  (Fig. 4.8), and the generalized torque  $T_l^*$  (Fig. 4.9), the parameter  $\beta$  is calculated and used in order to determine which motors

## Chapter 4. Longitudinal loading subsystem

---

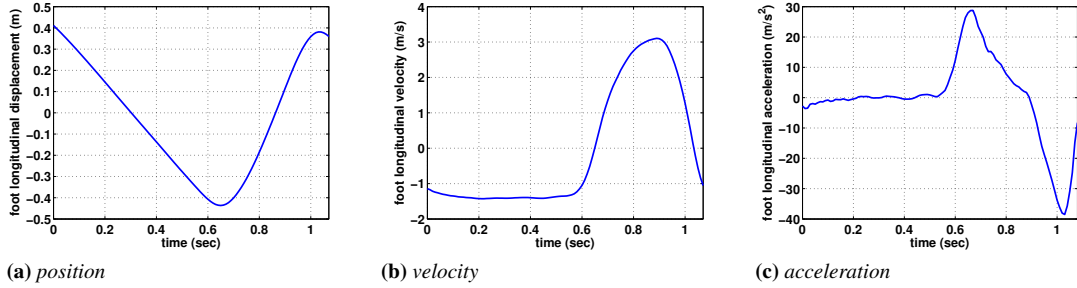


**Figure 4.6:** Law of motion of the foot in longitudinal direction

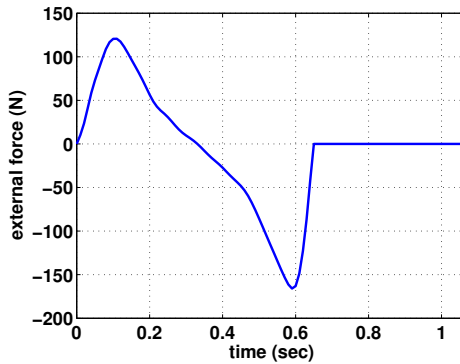


**Figure 4.7:** External load applied to the carriage

are suitable for the application (Tab. 4.2). From this point of view, it is worth noting that the accelerating factor is always greater than the load factor. As a consequence, all the motors are acceptable.

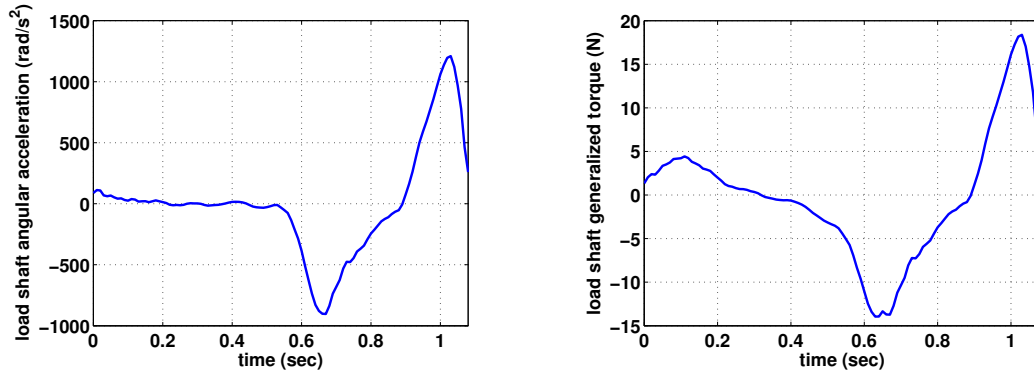


**Figure 4.8:** Reference hip linear displacement components

**Figure 4.9:** Reference hip angular displacement components

The useful reduction ratio range associated to each motor is then calculated. The value of the corresponding parameters are reported in the following table (Tab. 4.2).

The motor-reducer unit is finally chosen according to the reducer ratio available on the catalog, i.e. 1/3, 1/4, 1/5, 1/7, 1/10, 1/25, 1/35, 1/70, 1/100. This task is performed graphically using the following chart (Fig. 4.10):

## 4.2. Longitudinal axis design

**Table 4.2:** Parameters for the selection of the motor-reducer unit

Motor	$\alpha$	$\beta$	$\tau_{min}$	$\tau_{max}$	$\tau_{lim}$
MCS06C41	22500	12161	0.0137	0.0703	0.1057
MCS06I41	75000	12161	0.0090	0.2002	0.1057
MCS09L41	72321	12161	0.0281	0.5994	0.1057
MCS09D41	48090	12161	0.0221	0.2989	0.1057
MCS12L41	114150	12161	0.0427	1.4902	0.1057
MCS14P32	127089	12161	0.0731	2.8532	0.1327
MCS19F30	67846	12161	0.1401	2.7886	0.1427
MCS19P30	256000	12161	0.1092	8.8047	0.1427

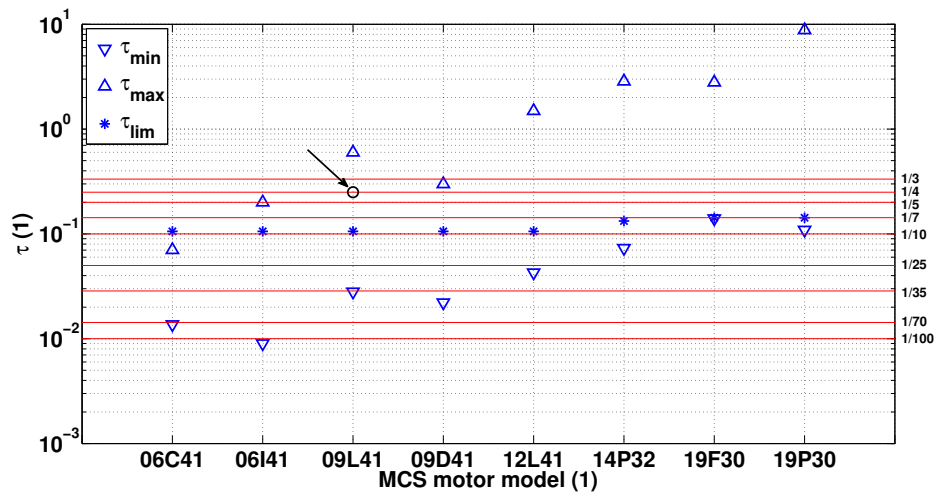


**Figure 4.10:** Useful reduction ratio range associated to each motor

The characteristics of both the brushless motor - Lenz MCS09L41 (Fig. 4.13) - and the planetary gearbox - Wittenstein LP+ Generation 3 (Fig. 4.13) - selected according to the aforementioned procedure are given in the following tables (Tab. 4.11, 4.12).

**Figure 4.11:** Brushless motor kinematic and dynamic data

$\omega_N$	4050 rpm
$\omega_{max}$	7000 rpm
$T_N$	4.5 Nm
$T_{max}$	32 Nm
$J_m$	2.8 Kgm <sup>2</sup>

**Figure 4.12:** Planetary gearbox kinematic data

$$\boxed{\tau} \quad 1/4$$



**Figure 4.13:** Representative picture of the motor-reducer unit

Finally, an inverter - Lenz 9400 Highline - equipped with an additional module that allows the analog signal from the resolver of the motor to be converted into digital, emulating the signal produced by an encoder, is associated to the linear actuator.

## Chapter 4. Longitudinal loading subsystem

---

Once the motor-reducer unit has been selected, the equations describing the dynamics of the system are written and implemented numerically in order to define a suitable control strategy. First, however, it is useful to recall the operating procedure of the system already described in Section 3.5.

### 4.3 Operation procedure

---

From a functional point of view, due to the need to run several cycles of gait by means of a single test procedure, the use of a linear guide determines the need to alternately implement two control logics:

- force control;
- position control.

The former is active during the entire stance phase so as to reproduce the correct value of the force acting on the foot due to reaction with the ground in the longitudinal direction. On the other hand, the latter concurs to return the carriage to its initial position before the beginning of the next cycle, that is, before the end of the swing phase. These strategies are developed separately in the following sections.

### 4.4 Control architecture

---

There are different methods to control the behavior of a system alternately in terms of force or position during a single application. These have been developed in order to cope with situations that might involve interactions between the manipulators and the surrounding environment [33, 67]. For instance, this need is quite common whenever robots are used to manipulate objects (assembling) or to perform operations on surfaces (drilling, finishing, deflashing).

Initially attention was mainly focused on the realization of sensors that can provide precise information about the progress of interactions with the environment. Nowadays, the development of control architectures and computing techniques for taking advantage of such sensory information is more important.

From this point of view, the transition from position to force control, and vice versa, may be simply regulated by means of a selection matrix, i.e. a diagonal matrix whose size equals the number of degrees of freedom to be controlled in the system. Matrix inputs can assume either 1 or 0 value as a function of the current working condition. As a consequence, the control signals once multiplied by the matrix may be either processed or not by the corresponding controllers. Figure 4.14 illustrates the block diagram of the control architecture incorporating this idea, even known as ‘Hybrid control’.

In systems having one degree of freedom, this matrix corresponds to a button that switches when a particular event occurs. For example, in this context the transition may be associated to the value assumed by the contact force in the vertical direction. Such information allows to detect the walking phase, either swing or stance, and therefore to choose the control strategy to be applied.

The main advantage of this technique is the possibility to separately deal with the two control branches and perform the synthesis of the control laws without an accurate

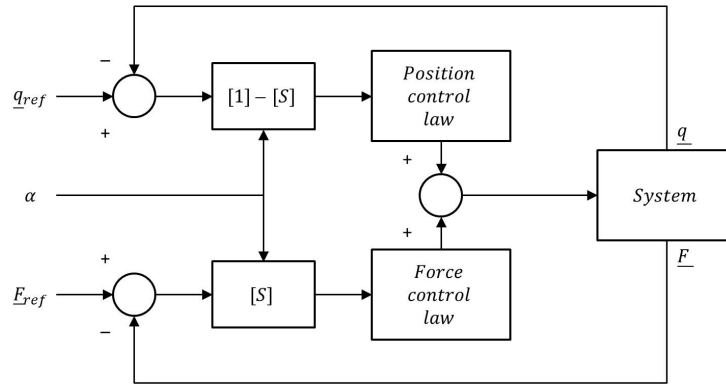


**Figure 4.14:** Schematic representation of the hybrid control architecture

model of the problem under study. Generally speaking, the control parameters, such as gains, may therefore be tuned empirically, that is, without applying any analytical optimization criteria/theoretical technique. However, a matrix accepting only two logical selection levels (boolean logic) results in sudden reference changes that may undermine the stability of the system and therefore its ability to achieve the expected result.

An alternative approach to cope with the dynamic interaction between a manipulator and its environment without changing the controller structure is the ‘Impedance control’ [38]. The key theory behind the method is to treat the environment as an admittance and the manipulator as an impedance. From a practical point of view, such control architecture does not regulate force or position separately. Instead a regulation of the relationship between force on the one hand and position, velocity and acceleration on the other hand is performed. Intuitively, this relation is called impedance. No matter the nature of the impedance, it can be nonlinear or even discontinuous, as long as it specifies the force produced by the manipulator in response to the motion imposed by the environment. For instance, the relation may be reproduced by means of a spring-mass-damper model. If this is the case, the dynamic relationship between force, and position, velocity and acceleration is given by the following relation:

$$F = Ma + Cv + Kx.$$

Mass and spring are energy storing elements, while the damper is an energy dissipating element. The dynamic interaction between the manipulator and the environment may then be modulated, regulated and controlled by changing the impedance parameters. Thus, a very general strategy for controlling a manipulator is to control its motion (as in conventional robot control) and in addition give it a ‘disturbance response’ for deviations from that motion which has the form of an impedance.

Evidently, the possibility to regulate the behavior of the system by acting just on one variable, i.e. the position, eliminates the risks to jeopardize the stability such as the hybrid control does. On the other hand, the need to define the relation between the kinematic and dynamic quantities as realistically as possible involves the development of a detailed model of the system, nonlinearities included. In the case under study, the nonlinearities and the characteristics of the system are not completely known:

- the horizontal force component to be regulated is introduced by the friction between the prosthetic foot and the support surface representing the ground;

## Chapter 4. Longitudinal loading subsystem

---

- the intrinsic mechanical properties of the elements involved, such as the belt of the linear guide and the prosthetic foot, are unknown;
- the behavior of the prosthesis itself is not predictable, being under development.

As a consequence, the hybrid control strategy is initially adopted. As previously hinted, such strategy allows to separately deal with the two control branches. The position and the force controller are therefore defined individually in the next sections. In particular, the possibility to track both the position and the force reference by means of a linear regulator is evaluated.

### 4.5 Position control

---

A linear model of the system is essential for developing a PID controller with the theoretical design techniques. Thus, the equations describing the problem are collected and linearized in this section. Successively, the gains are calculated in order to satisfy the dynamic requirements of the applications. Finally, some considerations about how to compute a suitable law of motion to take the carriage back in the initial position are performed.

#### 4.5.1 Mathematical model

As previously hinted, the theoretical development of the controller presupposes the availability of a mathematical model of the system under study. Such system, during position control, consists of three main elements:

- motor;
- load;
- transmission.

Depending on the function to be performed, the equations describing the dynamic behavior of these elements may be written adopting different accuracy levels. In this context, the ability to recover the initial position within the predetermined time limit is more important than the ability to exactly track the computed trajectory. The model can therefore be defined neglecting many aspects that unnecessarily complicate the issue. For example, the equivalent electrical model of the brushless motor is not considered during this study. Similarly, the dynamic effect of the main nonlinearities is neglected:

- the friction acting on the carriage;
- the flexibility of both the toothed belt and the transmission;
- the backlash of the reducer.

Eventually, these components are introduced as noise. According to these considerations, the equations reported in section 4.2.2 may be recalled to describe the behavior of each mechanical element:

- motor:  $J_m \ddot{q}_m + D_m \dot{q}_m = T_m - T_{lm}$
- load:  $J_l \ddot{q}_l = T_{ml} - T_l$
- transmission:  $\tau = \omega_l / \omega_m$

where  $q_m$  and  $q_l$  are respectively the angular position of the motor and the load,  $J_m$  and  $D_m$  are the inertia and the friction of the motor,  $J_l$  is the inertia of the load,  $\tau$  is the kinematic ratio,  $T_m$  is the torque applied by the motor,  $T_l$  the resistive torque applied by the load,  $T_{lm}$  is the equivalent torque of the load at the motor shaft and finally  $T_{ml}$  is the equivalent torque of the motor at the load shaft. Such a system is linear and therefore suitable for the development of classical control logics. By combining these expressions and rearranging the terms, it's possible to achieve the equation describing the behavior of the system:

$$(J_m + \tau^2 J_l) \ddot{q}_m + D_m \dot{q}_m = T_m - \tau T_l.$$

By applying the Laplace transformation it evolves into:

$$(J_m + \tau^2 J_l)s\dot{Q}_m(s) + D_m\dot{Q}_m(s) = T_m(s) - \tau T_l(s).$$

Since during the swing phase the application of external loads is not expected, the resistance torque,  $T_l$ , may be considered a noise like the other nonlinearities. Thus, it is possible to obtain the transfer function between the speed and the output torque of the motor:

$$\frac{\dot{Q}_m(s)}{T_m(s)} = G_2(s) = \frac{1}{(J_m + \tau^2 J_l)s + D_m}.$$

By neglecting the engine friction component, it's finally possible to write:

$$G_2(s) = \frac{1}{(J_m + \tau^2 J_l)s} = \frac{\mu}{s},$$

where  $\mu$  is the steady-state gain. The block diagram of the system, noise included, is represented in figure (Fig. 4.15).

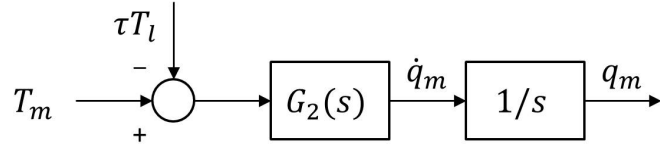


**Figure 4.15:** Block diagram of the mechanical system during position control

### 4.5.2 Control synthesis

According to the classical regulation strategies, the position control of a system having a single degree of freedom involves the use in cascade of a proportional regulator (P) in terms of position and a proportional integrative regulator (PI) in terms of speed. The block diagram of this P/PI controller is represented in figure (Fig. 4.16).

According to the information reported in the literature and being known the steady-state gain,  $\mu$ , the gains of the controllers can be estimated by setting the bandwidth both in terms of speed,  $\omega_{cv}$ , and position,  $\omega_{cp}$ , according to the following relations:

$$K_{P_p} = \omega_{cp}, \quad K_{P_v} = \frac{\omega_{cv}}{\mu}, \quad T_{I_v} = \frac{10}{\omega_{cv}}.$$

## Chapter 4. Longitudinal loading subsystem

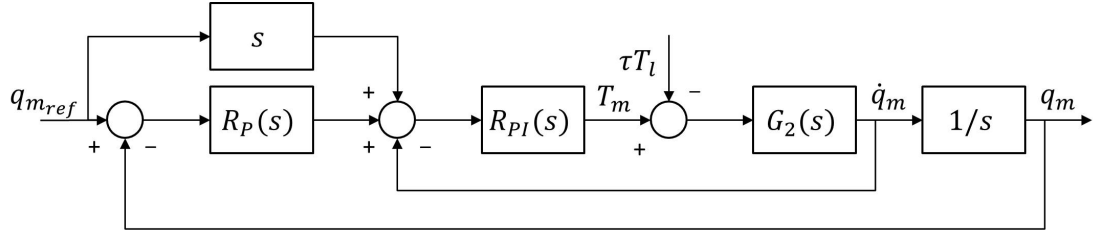


**Figure 4.16:** Block diagram of the P/PI position controlled system

However, the P/PI controller can be reduced into a PID if the actual speed is not directly measured but derived starting from the position signal (Fig. 4.17). In this case only the position signal is accessible through the encoder.

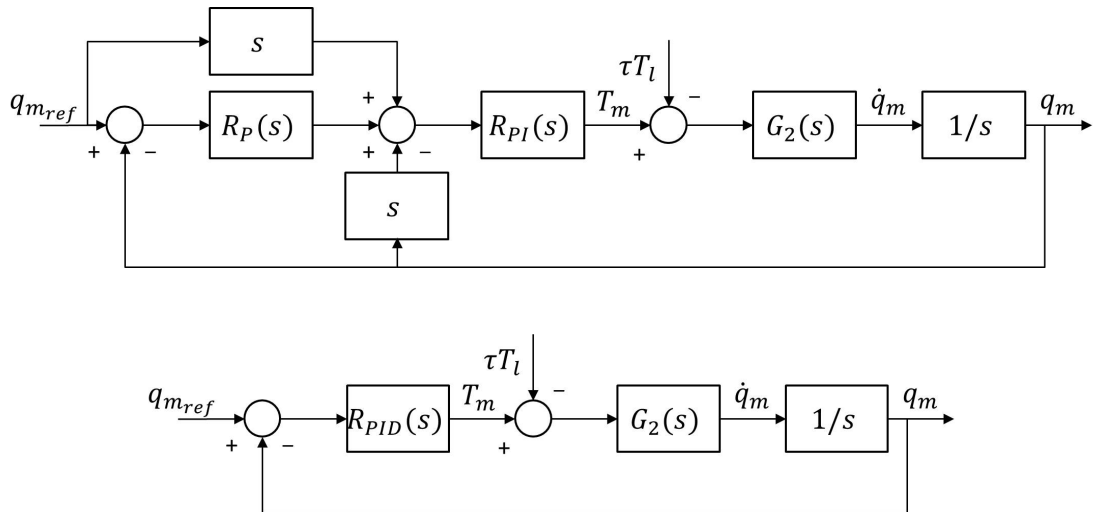


**Figure 4.17:** Block diagram of the resulting PID position controlled system

The PID parameters can be calculated starting from the gains of the P/PI architecture according to the following instructions:

$$K_P = K_{P_v} (K_{P_p} + 1/T_{I_v}), \quad T_D = \frac{K_{P_v}}{K_P}, \quad T_I = \frac{K_P T_{I_v}}{K_{P_p} K_{P_v}},$$

and gathered in the following form:

$$R_{PID}(s) = K_P \left( 1 + \frac{1}{sT_I} + \frac{sT_D}{1 + sT_D/N} \right)$$

where  $N = 5$  for introducing a pole at high frequency. Once bandwidths consistent with the frequency content of the signals to be reproduced both in terms of position and speed have been defined,

$$\omega_{c_v} = 100 \frac{\text{rad}}{\text{sec}}, \quad \omega_{c_p} = 10 \frac{\text{rad}}{\text{sec}},$$

the data of the engine, the reducer and the load, can be used to estimate the gain values (Tab. 4.3).

**Table 4.3:** Position control PID gains

$K_P$	$T_D$	$T_I$
2.25	0.05sec	0.2sec

After tuning, the analysis focuses on the static and dynamic performances of the closed loop system. In this regard, the step response and the frequency response function (FRF) are evaluated. Their graphs are presented below (Fig. 4.18, 4.19).

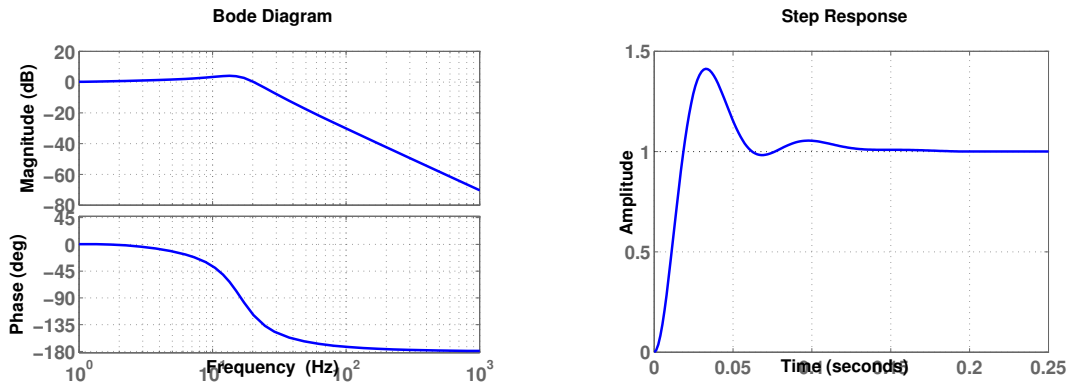


**Figure 4.18:** Frequency response function of the closed loop system

**Figure 4.19:** Step response function of the closed loop system

From this point of view, the FRF demonstrates suitable characteristics for the application:

- broadly constant module in the range of frequencies of interest (bandwidth);
- decreasing module beyond the bandwidth, so as to reduce the effect of high frequency disturbances;
- no dynamic amplification;
- almost null phase within the bandwidth.

On the other hand, the overshoot of the step response is quite high. This problem can be faced in two different ways:

- by tuning the PID gains;
- by smoothing the reference to be tracked.

Both are exploited in this work. The verification, calibration and optimization of the gains, as well as the assessment of the linear controller suitability, are performed at the end of the numerical simulation in which both the phases of the cycle are reproduced. On the other hand, attention now focuses on the law of motion to be applied in order to return the carriage to its initial position.

#### 4.5.3 Law of motion profile

This task is not as simple as it seems. Disturbances, uncertainties and unpredictable behaviors of the prosthesis limit the opportunity to use a standard law of motion. Indeed, the dynamics of the phenomenon under study may change from cycle to cycle. As a consequence the law of motion must be planned before each swing phase as a function of the actual state of the carriage, that is, according to actual kinematic quantities. Position, velocity and acceleration may indeed vary at each iteration. Obviously, the greater the amount of kinematic information taken into account, the higher the chance of minimizing the jerk<sup>2</sup> and consequently the stress of the motor.

Several standard laws of motion are available but not all of them are suitable. The available measurement equipment allows indeed just to measure the position of the carriage; furthermore not in loco but starting from the angular position of the motor shaft. All the laws requiring the actual value of the acceleration are therefore rejected so as to apply the derivative of the position signal just once for obtaining the velocity. In fact, the second derivative is inevitably compromised by the amplification of the noise. A law of motion with trapezoidal velocity profile meets this requirement (Fig. 4.20).

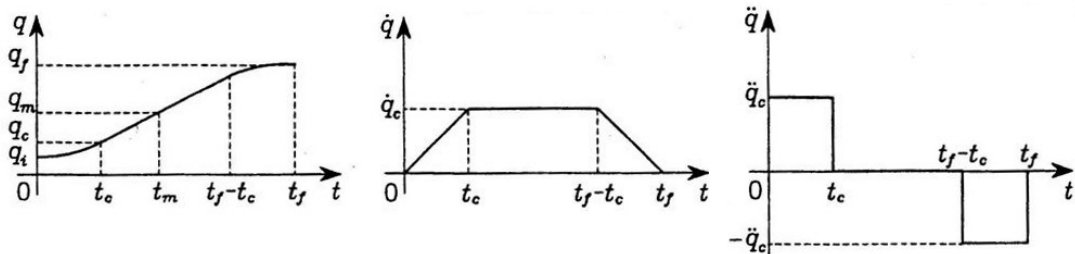


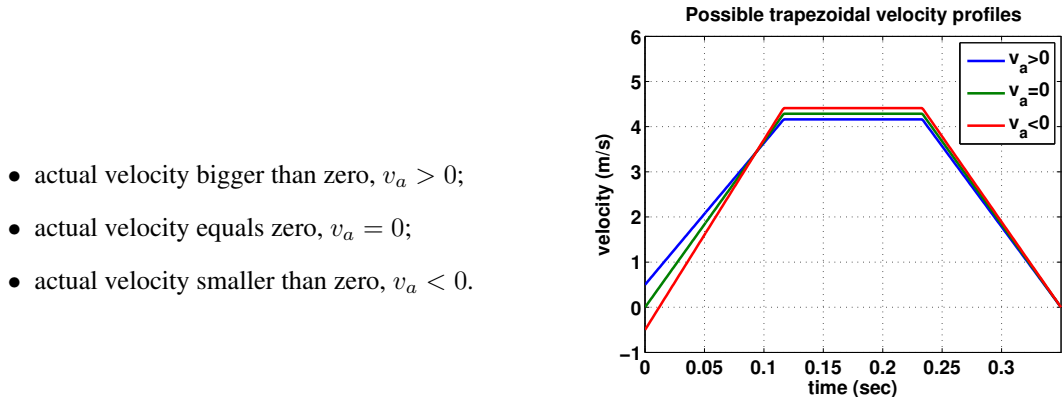
**Figure 4.20:** Position, velocity and acceleration profiles considered during this study

Once the law has been chosen, it is necessary to define a velocity profile whose underlying area equals the stroke necessary to move the carriage back to the initial position,  $p_0$ , within a suitable time period,  $\Delta t$ . As extensively observed, the stroke is computed based on the actual position,  $p_a$ , of the carriage. On the other hand, the time period is obtained being known that the swing phase lasts about 40% of the entire cycle during normal walking, that is, about 0.45 seconds in this case. Nevertheless, the limit is reduced to 0.35 seconds in order to ensure complete recovery of the position while respecting the speed limits [57]. However, the maximal speed value,  $v_{max}$ , depends also on other two parameters:

- the partitioning value,  $par$ .
- the actual speed value,  $v_a$ .

The former is defined so as to reduce the work of the motor, i.e.  $par = 1/3$ . As a consequence, the acceleration phase, the constant speed phase and the deceleration phase are equal in terms of time, that is, one-third of the entire period,  $\Delta t$ . Conversely, three situations may arise in terms of actual velocity (Fig. 4.21):

<sup>2</sup>In physics, jerk, also known as jolt, surge, or lurch, is the rate of change of acceleration, that is, the derivative of acceleration with respect to time.



- actual velocity bigger than zero,  $v_a > 0$ ;
- actual velocity equals zero,  $v_a = 0$ ;
- actual velocity smaller than zero,  $v_a < 0$ .

Figure 4.21: Possible velocity profiles

Regardless of the case considered, the proposed method requires the controller to compute the maximum speed value,  $v_{max}$ , every time so that the integral of the velocity profile equals the stroke required to take the carriage back to the initial position. This task is easily performed according to the following relation:

$$v_{max} = \frac{2(p_0 - p_a) - v_{apar}\Delta t}{2(1 - par)\Delta t} = \frac{2h - v_{apar}\Delta t}{2(1 - par)\Delta t}.$$

Once the velocity profile is known, it is possible to compute by integration the reference to be used when performing position control. Obviously, this calculus must be repeated by the processor before each swing phase according to actual kinematic quantities regardless of the computational burden.

## 4.6 Force control

The longitudinal force component to be regulated is introduced by the friction. Clearly, the identification, analysis and modeling of the interaction between the bodies could facilitate the definition of the control strategies to be adopted and consequently enhance the reproduction of the phenomenon.

However, a detailed description requires many pages of dissertation, rather than a mere analysis of the literature, as well as the execution of dedicated experimental tests. Since friction is not the scope of this study, but rather the possibility of exchanging forces between bodies, just the main aspects of interest are analyzed in this section. In particular, once reviewed the fundamental basics, a friction model compatible with the phenomenon to be reproduced is introduced. Further explanations may be found by the reader in the many textbooks about the topic.

### 4.6.1 Friction model

The study of the friction is such a complex subject that the microscopic phenomena causing the macroscopic effects are not yet fully known. For this reason, several friction models have been developed for simulating the different behaviors. These models may be grouped into two distinct categories:

- static friction models;

- dynamic friction models.

Dynamic models provide a more accurate description of the phenomenon, especially at the commencement of movement, due to the possibility of simulating special phenomena such as the variations of the force at which detachment occurs [34]. However, they are very difficult to implement because of the need to take into account micro-scale events. Thus, these models are discarded in favor of the static ones.

Basic static models are obtained as a combination of the primitive coulomb and viscous friction models. According to them, the reaction force produced by the friction is computed as a function of the relative sliding speed between the two contact surfaces.

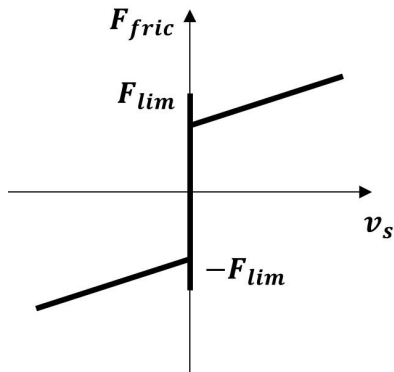


Figure 4.22: Coulomb friction model

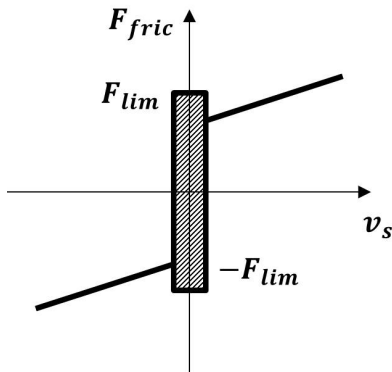


Figure 4.23: Karnopp friction model

These models are affected by the same limit. The discontinuity of the function, at the zero velocity point (Fig. 4.22), may lead to uniqueness solution problems when solving the motion equations. Such models are therefore suitable only in applications in which the sliding velocity is not null or the resting condition, i.e. the adhesion between the bodies, is occasional. Of course this is not the case, the model proposed by Karnopp is therefore introduced to avoid numerical problems.

This model presents a sticky region, i.e. a vector field rather than a zero velocity point, in which the relative speed can be considered null and the static friction force can vary from a minimum to a maximum (Fig. 4.23). Within the static region, the sliding velocity,  $v_s$ , is therefore null as long as the reaction force between the bodies (computed as a function of the other forces applied to the system),  $F_t$ , is lower than the static limit,  $F_{lim}$ . When such a limit is overcome, friction is computed as a function of the sliding velocity, that is, according to a primitive viscous friction model. This behavior is described by a set of three ordinary differential equations, one for the movement phase, one for the static friction phase, and one for the transitional phase between the previous two [72]. The equation to be considered, and thus the resulting friction force, is determined according to the state of the system and the resultant external force:

$$F_{fric} = \begin{cases} F_t & v_s = 0 \wedge |F_t| \leq \mu_s |F_n| \\ \mu_s |F_n| sgn(F_t) & v_s = 0 \wedge |F_t| > \mu_s |F_n| \\ \mu_d |F_n| sgn(v_s) & \text{else} \end{cases}$$

where  $\mu_s |F_n| = F_{lim}$  is the force determining the static friction limit.

This friction model is implemented in SimMechanics using the ‘joint stiction actuator’ block. A representative scheme of the model is given in figure (Fig. 4.24).

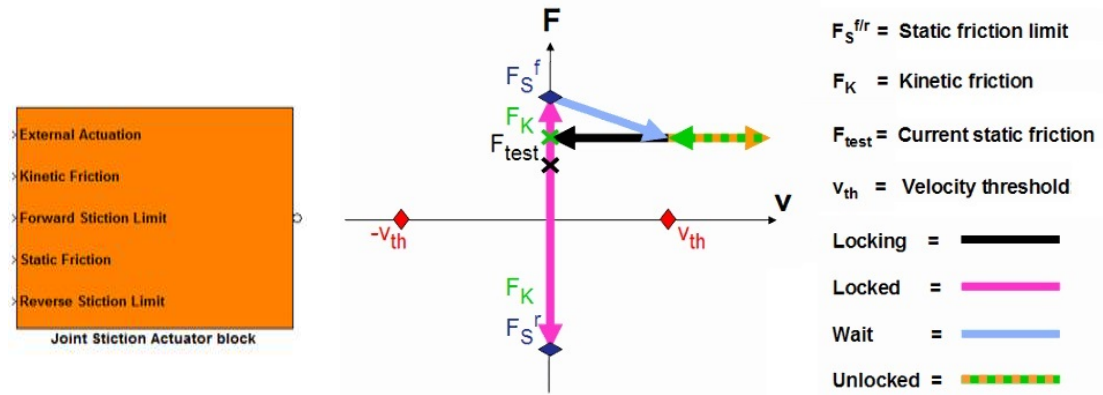


**Figure 4.24:** SimMechanics friction block

Since the equations given above are already implemented in the block, it is sufficient to define the values of the quantities distinguishing the static friction region from the dynamic one, i.e. the static friction coefficient,  $\mu_s$ , the dynamic one,  $\mu_d$ , and the velocity threshold,  $v_{th}$ . The first two parameters are obtained from the literature [74] (Tab. 4.4). The third parameter is defined instead so as obtain a fair compromise between realism and computational burden when performing the numerical analysis (Tab. 4.4).

**Table 4.4:** Friction model parameters

$\mu_s$	$\mu_d$	$v_{th}$
0.8	0.2	1mm/s

The other features of the model and the results obtained by means of it are analyzed below. Attention now focuses on the control strategy to be applied for reproducing the trend of the longitudinal force reference.

### 4.6.2 Control synthesis

The aim, during this first phase of the system development, is to exploit the PID controller to reproduce both the position and force reference. The logic behind this strategy is in fact relatively simple to understand, implement and calibrate compared to other control algorithms. A good level of performance can indeed be achieved, even if the exact model of the system is unknown, by calibrating the gains according to simple empirical rules. This opportunity is particularly appreciated given the complexity of the problem at hand. The nonlinear nature of the friction prevents indeed the possibility to univocally linearize the equations describing the behavior of the system, and therefore to define the gains of the PID controller through the theoretical regulation methods (Fig. 4.25).

Given the impossibility of conducting the synthesis of the regulator analytically, a numerical model of the problem is developed within the Simulink and SimMechanics simulation environment. This model allows indeed the application of the above

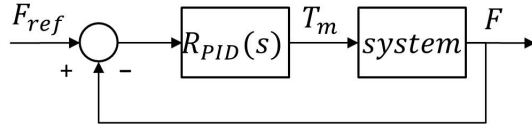


**Figure 4.25:** Block diagram of the PID force controlled system

mentioned empirical regulation techniques as well as the definition of compensation algorithms that allow better performance levels to be reached. Before undertaking this numerical analysis, the attention focuses on the identification of a method for computing a longitudinal force reference compliant with the target of the simulation.

#### 4.6.3 Force profile

A problem occurs when defining the longitudinal force reference: the interaction between the foot and the ground heavily relies on the response of the prosthesis, which is not known a priori. Thus, it is not possible to define the reference force as a function of time, since the duration of the contact phase, that is the stance phase, is uncertain. Correlations between the longitudinal and vertical force component are therefore investigated, under the hypothesis to faithfully reproduce the vertical load, in order to calculate the former as a function of the latter. In particular, analyzing the dynamic data, a total of 14 measurements on 4 able-bodied subjects (Sec. 2.3), a linear relationship between the trend of the vertical force and the first derivative with respect to time of the longitudinal force is found. An approximation of the reference may therefore be achieved in real time as a function of the actual vertical force value. Obviously, duration problems are avoided according to this method.

$$\frac{dF_x(t)}{dt} \approx AF_y(t) - B.$$

This analysis highlighted another important aspect. Although there are no universally valid values for A and B, given a subject, it is possible to reproduce the trend of the longitudinal force, regardless of the vertical trend considered, using the same parameters. On the other hand, this consideration is not true among different subjects. According to the literature, this inter-variability might depend on multiple factors such as weight, height, gender [23], age [62], pathologies and even geographic origin [4]. However, due to the lack of data, it is not possible to run a statistical analysis to verify the relevance of the correlations. Nevertheless, in support of this theory, the table below shows the results, in terms of A and B values, obtained by reducing the quadratic mean of the error (Tab. 4.5).

**Table 4.5:** Analysis of the force components correlation

Subject	$A_{mean}$ [ $s^{-1}$ ]	$\sigma_A$ [ $s^{-1}$ ]	$B_{mean}$ [N/s]	$\sigma_B$ [N/s]	$err_{rms}$ [N]
1	3	0	1900	0	31.42
2	3	0.5	1817	355	12.88
3	5	0.25	2225	96	25.92
4	5	0.5	2513	275	16.77

It is worth noting that in the worst case scenario, the use of this technique results

in an error value of just  $31.42N$ . This value is very small if considering that slight changes in speed can have big effects on the patterns of gait parameters and as a consequence on the force exchanged with the ground [78]. An additional demonstration of the merits of the proposed method are presented in the diagram showing the trends of the actual longitudinal force recorded during the laboratory trial and the corresponding approximation considered during this study (Fig. 4.26).

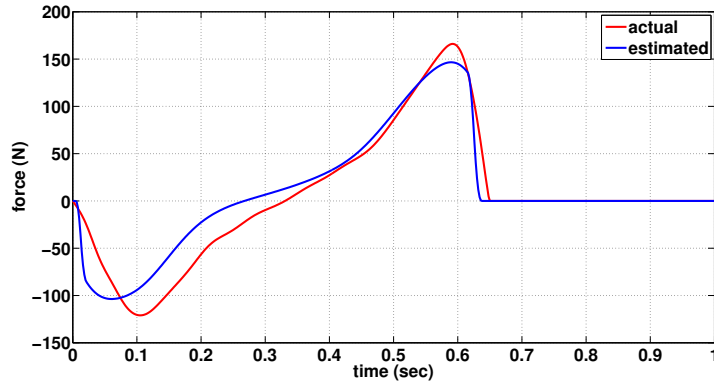


**Figure 4.26:** Actual and approximated longitudinal force reference

Although the signals do not perfectly overlap, their affinity is acceptable for the moment and the method proposed for calculating the aforementioned horizontal force reference on-line as a function of the vertical force component is implemented in the numerical model. Its description is given in the next section.

## 4.7 Numerical simulation

---

Under the hypothesis of having full access to the load measures, which argument is part of the next chapter (Chap. 5), this section deals exclusively with the development of the control strategies necessary to:

- reproduce the trend of the longitudinal force acting on the foot during the stance phase;
- return the carriage to its initial position during the swing phase.

In particular, the intention is to verify the suitability of the solutions proposed so far considering working conditions that are as real as possible. The aspects under evaluation are:

- the possibility of reproducing both the force and position reference by means of PID controllers;
- the suitability of the method proposed to compute the references themselves.

This task is accomplished by means of a numerical model of the problem under study.

## Chapter 4. Longitudinal loading subsystem

### 4.7.1 Nonlinear numerical model

The block diagram of the model developed using both the Simulink and SimMechanics modeling environment is shown in figure (Fig. 4.27). Its features are briefly analyzed below.

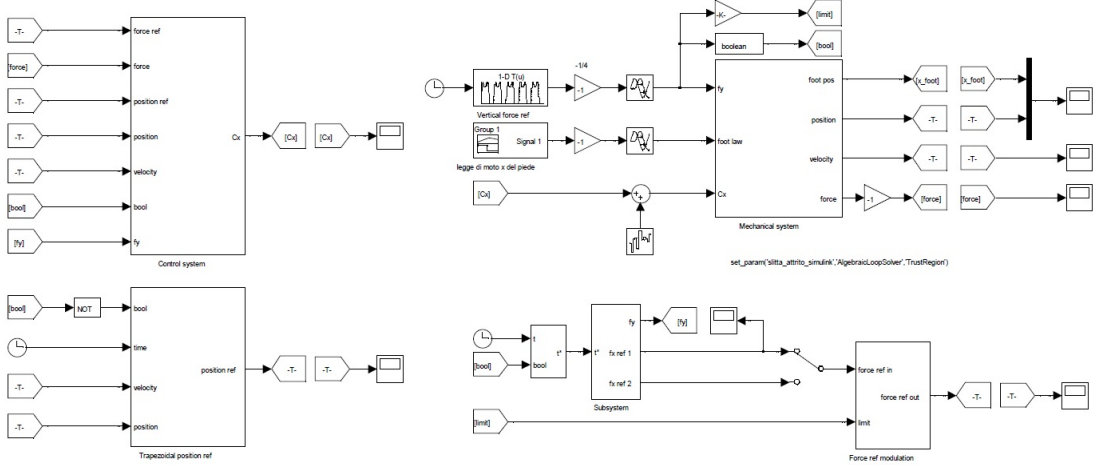


**Figure 4.27:** Block diagram of the horizontal actuating system numerical model

SimMechanics is used to model and simulate the mechanical properties and the motion possibilities of the bodies constituting the system, that is, the foot and the mechanism representing the ground. The foot is modeled as a massless point moving along the longitudinal direction according to a law of motion similar to the physiological one. On the other hand, the support surface mechanism is reproduced by means of a rigid body having a mass of  $15kg$  (Sec. 4.5.2) and moving in longitudinal direction. Also the foot-ground contact forces are modeled in SimMechanics. The vertical component is introduced as an external force, that is, under the hypothesis that it can be accurately reproduced through the vertical actuating subsystem (Chap. 5). On the other hand, the longitudinal component is introduced using the ‘joint stiction actuator’ block, that is, according to the Karnopp friction model presented before (Sec. 4.6.1).

Simulink is used instead to compute both the force and position reference signal on-line as a function of the current state of the system, and to implement the hybrid control architecture within which the PID control laws can be applied. From this point of view, the parameters of the position controller are obtained by iteratively modifying the first attempt gains computed before (Sec. 4.5.2). Conversely, the force controller gains are computed according to the MATLAB empirical techniques and then adjusted by trial and error. Finally, the simulations are conducted neglecting, for simplicity, the flexibility of the belt and any other friction force in the system. Moreover, the position of the carriage is ideally measured in loco whereas in reality it is deduced starting from the angular position of the motor shaft by means of the encoder. Results obtained thorough the model are presented in the next section.

### 4.7.2 Preliminary results

The graphs of the reference and the measured signals of the controlled variables are shown (Fig. 4.28, 4.29). Given a chart, comparison between curves is meaningful

#### 4.7. Numerical simulation

---

depending on whether the control is performed either in force or in position, that is respectively when the switch signal is high or low (Fig. 4.30). Graphs show that the control system manages to follow the reference in a satisfactory manner during both the stance and the swing phase.

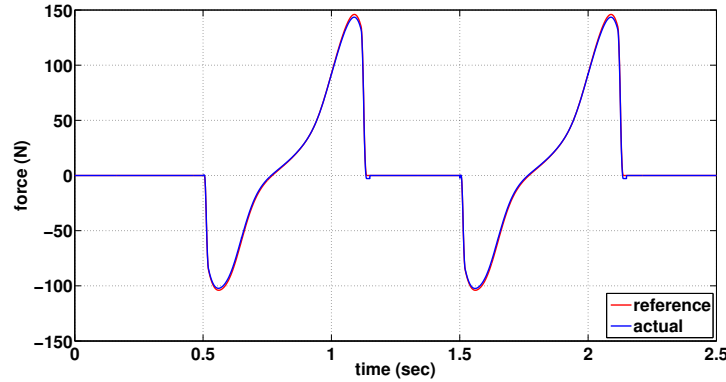


**Figure 4.28:** Force reference and actual trend

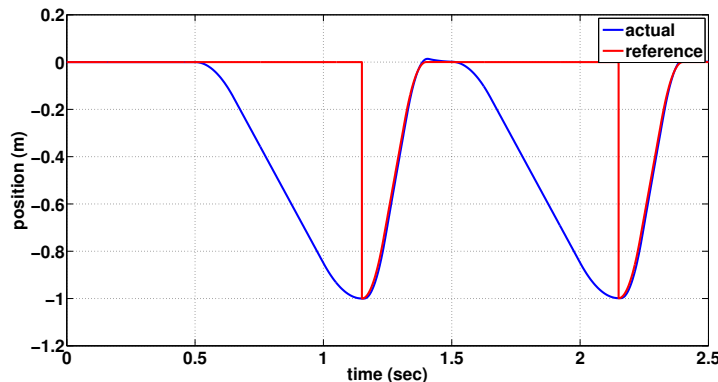


**Figure 4.29:** Position reference and actual trend

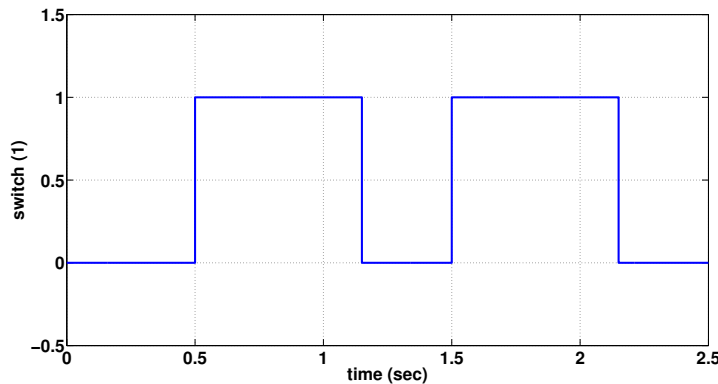


**Figure 4.30:** Switch signal

In addition, the support surface is able to recover the initial position before the foot,

## Chapter 4. Longitudinal loading subsystem

---

i.e. before the beginning of the next cycle (Fig. 4.31).

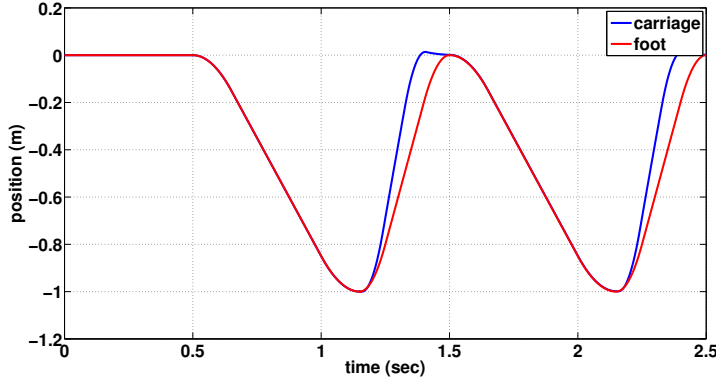


**Figure 4.31:** Actual position of both the carriage and the foot

Finally, the trend of the motor torque necessary for driving the carriage is presented (Fig. 4.32).

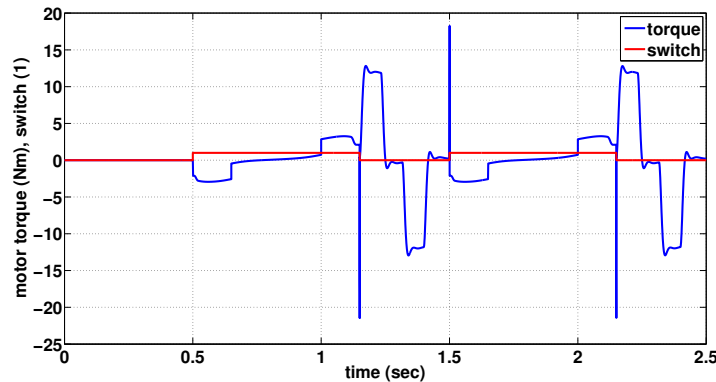


**Figure 4.32:** Torque supplied by the motor to drive the carriage according to the hybrid control strategy

Spikes occurring at the switching time reveal that the hybrid control architecture, together with the method proposed to compute the reference position, is actually not able to minimize the jerk. This aspect is important because it jeopardizes the system stability on the one hand, and increases the stress at the electric motor on the other hand. It's therefore necessary to find another method before performing any other considerations about the ability of the solution proposed to track the references.

### 4.7.3 Position/force control with self-adjusting matrix

Considering that the force spikes are caused by the sudden reference change, i.e. by the boolean logic of the selection matrix, a solution to the problem could be the use of functions that ensure a more gradual transition from one logic to another.

There is an ample array of methods meeting this objective in the literature, among which Zhang et al. [91]. From a practical point of view, the architecture of this method is equivalent to the hybrid one. However, the force information is not only used in a feedback loop, but also to modulate the selection matrix so as to change the control

## 4.7. Numerical simulation

mode as smoothly as possible. As a result, this method has the advantage of hybrid control:

- removing the need to develop a detailed model of the problem;

as well as the advantage of impedance control:

- limiting the discontinuity resulting from the passing from one control to another.

For this reason, it is frequently referred to as ‘Mixed control’. A representative scheme of the logic behind such control architecture is given in figure (Fig. 4.33).

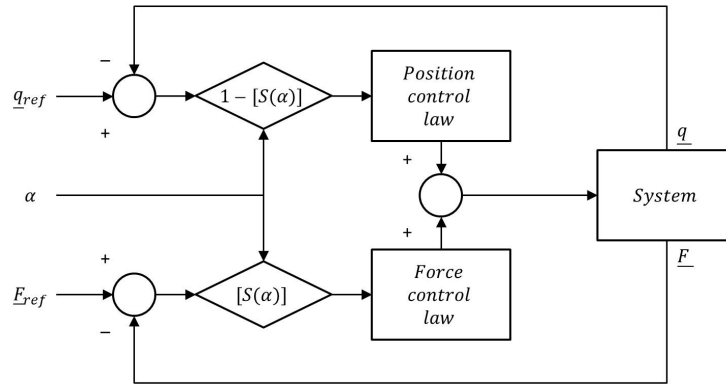


**Figure 4.33:** Schematic representation of the mixed control architecture

The application of this technique is particularly suitable for this context. The two previously developed control branches can in fact remain unchanged given their capacity to follow the corresponding references. The only change to be made is the selection matrix, which needs to be defined as a function of the feedback signal. Once again the vertical force component is used. However, this time the selection matrix is defined so as to assume all the values between 0 and 1 as a function of the force itself. In particular, the selection matrix is defined according to the hyperbolic secant function as follows:

$$S^2 = \begin{cases} 1 - \operatorname{sech}(\alpha F_y) & \text{if } F_y > 0 \\ 0 & \text{if } F_y \leq 0 \end{cases}$$

where  $\alpha$  is the coefficient determining the smoothness of the curve. The trend of  $S$  is represented in the following picture as a function of the vertical force considering different values of  $\alpha$  (Fig. 4.34).

Regardless of the value of  $\alpha$ , three main regions are noticeable:

- $S = 1$ , the control is performed only in terms of force;
- $S = 0$ , the control is performed only in terms of position;
- $0 < S < 1$ , the control is performed both in terms of force and position.

In this case  $\alpha$  is defined by trial and error so as to remove all the discontinuities of the driving force, in particular  $\alpha = 0.08$ . However, it is worth noting that this could

## Chapter 4. Longitudinal loading subsystem

---

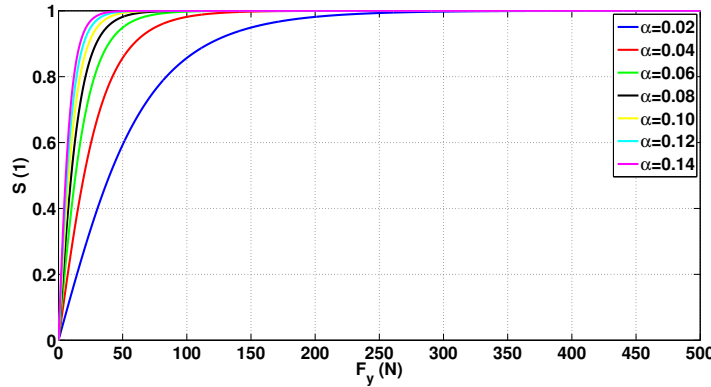


**Figure 4.34:** Trend of the selection matrix as a function of the vertical reaction force considering different values in terms of  $\alpha$

be modified to guarantee that the transition from position control to force control is completed only when the vertical contact force is sufficiently high to ensure a stable contact condition (Fig. 4.34). In fact, the higher the force exchanged in orthogonal direction with respect to the force plate, the larger the static friction limit is.

This safety feature should prevent adhesion loss and the problems linked thereto, such as stick slip phenomenon, enhancing the stability of the system despite the application of PID controllers. To further strengthen this, the previously computed longitudinal force reference is also modulated so as to ensure that the load to be applied is not higher than the current static friction limit,  $F_{x,lim} = \mu_s F_y$ . This aim is accomplished as shown in figure by means of the Z-shaped function (Fig. 4.35).

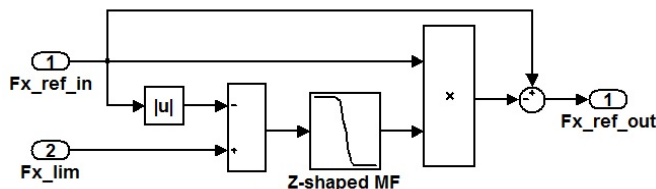


**Figure 4.35:** Block diagram of the strategy for modulating the reference force signal through the Z-shaped function

The value assumed by the Z-shaped spline-based function is computed on-line as a function of the difference between the horizontal reference force and the corresponding static friction limit as follow:

$$Z_{shaped} = \begin{cases} 1 & if \Delta F \leq 0 \\ 1 - 2(\Delta F / 150)^2 & if 0 < \Delta F < 0 \\ 2(\Delta F / 150 - 1)^2 & if 0 \leq \Delta F \leq 0 \\ 0 & if \Delta F \geq 0 \end{cases}$$

where  $\Delta F = F_{x,lim} - |F_{x,ref}| = \mu_s F_y - |F_{x,ref}|$ .

Even if the contact is lost, the self-adjusting matrix will guarantee a gradual passage from the force control mode to the position control mode taking the carriage back to its initial position without any risk for the system. The results obtained by means of such a control strategy are reported in the next section.

#### 4.7.4 Final results

The mixed control method does not add any benefit in terms of performance. The system capacity to reproduce the reference signals is therefore practically the same (Fig. 4.28, 4.29). On the other hand, the use of a logic that allows to gradually switch from one control logic to another eliminates the force spikes that might compromise the system stability (Fig. 4.36).

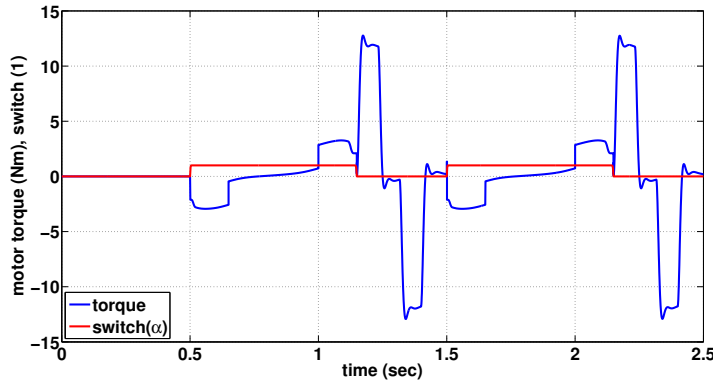


**Figure 4.36:** Torque supplied by the motor to drive the carriage according to the mixed control strategy

Once the dynamic problem is solved, the suitability of the motor-reducer units can be evaluated. This condition is verified if the root mean square values of both the velocity and the torque supplied by the motors ( $\frac{\omega_{l,rms}}{\tau}, \tau T_{l,rms}^*$ ) are included in its continuous working area:

$$\frac{\omega_{l,rms}}{\tau} \leq \omega_{m,N},$$

$$\tau T_{l,rms}^* \leq T_{m,N}.$$

In this case,  $\frac{\omega_{l,rms}}{\tau} = 3147 \text{ rpm}$  and  $\tau T_{l,rms}^* = 4.95 \text{ Nm}$ . The root mean square value of the torque supplied by the motor is therefore slightly bigger than the prescribed limit,  $T_{m,N} = 4.5 \text{ Nm}$ , suggesting the need to change the gearbox. For instance, the problem could be overcome by using a transmission with a reduction ratio corresponding to 1/5. However, the maximum achievable speed decreases proportionally to  $\tau$ . Thus, the current reduction ratio, 1/4, is kept to improve the kinematic performance rather than the dynamic one.

---

## 4.8 Experimental testing

Once the merits of the proposed method have been evaluated, tests are performed to gain confidence with the experimental set-up and extract additional parameters useful

## Chapter 4. Longitudinal loading subsystem

in the simulation phase. In particular, the friction force between the components of the linear guide is estimated in order to improve the reliability of the numerical model.

### 4.8.1 Experimental setup

Before the trials can be undertaken, it is necessary to assemble the test equipment, develop the electrical plant and build the data acquisition system useful for control purposes (Fig. 4.37). Below are the steps performed to achieve these goals.

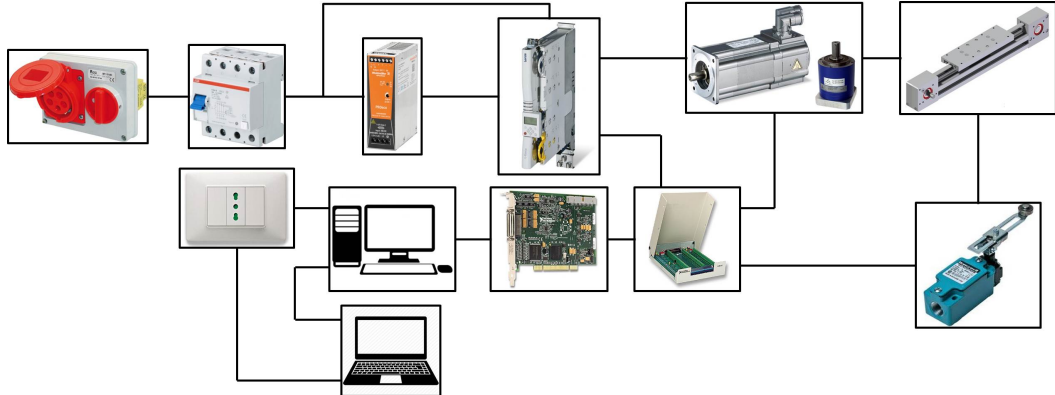


Figure 4.37: Connection diagram of the longitudinal actuating subsystem experimental setup

#### Test equipment

The principal devices composing the test equipment are: the linear guide and motor-reducer unit. Their assembly does not require any particular attention apart from fastening the frame of the linear mechanical unit to the ground. Sensors are then added.

The possibility to control the system in terms of either position or velocity requires the above mentioned module for emulating the signal of the encoder (Sec. 4.2) as well as limit switches. Apart from protecting the system from possible malfunctioning, these enable the identification of the reference positions about which performing the tasks. Also the limit switches are mounted on the frame of the linear guide.

#### Electrical plant

The electric plant is made up of two distinct circuits. In one case, the current coming from the three-phase electric socket passes through a differential switch, an AC/DC converter (24Vdc) and other electronic components that protect the instrumentation from possible power surges before supplying the inverter and the brushless motor. In the other one, the computers constituting the data acquisition system are directly connected to the 220V socket.

#### Data acquisition system

The data acquisition system makes exclusive use of products from National Instruments (NI). In particular, the communication between the hardware and the software is established through a NI-SCB 68 screw terminal connector block (Fig. 4.38) and a PCI NI-6229 DAQ board (Fig. 4.39) inserted into a desktop PC running the same

## 4.8. Experimental testing

Real-Time Operating System (RTOS) installed in the top quality platforms, such as NI cRIO. Although less powerful, the Desktop PC allows to save costs compared to other solutions. This aspect is important when testing the functionality of an early prototype.



**Figure 4.38:** NI-SCB 68 screw terminal connector block



**Figure 4.39:** PCI NI-6229 DAQ board

Once the necessary components are supplied, the operating systems, software and drivers are installed, and the connection between the devices is established, the rest of the work is carried out in LabVIEW 2014, the graphic programming environment developed by NI.

### 4.8.2 LabView control program

Aim of the control program is to drive the output of the mechanical system by manipulating the input in a closed loop. In this regard, LabVIEW defines the communication channels, processes the analog and digital signal coming from the sensors, calculates the command signal driving the motor, and saves on text files the results useful for post-processing.

Since delay can cause system failure, precise timing and long term reliability are fundamental prerequisites from a control point of view. It is therefore necessary to build the program so as to ensure that deterministic tasks receive enough processor resources (saving the results to a text file does not fall under this category). From this point of view, the LabVIEW Real-Time toolbox allows to define the period and the priority at which each operation is performed using the same intuitive LabVIEW graphical language. Once these priorities have been defined on the laptop, it is necessary to deploy the program on the desktop PC running the dedicated LabVIEW RTOS before each test procedure, so as to ensure its deterministic execution. Running a measurement or control program on a standard PC with a general-purpose OS installed (such as Windows) is indeed unacceptable. At any time, the operating system might delay execution of the program due to many reasons: to run a virus scan, update graphics, perform system background tasks, etc.. The graphic interface of one of the control programs used during the experimental trials is presented below (Fig. 4.40).

### 4.8.3 Experimental trial

Once the experimental setup has been configured and the control programs have been developed in LabVIEW-RT, some tests are performed to calibrate the control gains and estimate some parameters useful for modeling purposes. In particular, the relation between the friction coefficient,  $\mu(v)$ , and the speed of the carriage,  $v$ , has been evaluated.

## Chapter 4. Longitudinal loading subsystem

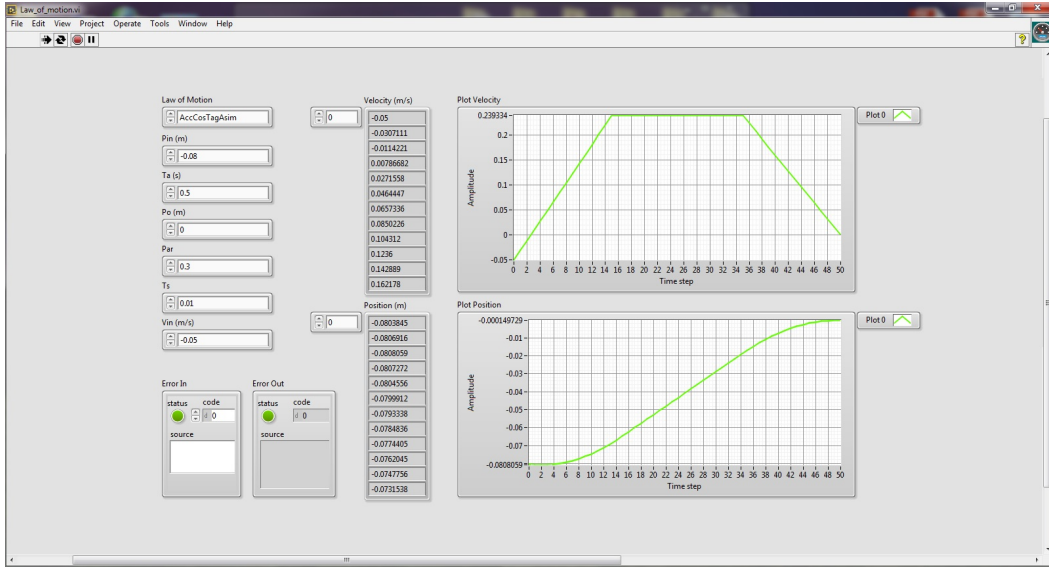


**Figure 4.40:** LabVIEW programming environment

The friction force can in fact be reproduced simply by adopting the law of Coulomb (Sec. 4.6.1):

$$F_{fric} = -\text{sign}(v)\mu(v)F_N,$$

where  $F_N$  is the reaction force between the bodies along the vertical direction, that is the weight of the carriage and the mass simulating the mechanism mounted on it.

The tests are conducted by measuring the torque necessary to move the system at a given constant velocity. Indeed, since no other external forces are applied, the friction force can be computed starting from the torque itself:

$$F_{fric} = T_{ml}/R,$$

as well as the friction coefficient:

$$\mu = T_{ml}/RF_N.$$

The procedure is repeated considering different velocities so as to obtain the map of friction coefficient. The velocity and the torque signal acquired during one trial are reported in the following figure (Fig. 4.41).

The results obtained suggest, in particular, that the friction coefficient is about 0.26 regardless of the velocity considered (Fig. 4.42).

The complete map of the friction coefficients to be implemented numerically in the final simulation phase is reported in the following figure (Fig. 4.43).

## 4.9 Longitudinal loading subsystem concluding remarks

This chapter has dealt with the definition of the subsystem necessary for reproducing the longitudinal load acting on the prosthetic foot during the stance phase. The final solution consists of a belt driven linear guide and a motor-reducer unit. This architecture

#### 4.9. Longitudinal loading subsystem concluding remarks

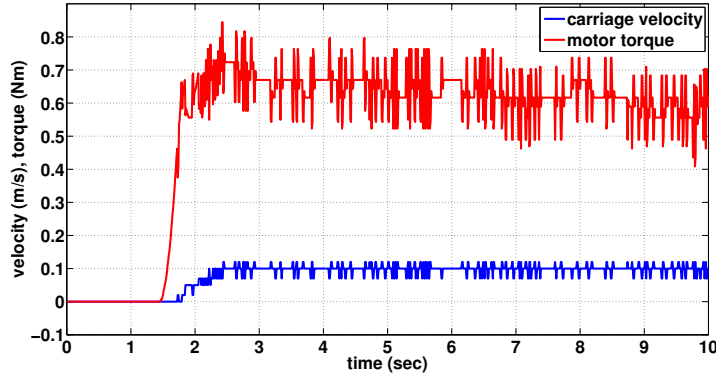


**Figure 4.41:** Experimental result in terms of torque supplied by the motor and velocity of the carriage

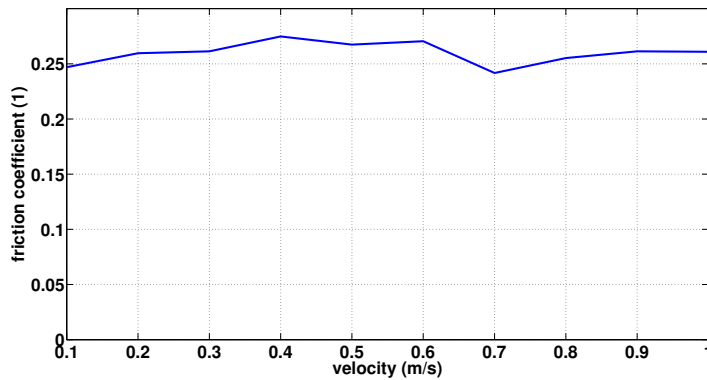


**Figure 4.42:** Experimental trend of the friction coefficient as a function of the carriage velocity

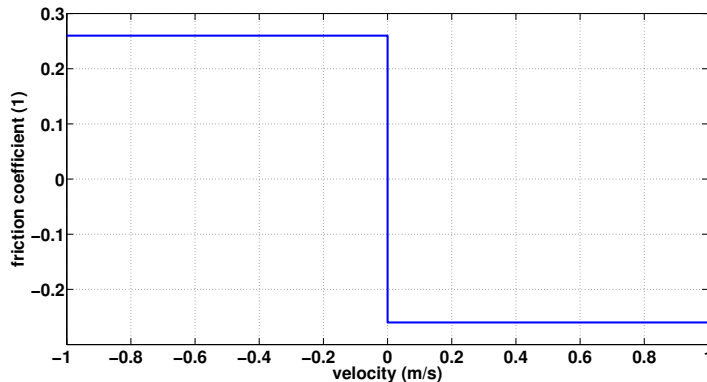


**Figure 4.43:** Numerical trend of the friction coefficient as a function of the carriage velocity

does not introduce any improvement compared to those existing in the literature from a mechanical point of view. Moreover, it leads the need to control the system alternately in terms of force and position. However, the good results obtained by other authors have prompted this choice.

Once selected the commercial components, the mathematical model of the system has been developed in order to define suitable control strategies for accurately repro-

## **Chapter 4. Longitudinal loading subsystem**

---

ducing both the force reference and the position reference. From this point of view, it is worth noting the need to implement suitable methodologies for computing the references on line as a function of the actual state of the system. Disturbances, uncertainties and unpredictable behaviors of the prosthesis limit indeed the opportunity to use standard profiles. In particular, a new method for estimating the longitudinal force component as a function of the vertical one has been introduced. Results are promising. However, the relevance of the suggested correlation should be verified by conducting further analysis.

The aforementioned algorithms have been tested and improved numerically.

Finally some experimental tests have been undertaken in order to estimate the values assumed by certain parameters, which are useful for modeling purposes.

---

# CHAPTER 5

---

## Vertical loading subsystem

---

### 5.1 Introduction

---

This chapter deals with the development of the solution necessary for reproducing the vertical load acting on the prosthetic foot due to reaction with the ground. Both the design choices and the mathematical modeling are analyzed. Then, attention is focused on the synthesis of a suitable controller to accomplish the objectives of the application. In particular, the possibility of using a linear regulator is evaluated. Finally, the system is realized and experimentally tested.

### 5.2 Mechanical architecture

---

As previously hinted, the development of the vertical loading subsystem may be largely undertaken regardless of the solution adopted in the longitudinal direction thanks to the possibility of decoupling the individual movements. On the other hand, the employment of the industrial 6-axis robot introduces some limitations that should be considered from the very beginning in order to avoid potential problems in the solution. This is worth for all the elements constituting the vertical loading subsystem which are analyzed below:

1. the actuator;
2. the mechanism architecture;
3. the measurement set-up.

### **5.2.1 Actuator**

The development process starts with the selection of the actuator that best meets the possibility to:

- apply the correct trend of the vertical force during the stance phase;
- regain and maintain the initial position before the end of the swing phase;
- introduce a compliant behavior in the load direction.

Considering these needs, the definition of the subsystem involves immediately a critical issue which requires consequently a choice: excluding electric actuators to avoid the risk of compromising the functionality of the robot rigidly connected to the prosthetic specimen. The high degree of stiffness of this kind of engine may indeed cause sudden stress changes and large disturbance forces that could compromise the functionality of the 6-axis industrial robot regardless of its load capability. This risk especially occurs when the prosthetic foot hits the force platform at the beginning of the contact stage. Indeed, this kind of commercial manipulator does not allow the application of many advanced control techniques since it is designed for common industrial applications, such as motion tracking. On the other hand, two benefits are related to the use of a pneumatic actuator:

- the compressibility of the gas inherently induces a compliant behavior in the vertical direction increasing the stability of the system and preventing potentially dangerous situations;
- the low mass of this kind of solution guarantees a reduction of the inertial loads and therefore the possibility to limit the stress at the motor driving the longitudinal loading subsystem.

However, there are also some obvious disadvantages related to the use of pneumatic actuators in servo-mechanical applications:

- the high nonlinear properties of the medium;
- the disturbances introduced by leakage at the valve and in the circuit;
- the bandwidth reduction of the system.

Nevertheless, this solution is finally adopted due to the great reliability shown in [61]. In particular, an active air spring is chosen among all the pneumatic actuators. This device is made up of a fabric rubber bellows, to contain a column of compressed air, and metallic elements, to facilitate the transfer of stored energy from the fluid to the mechanical units to be activated (Fig. 5.1).

There are two advantages related to the use of an air spring. First of all, the intrinsic stiffness of its elastic part ensures a smooth transfer of the load from the bellows to the foot during the initial contact phase. This consideration is examined more in detail during the description of the operation procedure of the vertical actuation system (Sec. 5.4). In addition, the elasticity of the bellows allows out of alignment working conditions (Fig. 5.2) and therefore the possibility to rely on bigger error margins during the design stage with respect to actuators having a rigid chamber.



**Figure 5.1:** Examples of air spring available on the market

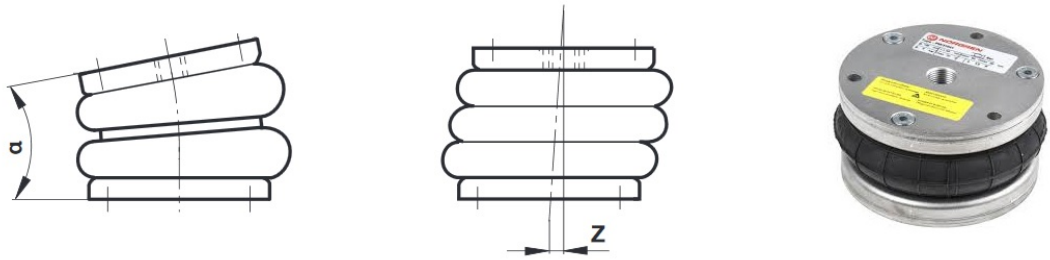


**Figure 5.2:** Out of alignment working conditions allowed by the air spring considered during this study

This device is therefore chosen to increase the robustness and stability of the system even though it substantially reduces the bandwidth of the vertical actuation subsystem. The effect of this limitation will be verified at the end of the design process when performing the numerical analyses and the experimental tests.

The air spring model is finally chosen to meet the kinematic and dynamic requirements of the application (Sec. 2.4). The model selected - NORGREN PM/31041 (Fig. 5.2) - offers the following characteristics:

- maximal stroke: 50mm;
- maximal operating pressure: 8bar;
- maximal force: 7kN;
- maximal force at maximal stroke: 2kN;
- diameter: 110mm.

### 5.2.2 Mechanism architecture

Once a suitable air spring for the application has been identified, it is necessary to develop the mechanism which transmits the vertical movement of the actuator to the support surface. During this work, the complex final architecture is obtained by iteratively modifying the basic configuration so as to meet all the requirements given below:

## Chapter 5. Vertical loading subsystem

---

- accommodate the air spring and protect it from damage;
- reduce overall dimensions and weight;
- exhibit proper structural properties;
- collect the fundamental kinematic and dynamic data;
- simplify the manufacture procedure;
- reduce the cost.

In particular, the basic configuration simply consists of the air spring and two plates used to connect the subsystem to the carriage of the linear guide and support the foot during the contact phase. Plates having a rectangular base of  $400mm \times 200mm$  are used considering that the sole of a foot covers an area of approximately  $300mm \times 100mm$ . Despite the hyperstaticity, 4 linear shafts prevent movements of the upper plate other than the vertical one. These are fixed to the top plate in order to exploit the space at the sides of the carriage of the linear guide driving the horizontal motion and consequently limit the upward development of the structure. Finally, some elements protect the pneumatic actuator from dangerous elongations (Fig. 5.3).

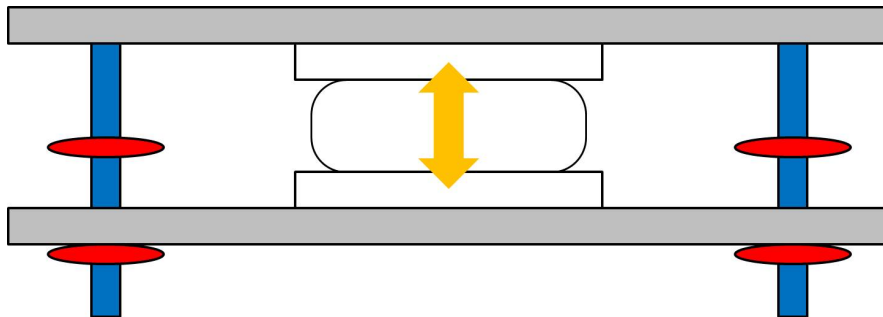


**Figure 5.3:** Basic configuration of the vertical actuating mechanism

Before defining the materials and the dimensions of the structural components so as to withstand the applied loads, the basic design is modified in order to introduce the measurement equipment.

### 5.2.3 Measurement set-up

The fundamental quantities to be collected during the test procedure are:

- the contact force between the foot and the support surface representing the ground;
- the vertical displacement of the support surface itself.

Apart from being useful parameters for evaluating the performance of the prosthesis, these quantities are essential for controlling the behavior of the vertical loading subsystem during both the stance and the swing phase. In particular, it is necessary to design and build a force plate that can separately collect data along two axes, despite the possibility of using multi-axial load cells, in order to avoid high costs and measurement interferences.

### Horizontal force component

The longitudinal force component is introduced into the system because of the friction between the prosthetic foot and the support surface representing the ground. A number of methods for obtaining this force information exist:

- measuring the current of the motor driving the carriage of the horizontal linear guide,
- measuring by means of a dynamometer the torque at the shaft of the motor;
- measuring by means of sensors the force applied by the foot at the support surface simulating the ground.

The first two techniques are limited by the lack of an accurate model of the system that allows to compensate the effect of the inertia, the friction and the flexibility on the measurement. On the other hand, plate-mounted force sensors pose challenging problem in terms mechanical design. However they are more sensitive and easier to use than joint sensors. This solution is therefore finally adopted. Obviously, this information must be collected through the sensors at the origin, that is, before the force is transmitted to the linear guides and consequently discharged at the constraints (Fig. 5.3). Moreover, it must not affect the measurement of the vertical force component.

The final solution satisfying these needs is developed starting from the equipment adopted by Tarabini et al. [80] (Fig. 5.4a) for identifying the mass matrix of people standing in a quiet upright position (Fig. 5.4b).

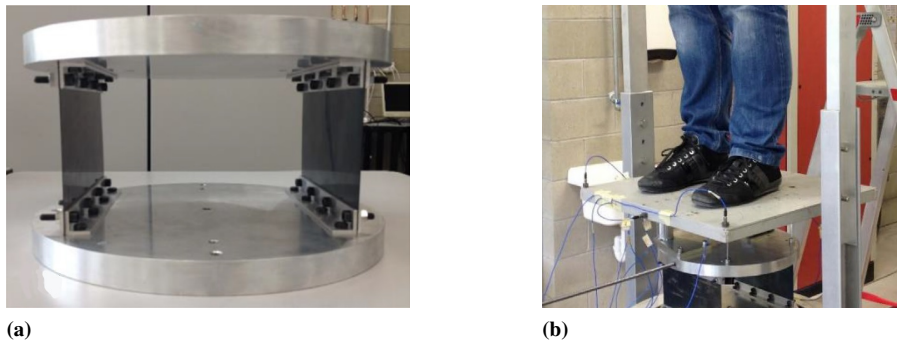


**Figure 5.4:** Solution developed by Tarabini et al. for identifying the mass matrix of people

This device consists of a rigid support plane and two flexible foils designed to offer:

- infinite rigidity in vertical direction;
- low rigidity in longitudinal direction.

As a consequence, the solution ensures complete transmission of the vertical force, so that it can be successively measured, and access to the horizontal loads starting from the deflection of the structure. Although strain gauges are probably the best solution, it is also possible to use load cells stiffer than the foils in the longitudinal direction. Once a suitable model has been identified, the foils are therefore appropriately scaled in order to satisfy the aforementioned need and to reduce the vertical encumbrance as

## Chapter 5. Vertical loading subsystem

---

much as possible. The available load cells - Honeywell Precision Miniature Load Cell (Fig. 5.5) - offer the following features:

- strain gauge technology;
- maximal load  $500N$ , both in tension and compression;
- deflection at full scale  $0.03mm$ .



**Figure 5.5: Load cell implemented**

Their axial stiffness is estimated starting from the awareness of the deflection of the cell at full scale, that is, about  $16500N/mm$ . Once this parameter is known, the steps performed in order to design the flexible foils are the following:

- define a section that can support the vertical loads;
- determine the minimum height required to ensure the necessary deflection rigidity.

Given the availability of  $0.5mm$  thick foils, once checked their ability to withstand loads 3 times higher than the maximum expected, it is sufficient to compute the height. In particular, a height of  $40mm$  provides a stiffness equal to  $32N/mm$  in the longitudinal direction, i.e.  $2/1000$  of the load cell stiffness. This ratio is further reduced to  $1/1000$  by considering two load cells in parallel. All the simulation are performed in Solidworks using the finite element method (FEM) toolbox.

However, this kind of solution does not exclude movements of the support surface within the horizontal plane different from the longitudinal one. The deflection produced by these phenomena may negatively influence the measurement. Different options are available to cope with this problem:

- spherical joints;
- spherical washers;
- slender beams.

The choice is strictly limited by the necessity to exclude backlash at the connection level so as to avoid measurement errors when the force moves from positive to negative and vice versa. Spherical joints and spherical washers do not guarantee this opportunity. Thus, slender beams are necessarily implemented. These must prevent the transmission of bending loads as well as instability due to buckling. The thinnest rod meeting this description is  $200mm$  long and has a diameter of  $4mm$ . However, the diameter is augmented to  $5mm$  in order to increase the resistance and facilitate the manufacturing process. A schematic representation of the solution described so far is shown below (Fig. 5.6).

### Vertical force component

Four load cells of the same type as those used in the longitudinal direction are placed between the spring and the upper plate in order to measure the vertical force component. Given the impossibility of attaching the cells directly to the pneumatic actuator, it is necessary to insert an additional support plate. In particular, this plate is designed to meet the following two criteria:

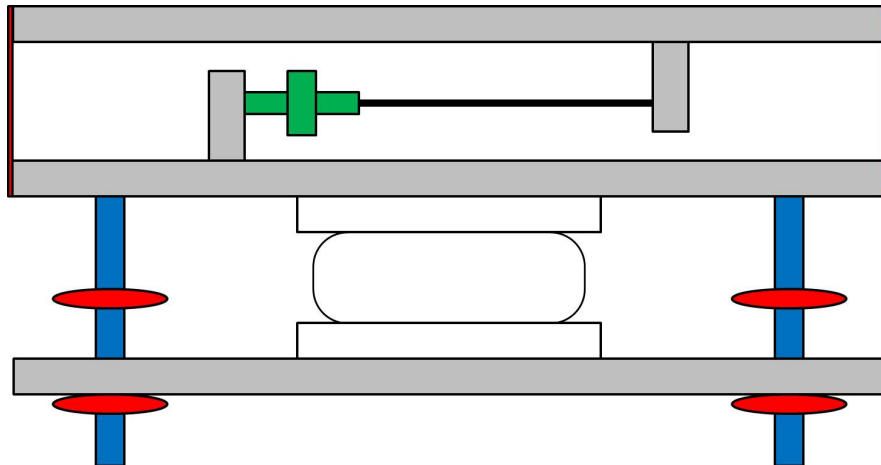


**Figure 5.6:** Solution for measuring the load in longitudinal direction

- contain the vertical development of the system;
- place the load cells as near as possible to the corners of the upper plate in order to reduce the excessive stress resulting from the application of eccentric loads.

Since the measurement may be compromised by the deformation of the plates, the parts are finally connected through spherical joints (Fig. 5.8). The final result is shown in figure (Fig. 5.7).

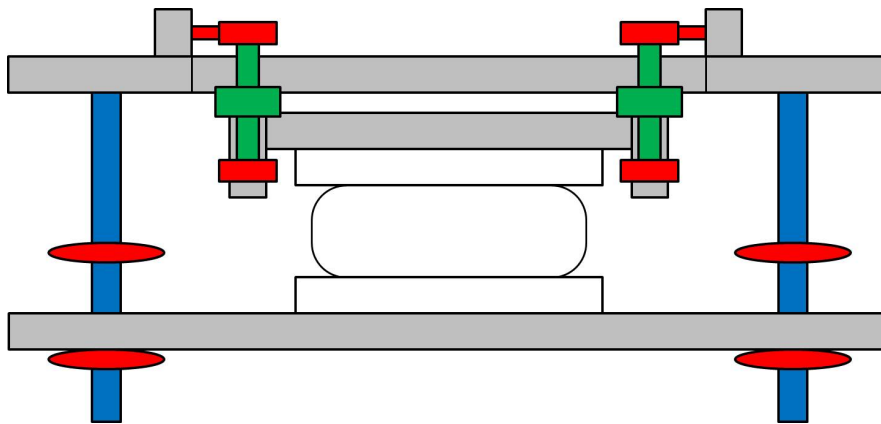


**Figure 5.7:** Solution for measuring the load in vertical direction

#### Vertical displacement

A linear potentiometer is used to determine the movement of the upper plate in respect of the lower plate. The maximal stroke of the transducer adopted - DSPM Industria CLS1322 (Fig. 5.9) - is 50mm, i.e. the same of the air spring.

Once the architecture of the system has been determined, it is possible to define the dimensions of its elements. The scheme of the whole structure is shown in the figure (Fig. 5.10).

## Chapter 5. Vertical loading subsystem

---



**Figure 5.8:** Spherical joints implemented



**Figure 5.9:** Linear potentiometer implemented

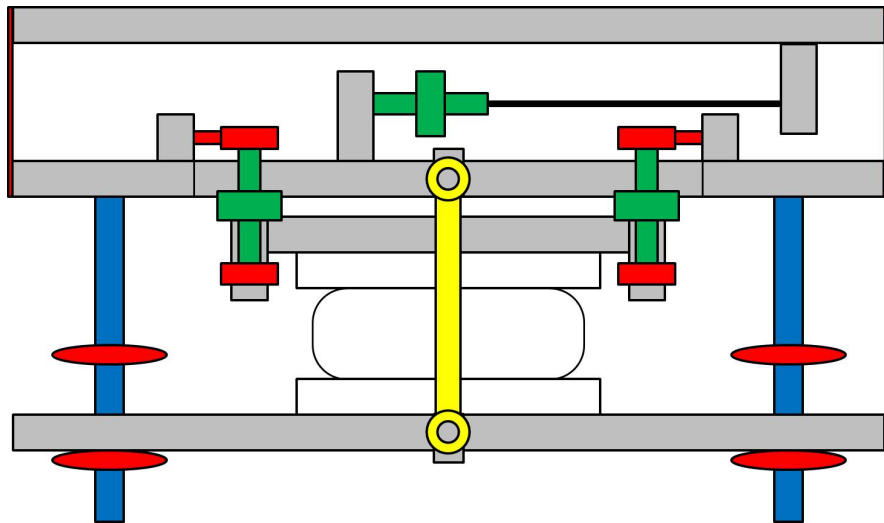


**Figure 5.10:** Schematic representation of the final solution

### 5.3 Structural design

---

There are five structural elements that need to be suitably designed:

1. vertical guide system (green);
2. lower plate (violet);
3. intermediate plate connected to the air spring (blue);
4. intermediate plate connected to the flexible foils (red);
5. upper plate (yellow).

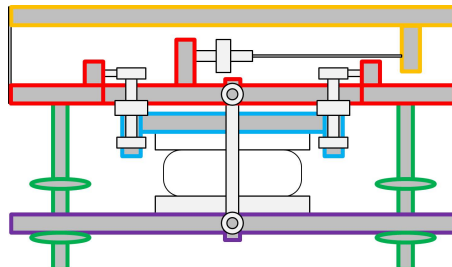


**Figure 5.11:** Mechanism sections

#### 5.3.1 Vertical guide system

The vertical guide system consists of four main elements:

- the linear shafts;
- the bushings;
- the corresponding supports;
- the collar clamps.

Since the structural failure of the shafts can have destructive consequences on the entire system, these elements are designed considering a high safety factor. In particular, the final diameter is calculated under the hypothesis that the entire load is supported only by one of the four steel shafts. These shafts are mainly stressed in terms of bending due to the horizontal force applied by the foot on the support surface. The maximum value of this force is rounded off to 200N (Sec. 2.4.).

The lever arm is computed starting from the awareness of the maximum height of both the air spring, 90mm, and the load cells, 44.45mm. The contribution of the spacers introduced to contain the vertical development of the structure is not considered (Fig. 5.7). Finally, their sum is conservatively rounded off to 150mm even if during operation the elongation of the actuator is likely lower.

It is therefore finally possible to compute the value assumed by the bending moment, 30Nm, and apply the Navier equation in order to compute the diameter of the shafts:

$$\sigma_{max} = S_F \frac{(M_f R)}{J},$$

where  $S_F$  is an additional safety factor, 2,  $\sigma_{max}$  is the yield strength of the mild steel, 215MPa,  $R$  and  $J$  are the radius and the moment of inertia of the shaft section about the neutral axis. As a result, the minimum acceptable diameter is about 14mm. Since this size is not available in the catalog, shafts having 16mm diameter are finally chosen. Sintered bronze bushings 5.12a, support devices 5.12b, and collar clamps 5.12c having the same size are consequently employed.



**Figure 5.12:** Commercial components constituting the vertical guide system

Thereafter, the sketch of the plates is defined. This task is initially accomplished so as to guarantee that they can properly perform their function. Then, their thickness is defined in order to reach a good tradeoff between weight reduction and structural properties. In particular, the final value is computed so as to ensure that their maximal deflection does not exceed 1/10mm under the application of 1000N in vertical direction. This property is assessed through the execution of finite-elements (FE) simulations in SolidWorks. Only plates made of aluminum are considered in order to reduce the weight of the system. Additional improvements are finally undertaken in order to further reduce the overall weight of the solution.

### 5.3.2 Lower plate

The main functions of the lower plate are:

## Chapter 5. Vertical loading subsystem

- accommodate the base of the actuator;
- suit the shape of the carriage of the linear guide;
- fit the bushings and give the opportunity to align them in concert with the linear shaft;
- host one extremity of the potentiometer.

Here are the top and frontal view of the sketch satisfying all these requirements (Fig. 5.13). Some dimensions are reported to give an idea of the overall size of the component. It is worth to note the decision to fit the bushings on additional blocks equipped with eyelets in order to cope with the hyperstaticity of the system.

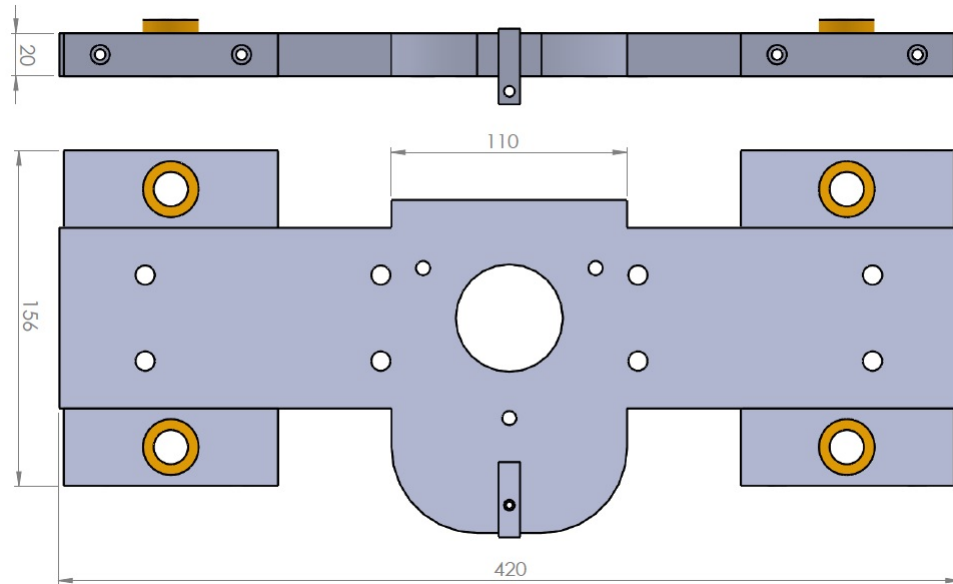


**Figure 5.13:** Final design of the lower plate

### 5.3.3 Intermediate plate connected to the air spring

The main functions of this component are:

- suit the top of the actuator;
- allow access to the air inlet;
- accommodate the spherical joints for connecting the load cells measuring the vertical load;
- reduce the overall height of the system.

The final design is obtained as the sum of three different blocks screwed together so as to facilitate the manufacturing. Its representation is shown in the following figure (Fig. 5.14).

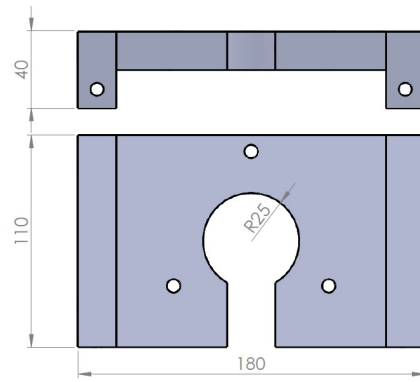


**Figure 5.14:** Final design of the intermediate plate connected to the air spring

#### 5.3.4 Intermediate plate connected to the flexible foils

The main functions of this component are:

- fit the shape of the upper plate to allow their connection through the flexible foils;
- accommodate the load cells for measuring both the vertical and longitudinal force components;
- accommodate the supports that allow to align and fasten the linear shafts.

The final design is realized by modifying a plate having a rectangular base of  $400mm \times 200mm$  so as to fit the dimensions of the upper surface and fulfill the above list of requirements. On the other hand, the final thickness is computed in SolidWorks in order to meet the above mentioned structural requirements, i.e. maximum deflection lower than  $1/10mm$ . Both the result of this simulation and the final design of the plate are reported in the following figures (Fig. 5.15, 5.16).

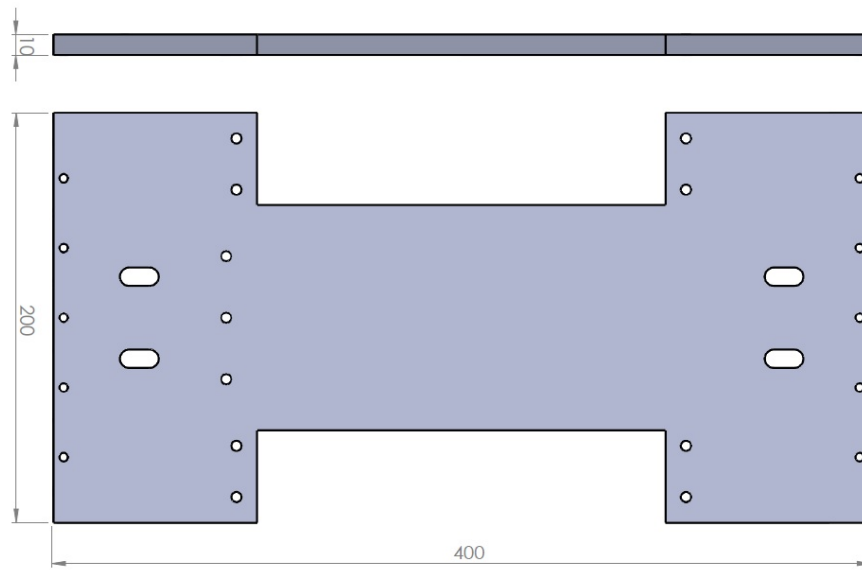


**Figure 5.15:** Final design of the intermediate plate connected to the flexible foils

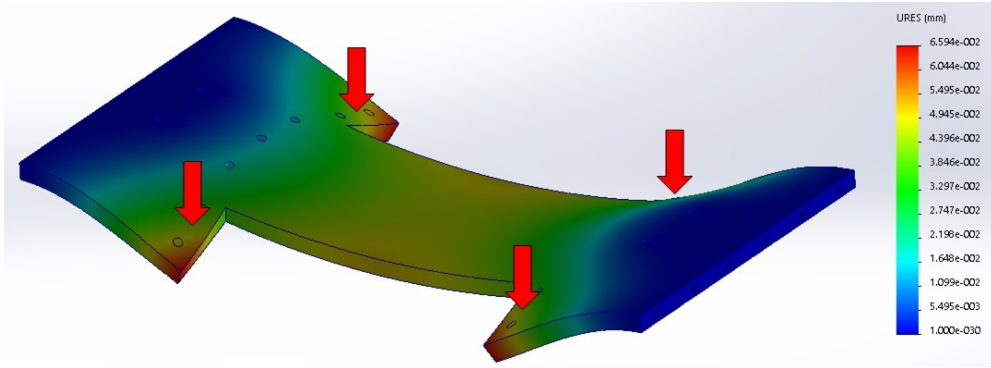


**Figure 5.16:** FE analysis of the intermediate plate connected to the flexible foils

### 5.3.5 Upper plate

Finally the requirements related to the design of the upper plate are given:

- facilitate the contact with the foot;
- fit the shape of the intermediate plate to allow their connection through the flexible foils;
- accommodate the loads cell for measuring the loads in longitudinal direction;
- host the upper extremity of the potentiometer.

Even in this case, FE simulations are performed in SolidWorks to verify that the maximal deflection is strictly lower than  $1/10\text{mm}$  regardless of the point where the force is applied by the foot. The results are shown in the following figures (Fig. 5.18,5.19).

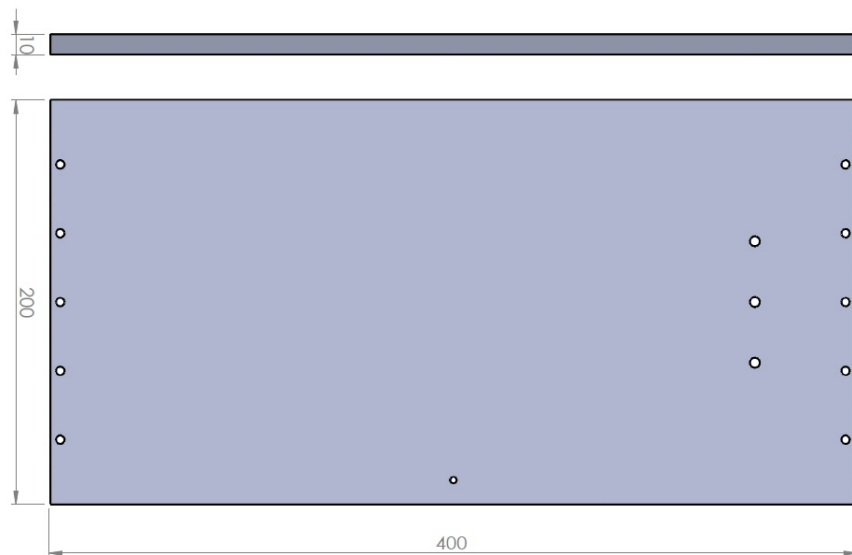


**Figure 5.17:** Final design of the upper plate

### 5.3. Structural design

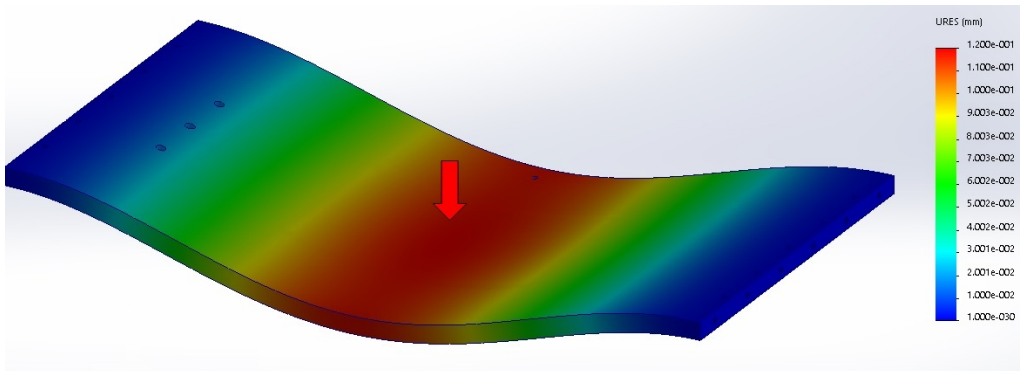


**Figure 5.18:** First FE analysis of the upper plate

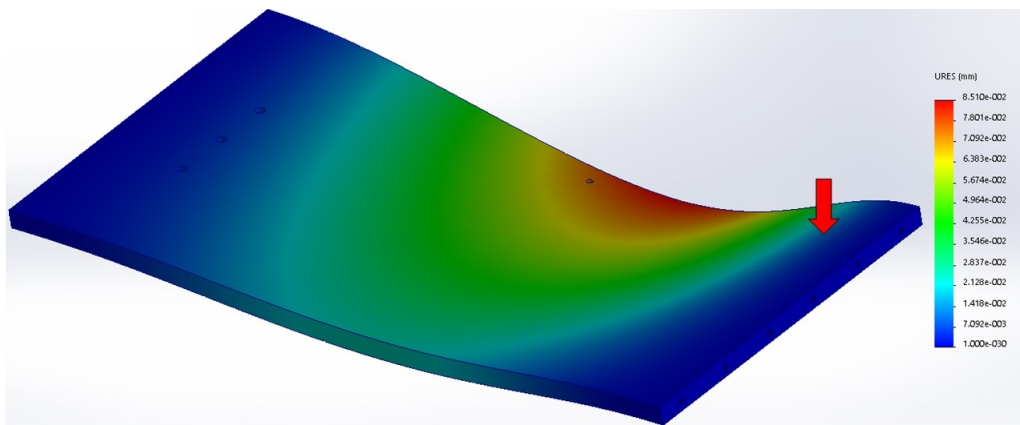


**Figure 5.19:** Second FE analysis of the upper plate

Despite the attempts to make it simple, the final solution is rather complex. After all, it is able not only to perform displacements and supply the forces in the vertical direction, but also to measure the motion of the upper plate and the forces due to reaction with the foot in the sagittal plane. The following figure shows the latest CAD version of the entire system (Fig. 5.20).



**Figure 5.20:** Final rendering of the vertical loading subsystem

## **Chapter 5. Vertical loading subsystem**

---

Before defining the mathematical model and developing the control logic of the vertical loading subsystem its operation procedure is reviewed.

### **5.4 Operation procedure**

---

From a functional point of view, the solution proposed so far allows to control the air spring exclusively in terms of force during all the phases of the test. As previously hinted, this opportunity is introduced by the intrinsic stiffness of the air spring bellows. In particular, the idea is to follow two types of reference:

- a constant offset value;
- the gait analysis trend of force.

Four main working phases are therefore recognizable:

1. Lack of contact:

When the foot is still moving up in the air (swing phase), the force (and therefore the inner pressure) required by the air spring to hold the subsystem at the maximal vertical height is constant and equals that necessary to support the weight of the subsystem itself and the elastic return of the spring bellows.

2. Initial stage of contact:

Subsequently, during the initial stage of contact, the pneumatic actuator continues to supply the same force (constant inner pressure) while being dragged downward by the movement of the foot, which in turn is subjected to an increasing force due to the simultaneous return of the spring to its resting length. In particular, the elastic characteristics of the air spring selected guarantees a linear increment of the force, i.e. in accordance with the slope of the actual reference force (Fig. 5.21).

3. Stable contact:

When the force applied to the foot reaches a predetermined offset value, the aim is to modulate the inner pressure so as to reproduce the correct gait analysis trend of force (Fig. 5.21).

4. End of contact:

Finally, when the force drops below the predetermined offset value, the application of the constant force results in a gradual decrease of the load applied to the foot and the return of the platform to the initial height. Once again, the trend of the force is linear like the reference thanks to elastic intrinsic characteristics of the air spring (Fig. 5.21).

Therefore, the transition from one reference to another occurs when the force applied to the foot is sufficiently high to ensure a stable contact condition. Considering that during the initial stage of contact, the spring is basically exploited almost passively (linear elastic characteristic at constant inner pressure) such a transition is even determinable on the basis of the vertical height of the support surface. The linear potentiometer is therefore used to measure its displacement and consequently to distinguish

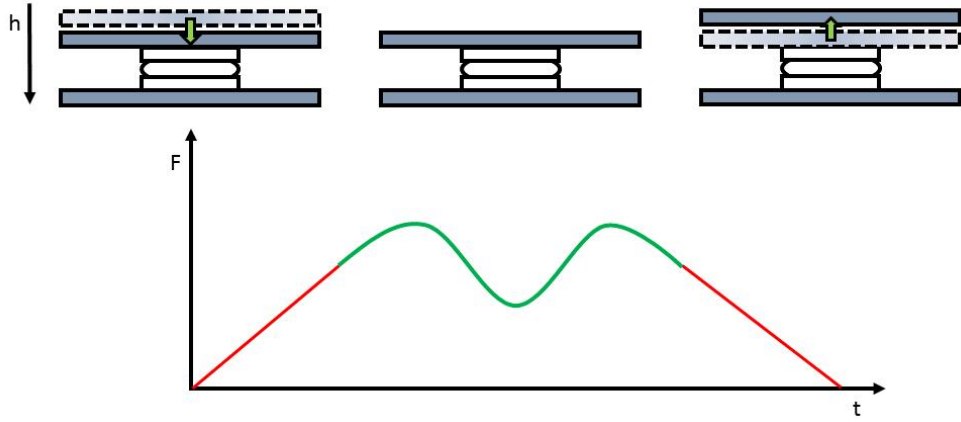


**Figure 5.21:** Working phases of the vertical loading subsystem

the stability of the contact condition. On the other hand, the load cells are used just to measure the force acting on the foot.

Once defined the operation procedure of the subsystem, the equations describing the phenomenon are written. Then, although it is not possible to predict the exact behavior of the subsystem before it is built and tested for data collection, the formulas are implemented in MATLAB to define a suitable control strategy, rate its performance, and evaluate any critical aspect of the proposed mechanical solution.

## 5.5 Mathematical model

Although complex, the system may be modeled as a mass moving vertically under the effect of the force generated by the pressure within the air spring and the load applied by the foot. The term related to pressure is significantly affected by the dynamic behavior of the air within reservoirs, compressors, tubes and servo-valves. Thus, these components cannot be neglected in the modeling phase unless simplifications. For instance, in this case the use of reservoirs, compressors and long pipes is not expected. As a consequence, only the air spring and the mass flow-rate in the servo-valve are modeled. The dynamics of the valve mechanics itself is not included because its bandwidth is reasonably greater than the closed-loop bandwidth of the system. Finally, the mechanical load is introduced. The model is therefore constituted by three main components:

1. the air spring;
2. the servo-valve;
3. the mechanical load.

Once their individual mathematical models are developed, the equations are collected and implemented in MATLAB, and the theoretical design techniques are used to address the synthesis of a linear controller. Finally, the performance of the regulator is evaluated through a numerical nonlinear model of the system developed using Simulink and SimMechanics.

### 5.5.1 Air spring model

The air spring is essentially constituted by a rubber fabric bellows and metallic elements that allow to fasten the device to the mechanical elements to be actuated or supported. The main purpose of the bellows is to contain a column of air to exploit the dynamic characteristics of the gas. Hence, the behavior of the air spring is related to both the intrinsic characteristics of the rubber and the compressed air. The net force provided by the air spring is therefore substantially given by the sum of two nonlinear stiffness contributions:

- the intrinsic stiffness of the elastic part;
- the variable stiffness related to the compressed gas.

The first parameter can be roughly obtained from the graphs provided by the manufacturer once the working height and the working pressure are known. Thus, the first contribution can be expressed as follows:

$$F_i = -km(y_m, p_m)(y_m - y_{m0}) - r_m \dot{y}_m,$$

where  $y_m$  and  $y_{m0}$  are the actual and resting length of the spring,  $k_m(y_m, p_m)$  and  $r_m$  are the stiffness and the damping of the bellows.

The thermodynamic transformations affecting the gas inside the spring are necessary instead to obtain the second contribution [5, 17]. Indeed, these phenomena are not negligible if the aim is to properly simulate the active usage of the pneumatic actuator. The steps that led to the final equations are reported below with reference to the schematic picture of the pneumatic system (Fig. 5.22).

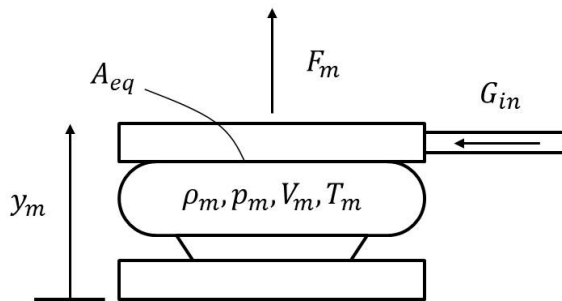


**Figure 5.22:** Schematic representation of the air spring

The following assumptions are considered in the process:

- the working fluid is an ideal gas satisfying the ideal gas law;
- the heat capacity ratio,  $k = c_p/c_v$ , is constant;
- the processes are adiabatic, i.e. there is no heat transfer between components and the environment;
- both the inertial and gravitational effects can be neglected.

First, the ideal gas law and the mass continuity equation are given,

$$p_m V_m = \rho_m V_m R T_m, \quad \frac{d(\rho_m V_m)}{dt} = G_{in},$$

where  $\rho_m$  is the air density,  $p_m$  and  $V_m$  are the inner pressure and volume of the spring,  $R$  and  $T_m$  respectively the universal constant and the temperature of the gas.  $G_{in}$  indicates the mass flow-rate entering the volume  $V_m$ . Assuming that the dynamics of the process is so rapid to not allow heat exchange, i.e. the transformation of the gas is adiabatic,

$$\frac{p_m}{\rho_m^k} = \frac{p_{m0}}{\rho_{m0}^k},$$

it is possible to derive the equation describing the state of the actuator according to the flow of air entering it,

$$\dot{p}_m V_m + k p_m \dot{V}_m = k G_{in} R T_m.$$

Obviously, the temperature inside the air spring is assumed to vary according to the adiabatic criteria,

$$T_m = \left( \frac{p_m}{p_{m0}} \right)^{\frac{k-1}{k}} T_{m0}.$$

In addition, the assumption that the volume varies linearly as a function of the spring length is carried out,

$$V_m = V_{m0} + A_{eq} (y_m - y_{m0}), \quad \dot{V}_m = A_{eq} \dot{y}_m,$$

where  $V_{m0}$  is the initial volume and  $A_{eq}$  the effective area of the spring. Finally, assuming that the effective area of the air spring is constant, it is possible to calculate the force due to the pressure,

$$F_p = A_{eq} (p_m - p_{atm}),$$

and the total amount delivered by the pneumatic actuator,

$$F_m = F_p + F_i = A_{eq} (p_m - p_{atm}) - k_m (y_m, p_m) (y_m - y_{m0}) - r_m \dot{y}_m.$$

### 5.5.2 Servo-valve model

A servo-valve model is necessary to express the flow rate of air entering the air spring,  $G_{in}$ , as a function of the other measurable physical quantities. Several models are available in the literature depending on whether the need is to have a more or less accurate description of the component [68]. In this section, a nonlinear model able to discern a choked flow condition is initially proposed. Since this is not suitable for analytically defining the parameters of a linear controller, a simplified model of the valve is subsequently introduced.

### Nonlinear servo-valve model

The more complex mathematical models are based on the observation that the valve can be considered a fixed-area sharp-edged orifice from a functional point of view [14]. Similarly, the mass flow-rate of the ideal gas through the valve is initially modeled following the flow equations originally proposed by Sanville [71] (in accordance with the standard ISO 6358) and discarding the temperature correction term during this work:

$$G_V = \begin{cases} C_V p_1 & \text{if } (p_2/p_1) \leq b_v \\ C_V p_1 \sqrt{1 - \left( \frac{(p_2/p_1) - b_v}{1 - b_v} \right)^2} & \text{if } (p_2/p_1) > b_v \end{cases},$$

where

$$C_V = \frac{C_{V,max}}{S_{V,max}} S_V, \quad b_v = \left( \frac{2}{k+1} \right)^{\frac{k}{k-1}}.$$

In this system:

- $G_V$  is the mass flow-rate of air through the servo-valve;
- $C_V$  is the flow coefficient of the servo-valve;
- $S_V$  represents the valve opening;
- $p_1$  and  $p_2$  are the upstream and downstream pressures of the valve;
- $b_v$  is the critical pressure ratio;
- $k$  is the heat capacity ratio.

Since in this case the use of long pipes is not expected, the mass flow-rate entering the air spring volume,  $G_{in}$ , is easily computable once  $p_1$  and  $p_2$  are known. During the loading phase, that is, the inflation of the air spring, the upstream pressure relates to the supply tank, while the downstream to the air spring. Therefore,  $G_{in} = G_V$ . In the unloading phase the upstream pressure relates to the air spring and the downstream one to the atmosphere. Since the air flow is outgoing from the volume of the air spring  $G_{in} = -G_V$ .

In the light of the above information, the behavior of a nozzle is rather complex. Indeed, its equation is nonlinear and radically different depending on whether the phase is that of inflation or deflation. Therefore, an alternative method, but reasonably valid in view of the wide spread in the literature, is introduced in order to perform the preliminary linear analysis. This model is shown below.

### Linear servo-valve model

The linear model of the valve is simply based on the following two observations:

- the relation between the supply voltage,  $V_c$ , and the controlled pressure,  $p_c$ , is assumed purely linear;
- the change in the valve downstream pressure,  $p_c$ , is not instantaneous.

This component is therefore generally treated as a second-order linear dynamic system:

$$\ddot{p}_c + 2\xi\omega_0\dot{p}_c + \omega_0^2 p_c = \omega_0^2 k_e V_c$$

where:

- $k_e$  is the static gain of the valve;
- $\omega_0$  is the natural frequency in  $rad/s$ ;
- $\xi$  is the damping ratio.

However, this model does not directly return the value of air mass flow-rate. As a consequence, it is necessary to introduce the relation between the pressure drop and the air flow passing through the tube connecting the servo-valve and the air spring,

$$p_c - p_m = R_{eq}G_{in}.$$

By introducing a constant resistance value this relation results linear.

### 5.5.3 Mechanical load model

The load supported by the air spring is constituted by the gravitational and inertial effects of the mechanical apparatus as well as by the contact force exchanged between the prosthetic foot and the support surface. The former contribution is simulated by introducing a mass comparable to that of the physical set-up shown in the previous section:

$$F_M = -M(g + \ddot{y}_m).$$

On the other hand, the foot-ground contact force is defined according to the penetration model stated in [74] to investigate the dynamic characteristics of normal and transfemoral amputee locomotion. Figure 5.23 reports a schematic illustration of the model. Clearly, the vertical component is calculated as the sum of an elastic and a viscous contribution,

$$F_c = -k_c d - r_c(d)\dot{d},$$

where the stiffness,  $k_c$ , is constant, while the damping,  $r_c$ , a nonlinear function of the bodies penetration value,  $d$ ,

$$r_c = \begin{cases} r_{c,max} \left| \frac{3d^2}{h^2} - \frac{2d^3}{h^3} \right| & \text{if } 0 \leq d < h \\ r_{c,max} & \text{if } d \geq h \end{cases}.$$

The penetration value,  $d$ , is computable based on the vertical position of both the foot,  $y_f$ , and the air spring,  $y_m$ ,

$$d = y_m - y_f.$$

on the other hand, the constant parameters of the foot-ground contact model are obtained from the literature [74] and illustrated in the following table (Tab. 5.1).

**Table 5.1:** Parameters of the foot-ground contact model

Parameter	Value
$k_c$	$7.5 \cdot 10^4 N/m$
$r_{c,max}$	$7500 Ns/m$
$h$	$0.01 m$

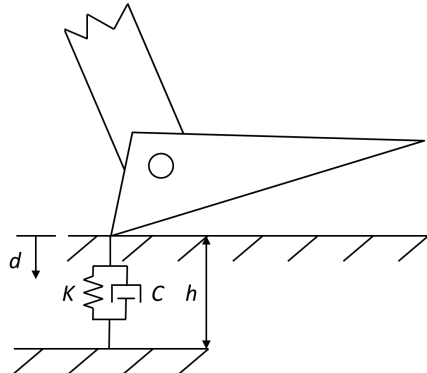


**Figure 5.23:** Foot ground penetration contact model

## 5.6 Numerical simulation

---

The aim of the aforementioned system is to apply the vertical reference force identified during the gait analysis (Sec. 2.4) to the prosthetic foot. The air flow entering the air spring should therefore be accurately regulated in real time according to a suitable logic. Due to the innate nonlinear properties of the medium and unknown disturbances, such as leakage at the valves, the control of pneumatic manipulators can be a challenging problem. From this point of view, it's claimed that conventional PID feedback controllers do not yield sufficient control performance when high precision is required. Indeed, when the state of the system is far from the linearization point, nonlinearities can degrade system performance and sometimes impair the stability of the system. Various approaches have been proposed to cope with this problem. Among these, 'sliding mode' techniques have proven to be efficient tools to control complex high-order nonlinear dynamic plants operating under uncertainty conditions. Nevertheless, the intention, during the first stage of study of the bench, is to assess the possibility of using a linear controller to reproduce the correct response, thereby avoiding unnecessary complications such as the definition of nonlinear control algorithms. The steps performed to accomplish this objective are analyzed below.

### 5.6.1 Linear analysis

A linear model of the entire system is essential for developing a PID controller with the theoretical design techniques. Thus, the equations described above are collected and linearized in this section. In particular, the synthesis of the controller is undertaken considering for simplicity just the stable contact phase. The system physical quantities are indeed subjected just to small deviations around such equilibrium point. Moreover, the modeling of the passive behavior of the air spring is useless from the control point of view. In fact, during this period, the constant pressure within the spring is controlled by the valve inner logic, which is inaccessible (Fig. 5.24, 5.25).

As a consequence, reference is made to the scheme shown in figure during this analysis (Fig. 5.26). For further explanation refer to the description of the operation procedure given before (Sec. 5.4).

## 5.6. Numerical simulation



**Figure 5.24:** Block diagram of the air spring open loop control system

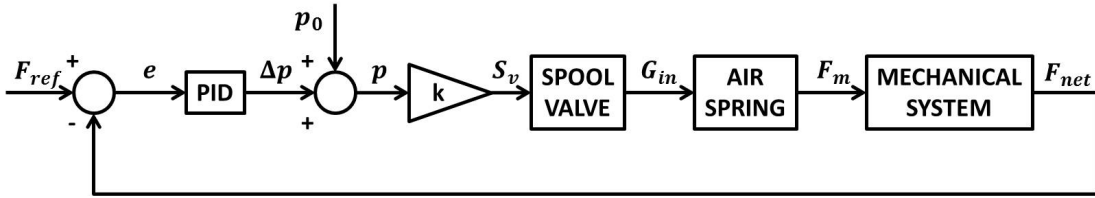


**Figure 5.25:** Block diagram of the air spring closed loop control system

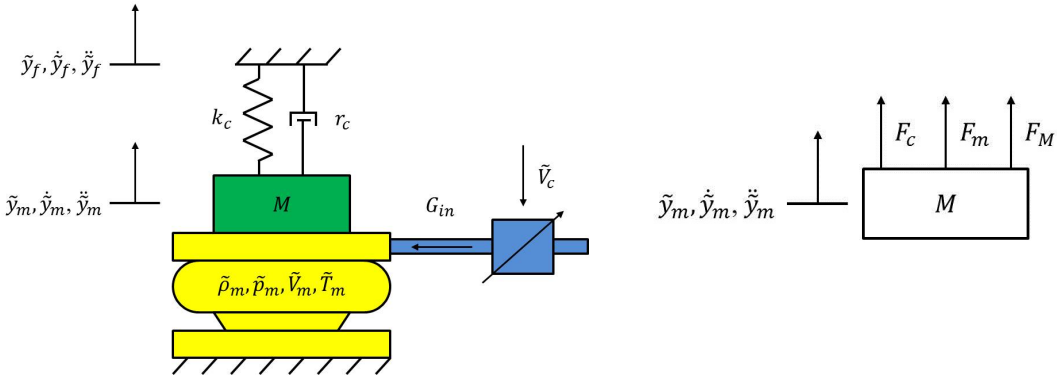


**Figure 5.26:** Schematic representation of the vertical loading subsystem during the stable contact phase

**Figure 5.27:** Model considered during the application of the Euler method

### System linear model

The equation describing the dynamics of the apparatus composed by the mechanical load and the air spring is first derived using the Newton-Euler method (Fig. 5.27),

$$\Sigma F_y = F_m + F_M + F_c = 0.$$

By replacing the relative expressions, discarding the constant forces at the equilibrium, and rearranging the terms, the previous equation becomes

$$M\ddot{y}_m + (r_m + r_c)\dot{y}_m + (k_m + k_c)\tilde{y}_m = r_c\dot{\tilde{y}}_f + k_c\tilde{y}_f + A_{eq}\tilde{p}_m,$$

and the set of equations of the entire system assumes the following form according to the same set of coordinates

$$\begin{cases} M\ddot{y}_m + (r_m + r_c)\dot{y}_m + (k_m + k_c)\tilde{y}_m = r_c\dot{\tilde{y}}_f + k_c\tilde{y}_f + A_{eq}\tilde{p}_m \\ \dot{\tilde{p}}_m A_{eq}\tilde{y}_m = kG_{in}R\tilde{T}_m - k\tilde{p}_m A_{eq}\dot{\tilde{y}}_m \\ \ddot{\tilde{p}}_c + 2\xi\omega_0\dot{\tilde{p}}_c + \omega_0^2\tilde{p}_c = \omega_0^2 k_e \tilde{V}_c \\ \tilde{p}_c - \tilde{p}_m = R_{eq}G_{in} \\ \tilde{F}_n = k_c(\tilde{y}_m - \tilde{y}_f) + r_c(\dot{\tilde{y}}_m - \dot{\tilde{y}}_f) \end{cases},$$

## Chapter 5. Vertical loading subsystem

---

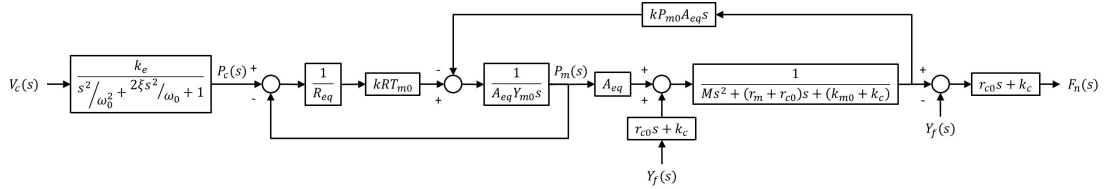
where obviously the linear model of the servo-valve is considered (even if it is not suitable for choked flow condition) and  $\tilde{F}_n$  corresponds to the change in the net force applied to the foot. This set of equations is still nonlinear and therefore not useful to assess the possibility of using a PID controller. However, by applying linearization about an arbitrary equilibrium point (whose initial conditions ( $p_{m0}, T_{m0}, y_{m0}, y_{f0}$ , etc.) are computed by performing the static equilibrium) the system becomes:

$$\begin{cases} M\ddot{y}_m + (r_m + r_{c0})\dot{y}_m + (k_{m0} + k_c)\tilde{y}_m = r_{c0}\dot{\tilde{y}}_f + k_c\tilde{y}_f + A_{eq}\tilde{p}_m \\ \dot{\tilde{p}}_m A_{eq}y_{m0} = kG_{in}RT_{m0} - kp_{m0}A_{eq}\dot{\tilde{y}}_m \\ \ddot{\tilde{p}}_c + 2\xi\omega_0\dot{\tilde{p}}_c + \omega_0^2\tilde{p}_c = \omega_0^2k_eV_c \\ \tilde{p}_c - \tilde{p}_m = R_{eq}G_{in} \\ \tilde{F}_n = k_c(\tilde{y}_m - \tilde{y}_f) + r_{c0}(\dot{\tilde{y}}_m - \dot{\tilde{y}}_f) \end{cases},$$

and applying the Laplace transformation it evolves into:

$$\begin{cases} Ms^2Y_m(s) + (r_m + r_{c0})sY_m(s) + (k_{m0} + k_c)Y_m(s) = r_{c0}sY_f(s) + k_cY_f(s) + A_{eq}P_m(s) \\ sP_m(s)A_{eq}Y_{m0} = kG_{in}(s)RT_{m0} - kP_{m0}A_{eq}sY_m(s) \\ s^2P_c(s) + 2\xi\omega_0sP_c(s) + \omega_0^2P_c(s) = \omega_0^2k_eV_c(s) \\ P_c(s) - P_m(s) = R_{eq}G_{in}(s) \\ F_n(s) = k_c(Y_m(s) - Y_f(s)) + r_{c0}s(Y_m(s) - Y_f(s)) \end{cases},$$

This is a Multi-Input-Single-Output (MISO) system whose block diagram representation is:

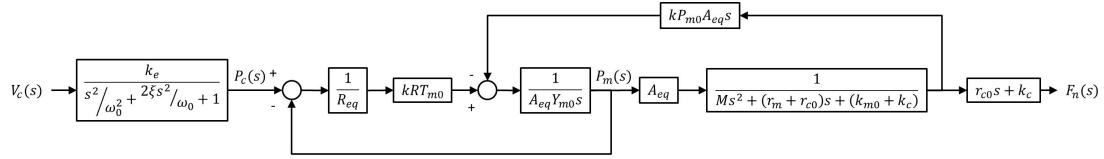


Clearly, the change in the net force depends on the amount of pressure in the air spring as well as on the motion of the foot. However, the movement performed by the latter in vertical direction during the stable phase of contact is small enough to be negligible (Sec. 2.4). By blocking the movement of the foot,  $y_f = 0$ , the set of equations then becomes:

$$\begin{cases} Ms^2Y_m(s) + (r_m + r_{c0})sY_m(s) + (k_{m0} + k_c)Y_m(s) = A_{eq}P_m(s) \\ sP_m(s)A_{eq}Y_{m0} = kG_{in}(s)RT_{m0} - kP_{m0}A_{eq}sY_m(s) \\ s^2P_c(s) + 2\xi\omega_0sP_c(s) + \omega_0^2P_c(s) = \omega_0^2k_eV_c(s) \\ P_c(s) - P_m(s) = R_{eq}G_{in}(s) \\ F_n(s) = (k_c - r_{c0}s)Y_m(s) \end{cases},$$

and the block diagram assumes the following simplified form:

## 5.6. Numerical simulation



i.e. the form of a Single-Input-Single-Output (SISO) system.

This set of equations is finally useful to derive the transfer function between the net force applied to the foot and the supply voltage of the valve,  $G_2(s) = (F_n(s))/(V_c(s))$ , and perform both the stability analysis of the system and the synthesis of the controller.

### Stability analysis and control synthesis

The stability analysis of the system is performed numerically. In particular, during this work, MATLAB is chosen because of its usage easiness and its computational robustness.

The stability is assessed by analyzing the poles of the transfer function  $G_2(s)$ . Clearly the expression of this function rely on the value assumed by the various physical quantities about the linearization point. As a consequence, it was first necessary to distinguish the possible working conditions. Six equilibrium configurations are identified in the end, i.e. one for each value of stable contact force considered:

$$F_{n0} = [500, 600, 700, 800, 900, 1000] \text{ N.}$$

It is worth noting that such force values correspond to the possible weight of the user of the prosthesis. The values assumed by the other physical quantities are reported in the following table as a function of the weight category (Tab. 5.2).

It is also worth noting that the pressure,  $P_{m0}$ , is constant and equals to that necessary to hold the subsystem at the maximal vertical height during the swing phase, that is when the foot is moving in the air. As a consequence also the inner stiffness of the bellows,  $k_{m0}$ , is constant. According to the data reported in the corresponding datasheet (Fig. 5.28), the relation between the supplied force and the elongation is indeed almost linear given a pressure value and under the hypothesis of constant equivalent area. Thus, the stiffness value is just a function of the inner pressure:  $k_m = k_m(p_m)$ . The corresponding trend and equation are shown in the following figure (Fig. 5.29).

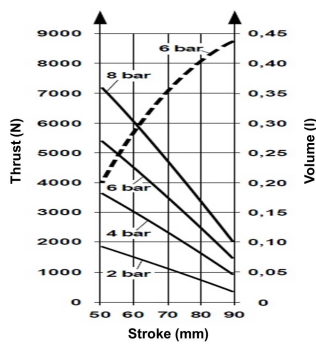


**Figure 5.28:** Datasheet diagram of the thrust force supplied by the spring as a function of the inner pressure and the elongation

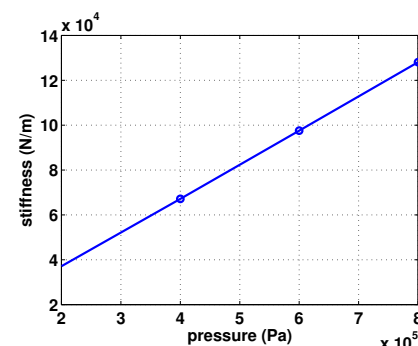


**Figure 5.29:** Stiffness of the air spring as a function of the inner pressure

## Chapter 5. Vertical loading subsystem

---

**Table 5.2:** Initial conditions of the dynamic system about each equilibrium position

$F_{n0} = 500N$ $P_{m0} = 384180Pa$ $T_{m0} = 293.15K$ $Y_{m0} = 0.0823m$ $Y_{f0} = 0.0756m$ $k_{m0} = 64748N/m$ $r_m = 2.5 \cdot 10^3 Ns/m$ $k_c = 7.5 \cdot 10^4 N/m$ $r_{c0} = 5.5556 \cdot 10^3 Ns/m$ $M = 10kg$ $A_{eq} = \pi(0.11/2)^2 m^2$ $k = 1.4$ $R = 8.314472 J/molK$ $R_{eq} = 1448.5 Pa \cdot s/mol$ $k_e = 100000 Pa/V$ $\omega_0 = 10\pi rad/s$ $\xi = 0.707$	$F_{n0} = 600N$ $P_{m0} = 384180Pa$ $T_{m0} = 293.15K$ $Y_{m0} = 0.0807m$ $Y_{f0} = 0.0727m$ $k_{m0} = 64748N/m$ $r_m = 2.5 \cdot 10^3 Ns/m$ $k_c = 7.5 \cdot 10^4 N/m$ $r_{c0} = 6.7200 \cdot 10^3 Ns/m$ $M = 10kg$ $A_{eq} = \pi(0.11/2)^2 m^2$ $k = 1.4$ $R = 8.314472 J/molK$ $R_{eq} = 1448.5 Pa \cdot s/mol$ $k_e = 100000 Pa/V$ $\omega_0 = 10\pi rad/s$ $\xi = 0.707$	$F_{n0} = 700N$ $P_{m0} = 384180Pa$ $T_{m0} = 293.15KN$ $Y_{m0} = 0.0792m$ $Y_{f0} = 0.0699m$ $k_{m0} = 64748N/m$ $r_m = 2.5 \cdot 10^3 Ns/m$ $k_c = 7.5 \cdot 10^4 N/mN$ $r_{c0} = 7.4044 \cdot 10^3 Ns/m$ $M = 10kg$ $A_{eq} = \pi(0.11/2)^2 m^2$ $k = 1.4$ $R = 8.314472 J/molK$ $R_{eq} = 1448.5 Pa \cdot s/mol$ $k_e = 100000 Pa/V$ $\omega_0 = 10\pi rad/s$ $\xi = 0.707$
$F_{n0} = 800N$ $P_{m0} = 384180Pa$ $T_{m0} = 293.15K$ $Y_{m0} = 0.0776m$ $Y_{f0} = 0.0670m$ $k_{m0} = 64748N/m$ $r_m = 2.5 \cdot 10^3 Ns/m$ $k_c = 7.5 \cdot 10^4 N/m$ $r_{c0} = 7.5 \cdot 10^3 Ns/m$ $M = 10kg$ $A_{eq} = \pi(0.11/2)^2 m^2$ $k = 1.4$ $R = 8.314472 J/molK$ $R_{eq} = 1448.5 Pa \cdot s/mol$ $k_e = 100000 Pa/V$ $\omega_0 = 10\pi rad/s$ $\xi = 0.707$	$F_{n0} = 900N$ $P_{m0} = 384180Pa$ $T_{m0} = 293.15K$ $Y_{m0} = 0.0761m$ $Y_{f0} = 0.0641m$ $k_{m0} = 64748N/m$ $r_m = 2.5 \cdot 10^3 Ns/m$ $k_c = 7.5 \cdot 10^4 N/m$ $r_{c0} = 7.5 \cdot 10^3 Ns/m$ $M = 10kg$ $A_{eq} = \pi(0.11/2)^2 m^2$ $k = 1.4$ $R = 8.314472 J/molK$ $R_{eq} = 1448.5 Pa \cdot s/mol$ $k_e = 100000 Pa/V$ $\omega_0 = 10\pi rad/s$ $\xi = 0.707$	$F_{n0} = 1000N$ $P_{m0} = 384180Pa$ $T_{m0} = 293.15KN$ $Y_{m0} = 0.0746m$ $Y_{f0} = 0.0612m$ $k_{m0} = 64748N/m$ $r_m = 2.5 \cdot 10^3 Ns/m$ $k_c = 7.5 \cdot 10^4 N/mN$ $r_{c0} = 7.5 \cdot 10^3 Ns/m$ $M = 10kg$ $A_{eq} = \pi(0.11/2)^2 m^2$ $k = 1.4$ $R = 8.314472 J/molK$ $R_{eq} = 1448.5 Pa \cdot s/mol$ $k_e = 100000 Pa/V$ $\omega_0 = 10\pi rad/s$ $\xi = 0.707$

Once again, this relation is linear. The stiffness value corresponding to the amount of pressure at the equilibrium is reported in the following table (Tab. 5.3).

**Table 5.3:** Bellows stiffness as a function of the inner pressure

$p$	2bar	4bar	6bar	8bar
$K$	$37135 N/m$	$67120 N/m$	$97524 N/m$	$128056 N/m$

The poles and the sole zero of each transfer function are successively calculated and represented in a single graph (Fig. 5.30). Since the system is a fifth-order one, the poles are 5 in total. However, it can be reduced to a second-order one because only the complex conjugate poles are dominant.

## 5.6. Numerical simulation

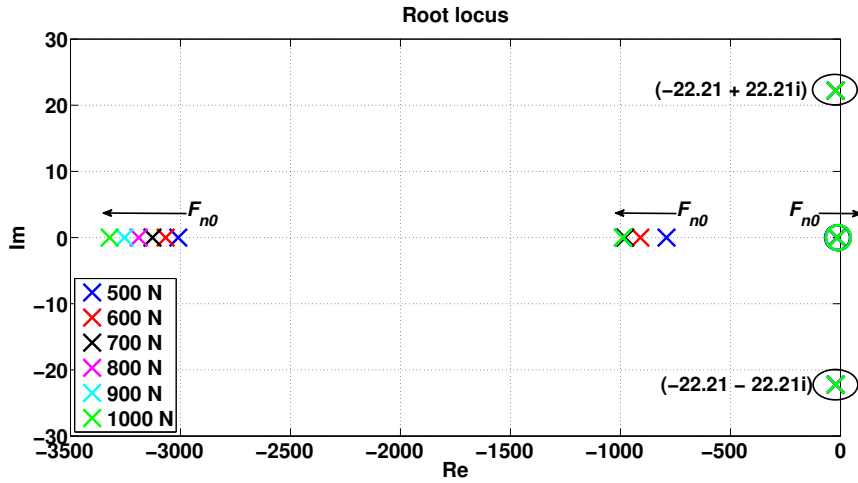


**Figure 5.30:** Root locus of the system about each equilibrium point

As expected, the root locus varies according to the equilibrium point under study. Nevertheless, the system is always stable, i.e. the real part of each pole is always negative.

Once the stability problem is solved, the system performance analysis is undertaken. Indeed, even if stable, the vertical loading subsystem might not have adequate dynamic characteristics. From this point of view, the frequency response function (FRF),  $G_2(i\Omega)$ , provides useful information. The trends of the modulus and phase of the FRFs obtained about each equilibrium point are therefore shown in the following figure (Fig. 5.31).

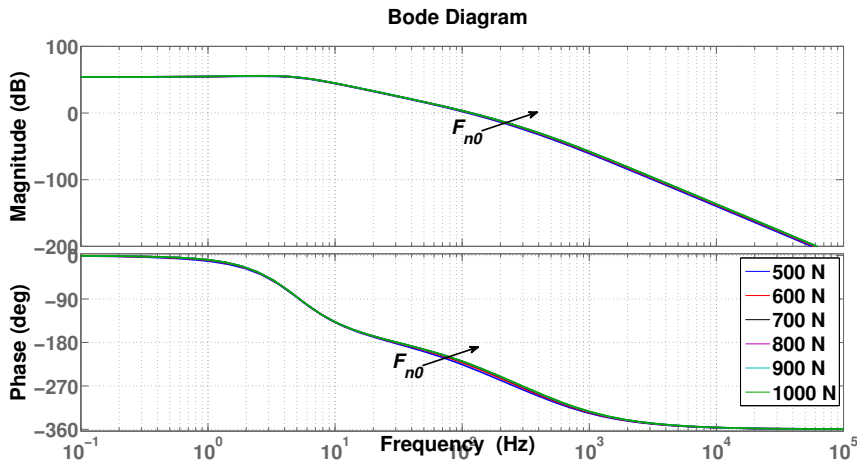


**Figure 5.31:** Bode frequency response of the dynamic system about each equilibrium point

As expected, the trend is typical of a second-order system at low frequencies. In addition, since the two dominant poles are fixed and the steady-state gains are more or less equal regardless of the contact force considered, the trends of the FRFs are practically identical to each other. From the performance point of view, each FRF demonstrates suitable characteristics for the application:

## Chapter 5. Vertical loading subsystem

---

- broadly constant module, albeit not unitary, in the range of frequencies of interest (bandwidth);
- decreasing module beyond the bandwidth, so as to reduce the effect of high frequency disturbances;
- no dynamic amplification;
- almost null phase within the bandwidth.

In light of this, one could therefore pretend to use the model to compute the input that returns the desired output. However, due to unavoidable modeling uncertainties and external disturbances, the output may be different from that expected. Therefore, the need to control the system arises.

Various methods are available for tuning a linear PID controller. In this case, since the transfer function of the system is known, such a procedure is performed according to the theoretical design techniques. In this regard, the transfer function is first reduced to the typical expression of a second order system:

$$G_2^*(s) = \frac{\mu\omega_n^2}{s^2 + 2\xi\omega_n s + \omega_n^2},$$

where  $\xi$ ,  $\omega_n$  and  $\mu$  are respectively the damping ratio, the natural frequency and the steady-state gain of the system. The first two parameters are calculable knowing the values assumed by the real and imaginary part of the complex conjugate poles (Fig. 5.30). On the other hand, the steady-state gain must be computed about each equilibrium point evaluating  $G_2(s)$  for  $s = 0$ . The possible values of  $\mu$  are reported in the following table (Tab. 5.4) as a function of the weight category.

**Table 5.4: Steady-state gain corresponding to each equilibrium point**

500N	600N	700N	800N	900N	1000N
$\mu = 510.0235$					

As previously outlined, the steady-state gains are equal to each other as well as the complex conjugate poles of all the transfer functions. As a consequence, a good tradeoff between performance and robustness can be achieved regardless of the possible working condition about which the controller is defined. During this work, the synthesis of the controller is performed about the equilibrium point corresponding to  $F_{n0} = 500N$ . The reduced transfer function,  $G_2^*(s)$ , under study is therefore the following one:

$$G_2^*(s) = \frac{5.034 \cdot 10^5}{s^2 + 44.42s + 987}.$$

The graphs of the transfer function,  $G_2(s)$ , and its reduced version,  $G_2^*(s)$ , are shown in figure (Fig. 5.32).

Once identified  $G_2^*(s)$ , it is possible to determine the expression of the controller,  $G_1(s)$ , that ensures a suitable closed-loop transfer function,  $L^*(s)$ :

$$L^*(s) = \frac{N^*(s)}{D^*(s)} = \frac{G_1(s)G_2^*(s)}{1 + G_1(s)G_2^*(s)} = \frac{\hat{\omega}_n^2}{s^2 + 2\hat{\xi}\hat{\omega}_n s + \hat{\omega}_n^2},$$

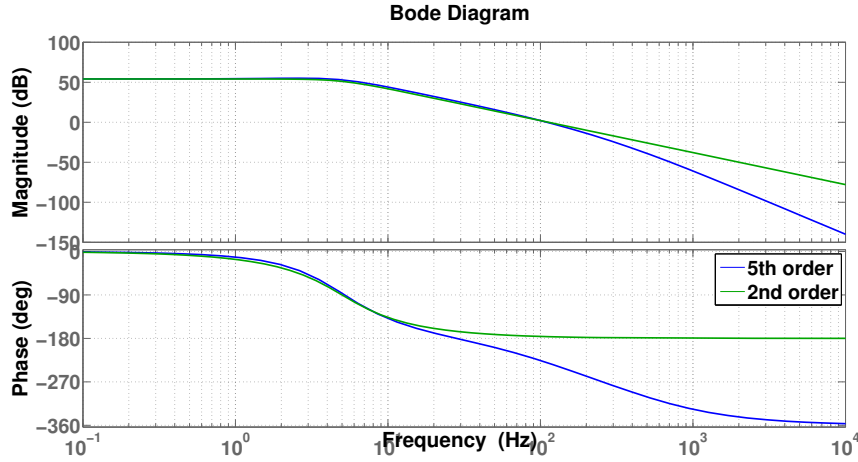


**Figure 5.32:** Bode frequency response of the dynamic system and its reduced version

where  $\hat{\omega}_n$  and  $\hat{\xi}$  are obtained as a function of the maximum acceptable overshoot,  $S$ , and the time when this is reached,  $T_S$ , according to the following relations:

$$S = 100 \cdot \exp^{\frac{-\pi\hat{\xi}}{\sqrt{1-\hat{\xi}^2}}} \quad T_S = \frac{\pi}{\hat{\omega}_n \sqrt{1-\hat{\xi}^2}}.$$

Assuming  $S = 0.75\%$  and  $T_S = 0.07s$ , the controller expression becomes:

$$G_1(s) = \frac{N^*(s)}{D^*(s) - N^*(s)} \cdot \frac{1}{G_2^*(s)} = \frac{6900s^2 + 3.065 \cdot 10^5 s + 6.81 \cdot 10^6}{5.034 \cdot 10^5 s^2 + 7.037 \cdot 10^7 s}.$$

Once the first attempt gains are identified, the optimization is simply performed by trial and error. The gains, and the transfer function of the controller, resulting from the optimization process are reported below:

$$K_p = 0.00366, \quad K_i = 0.0968, \quad K_d = 7.18 \cdot 10^{-5}, \quad T_f = 139.8$$

$$G_1(s) = K_p + K_i \frac{1}{s} + K_d \frac{T_f}{1 + T_f \frac{1}{s}} = \frac{0.01371s^2 + 0.6089s + 13.53}{s^2 + 139.8s}.$$

Once set the gains, the stability analysis of the full order controlled system may be executed by evaluating the poles of the corresponding closed-loop transfer function,

$$L(s) = \frac{G_1(s)G_2(s)}{1 + G_1(s)G_2(s)}.$$

However, an alternative criterion allows to evaluate the stability of the controlled system a priori, starting from the analysis of the open-loop transfer function,  $G(s) = G_1(s)G_2(s)$ . In particular, according to the Bode criterion, the closed-loop system is stable only if the real part of all the poles of  $G(s)$  is negative and both the gain and phase margins are positive. The gain and phase margin respectively equal  $21.2dB$  and  $65.8deg$  in this case (Fig. 5.33). The requirement is therefore fully respected.

## Chapter 5. Vertical loading subsystem

---

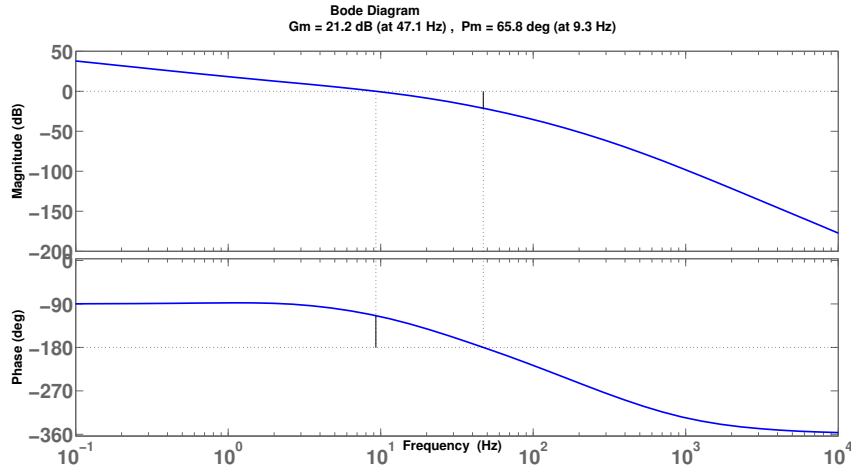


**Figure 5.33:** Gain and phase margins representation of the open loop controlled system

After stability, the analysis focuses on the static and dynamic performances of the fed-back system. In this regard, the step response and the FRF of the closed-loop system about each equilibrium point are evaluated. Their graphs are presented below (Fig. 5.34, 5.35). According to the step response function the system has restrained overshoot and short time constant regardless of the working condition considered. In addition, the FRFs Bode diagram shows unitary module and null phase at frequencies lower than 10Hz. Such a bandwidth is probably wide enough for the application.

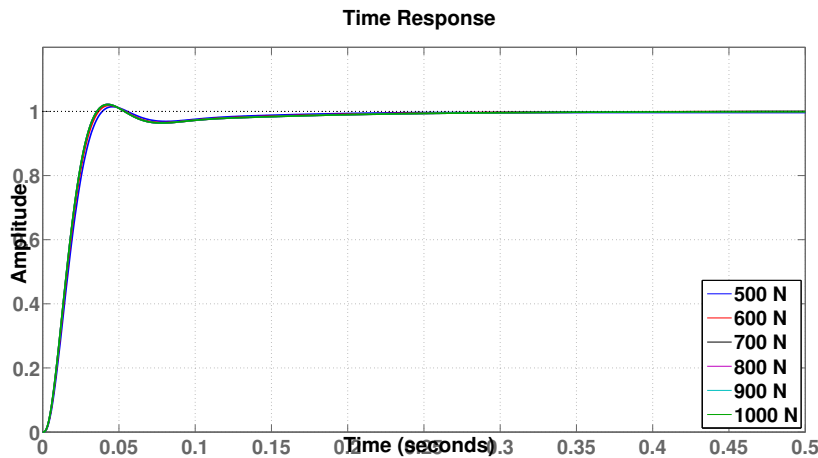


**Figure 5.34:** Step response of the closed-loop system about each equilibrium point

In light of these considerations, the solution proposed should be able to ensure the correct reproduction of the contact force and suppress the disturbances as rapidly as possible. Moreover, the loop design has enough gain and phase margin to allow for modeling errors or variations in system dynamics. However, nonlinearities (especially in the servo-valve) may undermine the validity of the analysis performed so far. It is therefore necessary to run a simulation considering more realistic working conditions.

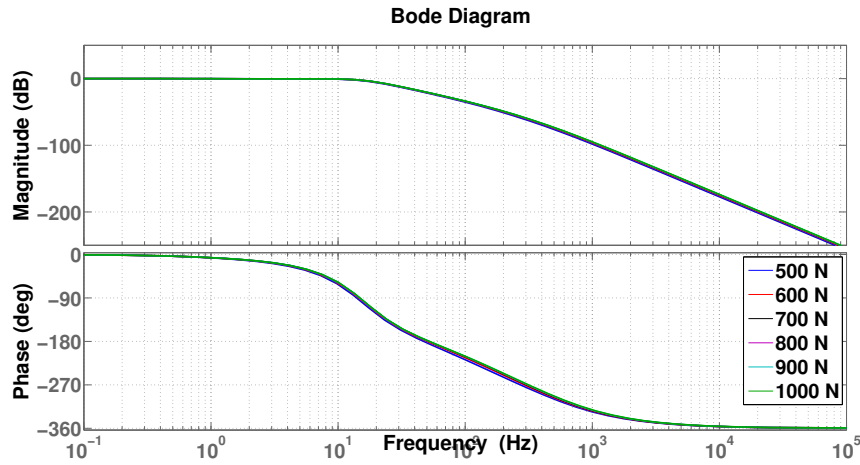


**Figure 5.35:** Bode frequency response of the closed-loop system about each equilibrium point

### 5.6.2 Nonlinear analysis

Aim of the present study is to rate the performance of the linear PID controller defined in the previous paragraph under more realistic working conditions, that is, simulating the entire operation procedure (Sec. 5.4) and considering the nonlinear characteristics of both the air spring and the servo-valve. The block diagram of the model developed using both the Simulink and SimMechanics modeling environment is shown in figure (Fig. 5.36). Its features are briefly analyzed below.

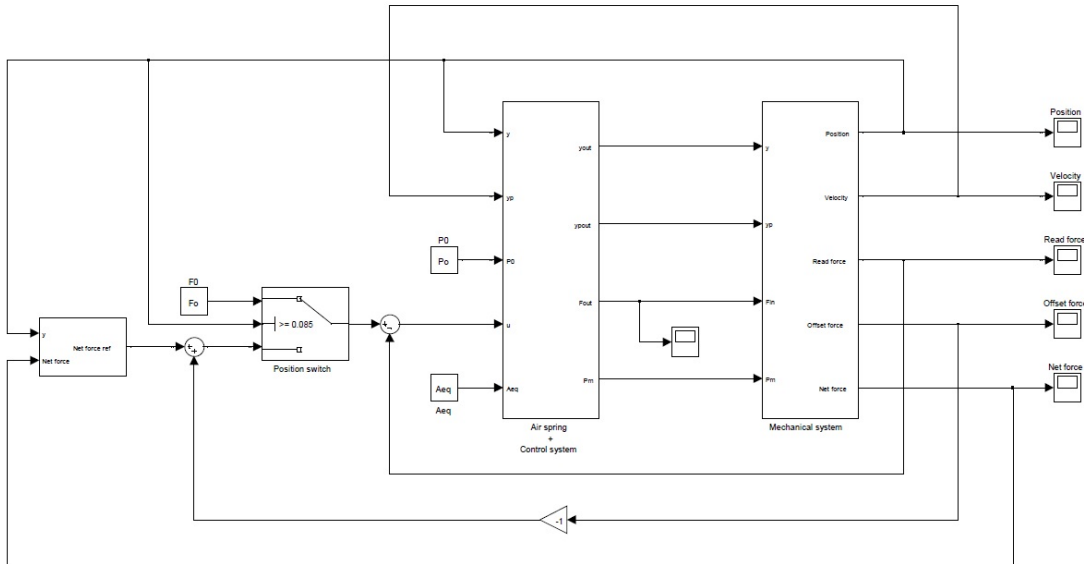


**Figure 5.36:** Block diagram of the vertical loading subsystem developed using Simulink and SimMechanics

SimMechanics is used to model and simulate the mechanical properties and the motion possibilities of the bodies constituting the system, i.e. the foot and the mechanism representing the ground.

## Chapter 5. Vertical loading subsystem

The foot is modeled as a massless point moving along the vertical direction according to a law of motion similar to the physiological one. On the other hand, the mechanism driven by the pneumatic actuator is reproduced by means of a rigid body having a mass comparable to that of the physical set-up previously presented (Sec. 5.3).

The foot-ground contact force is computed in Simulink according to the penetration model presented before (Sec. 5.5.3), i.e. as a function of the vertical position of the aforementioned two elements. On the other hand, the simulation is conducted neglecting for simplicity the friction of the vertical guides.

In addition, Simulink is used to model the dynamic behavior of the air within the air spring and the servo-valve, to compute the force introduced by the nonlinear stiffness of the bellows, and to implement the control logic. An overview of the model complexity is given in the following figure (5.37) representing the block diagram of the pneumatic actuator.

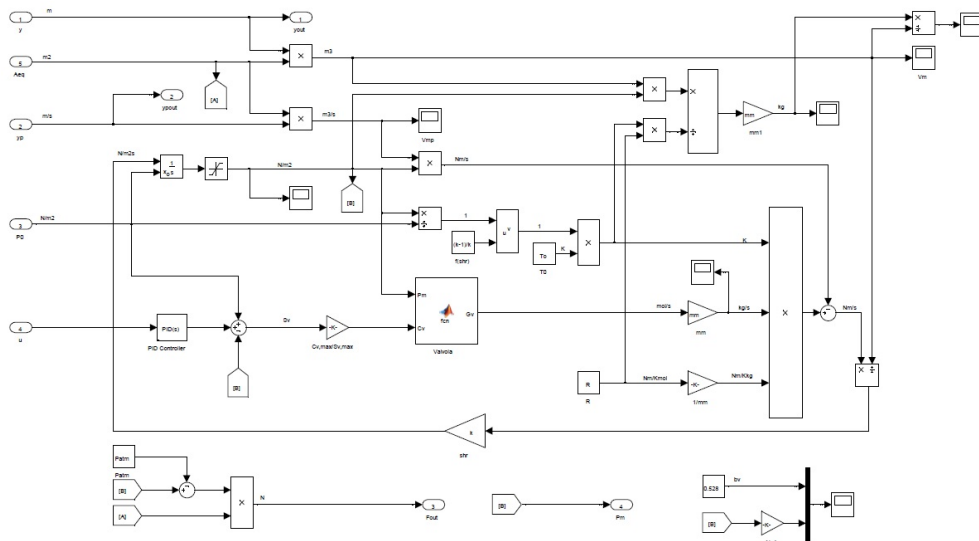


**Figure 5.37:** Block diagram of the pneumatic actuator developed using Simulink

The most significant results obtained by means of such a model are represented and described below.

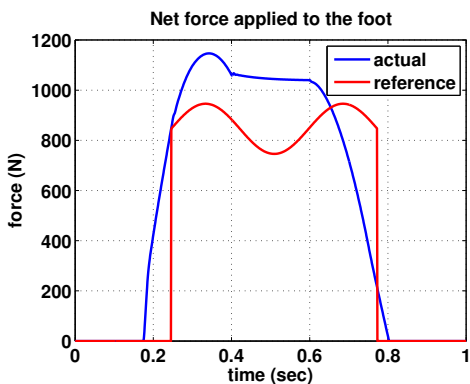


**Figure 5.38:** Approximated force reference and actual load applied to the foot

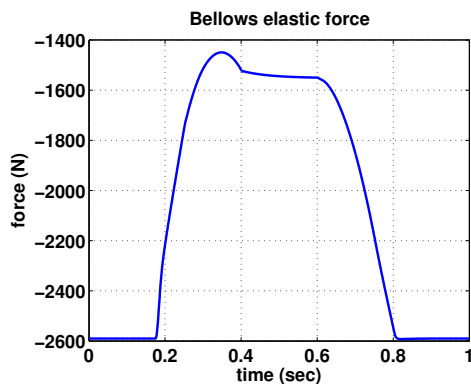


**Figure 5.39:** Elastic force due to the inner stiffness of the bellows

Clearly, a linear controller is not suitable to correctly reproduce the vertical reference force (Fig. 5.38) due to the innate nonlinear properties of both the medium and the valve. As a result the air spring is exploited almost passively during the entire stance period. The force applied on the foot by the spring is indeed principally related to the return of the bellows to its resting length (Fig. 5.39). However, satisfactory results may be achieved by replacing the analytical gains with the set of parameters computed in Simulink by applying the empirical regulation techniques rather than by applying more complex control strategies. In particular, the resultant controller is a PI whose gains are:  $K_p = 55.475$ ,  $K_i = 18007.8053$ . The need to use different gains is likely induced by the introduction of the nonlinear servo-valve model.

The trend of both the reference (red) and the actual (blue) vertical force obtained in these conditions are shown (Fig. 5.40). Comparison between curves is meaningful depending on whether the control is either active or not, that is respectively when the switch signal is high or low (Fig. 5.41).

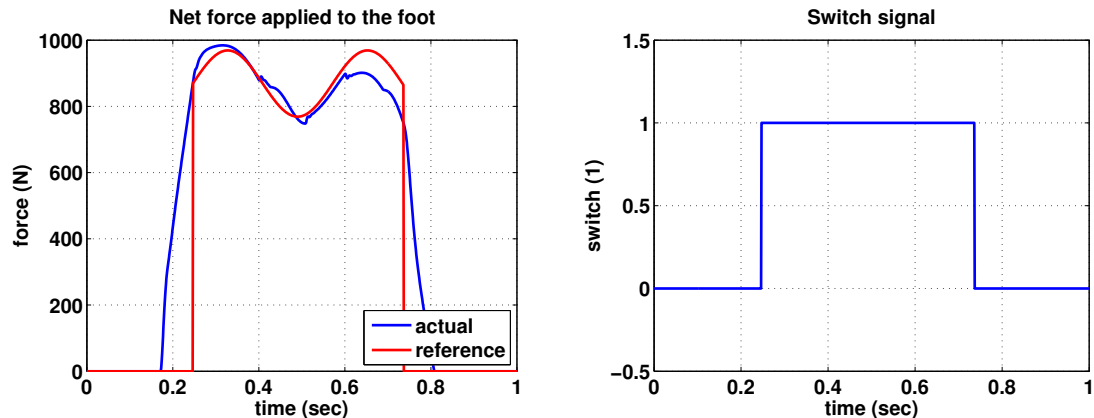


**Figure 5.40:** Approximated force reference and actual load applied to the foot with the new set of gains

**Figure 5.41:** Switch signal

The graphs show that the control system manages to follow the reference in a satisfactory manner despite the limitation introduced by the air spring in terms of bandwidth. However, the reference is not the actual vertical force recorded during the gait analysis session but an approximation thereof due to the need to exploit the spring almost passively at the initial and final stage of contact. This aspect is important because it increases the stability of the system. On the other hand, it prevents the possibility to track the desired trend (Fig. 5.42). Nevertheless, greater affinity may be achieved using different approximation technique when computing the reference. Anyway, the vertical loading subsystem fulfills the request of inputting full scale ground reaction force despite the observed deviation.

However, an additional problem linked to this aspect comes to light. The hypothesis under which the longitudinal loading subsystem was developed, that is the possibility to faithfully reproduce the vertical reaction force (Chap. 4), is not true. The possibility to reproduce the longitudinal force component as a function of the vertical one must therefore be reconsidered. This aspect is assessed during the final co-simulation (Chap. 7).

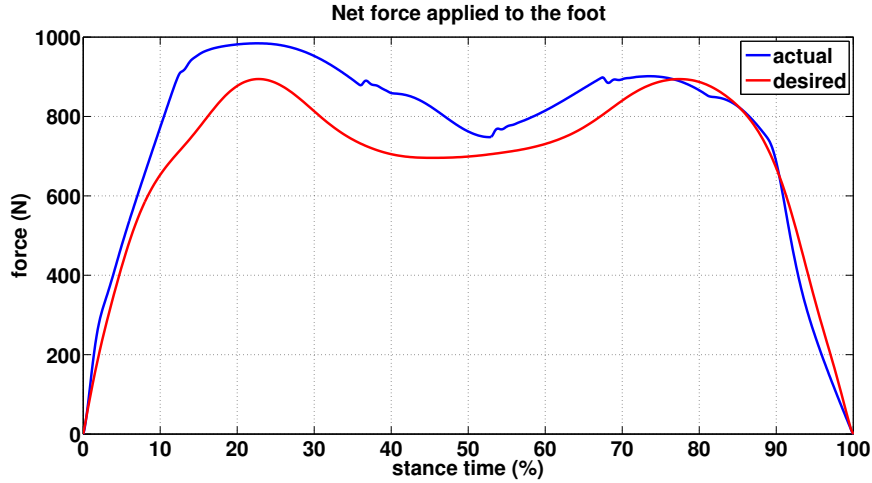


**Figure 5.42:** Vertical real force reference and actual load applied to the foot with the new set of gains

Finally, the vertical displacement of the support surface and the trend of the inner pressure are reported (Fig. 5.43,5.44) to verify the suitability of the selected actuator.

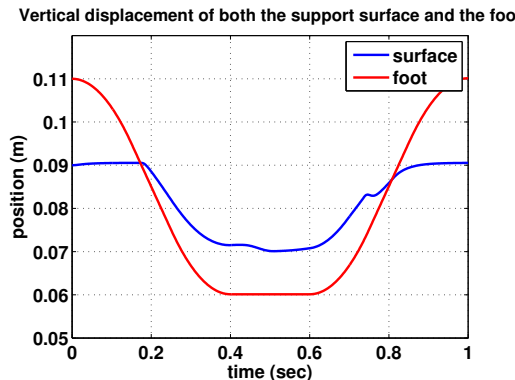


**Figure 5.43:** Vertical position of both the foot and the support surface

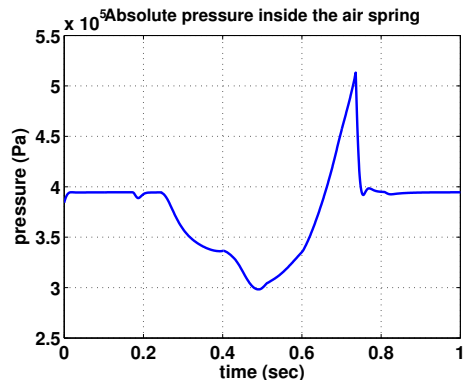


**Figure 5.44:** Absolute pressure within the air spring

The variation in terms of height of the support surface and thus of the air spring is about 2cm. This amount is in agreement with the stroke of the actuator (Sec. 5.2.1). The same consideration is valid in terms of absolute inner pressure since the maximum is strictly lower than 5.5bar. Finally, it is worth noting that the plate is able to return to its initial position before the beginning of the next cycle (Fig. 5.43).

## 5.7 Realization and characterization

---

Once numerically evaluated the goodness and the limits of the proposed solution, the mechanism is manufactured and assembled. Then, the control system is set up. Finally, some experimental test are performed in order to assess the performance of the solution and estimate some parameters useful for improving the reliability of the numerical model.

### 5.7.1 Realization and assembly

First of all, the commercial components are supplied while the custom ones are developed with the help of laboratory technicians and the use of numerical control machinery. The pieces are then assembled (Fig. 5.45). The upper and the lower part are initially mounted separately (Fig. 5.46). The two units are then overlaid and linked together so as to include the load cells and the potentiometer in between.

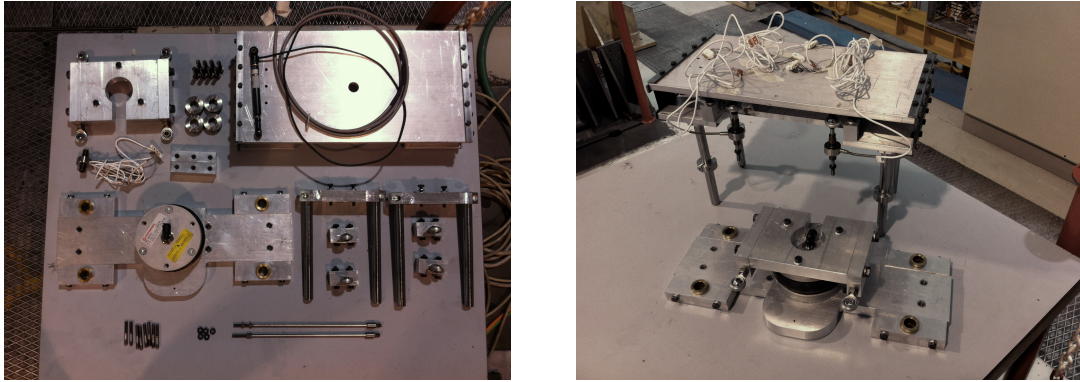


**Figure 5.45:** Commercial and custom made pieces

**Figure 5.46:** Upper an lower part constituting the vertical loading subsystem

Despite the high accuracy adopted during the manufacturing process, the assembly of the parts has been difficult due to the aforementioned hyperstaticity. Anyway, the eyelet foreseen during the design process, the additional manual improvement performed by the technicians, and the shaft greasing allowed to achieve the expected result. A representative picture of the assembly accommodated on the carriage of the horizontal linear guide is reported in the following picture (Fig. 5.47).

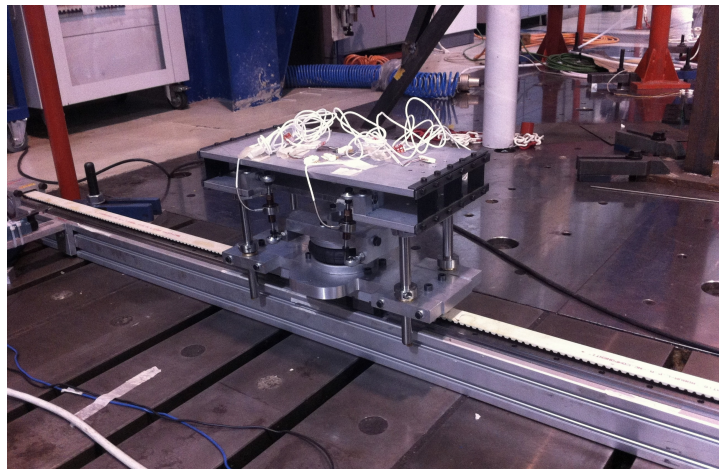


**Figure 5.47:** Representative picture of the vertical loading subsystem accommodated on the linear guide

It is clearly possible to discern the components constituting the mechanical setup, that is, the air spring, the architecture of the vertical mechanism and the transducers. On the other hand, the control system, which is the topic of the next section, is not present.

## Chapter 5. Vertical loading subsystem

### 5.7.2 Control system

The aim of the control plant is to regulate the behavior of the mechanical system, i.e. the pressure within the air spring. In particular, the command signal necessary for driving the opening of the servo-valve is generated by processing the data coming from the transducers. These shall therefore be powered and properly interpreted before performing the experimental tests. First, it is therefore essential to build the electrical plant and the data acquisition system. The connection diagram of the devices constituting the overall experimental setup is shown in figure (Fig. 5.48).

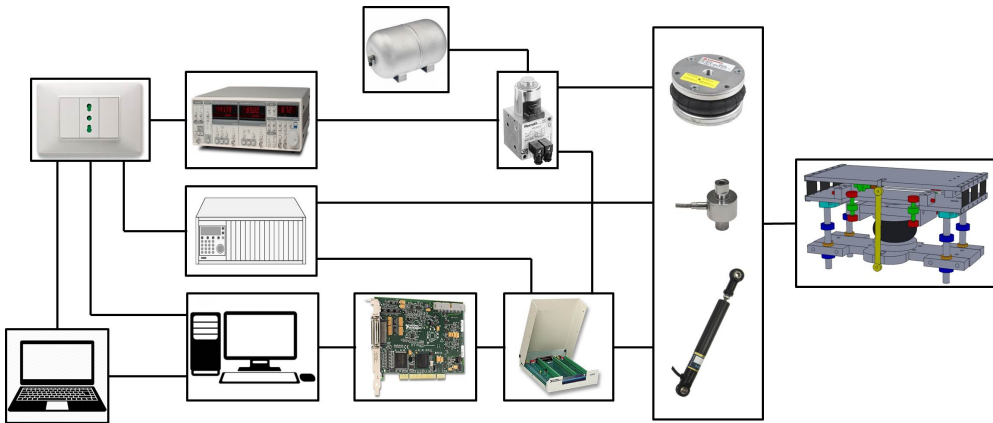


**Figure 5.48:** Connection diagram of the vertical loading subsystem

The data acquisition system is made up of the same National Instruments components (connector block NI-SCB 68, PCI NI-6229 DAQ board, desktop PC running the RTOS) previously used for testing the longitudinal loading subsystem. Since determinism is fundamental when performing this kind of control task, both the hardware and the software are installed and configured so as to ensure precise timing and long term reliability. Thereafter, the majority of the work is undertaken within the LabVIEW programming environment (Fig. 5.49).

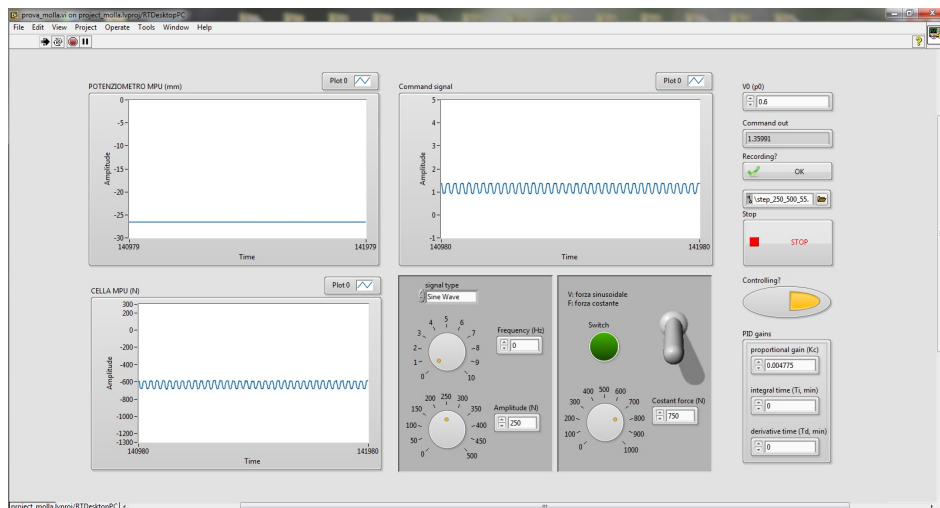


**Figure 5.49:** LabVIEW programming environment

## 5.7. Realization and characterization

As previously hinted, the program written in LabVIEW defines the communication channels, processes the analog signals coming from the sensors (load cells and linear potentiometer), calculates the command signal necessary for driving the opening of the servo-valve, and saves on text files the results useful for post-processing. Some of this tasks require a good awareness of the employed devices. It is therefore necessary to assess their characteristics by performing some preliminary tests.

- Strain gauge load cells

First of all, the load cells need to be powered; their operating voltage is  $10Vdc$ . In addition, the analogic signal coming from the strain gauges connected in the Wheatstone bridge configuration need to be amplified. Both these issues are solved using a devoted amplifier produced by HBM (Fig. 5.50a). The gains are in particular defined in order to enhance as much as possible the resolution of the transducers, i.e. in such a way that the maximum voltage value corresponds to the maximum representable load, that is, the full scale . Finally, some tests are conducted to check that the cells are linear as claimed in the datasheet (Fig. 5.50b). This property is verified as well as the absence of hysteresis. On the other hand, some deviations are noticed in terms of sensitivity. (Tab. 5.5).

**Table 5.5:** Load cells sensitivity

	Cell 1	Cell 2	Cell 3	Cell 4	Cell 5	Cell 6
[Kg/V]	9.33	9.07	9.14	8.90	9.01	9.43

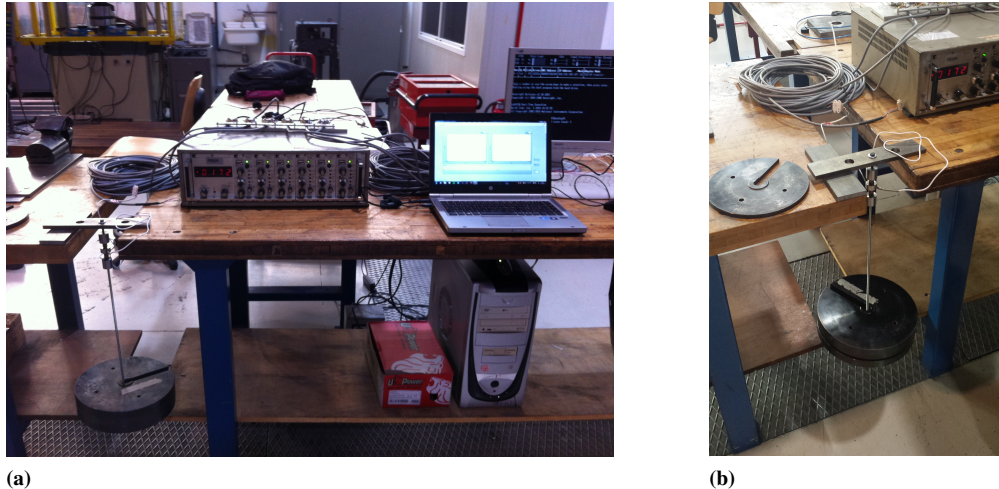


**Figure 5.50:** Load cells calibration experimental setup

- Linear potentiometer

This device can be powered and acquired directly through the NI connector block. Since the maximum voltage value supplied by the connector block is  $10Vdc$  and the maximum stroke is  $50mm$ , the relation existing between the displacement and the tension is the following one:  $5mm = 1V$ .

## Chapter 5. Vertical loading subsystem

- Servo-valve

The device employed - Bosch Rexroth AG serie ED05 (Fig. 5.51a) - is a pressure proportional valve. The position of the spool is therefore regulated by the inner control loop of the valve itself in order to ensure that the downstream pressure correspond to the desired one. In particular, the relation between relative pressure and input voltage command is the following:  $1\text{bar} = 1\text{V}$ . The inlet of the servo-valve is connected to the line of the laboratory, whose pressure is about  $7\text{bar}$ . On the other hand, the outlet is connected to the air spring by means of a tube and an elbow gasket (Fig. 5.51b). Finally, an AC/DC converter is used to supply  $24\text{Vdc}$  to the servo-valve.

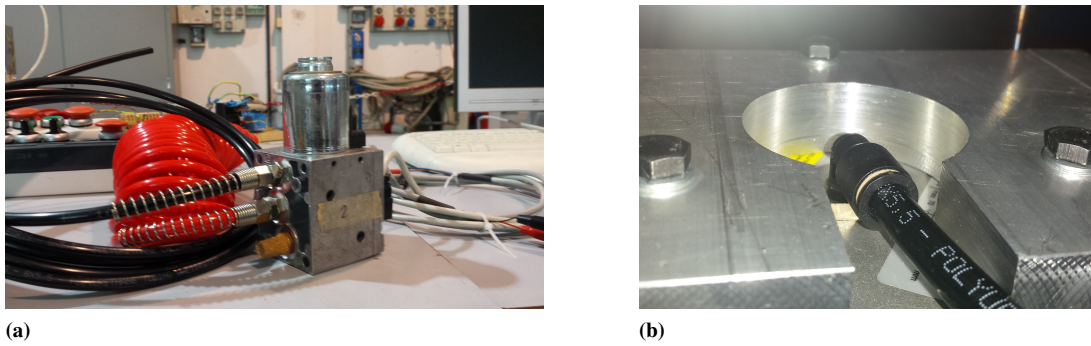


**Figure 5.51:** Servo-valve and elbow gasket implemented

After calibration some test are undertaken considering the overall system.

### 5.7.3 Calibration

The tests are performed at the laboratories of the Department of Mechanical Engineering of Politecnico di Milano in order to:

- evaluate the actual stiffness of the air spring;
- assess the reliability of the vertical force signal acquired through the load cells;
- estimate the friction acting on the vertical guide mechanism;
- investigate some characteristics of the servo-valve employed;
- assess the suitability of the control logic implemented.

Both static and dynamic tests are performed using an universal testing machine in order to fulfill the aforementioned purposes. The experimental setup, the test protocols and the results achieved are analyzed in the next sections.

### Experimental setup

The universal machine employed - Instron 8511 (Fig. 5.52) - can be operated either in terms of force or displacement. Its key features are listed below:

- maximum stroke of the hydraulic cylinder:  $\pm 25\text{mm}$ ;

## **5.7. Realization and characterization**

- maximum force range:  $\pm 20kN$ ;

Moreover, it allows to measure both the actual force and actual position using the following accessories:

- load cell with a full scale of  $\pm 20kN$ ;
- LVDT with a full scale of  $\pm 50mm$ .

The corresponding signals can be displayed directly on the video terminal or acquired through the BNC connectors. Both these option are exploited during the trials.

Finally, the possibility to vary arbitrarily the height of the crosshead allows to easily accommodate specimens having different vertical size. The vertical loading subsystem under study is connected as follows. The lower part of the apparatus is connected to the load cell at the base of the testing machine through a flange, that is, a threaded connecting tube (Fig. 5.52). On the other hand, the upper part is connected to the piston rod via a spherical joint so as to avoid redundant constraints that could undermine the reliability of the test (Fig. 5.52).

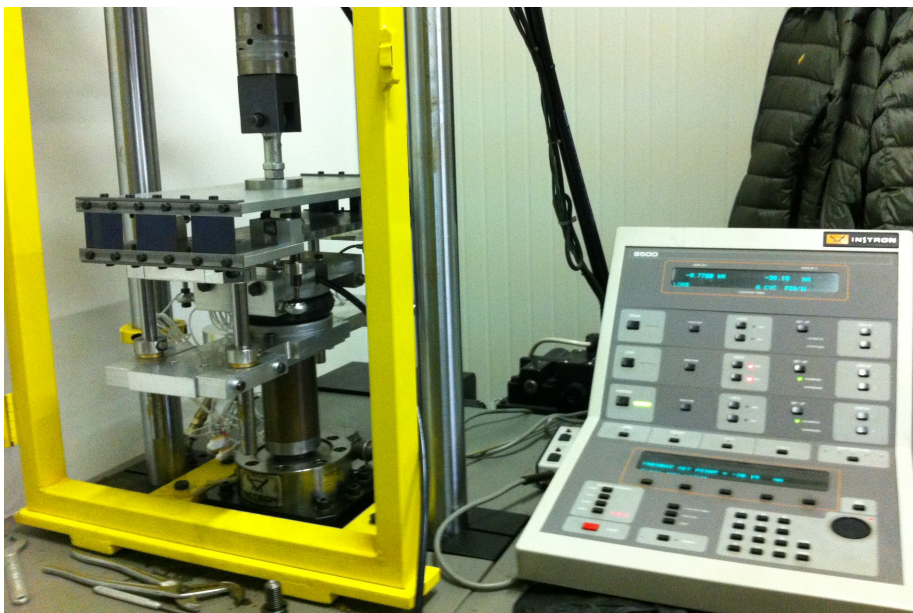


**Figure 5.52:** Vertical loading subsystem accommodated on the universal testing machine

The diagram of the experimental setup is shown in figure (Fig. 5.53).

Five different tests are performed using this setup. Since the machine is operated only in terms of position, the tests are respectively referred to as static or dynamic, in order to distinguish situations in which the piston is either fixed or in motion. Their features are analyzed in the next two sections.

### **Static tests**

- Test 1

Aim of the first static test is to obtain more realistic information about the stiffness of the air spring so as to improve its numerical model. Generally speaking, the

## Chapter 5. Vertical loading subsystem

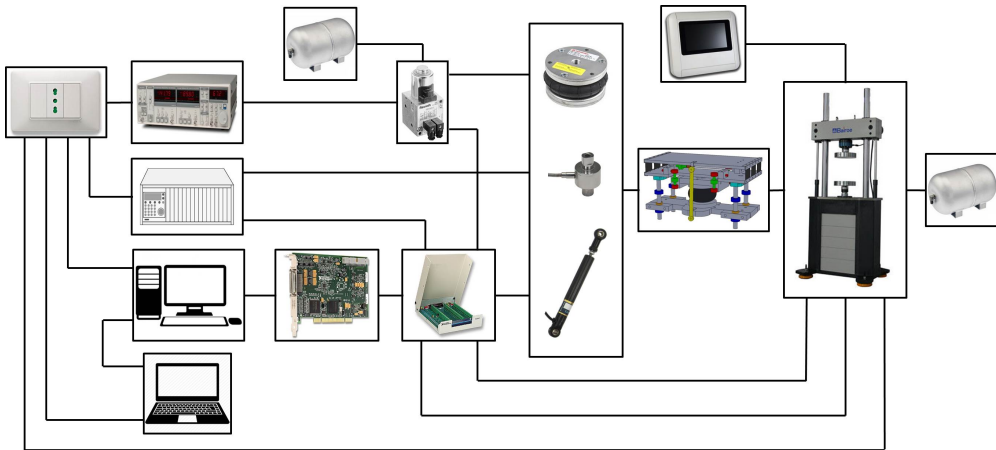


**Figure 5.53:** Block diagram of the overall experimental setup

nonlinear stiffness of the air spring changes according to both the elongation of the bellows and the amount of inner pressure. As a consequence the test is performed so as to examine all the possible combinations compliant with the working ranges of the equipment employed. The relative pressure is varied between 0bar and 6bar with steps of 0.5bar by driving the servo-valve through an additional external power source. On the other hand, the elongation of the spring is varied between 55mm and 85mm with steps of 5mm by moving the piston rod. The amount of thrust force delivered by the system under study is read by means of the Instron load cell directly at the video terminal. Results obtained via this procedure are summarized in the following chart (Fig. 5.54).

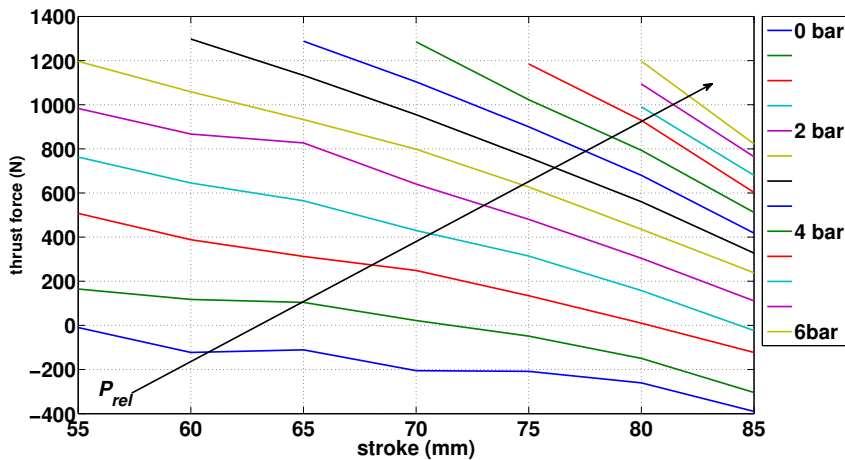


**Figure 5.54:** Thrust force supplied by the vertical loading subsystem as a function of the relative pressure and the elongation of the spring

Given a pressure and under the hypothesis of constant equivalent area, the relation between the thrust force and the elongation is almost linear. As expected, the stiffness is therefore independent from the position (Sec. 5.6.1). The resultant trend of the stiffness as a function of the pressure is represented in the following

## 5.7. Realization and characterization

figure (Fig. 5.55).

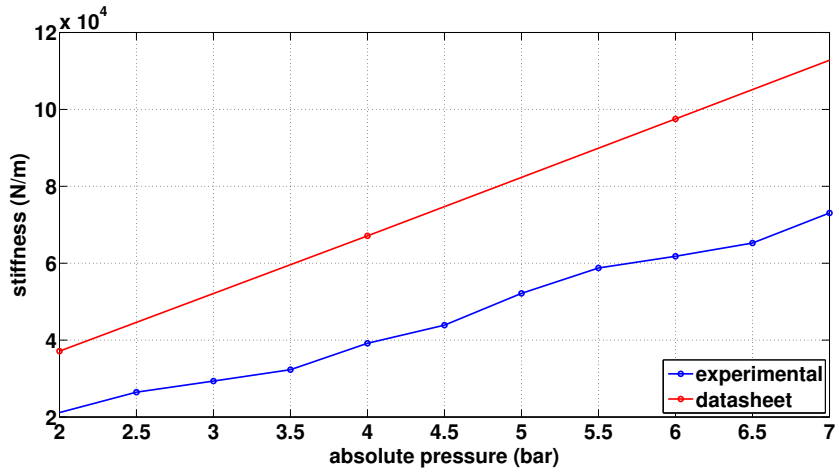


**Figure 5.55:** Stiffness of the vertical loading subsystem in vertical direction as a function of the absolute pressure

Once again, the trend is almost linear. However, the slope is lower than that expected. This behavior is definitely produced by the flexibility of the structure. As a consequence the system may be considered as the series of two springs, whose resultant stiffness is lower than that of the sole pneumatic actuator.

The first static test revealed another important aspect: the force signal acquired through the custom measurement setup (Sec. 5.2.3) and the force signal acquired through the universal testing machine load cell are equal in terms of magnitude (Fig. 5.56).

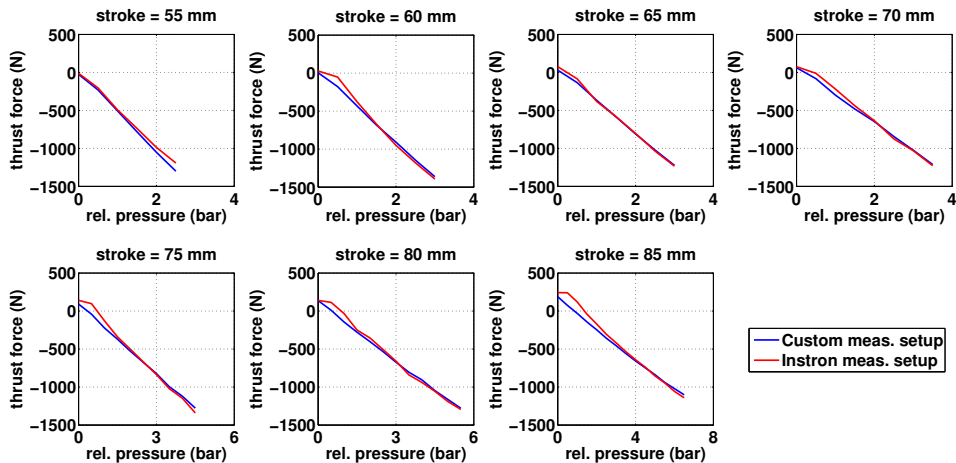


**Figure 5.56:** Comparison of the force through the custom measurement setup and the universal testing machine load cell

Differences between the signal occur only when the pressure within the air spring is so low that the bellows is stretched rather than compressed. This working condition is not expected during the operation of the test bench. Thus, it is not a

problem and the reason of the error is not investigated. Anyways, the trend of the average error is shown in figure as a function of the relative pressure (Fig. 5.57).

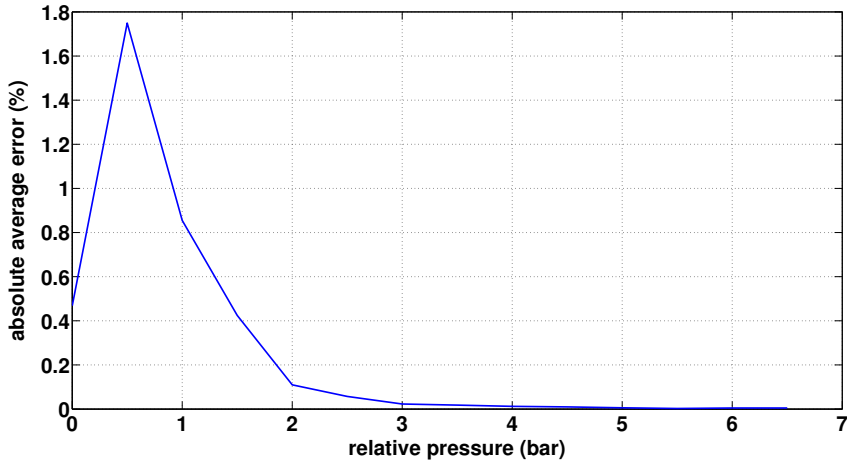


**Figure 5.57:** Average error committed through the custom measurement setup as a function of the relative pressure

Its amplitude is rather low if considering that the amount of pressure during operation is likely higher than 2bar.

- Test 2

The second static test is undertaken in order to achieve the frequency response function of the servo-valve. This test is performed at a given piston height (constant spring elongation) so as to exploit, on the basis of the air spring mathematical model introduced before (Sec. 5.5.1), the linear relationship between the thrust force and the pressure within the pneumatic actuator. By neglecting the inner stiffness of the bellows, the transfer function of the valve may indeed be achieved (both in term of module and phase) by evaluating the correlation between the force end the tension command signal. In particular, the dynamics of the regulator is evaluated by supplying the servo-valve with a sinusoidal signal having 0.5V amplitude (the offset changes according to the height so as to respect the working range of all the equipment elements). Only frequencies between 0 and 1Hz are considered. The test is repeated considering different elongations of the air spring (55, 70, 85mm). The trend of the module and the phase are shown in the following graph (Fig. 5.58).

Clearly, the module is constant within the range of frequencies considered. On the other hand, the delay increases together with the frequency and the elongation considered.

- Test 3

The final static test is performed to experimentally verify what stated during the numerical linear analysis (Sec. 5.6.1), that is, the possibility to achieve a good tradeoff between performance and robustness using the same set of PID gains regardless of the equilibrium position considered. This opportunity is assessed

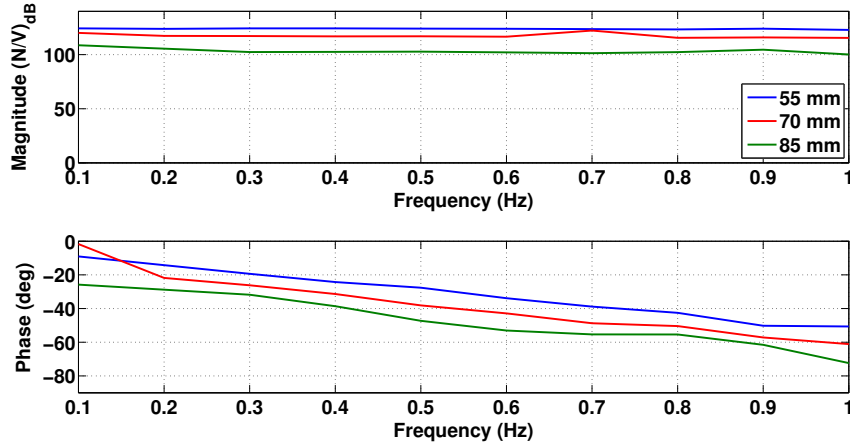


**Figure 5.58:** Bode diagram of the servo-valve transfer function

by comparing the gains obtained, around three different equilibrium conditions (55mm, 70mm, 85mm), through the Ziegler-Nichols empirical method. Results obtained in terms of proportional gain and oscillation period are reported in the following table (Tab. 5.6). The corresponding gains can be computed according to the following relations (Tab. 5.7).

**Table 5.6:** Parameters obtained by applying the Ziegler-Nichols method about each equilibrium point

	55mm	70mm	85mm
$\hat{K}_p$	0.0048	0.0073	0.0142
$\hat{T}$	0.28s	0.3s	0.33s

**Table 5.7:** Relations for computing the PID according to the Ziegler-Nichols

$K_p$	$T_i$	$T_d$
$\hat{K}_p$	$\hat{T}/2$	$\hat{T}/8$

Different values result in different set of gains. Probably, the linear regulator is therefore not suitable for the application due to the high nonlinearity of the equipment employed. Anyway, differences are so small that the opportunity to use the same set of gains is not completely excluded.

#### Dynamic tests

- Test 4

The first test is performed to estimate the friction of the vertical guide system. This information is achieved by imposing a constant value of pressure within the air spring and a sinusoidal variation of its elongation (10mm of amplitude) around its average stroke (70mm). The same procedure is conducted considering different frequencies (from 0 to 1Hz with steps of 0.1Hz) in order to achieve different excursion velocities. From this point of view, the available equipment allowed to reach only speed up to 0.15m/s. A graphical representation of the forces read

## Chapter 5. Vertical loading subsystem

through the universal machine load cell and the custom measurement setup is reported below (Fig. 5.59).

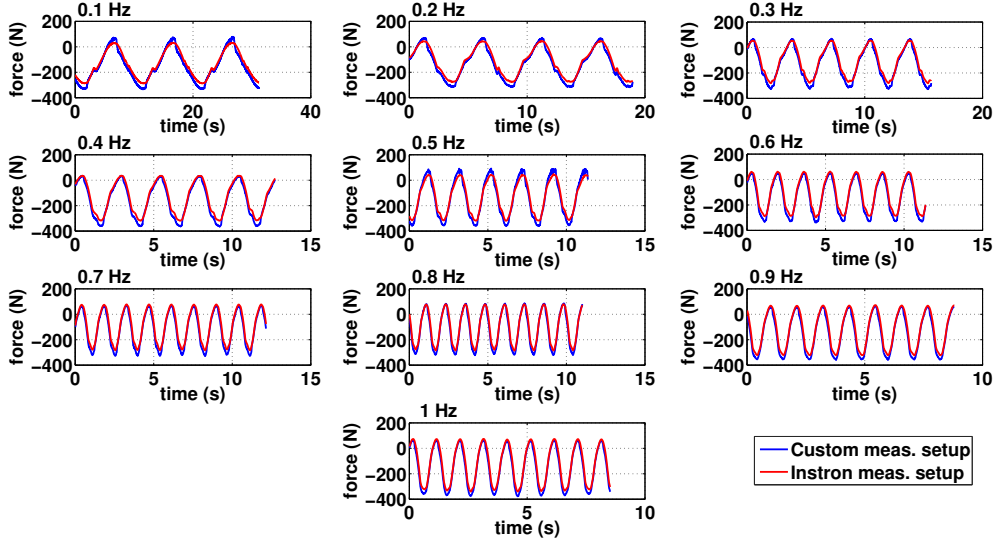


**Figure 5.59:** Force read through the custom measurement setup and the universal testing machine during the first dynamic test

The trend of the friction as a function of the velocity is then obtained by combining the force signals acquired during this session with the information achieved during the static test (the stiffness contribution at the given pressure)(Fig. 5.60).

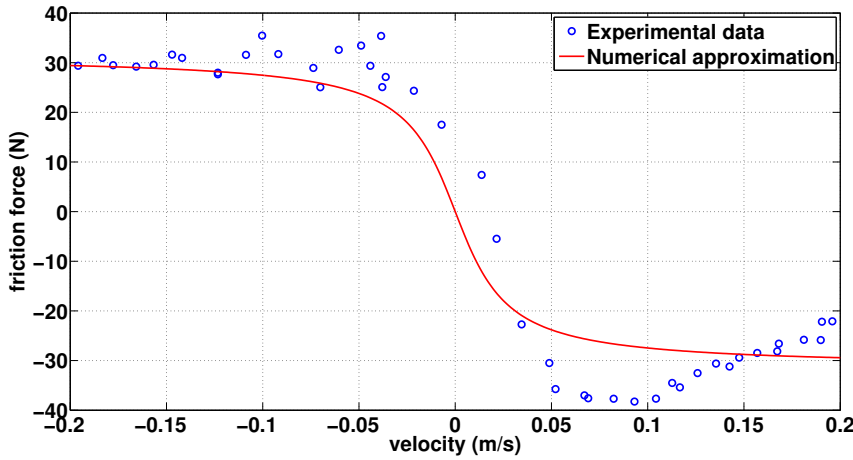


**Figure 5.60:** Trend of the friction force of the vertical loading subsystem

- Test 5

The aim of the last test is to verify the ability of the closed loop system to track a constant force reference ( $500\text{N}$  and  $700\text{N}$ ) despite the disturbance introduced by the piston in terms of motion (a sine wave with  $10\text{mm}$  amplitude). In particular, the gains of the PID controller employed are computed about the average stroke of the spring by applying the Ziegler-Nichols empirical method. From a

## 5.8. Vertical loading subsystem concluding remarks

practical point of view, this working condition is similar to the initial and final stage of contact, that is, when the spring is exploited almost passively. The test is repeated considering different motion frequencies between 0 and 1 Hz. Results are shown in the following figure (Fig. 5.61). Clearly, the system is able to track the force reference only at low frequencies. This problem is likely induced by the low dynamic characteristic of the pneumatic system (Test2). Also the linear PID controller is probably not suitable for the application (Test3).

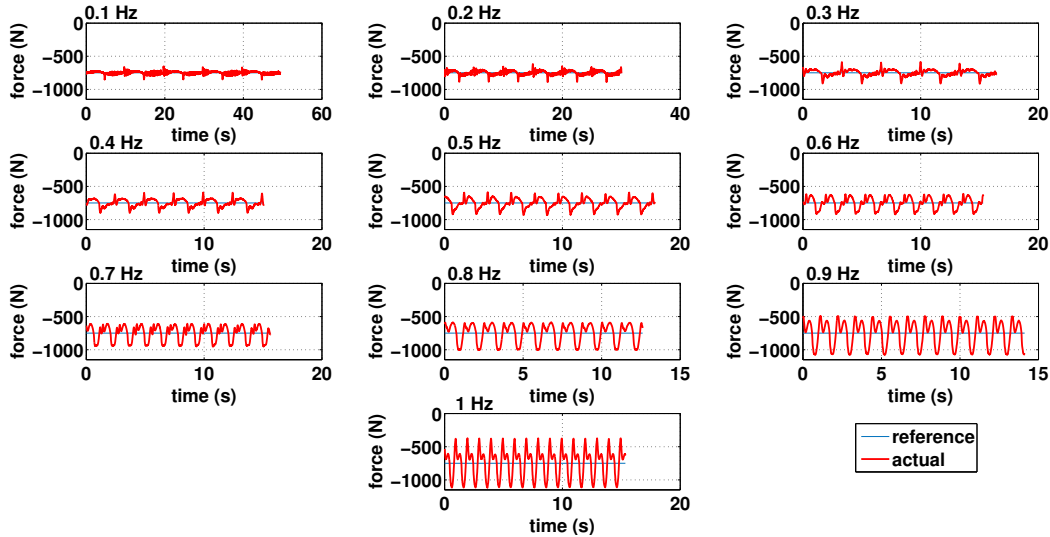


**Figure 5.61:** Ability of the system to track a constant force reference despite the disturbance imposed in terms of motion

## 5.8 Vertical loading subsystem concluding remarks

The innovative ideas implemented in the design of the vertical loading subsystem have led to the synthesis of a novel solution compared to those proposed in the literature by other authors. The main differences relate to the measurement set-up and the actuation system. In particular, the use of an active air spring as actuator introduced promising advantages in terms of test execution.

First of all, the compressibility of the air ensures a gradual transfer of the load during the initial stage of contact between the foot and the plate avoiding phenomena which could compromise the functionality of the bench. In addition, the intrinsic stiffness of the bellows allows to control the vertical axis only in terms of force throughout the entire gait cycle. Thus, the air spring physical characteristics allow to enhance the stability of the system and to automatize the test procedure.

However, there are also disadvantages related to the use of this solution. The aforementioned features respectively determine a reduction of the bandwidth and the need to recompute an approximated force reference at each cycle.

Nevertheless, these limits have not prevented the possibility to achieve satisfactory results during the numerical simulations. In particular, the load applied to the foot is qualitatively very similar to that acquired during the gait analysis session, both in terms of amplitude and duration.

## **Chapter 5. Vertical loading subsystem**

---

The experimental results have confirmed these considerations only in part. Indeed, the available servo-valve determined a further reduction of the bandwidth and consequently the impossibility to reliably evaluate the merits of the air spring as a single unit and the suitability of the PID linear controller.

Anyway, this solution have proven to be successful according to the author's opinion.

---

# CHAPTER 6

---

## Residual limb subsystem

---

### 6.1 Introduction

---

Once completely defined the subsystem necessary for reproducing the load acting on the foot, it is necessary to identify a commercial robot to simulate the motion of the hip. As highlighted in the gait analysis chapter (Chap. 2), besides guaranteeing the correct reproduction of the 6 movement components, such a robot must withstand the large loads acting on it. For this reason, once identified a solution suitable for the application some simulations are performed in ABB RobotStudio and MSC Adams in order to validate the choice. Finally, some custom pieces are design to accommodate and sustain the prosthesis under test.

### 6.2 ABB IRB 6620

---

A commercial six-axes industrial robot is selected for actuating the prosthetic specimen. This solution inherits indeed some advantages with respect to other commercial solutions (such as PKM) and custom built robots:

- less expensive;
- more accessible;
- more reliable.

The robot is selected based on both the capabilities to generate the range of motion and to withstand the loads outlined in the previous sections of this thesis. In particular, the end-effector of the manipulator shall:

## Chapter 6. Residual limb subsystem

- perform linear movements up to  $65mm$  with respect to the initial position with peak velocity around  $0.4m/s$ ;
- perform angular movements up to  $60deg$  with respect to the initial orientation with peak velocity around  $220deg/s$ ;
- withstand forces up to  $800N$  in the main load direction, that is, the vertical one;
- withstand torques up to  $400Nm$  within the main load plane, that is the sagittal one.



**Figure 6.1:** ABB IRB 6620 industrial 6-axis robot

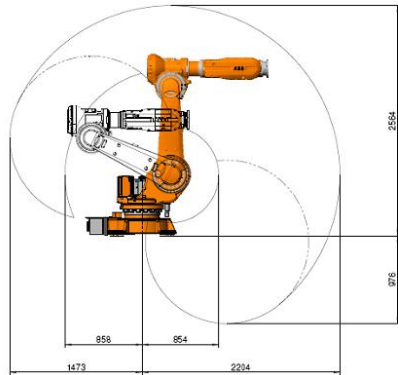


**Figure 6.2:** ABB IRB 6620 available workspace

Among the commercially available solutions the ABB IRB 6620 model is identified (Fig. 6.1). This system has a load capacity up to  $150kg$ . The motion possibilities of each independent axis are reported instead in the following table (Tab. 6.1).

**Table 6.1:** Primary kinematic information of the ABB IRB 6620 robot

Axis	Working range	Max speed
1	$-170deg$ to $+170deg$	$100deg/s$
2	$-65deg$ to $+140deg$	$90deg/s$
3	$-180deg$ to $+70deg$	$90deg/s$
4	$-300deg$ to $+300deg$	$150deg/s$
5	$-130deg$ to $+130deg$	$120deg/s$
6	$-300deg$ to $+300deg$	$190deg/s$

According to these data, the robot is compliant with the kinematic requirements of the application in terms of workspace. The motion capabilities of the axes (Tab. 6.1) allow indeed the replication of all the hip possible configurations by means of a single test procedure within the available range. Moreover, they facilitate the installation of the rest of the equipment avoiding space problems (Fig. 6.2). Some issues exist instead about the manipulator ability to reproduce the dynamic conditions exposed. In the data-sheet are not reported further information than the payload capability since this kind of manipulator is generally adopted for moving loads in a quasi-static manner. Moreover the maximal angular velocity achievable by each single axis is lower than the maximum requested at the end-effector. Some numerical simulations are therefore undertaken to definitely evaluate the suitability of the solution proposed both in terms of kinematics and dynamics.

### 6.3 Kinematic and dynamic analysis

The relative hip movements (Fig. 6.3, 6.4) and the loads acting on the articulation (Fig. 6.5, 6.6) calculated in MATLAB are used within the MSC Adams commercial software (Fig. 6.7) to estimate the rotations and torques at the joints of the 6-axis ABB IRB 6620 robot. The tasks performed in order to build the multibody (MTB) model of the mechanical system are:

- import the CAD model of the robot in the working environment;
- define the inertial properties of its parts;
- apply appropriate joints among individual axes;
- create pertinent reference systems for defining the kinematic and dynamic quantities useful in terms of simulation.

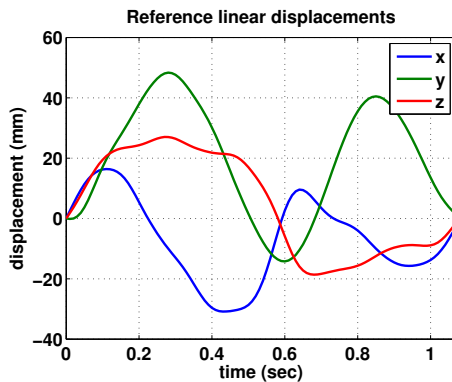


**Figure 6.3:** Reference hip linear displacement components

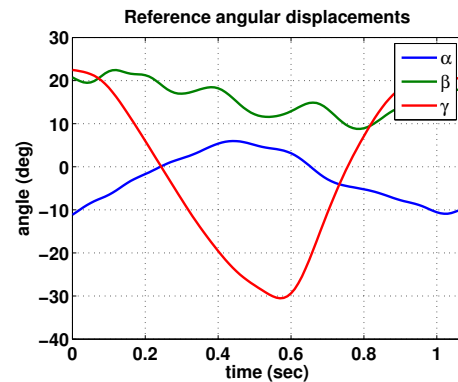


**Figure 6.4:** Reference hip angular displacement components

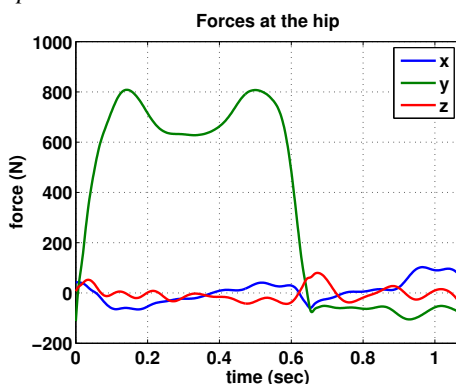


**Figure 6.5:** Reference hip linear displacement components

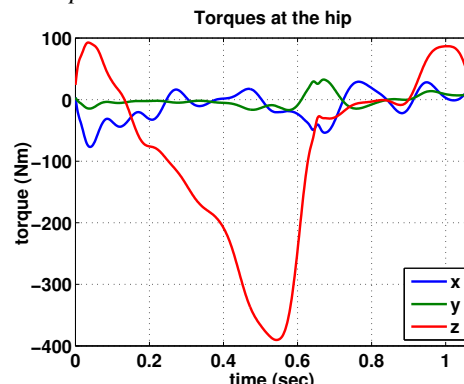


**Figure 6.6:** Reference hip angular displacement components

The latter task implies multiple solutions. There exist indeed infinite reference systems, better known as Work Object (WO) according to the high-level ABB programming language [70], with respect to which define the motion instructions of the Tool Frame (TF) within the robot workspace (Fig. 6.8).

## Chapter 6. Residual limb subsystem

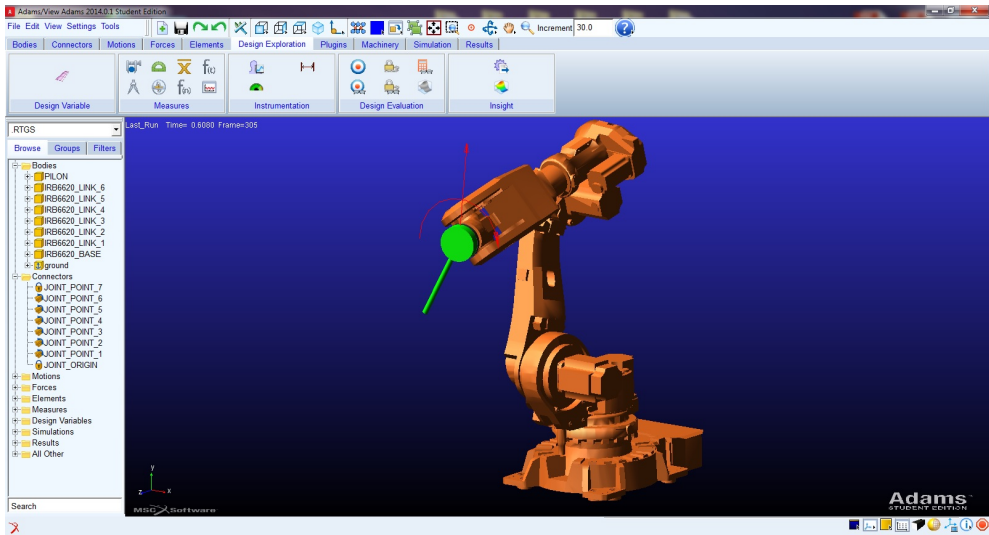


**Figure 6.7:** Representation of the robot model built in MSC Adams

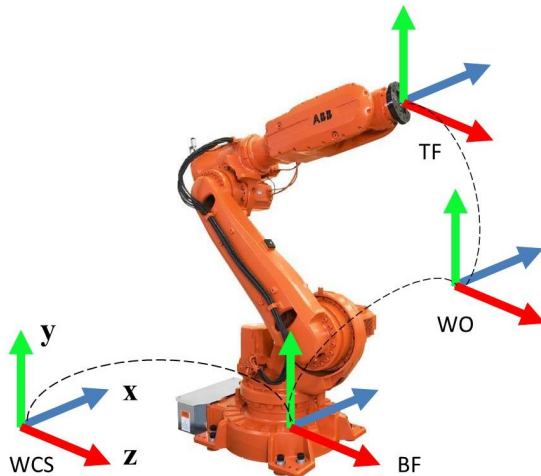


**Figure 6.8:** Main robot reference frames

Despite working in the neighborhood of some WO is clearly more convenient, the optimization process is postponed to the next paragraph (Sec. 6.4). On the other hand, during the initial validation activity of the robot, one of the many triads compliant with the need to facilitate the installation of the rest of the equipment is considered. Such WO is in  $[0, 1600, 1200] \text{ mm}$  with respect to the origin of the Base Frame (BF), that is, the main coordinate system of the robot, and is oriented like the BF itself (Fig. 6.8), that is, according to the reference system with respect to which the gait data are expressed (Chap. 2.4). Once defined the WO two kinds of simulation are performed:

- kinematic analysis;
- dynamic analysis.

Both the angular displacements and velocities at the joints achieved by performing the inverse kinematic analysis are represented below (Fig. 6.9, 6.10).

### 6.3. Kinematic and dynamic analysis

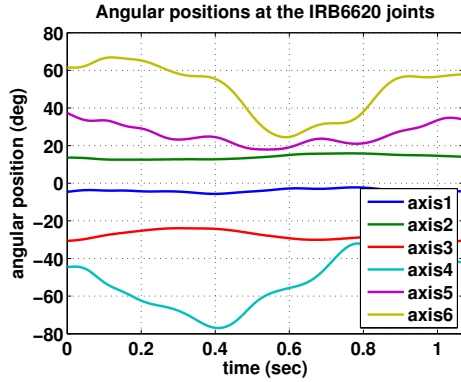


**Figure 6.9:** Joints angular position computed in MSC Adams before optimization

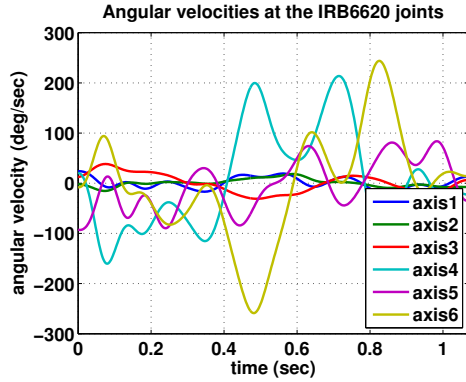


**Figure 6.10:** Joints angular velocity computed in MSC Adams before optimization

Thereafter, these trends are applied to the joints in order to perform the inverse dynamic analysis. In particular, the torques are computed taking into account two different working conditions:

1. neglecting the loads acting on the end-effector;
2. considering the loads acting on the end-effector.

This approach is adopted because the lack of knowledge about the inertial characteristics of the manipulator. Their calculation is indeed necessarily performed by associating the same density ( $2740\text{kg/m}^3$ ) to each solid part constituting the CAD model of the robot ([www.abb.com](http://www.abb.com)). There is no other way to access this confidential information. Obviously, the resulting mass distribution does not correspond to the real one. However, it should be very similar. In fact, the difference between the estimated total weight,  $860\text{kg}$ , and that declared by the manufacturer,  $900\text{kg}$ , is very small. The first simulation is therefore used as a benchmark. The corresponding torques, albeit different from the real ones, are indeed necessarily acceptable as long as the speed and position limits defined by the manufacturer are respected when no load is applied to the end-effector. The obtained results are reported in graphics 6.11 and 6.12.

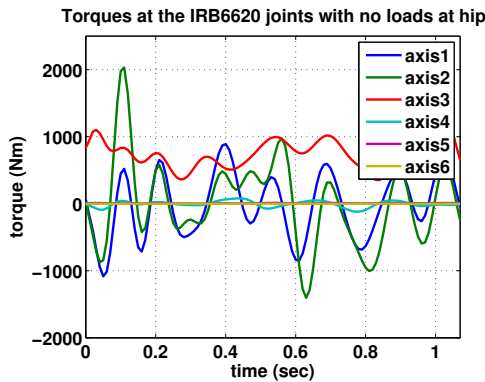


**Figure 6.11:** Joints torques computed in MSC Adams considering no loads at the hip

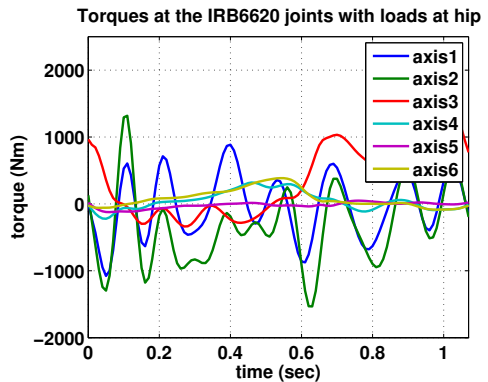


**Figure 6.12:** Joints torques computed in MSC Adams considering the loads at the hip

Finally, the trend of the power required at joints is shown (Fig. 6.13).

## Chapter 6. Residual limb subsystem

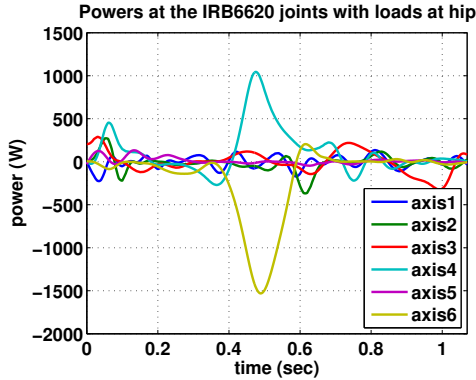


**Figure 6.13:** Joints powers computed in MSC Adams considering the loads at the hip

The analysis of the results reveals the following principal aspects. The torques computed according to the second working condition (Fig. 6.12) are not so much different from those computed according to the first one (Fig. 6.11). The action in some cases is even lower. In fact, the weight of the system allows to load the prosthetic device almost passively, that is, limiting the effort of the engines even if the loads acting on the end-effector of the robot are very high. Thus, the actions of the motors mainly contribute to overcome the inertia of the structure. The robot might therefore be able to perform the required task, thanks to its ability to reproduce the simple motion of the hip in the neighborhood of the WO considered. Such ability has been verified by performing numerical simulations in the devoted robot programming software, ABB RobotStudio (Fig. 6.14), and qualitative tests directly on the machine at the ABB Italian headquarters.

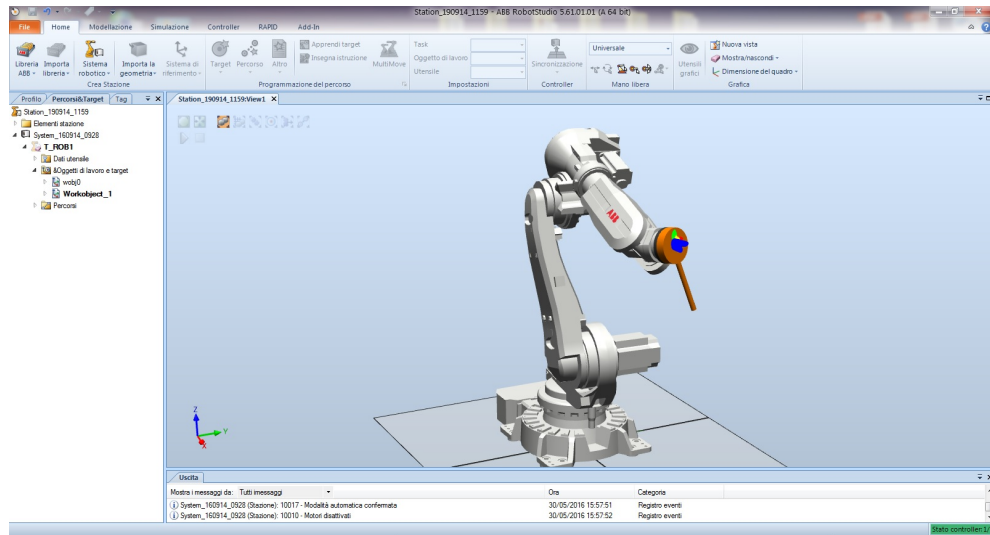


**Figure 6.14:** ABB RobotStudio simulation environment

Anyway, the influence of the working configuration over the joints in terms of speed and torque is investigated so as to further reduce the actions required at the engines. Indeed, the current speeds of the joints 4 and 6 (Fig. 6.10) exceed, albeit not significantly, the maximum limits recommended by the manufacturer and shown in the above table (Tab. 6.1). The MSC Adams optimization tool has been used to improve the design of

the test configuration.

## 6.4 ABB IRB 6620 optimization analysis

---

The aim of an optimization process is to find the best set of design variables that:

- minimizes or maximizes a suitable objective function;
- satisfies the design constraints relevant for the application.

The objective function, better known as cost function, is a numerical quantification of a relevant quality of the system under study. Changes in the design variables result in changes of the value assumed by such function. These parameters are therefore altered, within the admissible ranges, to find the solution that enhances the goodness of the system. However, not all the combinations are possible. Indeed, some sets of design variables result in incompatible states of the system. For this reason, design constraints are defined to discard unacceptable solutions.

In this case the objective function must be a numerical representation of the effort of the robot when performing the typical gait movements. It is therefore computed as the maximum value assumed by the sum of the squared torques,  $T_i$ , applied by the motors during the simulation. The value assumed by this function changes according to the working configuration of the robot and therefore according to two different sets of design variables:

- the three position components of the WO within the workspace,  $(x, y, z)$ ;
- the three orientation components of the TF with respect to the end-effector of the robot,  $(\alpha, \beta, \gamma)$ .

The first three parameters determine the working point. The others define instead how the prosthesis is fixed at the end-effector of the robot, and consequently the configuration assumed by the manipulator during the execution of the movements. From a practical point of view, the same result may be achieved by varying the orientation of the WO rather than the TF (Fig. 6.15). However, this approach induces the need to update the gait kinematic data according to the new set of orthogonal axes before performing each simulation. As a consequence, the TF orientation is varied so as to make the procedure faster and less tedious (Fig. 6.15).

Regardless of the variables considered, aim of the solver is to find the solution minimizing the objective function, whose expression is:

$$F(x, y, z, \alpha, \beta, \gamma) = \max\left(\sum_{i=1}^6 T_i^2(x, y, z, \alpha, \beta, \gamma)\right)$$

However, not all the possible configurations are suitable. Some of them result indeed in velocities at the joints higher than the prescribed limits (Tab. 6.1). Some constraints are therefore imposed to prevent working conditions potentially dangerous for the system. Although essential, these constraints prevent the procedure to converge towards the absolute minimum of the objective function. Anyway, achieving the optimal condition is useless if not applicable. Its value may even raise rather than diminish so as

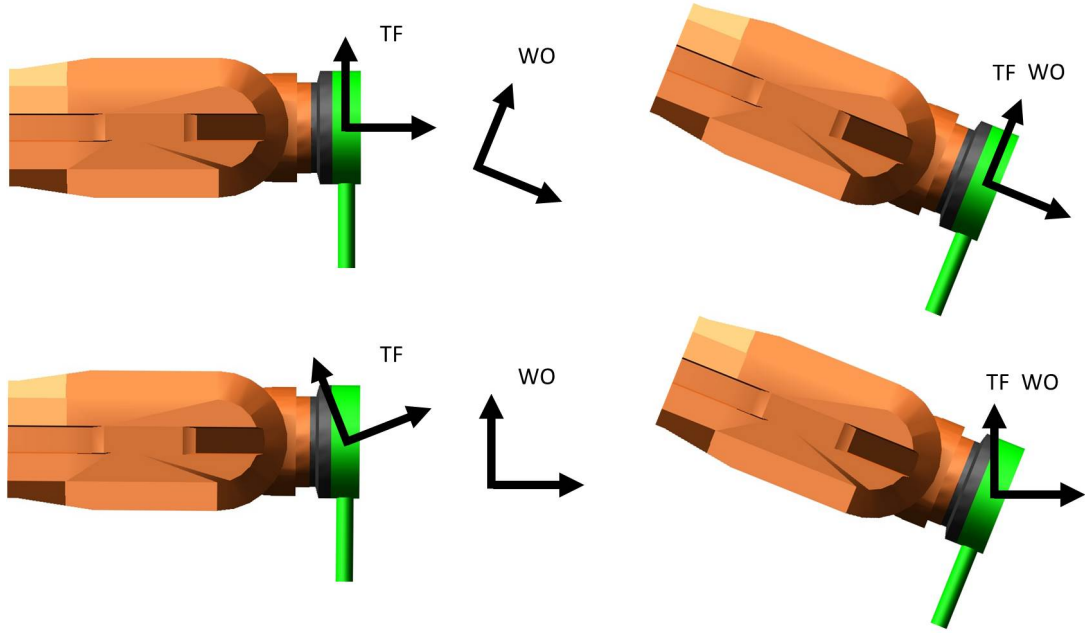


**Figure 6.15:** Orientation of the TF with respect to the end-effector

to meet the design constraints. In the present case, for example, the value of the objective function increases by 66.3% before finding the solution that meets the design constraints (Fig. 6.16).

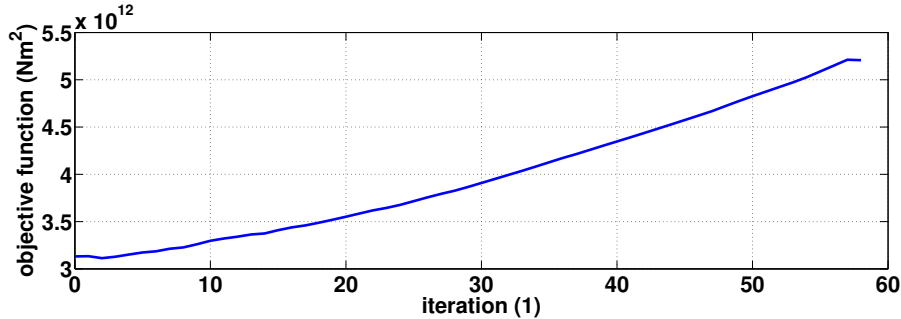


**Figure 6.16:** Trend of the objective function during the optimization procedure

At the end of the process, the TF final orientation differs so little from the initial one to not justify its adoption since this would unnecessarily complicate the design of the prosthesis grasping system. The origin of the WO moves instead to the point  $[-132, 1481, 1086] mm$  with respect to the BF.

Once completed the optimization process, the rotations and the torques applied at the joints of the robot are evaluated again. Both the angular displacements and velocities at the joints achieved by performing the inverse kinematics analysis are represented below (Fig. 6.17, 6.18).

In comparison with the previous case, the speed of each joint is confined within the recommended limits (Tab. 6.1). Subsequently, the kinematic information are used to

#### 6.4. ABB IRB 6620 optimization analysis

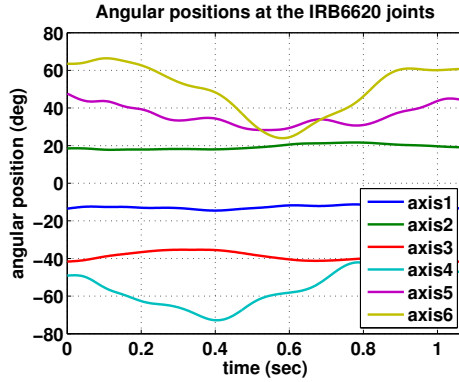


**Figure 6.17:** Joints angular position computed in MSC Adams after optimization

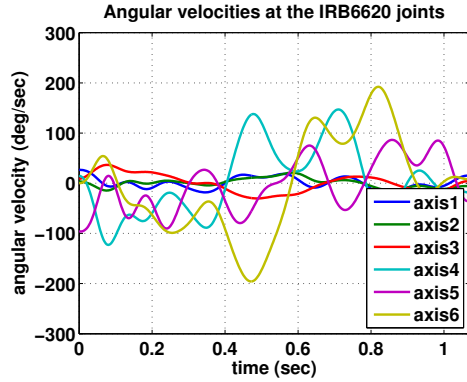


**Figure 6.18:** Joints angular velocity computed in MSC Adams after optimization

perform the inverse dynamic analysis. Such simulation is undertaken considering both the loads acting on the end-effector and the inertial characteristics of the mechanical system. The results are reported in the following figure (Fig. 6.19).

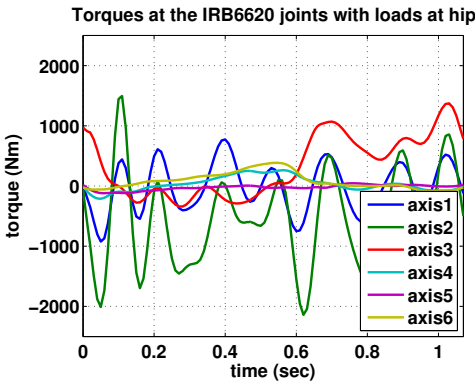


**Figure 6.19:** Joints torques computed in MSC Adams after optimization

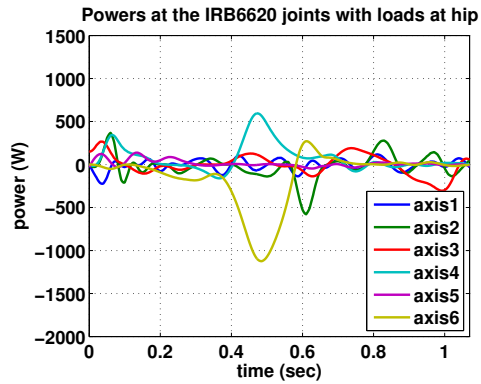


**Figure 6.20:** Joints powers computed in MSC Adams after optimization

The trends of the torques are quite similar to the previous ones (Fig. 6.12) except for the second joint (axis2). Its absolute maximum value is indeed about 30% higher. Nevertheless, it is not greater than the absolute maximum calculated for the same joint according to working condition number 1, that is, neglecting the loads acting on the end-effector (Fig. 6.11). Thus, the increment is potentially acceptable. Moreover, the lower velocities result in powers reduction, especially at the joints 4 and 6 (Fig. 6.20).

As a consequence, the system benefits from the optimization process despite the torque increment, and the computed position of the WO is definitely adopted. The same working point is considered when running the final simulation, i.e. when the numerical models of the systems separately analyzed so far, are imported into a single simulation environment in order to:

- evaluate the behavior of the gait simulator as a whole;
- identify any limitations of the proposed solution;
- provide a tool that allows to further develop the system.

## Chapter 6. Residual limb subsystem

---

Before carrying out this task (Chap. 7), the prosthesis grasping solution is designed being known that the orientation of the TF has not been affected by the optimization process.

### 6.5 Prosthesis grasping solution

---

The development of the system necessary for rigidly connecting the prosthesis to the end-effector of the industrial robot is not particularly difficult. There are three main design requirements to be considered:

- properly align the prosthesis to the system;
- correctly transfer the movements from the robot to the prosthesis;
- simulate subjects having different heights.

To meet each of these aspects, the system is divided into three parts:

1. one for simulating the mechanical axis of the femur;
2. one for connecting the artificial limb to the end-effector of the robot;
3. one for aligning and assembling the previous two.

The considerations and the choices that influenced the development of these three components are analyzed below starting from the first.

By excluding the socket (Chap. 1), the mechanical axis of the femur may be easily reproduced by means of a tube having:

- the length of the corresponding biological counterpart;
- the section big enough to be considered as rigid.

From this point of view, a tube having an external diameter of 30mm is probably thick enough and introduces one major advantage: the possibility to connect the prosthetic knee to the system using a solution widely used on the market, the prosthetic tubular adapter (Fig. 6.21).



**Figure 6.21:** Prosthetic tubular adapter

## 6.5. Prosthesis grasping solution

This solution besides being reliable, allows to vary the alignment of the prosthesis arbitrarily and therefore to increase the versatility of the system. The length of the tube may instead be calculated using anthropometric relations, i.e. formulas that allow to estimate the size of the body segments, starting from the height of the subject under study. In this case a tube 500mm long is suitable for the application [87].

The purpose of the second element is to connect the artificial limb to the robot end-effector in a simple and reliable way. From this point of view, the choice is to use a pierced plate modeled so as to fit the geometry of the end-effector itself.

The third component, i.e. the connection element, is finally developed so as to guarantee a stable connection of the aforementioned ones during the test procedure. The proposed solution allows to transmit torques and forces in terms of interference when tightening the screws. Below are two SolidWorks representations of the elements described above (Fig. 6.22, 6.23).

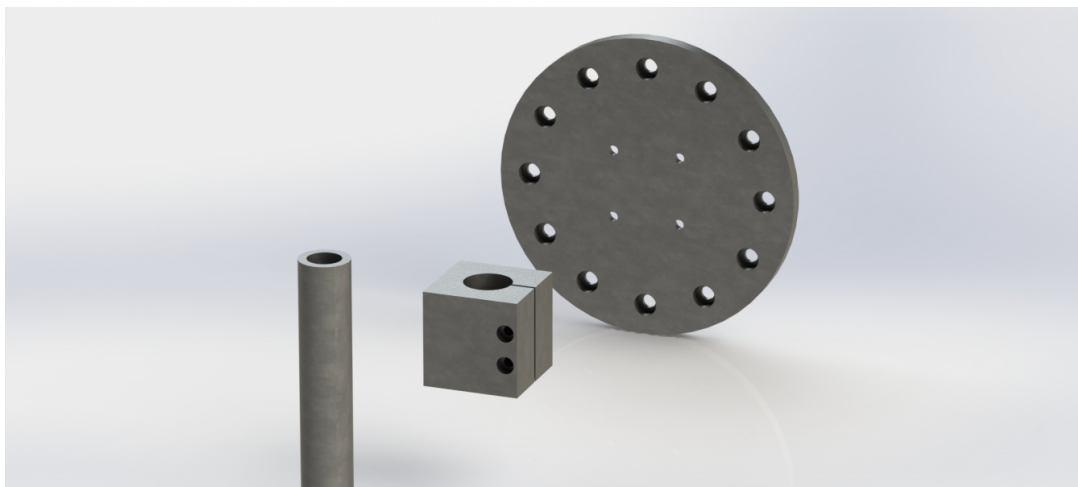


**Figure 6.22:** SolidWorks representation of the grasping solution

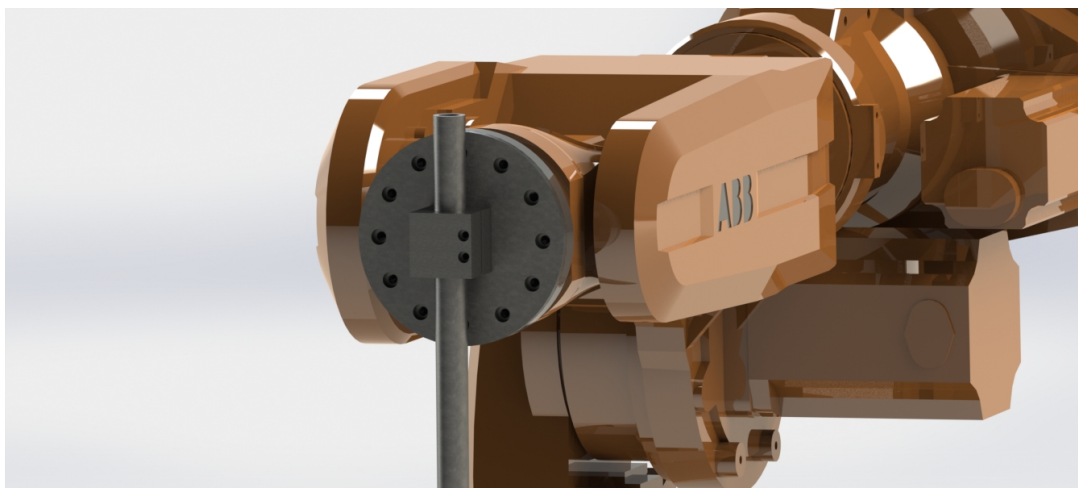


**Figure 6.23:** SolidWorks representation of the grasping solution mounted on the robot

## **6.6 Residual limb subsystem concluding remarks**

---

Despite a custom-made system would ensure higher performance, only 6-axis industrial robots are considered for reproducing the motion of the hip during the first development stage of the test bench.

However, no information about the possibility to use this kind of manipulator for simulating human gait features is available in the literature, to the best of the author's knowledge. Thus, some simulations have been carried out to estimate the suitability of the model under study.

According to the results, such a robot - ABB IRB 6620 - has a work space wide enough to fulfill the kinematic requirements as well as a payload capacity sufficiently high to withstand the loads acting at its end-effector during motion.

Two key aspects support this possibility. First, the actions of the motors mainly contribute to overcome the inertia of the structure. In addition, the weight of the system allows to load the prosthetic device almost passively, that is, reducing the effort of the engines themselves. The robot might therefore be able to perform the required task due to its ability to simulate the same motion when no load is applied at the end-effector.

Nevertheless, the working point has been optimized in order to reduce the stress at each axis. The corresponding results have been finally considered during the design of the solution necessary for accommodating the prosthesis on the robot.

---

# 7

## CHAPTER

---

## Numerical model of the entire system

---

### 7.1 Introduction

In this section the models developed so far, considering one by one the three main units of the bench, are grouped in order to evaluate the merits and the limits of the entire system as a whole.

### 7.2 ADAMS-MATLAB/Simulink co-simulation

The development of a mechatronic system, such as the test bench proposed in this document, generally passes several times through the design process before the final result meets all the project requirements. Due to either simplifications or unpredictable mutual interactions, the individually defined/selected parts (such as mechanics, actuators, sensors, control algorithms, etc.) may indeed be not suitable to achieve the ultimate purpose as an assembly.

For instance, the solution developed for reproducing the loads acting on the foot in longitudinal direction has been defined under the hypothesis to accurately reproduce the vertical force component (Chap. 4). Results obtained successively demonstrate that this assumption is not valid. The need to exploit the air spring almost passively during the initial and final stage of contact prevents indeed the possibility to track the actual force reference in vertical direction. On the other hand, an approximation is reproduced (Chap. 5). The ability of the vertical actuating subsystem itself to reproduce such reference was assessed under simplifying assumptions. As a matter of fact, the foot was modeled as a massless point moving along the vertical direction according to a law of motion similar but not equal to the physiological one. In addition, some mechanical properties are either wrong or missing. Among these are the inner stiffness of the

## Chapter 7. Numerical model of the entire system

mechanism in vertical direction and the friction between some connection elements, whose nature has been investigated experimentally just after modeling.

Once defined the individual units, a tool that allows to directly evaluate how each parameter influences the final result of the overall system is therefore strictly necessary. This approach removes the need to perform these considerations separately, making the process more reliable, light and fast. From a practical point of view, this means integrating into a single model the mathematical representation of all the mechanical and the control systems developed so far.

This issue is supported by several simulation and engineering tools. The majority of commercial software allows indeed to create within their own simulation environment both the aforementioned systems. Although very powerful, these software provide tools for accomplish detailed operations in just one domain. Thus, the co-simulation, namely the usage of two software in parallel, is many times the best approach. Among all the available techniques, a co-simulation based on ADAMS and MATLAB/Simulink cooperation can be a useful tool for testing the solution proposed and improving the development process of the rig [18]. This technique has already demonstrated to be a suitable tool for studying the mechanical design and dynamic behavior of complex mechatronic systems like robots, manipulators and cars, and for testing the corresponding control logics. As a consequence, this chapter deals with the development of a model based on direct embedding of dynamic model of the mechanical system implemented in ADAMS into the control plant developed in MATLAB/Simulink environment (Fig. 7.1).

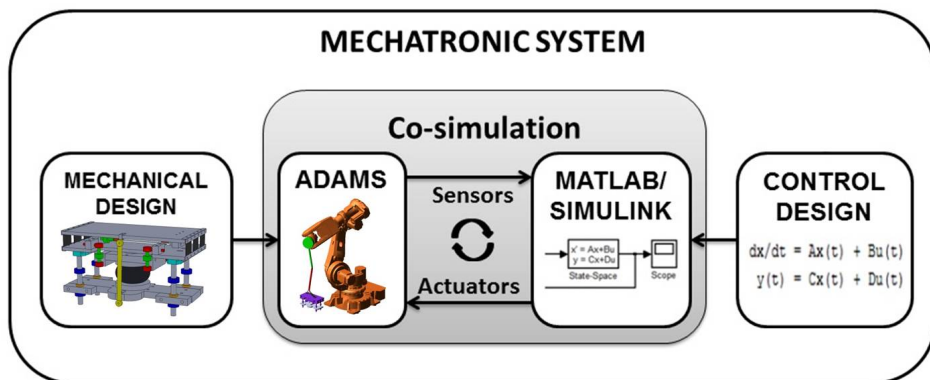


**Figure 7.1:** Schematic representation of the co-simulation model

### 7.3 Numerical model of the mechanical system

ADAMS is a multibody dynamics simulation software for studying the dynamic behavior of interconnected rigid or flexible bodies, each of which may undergo large translational and rotational displacements. It is used to build the model of the mechanical system because of some features making it superior than MATLAB/SimMechanics:

- the possibility to import and graphically display the solid models of the components constituting the system;
- the opportunity to define kinematic and dynamic relations between bodies in an automatic way by means of built in functions;

### 7.3. Numerical model of the mechanical system

- the ability to define in parametric form some of the design variables.

The elements constituting the mechanical systems:

- the 6-axis industrial robot;
- the ground subsystem mechanism;
- the prosthetic components;
- the prosthesis grasping device;

are first designed and assembled in SolidWorks. The assembly is then imported into the ADAMS simulation environment. Here, the constraints and the mass properties of each single part are defined.

In addition, all the forces and measures necessary both for control and validation purposes are specified. Here is a representation of the resulting mechanical system (Fig. 7.2).

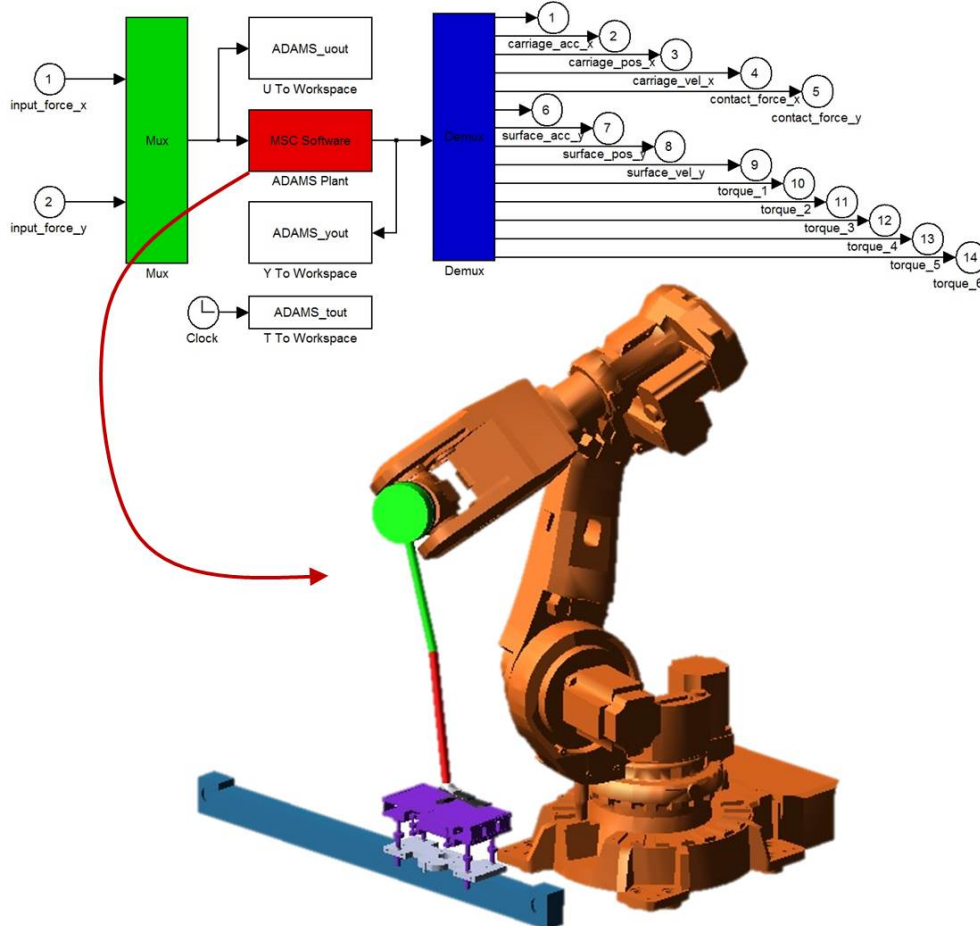


**Figure 7.2:** Representation of the mechanical model of the overall system built in ADAMS

Such a MTB model is finally imported into the MATLAB/Simulink simulation environment using the ADAMS/Control toolbox [54]. During this procedure the input and

## **Chapter 7. Numerical model of the entire system**

---

output state variables are identified. The outputs describe the variables that go to the controls application. The inputs describe the variables that come back into ADAMS and, therefore, complete the closed loop between ADAMS and the control application, i.e. MATLAB/Simulink.

Inputs state variables to the MTB model are:

- the net external forces driving the displacement of the force plate both in horizontal and vertical direction;
- the contact forces between the prosthetic foot and the force plate both in horizontal and vertical direction.

The first contributions determine, together with the inertial forces computed in ADAMS, the motion of the force plate within the sagittal plane. On the other hand, the second contributions are applied to the prosthetic foot so as to compute the torques required at the joints of the robot under more realistic conditions.

Outputs state variables from the MTB model are instead:

- the position and velocity of the force plate both in horizontal and vertical direction;
- the position and velocity of the prosthetic foot both in horizontal and vertical direction;
- both the kinematic and dynamic actions at the joints of the 6-axis industrial robot.

The first and the second sources of information are used in Simulink to compute the forces acting on the mechanics of the system, such as the frictions and the contact forces, as well as the reference signals to be tracked during both the stance and the swing phase. These signals are then processed by the controller in order to evaluate the command of the actuators and compute the net forces to be applied in ADAMS. On the other hand, the kinematic and dynamic quantities describing the behavior of the manipulator are output for verdict purposes, i.e. for assessing the suitability of the robot under more realistic conditions.

Once completely defined the MTB model and exported its plant, most of the operations are performed in MATLAB.

### **7.4 Numerical model of the control system**

---

MATLAB/Simulink is a powerful environment for mathematical modeling and result processing. Its strong points are:

- the usage easiness;
- the computational robustness.

The control system of each mechanical system is already implemented in Simulink as well as the equations describing the pneumatic actuator and the contact between the prosthetic foot and the force plate. Compared to the previous individual cases the only difference is the modeling of the mechanical system in ADAMS. In addition, for increasing the reality and reliability of the simulation also the mechanical properties experimentally evaluated are implemented. In particular, the aspects introduced are:

## 7.5. Operation and results

- the nonlinear stiffness of the ground subsystem in vertical direction (Sec. 5.7.3);
- the friction acting on the ground subsystem in vertical direction (Sec. 5.7.3);
- the friction acting on the ground subsystem in horizontal direction (Sec.4.8.3).

An overview of the control plant is given in figure (Fig. 7.3).

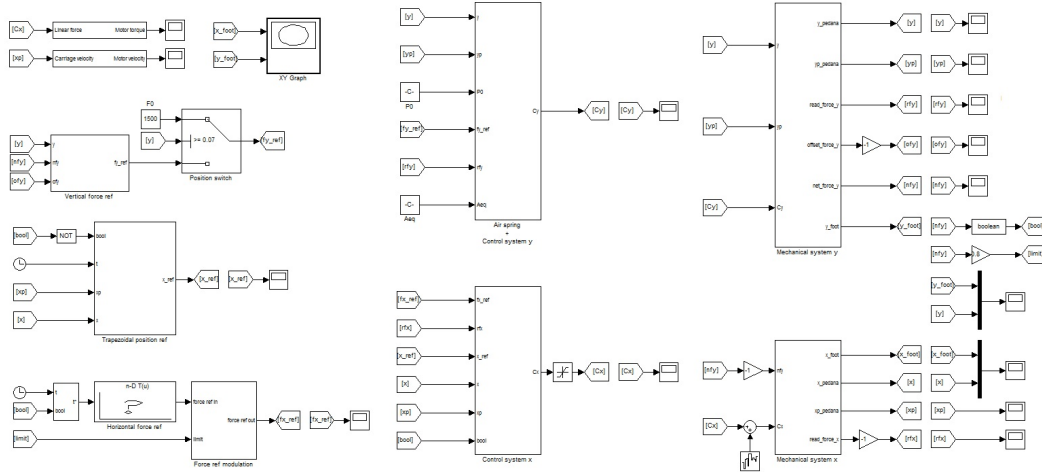


**Figure 7.3:** Representation of the control system built in MATLAB/Simulink

Once connected the ADAMS plant model into the block diagram created in Simulink is therefore sufficiently to define the simulation parameters and run it. The final results obtained through this numerical model are analyzed below.

## 7.5 Operation and results

The behavior of the gait simulator is first qualitatively assessed in ADAMS through its graphical interface; here are the pictures of the main simulation instants (Fig. 7.4).

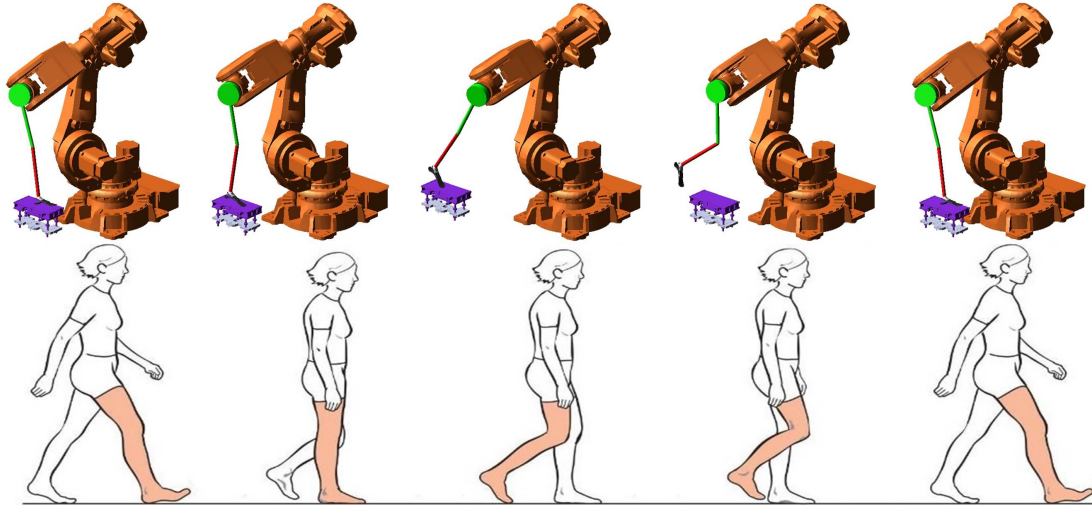


**Figure 7.4:** Comparison of the main co-simulation results with the corresponding gait instants

## Chapter 7. Numerical model of the entire system

---

The behavior of the system is then quantitatively analyzed in MATLAB in order to evaluate the merits and the limits of the gait simulator as a whole. First of all, the trajectory of the foot within the sagittal plane is analyzed (Fig. 7.5).

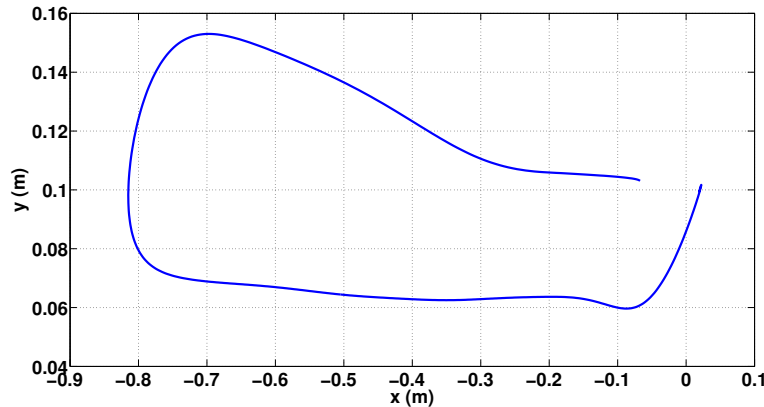


**Figure 7.5:** Trajectory followed by the foot in the sagittal plane

It is worth noting that the height at which the foot is moving during the contact phase is not constant as previously assumed (Sec. 5.6.2, Fig. 5.43) but oscillating. Even if restrained, such unnatural behavior is definitely induced by the decision to model the prosthetic foot as a rigid body and by the simplifications inevitably introduced when computing the length of the lower limb segments via the anthropometric relations. Greater affinity could probably be obtained by introducing the flexible model of the foot and by measuring the length of the limb segments directly on the subject. Nevertheless, the deviations are small enough to be neglected. Moreover, despite the noise, the vertical loading subsystem manages to maintain the contact during the entire stance phase and to acceptably reproduce the corresponding vertical force component both in terms of amplitude and duration (Fig. 7.6).

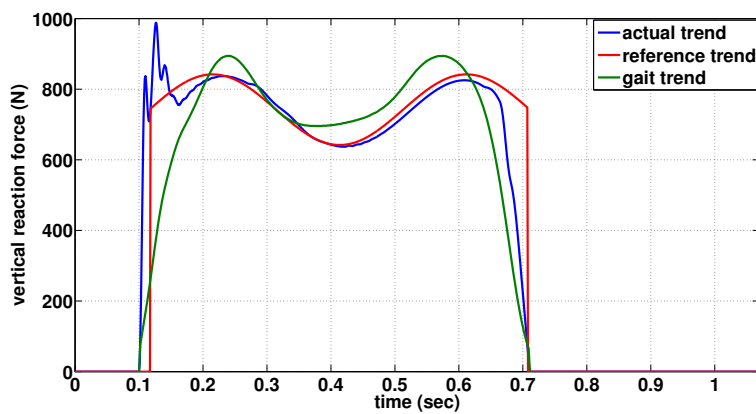


**Figure 7.6:** Vertical reaction force achieved by means of the model and corresponding gait trend

Reproducing the vertical force by means of an air spring is therefore successful. Besides restraining the sudden stress changes at the beginning of the contact phase, it has a bandwidth sufficiently wide to allow for a correct reproduction of the reference.

## 7.5. Operation and results

From this point of view, it is worth to remind that the reference force to be reproduced is not the real one but an approximation thereof. Nevertheless, such approximation has been modified in order to fit as much as possible the signal acquired during the gait analysis session (Fig. 7.6). This aspect is very important because the correct reproduction of the vertical force allows to test the functionality of the prosthesis under more realistic conditions. Furthermore, it is important in terms of computation of the longitudinal force reference. Its trend is reported in figure (Fig. 7.7).

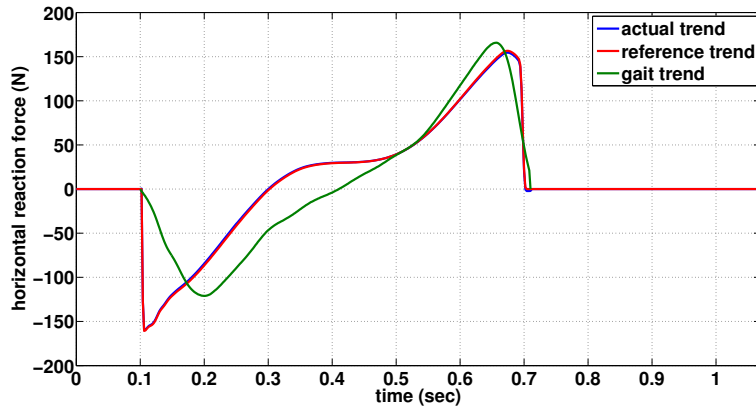


**Figure 7.7:** Horizontal reaction force achieved by means of the model and corresponding gait trend

Despite the attempts to achieve a more realistic trend, deviations from the gait pattern are rather obvious in terms of longitudinal direction (Sec. 4.6.3). This increment is definitely due to the different trend of the force applied to the foot in vertical direction and the peaks at the beginning of the contact phase. Nevertheless, the aim to apply full scale force in longitudinal direction is achieved. The trends are therefore comparable just qualitatively.

The performance of the ground subsystem are better in terms of position recovery during the swing phase. The system is indeed able to recover the initial position, both in vertical and horizontal direction, before the beginning of a new cycle (Fig. 7.8, 7.9).

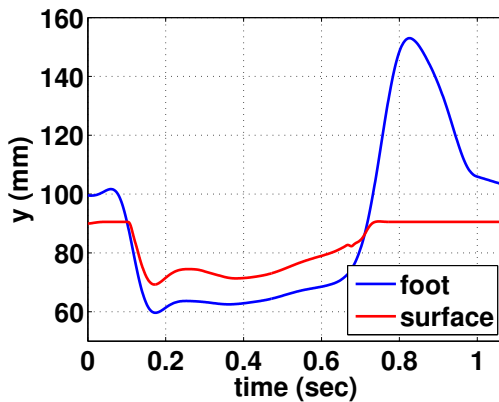


**Figure 7.8:** Vertical displacement of both the force plate and the foot

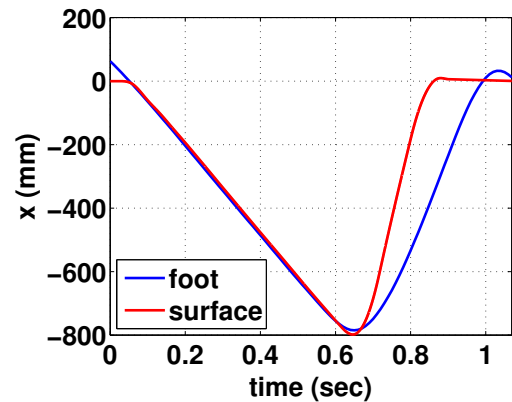


**Figure 7.9:** Horizontal displacement of both the force plate and the foot

Finally, here are the trends of the actions of the air spring (Fig. 7.10) and the brush-

## Chapter 7. Numerical model of the entire system

---

less motor (Fig. 7.11), as well as the torques applied at the joints of the robot (Fig. 7.12).

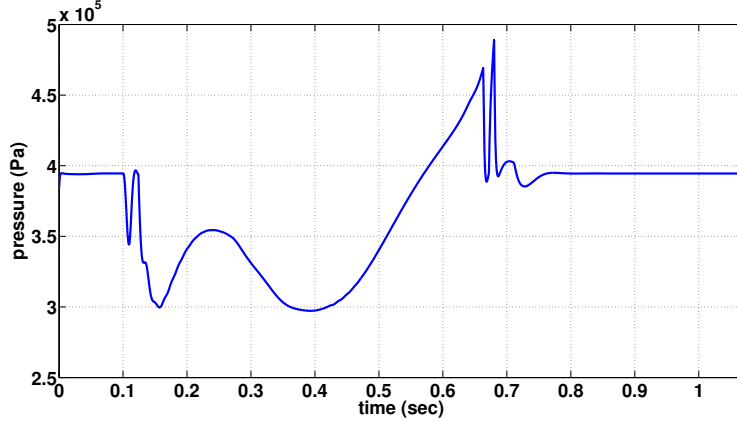


**Figure 7.10:** Absolute pressure within the air spring

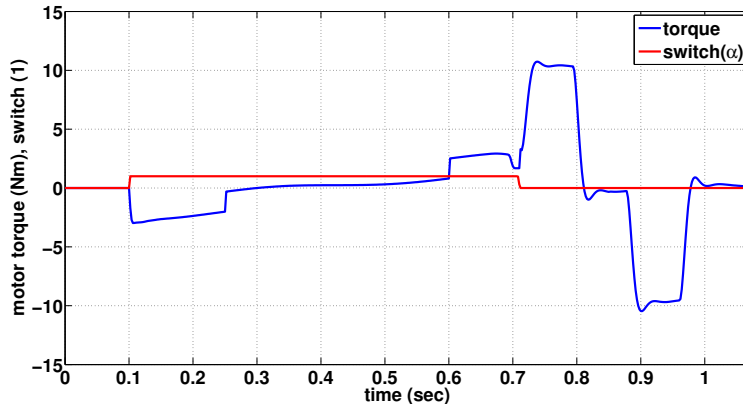


**Figure 7.11:** Torque applied by the brushless motor connected to the linear guide

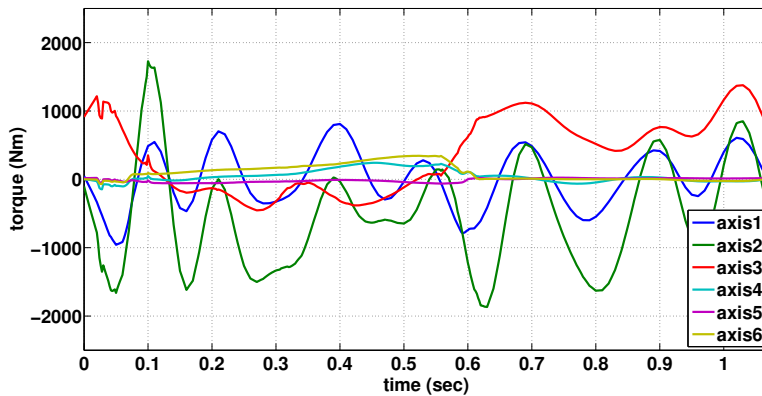


**Figure 7.12:** Torques at the joints of the robot

As expected, robot torques are quite similar to the previous one (Fig. 6.19). Dif-

## **7.6. Numerical model of the entire system concluding remarks**

---

ferences in terms of force applied to the foot are indeed very small and, as previously stated, the contribution of the inertial loads is more significant. Also the force peaks at the initial stage of contact do not generate torque variations so abrupt to compromise the functioning of the manipulator. The robot may therefore be able to perform the required task, i.e. to correctly reproduce the hip kinematics at near physiologically correct velocities.

## **7.6 Numerical model of the entire system concluding remarks**

---

The results achieved by means of the numerical model of the entire system support the considerations already undertaken considering each subsystem as a single unit from a mechanical point of view. On the other hand, the algorithms developed for computing the force references in real time as a function of the current state of the system require additional improvements. The performance of the system heavily relies indeed on the possibility to correctly reproduce the vertical force component. Further clarification are given in the next chapter.



---

# CHAPTER 8

---

## Conclusions

---

This research topic has dealt with the development of a bench for testing lower limb transfemoral prostheses, especially modern ones (Chap. 1). The idea of developing such a bench was established after a careful evaluation of the requirements and test methods defined by the International Standards Organization to assess the conformity of the mentioned devices. These standards merely identify structural tests to verify that the prostheses, and their individual components, are able to ensure adequate strength properties during their use. As a consequence, they are not suitable for assessing the functional performance of the prosthetic devices, that is, the ability to assist the amputee while walking. Standards limits are even more evident when considering that, in the recent past, the technological advancement mostly concerned the possibility of integrating ever smaller and more powerful electronic components instead of new materials and topologies. For instance, the knee prosthetic joints currently on the market guarantee maximum yield by means of sensors and actuators that allow to adjust in real time the physical characteristics and thus the response of the device itself. Meanwhile, researchers are developing new devices for restoring many locomotive functions corrupted by the disability, such as sit-to-stand maneuvers, stair/slope ascent ambulation, as well as level walking. However, a prosthesis having such characteristics is far from being realizable in short time. On the one hand, developing a commercially viable active prosthesis that is humanlike in its weight, size, strength, and impedance, while still being energetically economical and noise free, is a challenging design problem. On the other hand, suitable development and verification methods for assessing the functional properties of the prostheses are missing.

The need to perform this kind of test is not recent, several solutions have been proposed in the literature. Among these, in-vitro prostheses experimentations demonstrate several advantages over in-vivo ones in terms of reliability, versatility and safety. It is

## Chapter 8. Conclusions

---

therefore foreseen that robotic testing will play a greater role than human gait trials in the development process of prosthetics.

According to these considerations, in the present work a novel in-vitro test bench for assessing the functional properties of transfemoral prostheses has been developed. In particular, the definition process was performed in order to overcome the three main significant challenges of the current gait simulators:

- operating at near physiologically correct velocities;
- inputting full scale ground reaction forces;
- simulating motion in all three planes (sagittal, coronal and transverse).

To this end, the kinematic and dynamic data obtained during a gait analysis session (Chap. 2) have been used to:

- define the mechanical architecture of the system;
- identify the essential components and verify their commercial accessibility;
- develop the custom made parts which are not yet available on the market.

At the end of this procedure, the gait simulator exhibits 8 DOFs and is made of two main subsystems with 6 and 2 DOFs. These are respectively used to replicate the series of motion patterns performed by the residual segment of the limb and the loads acting on the prosthetic foot due to reaction with the ground. The first task is realized by means of a six-axes industrial manipulator having suitable motion and payload capabilities and controlled in terms of position during the entire gait cycle. On the other hand, the contact forces are reproduced through an innovative force plate, controlled both in terms of force and position, whose longitudinal and vertical progression are respectively driven by means of a linear guide and an active air spring. Finally, specific mounting devices have been designed to accommodate the aforementioned units and the prosthetic specimen under test.

Once defined the mechanical architecture, the individual units have been studied separately by performing numerical simulations and experimental test in order to:

- evaluate the merits and the limits of the proposed solutions;
- develop specific control logics.

Then, their models were integrated within a single simulation environment to evaluate the performance of the system as a whole. Here are reported the main considerations achieved during the development of the test bench.

The sudden stress changes at the initial stage of contact determined the necessity to introduce a compliant behavior in the main load direction. Since the low level control plant of the robot is not accessible, a pneumatic actuator has been used for reproducing the vertical force so as to exploit the compressibility of the gas. In particular, an air spring was selected. However, this solution did not allow to correctly reproduce the actual trend of force obtained during the gait analysis session. Firstly, the need to exploit this kind of actuator almost passively (constant inner pressure) during the initial and final stages of the contact introduced the need to track a force reference which is

---

an approximation of the real one. Even if the strategy can be improved, a trend equal to the real one is far from being achievable. Anyway, this might not be a problem since a standard pattern does not exist to the best of the author's knowledge. Therefore, it is sufficient to reproduce a trend comparable to the physiological one in its recurring characteristics. Secondly, the frequency content of the actual vertical force signal is higher than the bandwidth of this kind of actuator as well as of the servo-valve used during the experimental tests. Although this limitation has not prevented to achieve satisfactory results, an actuation system having a higher dynamic response would be preferable. However, such actuators would require oriented solutions for introducing the compliant behavior either in terms of hardware or control logic. Moreover, they likely entail an increment of the mass and consequently the risk to exceed the operation range of the available brushless motor. It is therefore more convenient to evaluate the benefits related to the application of more sophisticated control strategies rather than different hardware solutions. Indeed, during this study only the possibility to implement linear control logics was considered for the sake of simplicity. This solution, in conjunction with the Mixed control architecture, allowed to achieve good results in longitudinal direction (Chap. 4). On the other hand, both the numerical simulation and the experimental tests performed revealed the limits of this approach when dealing with high nonlinear systems as the pneumatic actuator used in this work (Chap. 5). An adaptive or a nonlinear control would probably improve the performance of the vertical loading subsystem and therefore, according to the study performed, the reliability of the entire simulator. Also the computation of the longitudinal force would benefit from this enhancement since it is computed in real time as a function of the vertical force itself. From this point of view, it is also worth to check the possibility to achieve a more realistic longitudinal reference force trend by considering different approximation techniques.

Finally, the decision to split the bench in two subsystems for separately reproducing the kinematic and dynamic aspects of gait is successful. In fact, as stated in the literature, robots compliant with the gait kinematic and dynamic requirements have indeed an inertia so high to prevent the correct reproduction of the force reference whenever controlled in terms of position. On the other hand, strategies directed toward the control of the force may result in deviations of the hip from the expected trajectory resulting in a wrong kinematic reproduction of the phenomenon.

Despite the limitations highlighted, the initial objectives are achieved. According to author's opinion the method proposed is therefore successful. Thus, if the conditions are satisfied also experimentally, the method could be applied in the design and development process of the lower limb prostheses in order to ensure a wider range of locomotive advantages for people affected by disability. Finally, it is worth to outline and share with the authors involved in the topic the relevance of the clinical outcomes in the prosthetic design process as they have been of fundamental importance in the development of the present test bench.



---

# APPENDIX A

---

## Anatomical frames

---

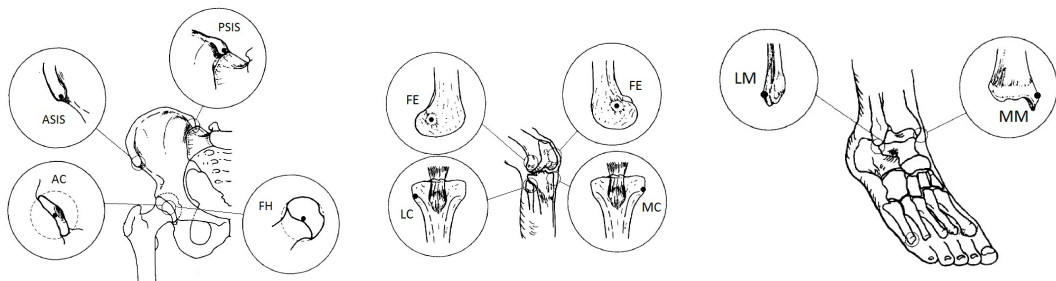


**Figure A.1:** Anatomical landmarks

---

### A.1 Thigh coordinate system

---

Anatomical landmarks (Fig.A.1):

FE: Femoral epicondyle.

FH: Femoral head (equal to AC).

Embedded axes:

$O_t$ : The origin coincident with the right (or left) hip center of rotation.

$Y_t$ : The line joining the midpoint between the medial and lateral FEs and the origin, and pointing cranially.

$Z_t$ : The line perpendicular to the  $Y_t$ -axis, lying in the plane defined by the origin,  $O_t$ , and the two FEs, pointing to the right.

## **Appendix A. Anatomical frames**

---

$X_t$ : The line perpendicular to both  $Y_t$ - and  $Z_t$ -axis, pointing anteriorly [20].

### **A.2 Shank coordinate system**

---

Anatomical landmarks (Fig.A.1):

MM: Tip of the medial malleolus.

LM: Tip of the lateral malleolus.

MC: The most medial point on the border of the medial tibial condyle.

LC: The most lateral point on the border of the lateral tibial condyle.

IM: The inter-malleolar point located midway between MM and LM.

IC: The inter-condylar point located midway between the MC and LC.

Anatomical planes:

Frontal plane: The plane containing points IM, MC and LC.

Torsional plane: The plane containing points IC, MM and LM.

Sagittal plane: The plane perpendicular to the frontal plane and containing the long axis of the shank (the line connecting points IC and IM).

Transverse plane: The mutual plane perpendicular to the frontal and sagittal planes.

Embedded axes:

$O_s$ : The origin coincident with IM.

$Z_s$ : The line connecting MM and LM, and pointing to the right.

$X_s$ : The line perpendicular to the torsional plane of the shank, and pointing anteriorly.

$Y_s$ : The line perpendicular to both  $X_s$ - and  $Z_s$ -axis.

### **A.3 Foot coordinate system**

---

Anatomical landmarks (Fig.A.1): Same as for shank.

Embedded axes:

$O_f$ : The origin coincident with that of the shank coordinate system ( $O_s$ ) in the neutral configuration.

$Y_f$ : The line coincident with the long axis of the shank in the neutral configuration, and pointing cranially.

$X_f$ : The line perpendicular to the frontal plane of the shank in the neutral configuration, and pointing anteriorly.

$Z_f$ : The common line perpendicular to  $X_f$ - and  $Y_f$ -axis.

#### **A.4 Global coordinate system**

---

Finally, a right-handed orthogonal triad fixed to the ground with the positive  $Y_g$ -axis upward and parallel to the field of gravity and the positive  $X_g$ -axis lying on the floor and pointing in the progression direction of walking, is used as global reference frame.



---

# APPENDIX $\mathcal{B}$

---

## Angular convention

---

The mathematics useful to specify the relative orientation of two sets of coordinates is analyzed in this section.

### B.1 Cardan and Eulerian angles

---

The final orientation of one triad with respect to another can be achieved by applying three consecutive rotations  $\alpha, \beta, \gamma$  about the axes  $U_1, U_2, U_3$  of either the moving or fixed coordinate system, starting from an alignment situation. Because of these three rotations, the moving triad initially in  $X_0Y_0Z_0$  evolves into  $X_1Y_1Z_1$ , then in  $X_2Y_2Z_2$  and finally in  $X_3Y_3Z_3$ .

$$\begin{array}{cccccc} X_0Y_0Z_0 & \xrightarrow[U_1]{\alpha} & X_1Y_1Z_1 & \xrightarrow[U_2]{\beta} & X_2Y_2Z_2 & \xrightarrow[U_3]{\gamma} \\ (0) & & (1) & & (2) & & (3) \end{array}$$

Each rotation as well as the final orientation is described by means of a matrix. In particular, the value assumed by the elements of the latter may be computed alternately according either the Cardan or Euler convention. Twelve combinations are possible if considering only intrinsic rotation, that is, rotations about the axes of the moving triad. Only the Cardan are considered below.

### B.2 Cardan convention: position

---

The final orientation matrix can be expressed as the product of the 3 matrices as follow:

$$R = Rot(i, \alpha)Rot(j, \beta)Rot(k, \gamma) \quad (i \neq k)$$

---

## Appendix B. Angular convention

where  $i, j, k$  represent the axes of the moving triad about which the rotations  $\alpha, \beta, \gamma$  occur (Tab. B.1).

**Table B.1:** Cardan convention for computing the orientation matrix

Axis	$ijk$	$\lambda$
$xyz$	123	
$yzx$	231	+1
$zxy$	312	
$zyx$	321	
$xzy$	132	-1
$yxz$	213	

Starting from this consideration, the final orientation matrix  $R(\alpha, \beta, \gamma)$  may be directly computed according the following relations being known the angles  $\alpha, \beta, \gamma$ :

$$R(\alpha, \beta, \gamma) = \begin{bmatrix} r_{ii} = C_\beta C_\gamma & r_{ij} = -\lambda C_\beta S_\gamma & r_{ik} = \lambda S_\beta \\ r_{ji} = S_\alpha S_\beta C_\gamma + \lambda C_\alpha S_\gamma & r_{jj} = -\lambda S_\alpha S_\beta S_\gamma + C_\gamma C_\alpha & r_{jk} = -\lambda S_\alpha C_\beta \\ r_{ki} = -\lambda C_\alpha S_\beta C_\gamma + S_\alpha S_\gamma & r_{kj} = C_\alpha S_\beta S_\gamma + \lambda S_\alpha C_\gamma & r_{kk} = C_\alpha C_\beta \end{bmatrix}$$

Conversely, the value of the angles may be deducted from the final orientation matrix according to the following relations:

$$\begin{cases} \alpha = \text{atan}2(-\lambda r_{jk}, r_{kk}) & -\pi \leq \alpha \leq \pi \\ \beta = \text{asin}(\lambda r_{ik}) & -\pi/2 \leq \beta \leq \pi/2 \\ \gamma = \text{atan}2(-\lambda r_{ij}, r_{ii}) & -\pi \leq \gamma \leq \pi \end{cases}$$

---

## B.3 Cardan convention: velocity and acceleration

### B.3.1 Angular velocity

The relations among the derivatives with respect to time of the cardan angles and the angular velocity of the moving triad with respect to the fixed reference frame, can be expressed according the following matrix:

$$\begin{aligned} \begin{bmatrix} \omega_i \\ \omega_j \\ \omega_k \end{bmatrix} &= \begin{bmatrix} 1 & 0 & \lambda S_\beta \\ 0 & C_\alpha & -\lambda S_\alpha C_\beta \\ 0 & \lambda S_\alpha & C_\alpha C_\beta \end{bmatrix} \begin{bmatrix} \dot{\alpha} \\ \dot{\beta} \\ \dot{\gamma} \end{bmatrix} \\ \begin{bmatrix} \dot{\alpha} \\ \dot{\beta} \\ \dot{\gamma} \end{bmatrix} &= \begin{bmatrix} 1 & S_\alpha S_\beta / C_\beta & -\lambda C_\alpha S_\beta / C_\beta \\ 0 & C_\alpha & \lambda S_\alpha \\ 0 & -\lambda S_\alpha / C_\beta & C_\alpha C_\beta \end{bmatrix} \begin{bmatrix} \omega_i \\ \omega_j \\ \omega_k \end{bmatrix} \end{aligned}$$

### B.3.2 Angular acceleration

The accelerations can be obtained by simple derivation with respect to time of the speed relationships. In matrix form results:

---

**B.3. Cardan convention: velocity and acceleration**

---

$$\begin{bmatrix} \dot{\omega}_i \\ \dot{\omega}_j \\ \dot{\omega}_k \end{bmatrix} = \begin{bmatrix} 1 & 0 & \lambda S_\beta \\ 0 & C_\alpha & -\lambda S_\alpha C_\beta \\ 0 & \lambda S_\alpha & C_\alpha C_\beta \end{bmatrix} \begin{bmatrix} \ddot{\alpha} \\ \ddot{\beta} \\ \ddot{\gamma} \end{bmatrix} + \begin{bmatrix} \lambda C_\beta & 0 & 0 \\ \lambda S_\alpha S_\beta & -\lambda C_\alpha C_\beta & -S_\alpha \\ -C_\alpha S_\beta & -S_\alpha C_\beta & \lambda C_\alpha \end{bmatrix} \begin{bmatrix} \dot{\beta} \dot{\gamma} \\ \dot{\alpha} \dot{\gamma} \\ \dot{\alpha} \dot{\beta} \end{bmatrix}$$



---

## Bibliography

---

- [1] ISO 10328:2006. *Prosthetics - Structural testing of lower-limb prostheses - Requirements and test methods*.
- [2] B Aeyels, W Van Petegem, J Vander Sloten, Georges Van der Perre, and Louis Peeraer. An emg-based finite state approach for a microcomputer-controlled above-knee prosthesis. In *Engineering in Medicine and Biology Society, 1995., IEEE 17th Annual Conference*, volume 2, pages 1315–1316. IEEE, 1995.
- [3] Erhan Akdoğan and Mehmet Arif Adli. The design and control of a therapeutic exercise robot for lower limb rehabilitation: Physiotherabot. *Mechatronics*, 21(3):509–522, 2011.
- [4] Saud Al-Obaidi, James C Wall, Alia Al-Yaqoub, and Muneera Al-Ghanim. Basic gait parameters: A comparison of reference data for normal subjects 20 to 29 years of age from kuwait and scandinavia. *Journal of rehabilitation research and development*, 40(4):361, 2003.
- [5] Stefano Alfi, S Bruni, G Diana, A Facchinetto, and Laura Mazzola. Active control of airspring secondary suspension to improve ride quality and safety against crosswinds. *Proceedings of the Institution of Mechanical Engineers, Part F: Journal of Rail and Rapid Transit*, 225(1):84–98, 2011.
- [6] Erik K Antonsson and Robert W Mann. The frequency content of gait. *Journal of biomechanics*, 18(1):39–47, 1985.
- [7] Patrick M Aubin, Matthew S Cowley, and William R Ledoux. Gait simulation via a 6-dof parallel robot with iterative learning control. *Biomedical Engineering, IEEE Transactions on*, 55(3):1237–1240, 2008.
- [8] Nicolò Bachschmid. *Fondamenti di meccanica teorica e applicata*. McGraw-Hill, 2010.
- [9] Marko Bacic. On hardware-in-the-loop simulation. In *Decision and Control, 2005 and 2005 European Control Conference. CDC-ECC'05. 44th IEEE Conference on*, pages 3194–3198. IEEE, 2005.
- [10] Stacy J Morris Bamberg, Ari Y Benbasat, Donna Moxley Scarborough, David E Krebs, and Joseph A Paradiso. Gait analysis using a shoe-integrated wireless sensor system. *Information Technology in Biomedicine, IEEE Transactions on*, 12(4):413–423, 2008.
- [11] Stacy J Morris Bamberg, Paul LaStayo, Lee Dibble, Josh Musselman, and Swarna Kiran Dasa Raghavendra. Development of a quantitative in-shoe measurement system for assessing balance: sixteen-sensor insoles. In *Engineering in Medicine and Biology Society, 2006. EMBS'06. 28th Annual International Conference of the IEEE*, pages 6041–6044. IEEE, 2006.
- [12] Philipp Beckerle, L Lahnstein, Janis Wojtusch, Stephan Rinderknecht, and Oskar von Stryk. Conception and design of a hardware simulator for restoring lost biomechanical function. In *Systems, Man, and Cybernetics (SMC), 2013 IEEE International Conference on*, pages 1906–1911. IEEE, 2013.
- [13] Malte Bellmann, Thomas Schmalz, and Siegmar Blumentritt. Comparative biomechanical analysis of current microprocessor-controlled prosthetic knee joints. *Archives of physical medicine and rehabilitation*, 91(4):644–652, 2010.
- [14] James E Bobrow and Brian W McDonell. Modeling, identification, and control of a pneumatically actuated, force controllable robot. *Robotics and Automation, IEEE Transactions on*, 14(5):732–742, 1998.

## Bibliography

---

- [15] Roozbeh Borjian, James Lim, Mir Behrad Khamesee, and William Melek. The design of an intelligent mechanical active prosthetic knee. In *Industrial Electronics, 2008. IECON 2008. 34th Annual Conference of IEEE*, pages 3016–3021. IEEE, 2008.
- [16] John H Bowker. *Atlas of limb prosthetics: surgical, prosthetic, and rehabilitation principles*. Mosby Inc, 1992.
- [17] Francesco Braghin, Federico Cheli, Alan Facchinetto, and Edoardo Sabbioni. Design of an active seat suspension for agricultural vehicles. In *Structural Dynamics, Volume 3*, pages 1365–1374. Springer, 2011.
- [18] Tomas Brezina, Zdenek Hadas, and Jan Vetiska. Using of co-simulation adams-simulink for development of mechatronic systems. In *MECHATRONIKA, 2011 14th International Symposium*, pages 59–64. IEEE, 2011.
- [19] Aurelio Cappozzo. Gait analysis methodology. *Human Movement Science*, 3(1):27–50, 1984.
- [20] Aurelio Cappozzo, Fabio Catani, Ugo Della Croce, and Alberto Leardini. Position and orientation in space of bones during movement: anatomical frame definition and determination. *Clinical biomechanics*, 10(4):171–178, 1995.
- [21] Giuseppe Carbone, Conghui Liang, and Marco Ceccarelli. Using parallel architectures for humanoid robots.
- [22] EY Chao, RK Laughman, E Schneider, and RN Stauffer. Normative data of knee joint motion and ground reaction forces in adult level walking. *Journal of biomechanics*, 16(3):219–233, 1983.
- [23] SH Cho, JM Park, and OY Kwon. Gender differences in three dimensional gait analysis data from 98 healthy korean adults. *Clinical biomechanics*, 19(2):145–152, 2004.
- [24] Herman J De Straete, Pascal Degezelle, Joris De Schutter, and Ronnie JM Belmans. Servo motor selection criterion for mechatronic applications. *Mechatronics, IEEE/ASME Transactions on*, 3(1):43–50, 1998.
- [25] Ugo Della Croce, Patrick O Riley, Jennifer L Lelas, and D Casey Kerrigan. A refined view of the determinants of gait. *Gait & posture*, 14(2):79–84, 2001.
- [26] Aaron M Dollar and Hugh Herr. Lower extremity exoskeletons and active orthoses: challenges and state-of-the-art. *Robotics, IEEE Transactions on*, 24(1):144–158, 2008.
- [27] Janice J Eng and David A Winter. Kinetic analysis of the lower limbs during walking: what information can be gained from a three-dimensional model? *Journal of biomechanics*, 28(6):753–758, 1995.
- [28] A Facchinetto and S Bruni. Hardware-in-the-loop hybrid simulation of pantograph–catenary interaction. *Journal of Sound and Vibration*, 331(12):2783–2797, 2012.
- [29] Arnaud Faivre, Marc Dahan, Bernard Parratte, and Guy Monnier. Instrumented shoes for pathological gait assessment. *Mechanics research communications*, 31(5):627–632, 2004.
- [30] Kevin Fite, Jason Mitchell, Frank Sup, and Michael Goldfarb. Design and control of an electrically powered knee prosthesis. In *Rehabilitation robotics, 2007. ICORR 2007. IEEE 10th international conference on*, pages 902–905. IEEE, 2007.
- [31] H Giberti, F Resta, E Sabbioni, L Vergani, C Colombo, G Verni, and E Boccafogli. Development of a bench for testing leg prosthetics. In *Special Topics in Structural Dynamics, Volume 6*, pages 35–45. Springer, 2013.
- [32] Hermes Giberti, Simone Cinquemani, and Giovanni Legnani. A practical approach to the selection of the motor-reducer unit in electric drive systems. *Mechanics based design of structures and machines*, 39(3):303–319, 2011.
- [33] Hermes Giberti and Cristiano Marinelli. Vibration suppression of a flexible parallel kinematic manipulator. In *Nonlinear Dynamics, Volume 2*, pages 281–295. Springer, 2014.
- [34] Alessandro GIUA and Sergio LORRAI. Universita degli studi di cagliari facolta di ingegneria corso di laurea in ingegneria delle telecomunicazioni.
- [35] Donald Lee Grimes. *An active multi-mode above knee prosthesis controller*. PhD thesis, Massachusetts Institute of Technology, 1979.
- [36] Lina Hao, Xinhe Xu, and Jun Cheng. A test-bed for above-knee intelligent prosthesis. In *Robotics and Biomimetics, 2006. ROBIO'06. IEEE International Conference on*, pages 1311–1315. IEEE, 2006.
- [37] Sven Herrmann, Christoph Woernle, Michael Kaehler, Roman Rachholz, Robert Souffrant, János Zierath, Daniel Klüss, and Rainer Bader. Hil simulation for testing joint stability after total knee arthroplasty. *Multi-body System Dynamics*, 28(1-2):55–67, 2012.
- [38] Neville Hogan. Impedance control: An approach to manipulation. In *American Control Conference, 1984*, pages 304–313. IEEE, 1984.

## Bibliography

---

- [39] Carl D Hoover, George D Fulk, and Kevin B Fite. Stair ascent with a powered transfemoral prosthesis under direct myoelectric control. *Mechatronics, IEEE/ASME Transactions on*, 18(3):1191–1200, 2013.
- [40] Adam M Howell, Takehiko Kobayashi, Heather A Hayes, K Bo Foreman, and Stacy JM Bamberg. Kinetic gait analysis using a low-cost insole. *Biomedical Engineering, IEEE Transactions on*, 60(12):3284–3290, 2013.
- [41] Verne T Inman, Howard D Eberhart, et al. The major determinants in normal and pathological gait. *J Bone Joint Surg Am*, 35(3):543–558, 1953.
- [42] Jennifer L Johansson, Delsey M Sherrill, Patrick O Riley, Paolo Bonato, and Hugh Herr. A clinical comparison of variable-damping and mechanically passive prosthetic knee devices. *American journal of physical medicine & rehabilitation*, 84(8):563–575, 2005.
- [43] Mrn P Kadaba, HK Ramakrishnan, and ME Wootten. Measurement of lower extremity kinematics during level walking. *Journal of orthopaedic research*, 8(3):383–392, 1990.
- [44] Akin O Kapti and M Sait Yucenur. Design and control of an active artificial knee joint. *Mechanism and machine theory*, 41(12):1477–1485, 2006.
- [45] Kenton R Kaufman, Serena Frittoli, and Carlo A Frigo. Gait asymmetry of transfemoral amputees using mechanical and microprocessor-controlled prosthetic knees. *Clinical Biomechanics*, 27(5):460–465, 2012.
- [46] Jung-Hoon Kim and Jun-Ho Oh. Development of an above knee prosthesis using mr damper and leg simulator. In *Robotics and Automation, 2001. Proceedings 2001 ICRA. IEEE International Conference on*, volume 4, pages 3686–3691. IEEE, 2001.
- [47] Arthur D Kuo. The six determinants of gait and the inverted pendulum analogy: A dynamic walking perspective. *Human movement science*, 26(4):617–656, 2007.
- [48] Vasilios Kyriazis. Gait analysis techniques. *Journal of orthopaedics and traumatology*, 2(1):1–6, 2001.
- [49] Brian E Lawson, Huseyin Atakan Varol, Amanda Huff, Erdem Erdemir, and Michael Goldfarb. Control of stair ascent and descent with a powered transfemoral prosthesis. *Neural Systems and Rehabilitation Engineering, IEEE Transactions on*, 21(3):466–473, 2013.
- [50] Alberto Leardini, Aurelio Cappozzo, Fabio Catani, Soren Toksvig-Larsen, Aldo Petitto, Vincenzo Sforza, Giancarlo Cassanelli, and Sandro Giannini. Validation of a functional method for the estimation of hip joint centre location. *Journal of biomechanics*, 32(1):99–103, 1999.
- [51] Giovanni Legnani. *Robotica industriale*.
- [52] Flavia L Lombardo, Marina Maggini, Alessandra De Bellis, Giuseppe Seghieri, and Roberto Anichini. Lower extremity amputations in persons with and without diabetes in italy: 2001–2010. *PLoS One*, 9(1):e86405, 2014.
- [53] Ou Ma, Angel Flores-Abad, and Toralf Boge. Use of industrial robots for hardware-in-the-loop simulation of satellite rendezvous and docking. *Acta Astronautica*, 81(1):335–347, 2012.
- [54] MD ADAMS-User Manual. Msc. San Mateo, CA, 1999.
- [55] CRISTIANO MARINELLI. Definizione di modelli per l'esecuzione dell'analisi strutturale di un piede protesico in fibra di carbonio. 2012.
- [56] Ernesto C Martinez-Villalpando and Hugh Herr. Agonist-antagonist active knee prosthesis: A preliminary study in level-ground walking. *J. Rehabil. Res. Dev.*, 46(3):361–374, 2009.
- [57] Claudio Melchiorri. *Traiettorie per azionamenti elettrici*. Progetto Leonardo, 2000.
- [58] Pieter Meyns, Sjoerd M Bruijn, and Jacques Duysens. The how and why of arm swing during human walking. *Gait & posture*, 38(4):555–562, 2013.
- [59] Simcha Milo, Edmond Rambod, Chaim Gutfinger, and Morteza Gharib. Mitral mechanical heart valves: in vitro studies of their closure, vortex and microbubble formation with possible medical implications. *European journal of cardio-thoracic surgery*, 24(3):364–370, 2003.
- [60] WE Misselhorn, NJ Theron, and PS Els. Investigation of hardware-in-the-loop for use in suspension development. *Vehicle System Dynamics*, 44(1):65–81, 2006.
- [61] Tassos Natsakis, Josefien Burg, Greta Dereymaeker, Ilse Jonkers, and Jos Vander Sloten. Inertial control as novel technique for in vitro gait simulations. *Journal of biomechanics*, 48(2):392–395, 2015.
- [62] T Öberg, Alek Karsznia, and K Öberg. Basic gait parameters: reference data for normal subjects, 10-79 years of age. *Journal of rehabilitation research and development*, 30:210–210, 1993.

## Bibliography

---

- [63] Louis Peeraer, B Aeyels, and Georges Van der Perre. Development of emg-based mode and intent recognition algorithms for a computer-controlled above-knee prosthesis. *Journal of biomedical engineering*, 12(3):178–182, 1990.
- [64] Shabnam Pejhan, Farzam Farahmand, and Mohammad Parnianpour. Design optimization of an above-knee prosthesis based on the kinematics of gait. In *Engineering in Medicine and Biology Society, 2008. EMBS 2008. 30th Annual International Conference of the IEEE*, pages 4274–4277. IEEE, 2008.
- [65] Jacqueline Perry, Judith M Burnfield, and Lydia M Cabico. Gait analysis: normal and pathological function. 1992.
- [66] Serge Pfeifer, Anna Pagel, Robert Riener, and Heike Vallery. Actuator with angle-dependent elasticity for biomimetic transfemoral prostheses. *Mechatronics, IEEE/ASME Transactions on*, 20(3):1384–1394, 2015.
- [67] Marc H Raibert and John J Craig. Hybrid position/force control of manipulators. *Journal of Dynamic Systems, Measurement, and Control*, 103(2):126–133, 1981.
- [68] Edmond Richer and Yildirim Hurmuzlu. A high performance pneumatic force actuator system: Part i-nonlinear mathematical model. *Journal of dynamic systems, measurement, and control*, 122(3):416–425, 2000.
- [69] Hanz Richter, Dan Simon, William A Smith, and Sergey Samorezov. Dynamic modeling, parameter estimation and control of a leg prosthesis test robot. *Applied Mathematical Modelling*, 39(2):559–573, 2015.
- [70] ABB Robotics. Operating manual robotstudio.
- [71] FE Sanville et al. A new method of specifying the flow capacity of pneumatic fluid power valves. *Hydraulic Pneumatic Power*, 17(195):120–126, 1971.
- [72] Ulf Schaper, Oliver Sawodny, Tobias Mahl, and Uli Blessing. Modeling and torque estimation of an automotive dual mass flywheel. In *American Control Conference, 2009. ACC'09.*, pages 1207–1212. IEEE, 2009.
- [73] Henning Schmidt, Dieter Sorowka, Stefan Hesse, and Rolf Bernhardt. Design of a robotic walking simulator for neurological rehabilitation. In *Intelligent Robots and Systems, 2002. IEEE/RSJ International Conference on*, volume 2, pages 1487–1492. IEEE, 2002.
- [74] Mohsen Akbari Shandiz, Farzam Farahmand, Noor Azuan Abu Osman, and Hassan Zohoor. A robotic model of transfemoral amputee locomotion for design optimization of knee controllers. *International Journal of Advanced Robotic Systems*, 10, 2013.
- [75] S Strike and M Hillery. The design and testing of a composite lower limb prosthesis. *Proceedings of the Institution of Mechanical Engineers, Part H: Journal of Engineering in Medicine*, 214(6):603–614, 2000.
- [76] WJ Suntay, ES Grood, MS Hefzy, DL Butler, and FR Noyes. Error analysis of a system for measuring three-dimensional joint motion. *Journal of biomechanical engineering*, 105(2):127–135, 1983.
- [77] Frank Sup, Amit Bohara, and Michael Goldfarb. Design and control of a powered transfemoral prosthesis. *The International journal of robotics research*, 27(2):263–273, 2008.
- [78] Rawesak Tanawongsuwan and Aaron Bobick. A study of human gaits across different speeds. Technical report, Georgia Tech, Tech. Rep, 2003.
- [79] Weijun Tao, Tao Liu, Rencheng Zheng, and Hutian Feng. Gait analysis using wearable sensors. *Sensors*, 12(2):2255–2283, 2012.
- [80] Marco Tarabini, Stefano Solbiati, Bortolino Saggin, and Diego Scaccabarozzi. Apparent mass matrix of standing subjects exposed to multi-axial whole-body vibration. *Ergonomics*, pages 1–12, 2015.
- [81] Julius Thiele, Simon Gallinger, Peter Seufert, and Marc Kraft. The gait simulator for lower limb exoprostheses—overview and first measurements for comparison of microprocessor controlled knee joints. *Facta Universitatis, Series: Mechanical Engineering*, 13(3):193–203, 2015.
- [82] Jan F Veneman, Rik Kruidhof, Edsko EG Hekman, Ralf Ekkelenkamp, Edwin HF Van Asseldonk, and Herman Van Der Kooij. Design and evaluation of the lopes exoskeleton robot for interactive gait rehabilitation. *Neural Systems and Rehabilitation Engineering, IEEE Transactions on*, 15(3):379–386, 2007.
- [83] Rino Versluys, Anja Desomer, Gerlinde Lenaerts, Pieter Beyl, Michael Van Damme, Bram Vanderborght, Innes Vanderniepen, Georges Van Der Perre, and Dirk Lefever. From conventional prosthetic feet to bionic feet: a review study. In *Biomedical Robotics and Biomechatronics, 2008. BioRob 2008. 2nd IEEE RAS & EMBS International Conference on*, pages 49–54. IEEE, 2008.
- [84] RP Wells. The projection of the ground reaction force as a predictor of internal joint moments. *Bulletin of prosthetics research*, 10:15–19, 1980.
- [85] Michael W Whittle. *Gait analysis: an introduction*. Butterworth-Heinemann, 2014.

## Bibliography

---

- [86] Dietmar Winkler and Clemens Gühmann. Hardware-in-the-loop simulation of a hybrid electric vehicle using modelica/dymola. Citeseer.
- [87] David A Winter. *Biomechanics and motor control of human movement*. John Wiley & Sons, 2009.
- [88] Ge Wu and Peter R Cavanagh. Isb recommendations for standardization in the reporting of kinematic data. *Journal of biomechanics*, 28(10):1257–1261, 1995.
- [89] Ge Wu, Sorin Siegler, Paul Allard, Chris Kirtley, Alberto Leardini, Dieter Rosenbaum, Mike Whittle, Darryl D D'Lima, Luca Cristofolini, Hartmut Witte, et al. Isb recommendation on definitions of joint coordinate system of various joints for the reporting of human joint motion-part i: ankle, hip, and spine. *Journal of biomechanics*, 35(4):543–548, 2002.
- [90] Ge Wu, Frans CT Van der Helm, HEJ DirkJan Veeger, Mohsen Makhsoos, Peter Van Roy, Carolyn Anglin, Jochem Nagels, Andrew R Karduna, Kevin McQuade, Xuguang Wang, et al. Isb recommendation on definitions of joint coordinate systems of various joints for the reporting of human joint motion-part ii: shoulder, elbow, wrist and hand. *Journal of biomechanics*, 38(5):981–992, 2005.
- [91] Hui Zhang, Zhiqiang Zhen, Qing Wei, and Wenseng Chang. The position/force control with self-adjusting select-matrix for robot manipulators. In *Robotics and Automation, 2001. Proceedings 2001 ICRA. IEEE International Conference on*, volume 4, pages 3932–3936. IEEE, 2001.
- [92] Jian Zhang, Ling Shen, Lixing Shen, and Aiping Li. Gait analysis of powered bionic lower prosthesis. In *Robotics and Biomimetics (ROBIO), 2010 IEEE International Conference on*, pages 25–29. IEEE, 2010.
- [93] Adam Zoss and Hami Kazerooni. Design of an electrically actuated lower extremity exoskeleton. *Advanced Robotics*, 20(9):967–988, 2006.
- [94] Adam B Zoss, Hami Kazerooni, and Andrew Chu. Biomechanical design of the berkeley lower extremity exoskeleton (bleex). *Mechatronics, IEEE/ASME Transactions on*, 11(2):128–138, 2006.